

Towards Preliminary Surrogates To Biomechanically Model The Human Calvarium

by

Kevin Kojo Montero Adanty

A thesis submitted in partial fulfillment of the requirements for the degree of

Doctor of Philosophy

Department of Mechanical Engineering
University of Alberta

© Kevin Kojo Montero Adanty, 2023

ABSTRACT

Surrogate headforms are employed in injury biomechanics to reconstruct head impact scenarios and evaluate protective equipment. The development of human calvarium surrogates to mimic mechanical response at fracture would be an essential step forward in improving the biomechanical biofidelity of surrogate headforms. In order to develop and validate potential surrogates, it is important to gain knowledge of the physical properties and mechanical response of the calvarium. Therefore, the purpose of this dissertation was to determine the morphometry, geometry, and mechanical response of the human calvarium to guide the development of preliminary surrogate models of the calvarium with the intent to mimic mechanical response at fracture. To gain an appreciation for this body of work, it is important to accentuate the critical objectives concerning the characterization of morphometry, geometry, and the mechanical response of the human calvarium that were necessary to acquire before fabricating and evaluating the surrogate models.

Human calvarium specimens of beam geometry were extracted from male and female donors in the frontal and parietal regions of the calvarium. The specimens were micro-computed tomography (CT) scanned followed by computer-based imaging analyses to quantify morphometric and geometrical properties. Statistically significant morphological distinctions at the levels of sex, location, and layers of the calvarium were established. Geometrical properties such as thickness, cortical and diploë layer thickness, and radius of curvature were also determined to physically construct the surrogates. The specimens were then mechanically characterized under 4-point quasi-static and dynamic impact bending to quantify their mechanical response. In quasi-static loading, it was found that the trabecular bone pattern factor of the diploë was a significant predictor of force and bending moment at fracture. The inner cortical layer had the greatest number of morphometric and geometric properties that were significant predictors of mechanical response

including thickness, tissue mineral density, and porosity. In dynamic impact loading, it was found that the mechanical response between male and female calvaria was not significantly different. Overall, the average mechanical responses of the calvaria from both loading tests were required to evaluate how well they compared to the surrogate models.

Three surrogate prototypes were constructed using readily available and cost-effective materials, specifically epoxy and chalk. The average geometry of the prototypes including thickness and radius of curvature was consistent with the beamed-shaped calvaria. The prototypes were tested under 4-point quasi-static and dynamic impact bending. The prototypes exhibited the most significant differences in mechanical response to calvaria under quasi-static loading compared to dynamic impact loading. In dynamic impact loading, where the loading and strain rate conditions are most relevant to real-world head impacts, it was determined that an epoxy-chalk layered surrogate was the best prototype for further development because its force at fracture, bending moment at fracture, tensile strain at fracture, tensile and compressive stress at fracture, tensile effective bending modulus, and tensile strain rate was not significantly different to calvaria.

The morphometry, geometry, and mechanical response of the human calvarium were characterized to guide the construction and evaluation of surrogate models of the calvarium using readily available and cost-effective materials. This dissertation may be a first step towards the development of a full-size surrogate model of the calvarium that may be employed to mimic fracture response when reconstructing head impact events and testing countermeasure equipment.

PREFACE

This dissertation is an original work by Kevin Adanty. The research project, of which this dissertation is a part, received research ethics approval from the University of Alberta Research Ethics Board, Project Name “Towards a Biomechanically Valid Simulant Model of the Human Calvarium”, No: Pro00089219, Approved on June 13, 2019, Expired on May 4, 2023.

Chapters 1 to 4 presented in this dissertation forms part of a Cooperative Agreement (Number W911NF-19-2-0336) sponsored by the Army Research Laboratory, U.S.A. Acknowledgements of this sponsorship and agreement are presented in Chapters 1 to 4.

Chapter 1 – article 1 of this dissertation was published as:

Adanty, Kevin, Karyne N. Rabey, Michael R. Doschak, Kapil B. Bhagavathula, James D. Hogan, Dan L. Romanyk, Samer Adeeb, Simon Ouellet, Thomas A. Plaisted, Sikhanda S. Satapathy, Christopher R. Dennison. 2021. “Cortical and Trabecular Morphometric Properties of the Human Calvarium.” Bone 148 (July): 115931. <https://doi.org/10.1016/j.bone.2021.115931>.

Chapter 2 – article 2 is currently under review:

*Adanty, K., Bhagavathula, K. B., Rabey, K. N., Doschak, M. R., Adeeb, S., Hogan, J. D., Ouellet, S., Plaisted, T. A., Satapathy, S. S., Romanyk, D. L., & Dennison, C. R. (2023). “The Effect of Morphometric and Geometric Indices of The Human Calvarium On Mechanical Response”. *Clinical Biomechanics*.” Under Review.*

Chapter 3 – article 3 of this dissertation was published as:

*Adanty, K., Bhagavathula, K. B., Tronchin, O., Li, D. X., Rabey, K. N., Doschak, M. R., Adeeb, S., Hogan, J., Ouellet, S., Plaisted, T. A., Satapathy, S. S., Romanyk, D. L., & Dennison, C. R. (2023). *The Mechanical Characterization and Comparison of Male and Female Calvaria Under Four-Point Bending Impacts. ASME Journal of Biomechanical Engineering 145(5): 051009. <https://doi.org/10.1115/1.4056459>.**

Chapter 4 – article 4 of this dissertation has been submitted to the Annals of Biomedical Engineering:

*Adanty, K., Brice, A., Li, Y., Vakiel, P., Rabey, K. N., Adeeb, S., Ouellet, S., Romanyk, D. L., & Dennison, C. R. (2023). *A Preliminary Step Towards A Physical Surrogate of The Human Calvarium To Model Fracture. Annals of Biomedical Engineering. Submitted.**

Kevin Adanty was responsible for the conceptualization, methodology, software, formal analysis, investigation, data curation, writing – original draft, writing – review & editing, visualization, and project administration for all articles.

ACKNOWLEDGMENTS

Firstly, I would like to acknowledge and express an immeasurable thank you to my primary supervisor, Christopher Dennison, Ph.D. Dr. Dennison helped me gain wisdom and knowledge and provided academic and professional advice, unconditional guidance, and invaluable principles and values that have bolstered me as an individual and researcher throughout this degree. I want to express a special thank you to Dan Romanyk, Ph.D., my co-supervisor, who stepped up to be a part of my supervisory team mid-way through this degree. Dr. Romanyk's academic knowledge, advice and exceptional perspective on biomechanics offered me a unique avenue to view and critique my work which has also strengthened my research and individual skills. Dr. Dennison and Dr. Romanyk's time, support, dedication, and effort through each phase of my work were admirable and for that, I am truly grateful to them.

I would like to express my sincere appreciation for my committee members, Karyne Rabey, Ph.D. and Samer Adeeb, Ph.D. Not only did they deliver relentless support and time to improve the phases of my work, but each of them brought forth a diverse perspective and research background that was crucial to the advancement of my work. I would like to thank Michael Doschak, Ph.D. for granting me permission to use his micro-computed tomography scanner. I am most grateful to Dr. Doschak for spending an immense amount of time assisting me with operating the scanner and for the great discussions on bone morphology with me and Dr. Rabey. I would also like to thank Dr. Rabey and the Department of Anatomy for permitting me access to human cadavers to extract calvarium specimens. Finally, I would like to thank the individuals at the U.S. Army Research Laboratory and Defense Research and Development Canada for the sponsorship and funding and for providing insightful contributions to my work.

I would like to graciously thank all my past and current lab colleagues at the University of Alberta and the University of Victoria for providing support and advice during my research. I would also like to thank the many friends and colleagues I've made at the U of A and UVIC who have made a positive impact during my time as a doctorate student. Lastly, I must recognize and thank the many individuals I was fortunate enough to connect with during international conferences and symposiums.

I would like to acknowledge and thank my loving family. Although I have lived far apart from them since I began my journey as a university student, my father, mother, brother, and sister have been instrumental in providing unconditional love, motivation, and moral support in all dimensions of my life. I am truly blessed for the family I have. I would like to acknowledge the love and support from the small group of friends I've made in Edmonton and the many close friends from my Ottawa days who've kept in touch with me over these many years. Lastly, I must thank God for guiding me on the right path and blessing me with good health, strong faith, and patience throughout my life and this journey.

TABLE OF CONTENTS

ABSTRACT.....	ii
PREFACE.....	iv
ACKNOWLEDGMENTS	v
LIST OF TABLES	x
LIST OF FIGURES	xii
PART I.....	1
INTRODUCTION.....	2
Background.....	2
Problem Statement.....	5
DISSERTATION OBJECTIVES & SUB-OBJECTIVES	9
The Dissertation’s Objective	9
The Dissertation’s Sub - Objectives.....	9
DISSERTATION BREAKDOWN	12
REFERENCES.....	13
PART II.....	19
BACKGROUND: REVIEW OF LITERATURE	20
Basic Anatomy: Human Calvarium.	20
Skull Biomechanics	22
The Biomechanics of the Human Skull.....	23
The Mechanism of a Skull Fracture	27
The Flexural Biomechanics of Calvarium Specimens.....	29
Proposed Physical Surrogate Models of the Calvarium.....	36
REFERENCES.....	45
PART III	50
Chapter 1: The Morphometry and Geometry of The Human Calvarium.	51
ABSTRACT	53
1. INTRODUCTION.....	55
2. MATERIAL AND METHODS.....	59
2.1 Specimen Extraction.....	59
2.2 Micro-CT Scanning of Specimens.....	61
2.3 Statistical Analysis.....	69
3. RESULTS.....	72
3.1 Diploë Morphometry	72

3.2 Cortical Morphometry	76
4. DISCUSSION	78
4.1 Diploë morphometry	78
4.2 Cortical Morphometry	82
4.3 Future considerations and limitations	83
5. CONCLUSION.....	86
ACKNOWLEDGEMENTS.....	87
DECLARATIONS OF INTEREST.....	87
SUPPLEMENTARY MATERIAL A	88
SUPPLEMENTARY MATERIAL B	97
REFERENCES.....	99
Chapter 2: The Effect of Morphometric and Geometric Indices of The Human Calvarium On Mechanical Response.	104
ABSTRACT	105
1. INTRODUCTION.....	107
1.1 Problem statement.....	107
1.2 Purpose and relevance of this study.....	109
2. MATERIALS AND METHODS.....	111
2.1 The Specimens.....	111
2.2 Micro-Computed Tomography (μ CT).....	113
2.3 Morphometric and Geometrical Properties.....	114
2.4 The Preparation of Specimens for Mechanical Testing.....	118
2.5 Mechanical Testing: 4-Point Quasi-Static Bending Testing.....	119
2.6 Mechanical Response Variables	120
2.7 Statistical Analysis.....	123
3. RESULTS.....	125
4. DISCUSSION	130
4.1 Diploë morphometry and mechanical response.....	131
4.2 Cortical morphometry and mechanical response.....	133
4.3 Limitations	135
5. CONCLUSION.....	138
ACKNOWLEDGEMENTS.....	139
REFERENCES.....	140
CONFLICT OF INTEREST STATEMENT	145
Chapter 3: The Mechanical Characterization and Comparison of Male and Female Calvaria Under Four-Point Bending Impacts.....	146

ABSTRACT	147
1. INTRODUCTION.....	148
2. METHODS	151
2.1 Specimens	151
2.2 Specimen Preparation	154
2.3 Mechanical Testing: 4-Point Dynamic Bending Impacts.....	155
2.4 Statistical Analysis.....	160
3. RESULTS.....	161
4. DISCUSSION	167
5. LIMITATIONS	172
5.1 Specimens	172
5.2 Mechanical Testing.....	174
6. CONCLUSION.....	176
ACKNOWLEDGMENT.....	177
FUNDING	178
REFERENCES.....	179
Chapter 4: The Development of Preliminary Human Calvarium Surrogate Models to Mimic Mechanical Response at Fracture.	184
ABSTRACT	185
1. INTRODUCTION.....	186
2. MATERIALS AND METHODS.....	190
2.1 Surrogate Development – Prototype 1: Pure Epoxy	190
2.2 Surrogate Development – Prototype 2: Epoxy-Chalk Mix.....	191
2.3 Surrogate Development – Prototype 3: Epoxy-Chalk Sandwich Layered	192
2.4 Surrogate Geometry	193
2.5 Human Calvaria	194
2.6 Mechanical Testing Of The Surrogate Prototypes	196
2.7 Statistics.....	199
3. RESULTS.....	201
3.1 Group 1) Specimens and Surrogate Prototypes.....	201
3.2 Group 2) Specimens and Surrogate Prototypes.....	201
4. DISCUSSION	206
ACKNOWLEDGMENTS	212
FUNDING AND/OR CONFLICTS OF INTERESTS/COMPETING INTERESTS	213
REFERENCES.....	214
PART IV	217

CONCLUSIONS	218
CONTRIBUTIONS.....	220
LIMITATIONS AND FUTURE RECOMMENDATIONS	222
BIBLIOGRAPHY	227

LIST OF TABLES

Background: Review of Literature:

Table 1. The bending test results on adult calvaria reported in the literature prior to the presentation of this thesis.

Chapter 1:

Table 1. The average age and dimensions of the calvarium specimens.

Table 2. Definitions of the morphometric properties measured in this study along with their unit of measure.

Table 3. The statistical results for the interaction terms investigated for the diploë morphometry and cortical morphometry. The degree of freedom for each statistic was 1.

Table 4. Simple main effects: Averages [95% CIs] for FD with respect to sex, location, and all 50 specimens.

Table 5. Main effects: Averages [95% CIs] for diploë morphometry with respect to sex, location and all 50 specimens.

Table 6. Averages [95% CIs] for cortical morphometry with respect to sex, calvarium location, and cortical layer.

Table 7. CV (%) For A Male Frontal Specimen's Morphometry.

Table 8. CV (%) For A Male Parietal Specimen's Morphometry.

Table 9. CV (%) For A Male Frontal Specimen's Morphometry.

Table 10. CV (%) For A Male Parietal Specimen's Morphometry.

Table 11. CV (%) For A Female Frontal Specimen's Morphometry.

Table 12. CV (%) For A Female Parietal Specimen's Morphometry.

Table 13. CV (%) For A Female Frontal Specimen's Morphometry.

Table 14. CV (%) For A Female Frontal Specimen's Morphometry.

Chapter 2:

Table 1. The average geometrical properties of the specimens with 95% confidence intervals.

Table 2. Diploë and cortical morphometric and geometric properties computed in this work. The properties here are defined in accordance with work by Adanty et al (Adanty et al. 2021).

Table 3. Linear regression models for significant ($p < 0.05$) predictors of mechanical response.

Table 4. The means for all morphometric and geometric properties and mechanical response variables.

Chapter 3:

Table 1. The mean age and geometric properties of the calvaria (95% confidence interval).

Table 2. Mechanical response variables determined for each test.

Table 3. Descriptive statistics of the mechanical response variables according to sex.

Table 4. Descriptive statistics of the mechanical response variables across both sexes.

Table 5. Statistical report for the geometry of the calvaria presented in Table 1 where no significant differences in geometry were reported between sexes ($p>0.05$).

Table 6. A comparison between the present study's 4-point bending impact results to bending test results on adult calvaria reported in the current literature. F, P, T, and O are frontal, parietal, temporal and occipital respectively. R and L refer to right and left respectively.

Chapter 4:

Table 1. A schematic, composition, I_x and weight for each prototype.

Table 2. Mean and 95% confidence intervals (CI) for geometrical properties of Group 1) specimens.

Table 3. Mean and 95% CIs for geometrical properties of Group 2) specimens.

Table 4. Mean \pm standard deviation (SD), 95% CIs, and median for calvaria and each prototype.

Table 5. Mean \pm SD, 95% CI, and median for calvaria and each prototype.

LIST OF FIGURES

Background: Review of Literature:

Figure 1. a) The subdivisions of the skull. b) The human calvarium.

Figure 2. A lateral view of the human skull displays the sutures of the calvarium.

Figure 3. The three-layered structure of the calvarium.

Figure 4. A head acceleration-time tolerance curve adopted by Gurdjian and colleagues.

Figure 5. An illustration of the inbending-outbending effect (left image) resulting in a linear fracture that propagates towards the point of impact (black circle) (right image).

Figure 6. A beam under 4-point bending experiences its fibres under compression (shortening) from the beam's neutral axis to its outer surface where the load is applied, and fibres under tension (lengthening) from the beam's neutral axis to its inner surface.

Figure 7. Delille et al.'s physical head model (left image) and force-time response compared to the Hybrid III headform and Nahum et al.'s PMHS study (right image).

Figure 8. An image of a three-layered surrogate produced by Roberts et al. in a three-point bending test.

Figure 9. A calvarium specimen (top image) and its high-strength epoxy resin (Masterflow 622) model (bottom image).

Figure 10. Three commercially available bone surrogates. A, B, X, Y correspond to different densities used by Brown et al. The red arrows correspond to the two different loading conditions applied, transverse (top arrow) and longitudinal (bottom arrow).

Chapter 1:

Figure 1. Schematic representation of a calvarium showing the frontal and parietal locations where specimens were extracted from each cadaver.

Figure 2. Example images of a male frontal (a.), male parietal (b.), female frontal (c.), and female parietal (d) calvarium specimen. L, W (into the page) and T correspond to the location of where length, width, and thickness dimensions were measured respectively at the center of each specimen using digital calipers.

Figure 3. Example of a specimen stabilized in a centrifugal tube (a.) and the resulting reconstructed and filtered micro-CT image of the specimen (b.).

Figure 4. Diploë region of interest (ROI) shaded in red for a single cross-section of a calvarium specimen (a.). Resultant diploë VOI to be used for image analysis (b.).

Figure 5. The ROI for the inner (a.) and outer (b.) cortical table and their resulting VOIs to be used for image analysis.

Figure 6. An example of a binarized diploë cross-section illustrating the sphere (gold circles) method to compute Tb.Th and Tb.Sp.

Figure 7. An example of a binarized diploë cross-section illustrating rods and plates within the trabecular region.

Figure 8. Distribution and normality curves (red) for each diploë morphometric property.

Figure 9. Distribution and normality curves (red) for each cortical morphometric property.

Chapter 2

Figure 1. a) A simplified model of the human calvarium presenting the regions from which the frontal and parietal specimens were obtained. b) A human calvarium specimen, where L=length and T=thickness were measured at the center of the specimen. O.ROC=outer radius of curvature and I.ROC=inner radius of curvature was determined in Geomagic software (2014) by 3-Dimensional (3D) Systems (Rock Hill, South Carolina).

Figure 2. An example of a reconstructed μ CT BMP image at two different cross-sections for a calvarium specimen.

Figure 3. In this example of a reconstructed μ CT BMP cross-section, the ROI of the diploë is encapsulated with an irregular anatomic contour shown in red (left image). The irregular anatomic contour (in red) is also applied to the ROI on the outer cortical table (middle image) and inner cortical table (right image).

Figure 4. Reconstructed μ CT BMP images of the segmented layers for this calvarium. Top image: the VOI for a segmented outer cortical layer (note the possible vascular foramen perforating the outer cortical layer in this section). Middle image: the VOI for a segmented diploë. Bottom image: the VOI for a segmented inner cortical layer. At the approximate center of each layer, a. represents the outer cortical thickness, b. represents the diploë thickness, and c. represents the inner cortical thickness.

Figure 5. An example of a calvarium implemented with an FBG on its outer cortical surface. Note the red line representing the FBG is enhanced for illustrative purposes.

Figure 6. An example of a calvarium specimen in the Instron E3000 for quasi-static 4-point bending. All specimens were positioned such that the inner cortical table was in contact with the bottom fixtures.

Figure 7. A 2D diagram of the known forces acting on the specimen during quasi-static 4-point bending. The outer cortical FBG quantifies the outer cortical surface strain (compressive strain) and the inner cortical FBG quantifies the inner cortical surface strain (tensile strain).

Figure 8. Tensile and compressive strain rate was determined as the initial linear portion of the

strain-time plot.

Figure 9. A cross-section of a calvaria specimen annotated with parameters required to compute bending stress (equations 1).

Figure 10. Tensile and compressive effective bending modulus was determined as the initial linear slope of the stress-strain plot.

Figure 11. a) Scatterplots with linear regression fitted lines and 95% CIs (two curved lines) for Tb.Pf. The 95% CI indicates that there is a 95% probability that the true or population regression line is within the confidence bands.

Figure 11. b) Scatterplots with linear regression fitted lines and 95% CIs (two curved lines) for cortical morphometry and geometric properties. The 95% CI indicates that there is a 95% probability that the true or population regression line is within the confidence bands.

Figure 12. An image scheme reproduced from Hahn et al. to explain Tb.Pf. The highest connectivity in (a) has a Tb.Pf that is more negative or further left on the number line (-1.35 mm^{-1}) and the lowest connectivity in (c) has a Tb.Pf value that is less negative or further right on the number line (-0.20 mm^{-1}).

Chapter 3:

Figure 1. a) A top-view model of the human calvarium displaying the outline which the frontal and parietal specimens were extracted from. **b)** An example of a beam-shaped human calvarium specimen.

Figure 2. a) A cross-sectional micro-CT scanned image from a calvarium specimen, where c_1 and c_2 represent the half-thickness of the specimen from the centroid to the outer cortical and inner cortical surface, respectively. **b)** An STL model of a calvarium specimen in Geomagic software to compute outer ROC and inner ROC.

Figure 3. a) A 2D schematic of the 4-point bending impact and where the FBGs were placed on the surface of the calvaria. **b)** A frontal view of the custom-built 4-point impact apparatus. **c)** An isometric view of the custom-built 4-point impact apparatus.

Figure 4. An example of a strain-time plot (top graph) and its corresponding stress-strain plot (bottom graph) for a calvarium presenting where the slope was computed to obtain strain-rate and effective bending modulus respectively. The indicated slope on the stress-strain plot (bottom graph) to determine the effective bending modulus corresponds to the strain-rate (slope) in the strain-time plot (top graph).

Figure 5. Bar charts comparing the mechanical response between male and female. * indicates a Welch t-test was performed for violating homogeneity of variance.

Figure 6. Histograms for compressive modulus and tensile modulus with respect to sex.

Chapter 4:

Figure 1. A schematic to illustrate the double-syringe self-mixing nozzle epoxy applicator.

Figure 2. The silicone mold with each prototype's imprint.

Figure 3. a. An example of a frontal calvarium specimen. b. A z-y micro-CT image of the calvarium. c. A z-x micro-CT image of the calvarium.

Figure 4. a. A schematic of the 4-point quasi-static bending test. b. A schematic of the 4-point dynamic impact bending test.

Figure 5. a. An example of a calvarium specimen, b. prototype 1, c. prototype 2 and d. prototype 3 under 4-point quasi-static bending in an Instron E3000.

Figure 6. a. An example of a calvarium specimen, b. prototype 1, c. prototype 2 and d. prototype 3 under 4-point dynamic impact bending.

Figure 7. The bending stress of the calvaria (red), the surrogate prototypes (orange) and simulant skull materials (blue) from the previous studies (Falland-Cheung et al., 2017; Ondruschka et al., 2019; Roberts et al., 2013) that tested in 3-point quasi-static bending at 10 mm/min. US Foam #16 and BJB-TC were two-part expanding urethane foam (Roberts et al., 2013), PETG was modified polyethylene terephthalate glycol (Falland-Cheung et al., 2017), the self-cure acrylic was denture base resin (Falland-Cheung et al., 2017), and the PLA was polylactic acid used as a 3-D printing filament (Falland-Cheung et al., 2017).

Figure 8. The bending modulus of the calvaria (red), the surrogate prototypes (orange) and simulant skull materials (blue) from the previous studies (Falland-Cheung et al., 2017; Ondruschka et al., 2019; Roberts et al., 2013) that tested in 3-point quasi-static bending at 10 mm/min.

PART IV:

Figure 1. A schematic of the future design modification for the 4-point dynamic impact bending tests.

PART I

INTRODUCTION

Background

A skull fracture, particularly at the calvarium or neurocranium level, occurs when a blunt-force trauma at low or high velocity is delivered to the head exceeding the mechanical threshold of the calvarium (Jankovic et al., 2021; Vorst et al., 2003). If such a blunt-force trauma is significant enough, a skull fracture can be accompanied by traumatic brain injuries (TBI) such as brain contusions, subdural hematoma, epidural hematoma, and diffuse axonal injury (Macpherson et al., 1990). Consequently, when a skull fracture is diagnosed, it is unequivocally categorized as a life-threatening injury. Reporting on the prevalence of adult skull fractures is scarce, especially within North America. The United Kingdom reported skull fractures in 3% of accident and emergency department visits, while 62% of fractures occurred in patients with severe head injuries (Marks, 2005). Pediatric patients are more vulnerable to head trauma and skull fracture compared to adults given their head size is approximately 18% of their total body surface area and their relatively thinner skull (McGrath & Taylor, 2022). The incidence of a skull fracture from a head injury among children ranges from 2% to 20% in the U.S. (McGrath & Taylor, 2022). A cohort study from 10 Canadian pediatric teaching institutions between July 2001 and November 2005 found that of 3866 pediatric patients, 4.3% sustained a linear skull fracture (Osmond et al., 2010). Asia, exclusively India and China, reported a combined incidence rate of approximately 10 per 100,000 of TBI related to skull fracturing which is a considerable burden to their respective public health sectors' given their immense population (Puvanachandra & Hyder, 2009).

Skull fractures can occur in many civilian activities and settings. Of these civilian activities, motor vehicle accidents and falls are the most common scenarios where a skull fracture occurs (Carson, 2009; Komisar et al., 2022; Kremer et al., 2008; Marks, 2005; McGrath & Taylor, 2022;

Puvanachandra & Hyder, 2009; Shields et al., 2011). Recreational sports, including ice hockey, American football, and cycling remain susceptible activities in which a skull fracture may occur. However, modern-day helmets and protective strategies are refined to a high degree that enables them to reduce the risk of a skull fracture. The main focus for modern injury biomechanists is improving helmets to reduce the risk of mild traumatic brain injuries (mTBIs) including concussions (Adanty et al., 2020; Clark et al., 2020; Fahlstedt et al., 2021; Halldin & Aare, 2003; Hoshizaki & Brien, 2004; Karton et al., 2020; Kleiven, 2013; Knowles & Dennison, 2017). Sporting activities where skull fractures have been noticeably documented include skateboarding, motor crossing, ocean surfing, and snow skiing as these are classified as extreme-level sports (Sharma et al., 2015). Back face deformation (BFD) is a common occurrence in military helmets and has the potential to inflict a skull fracture and other severe head injuries among servicemen and women (Rafaels et al., 2015; Weisenbach et al., 2018). BFD occurs when a ballistic projectile is caught and absorbed by the helmet and as a result the helmet locally deforms towards the personnel's head which can lead to localized skull fractures (Weisenbach et al., 2018). Physical assault arising from violent criminal behaviour and workplace accidents are also common settings where skull fractures were reported (Chattopadhyay & Tripathi, 2010; Daughton, 1990; Kremer et al., 2008; Stables et al., 2005). In summary, a skull fracture has the potential to occur in various injury-prone circumstances, many of which occur at high-velocity impacts including motor vehicle accidents, falls, sports, military combat, the workplace, and physical assaults.

It is common for injury biomechanists to perform experimental studies encompassing the impact parameters of injurious scenarios. The purpose of these studies is to quantify the potential or the likelihood for which an injury can occur such as a skull fracture, and then develop countermeasures to reduce the risk of injury. One of the most important considerations during

experimental testing for head injury is the choice of a surrogate head model to employ during a blunt trauma impact (Crandall et al., 2011). Cadavers of the human head or skull are one of the earliest and most favourable models for studying fracture tolerances along with animal tissue (Félizet, 1873; Gurdjian et al., 1950; Gurdjian & Lissner, 1947). If accessible, these models are the superior choice for a surrogate due to their anatomical and physiological resemblances to a live human head (Crandall et al., 2011). In addition, cadaveric skulls have the advantage of replicating fracture and fracture patterns close to a live human skull (Gurdjian et al., 1950). Previous studies have utilized fresh, fresh-frozen, or fixed (embalmed) cadaveric head and skull models for impact studies to develop injury risk curves, qualitatively describe fracture patterns, and test the performance of protective devices (Delye et al., 2007; Gurdjian et al., 1950; Gurdjian & Lissner, 1947; Rafaels et al., 2015; Vorst et al., 2003; Weisenbach et al., 2018; Yoganandan et al., 1995).

A secondary option to consider as a surrogate model of the human head is the use of headform dummies. Headforms are engineered synthetic devices that can be composed of metal, hard urethane, isotropic polymers, and/or foam - some may be composed as a combination of these materials (Hubbard & McLeod, 1974; Li et al., 2021). A classic example is the Hybrid III headform which is typically used for helmet testing and performance evaluation. These headforms are instrumented with accelerometers and additional sensor equipment within the internal space of the headform to quantify head kinematics and internal brain pressure (Crandall et al., 2011; Li et al., 2021). The purpose of their resilient composition is to endure numerous impacts, and therefore achieve repeatable and reproducible head kinematics. At certain levels of head acceleration measured within the headform, researchers may correspond those magnitudes with probability risk functions of experiencing a concussion, skull fracture, or a TBI in a real-case scenario (Clark et al., 2020; Cripton et al., 2014; Gurdjian et al., 1966; Hoshizaki et al., 2017; Pellman et al., 2003;

Versace, 1971; Viano et al., 2012; Vorst et al., 2003; Zhang et al., 2004). In addition to cadaveric and headform surrogates, human volunteers – used in non-injurious experiments, animal head models, and computational head models are alternative options to employ to study trauma-related head impacts.

Problem Statement

Despite the available selections of surrogate models to study head injury, each surrogate, particularly the cadaver and headform models, has its drawbacks when modelling a skull fracture or other forms of head injury. To gain access to cadavers, one requires a legal donor source of bodies such as an anatomical gift program or a regulated service that may provide unclaimed bodies (Habicht et al., 2018). One will also require an ethical agreement to transport and store the cadavers in a certified biosafety laboratory and then perform relevant research. Due to differences in national laws and ethical requirements across the globe, many researchers and scientists do not have access to cadaveric tissue in any event. Moreover, considerable time and financial resources are required to purchase and maintain the cadaveric tissue in ideal conditions (Crandall et al., 2011; Habicht et al., 2018). Lastly, cadaveric tissue is also susceptible to sizeable variations in its biomechanical response due to the distinct morphology between donors. As for headforms, it is not possible to model skull fractures due to their non-frangible material composition destined for achieving repeatable and reproducible results. Consequently, during injury reconstruction and testing of protective devices, researchers would need to be cautious in suggesting whether a fracture occurred or not. A surrogate with frangible capabilities up to the level of a skull fracture would allow for studying the coupling between the impacting object and the head, and between the head and the brain during skull deformation. Like cadavers, headforms or full dummies are

also costly devices for both first-time purchases and repairs which lessen their availability for experimental testing.

Injury biomechanists, materials scientists, and those in the forensic field have recently commenced efforts toward potential synthetic bone simulants to model skull fracture (Brown et al., 2019; Delille et al., 2007; Falland-Cheung et al., 2017; Ondruschka et al., 2019; Plaisted et al., 2015; Roberts et al., 2013; Thali et al., 2002). Surrogate models of the calvarium with frangible capabilities can relieve the drawbacks concerning cadaveric tissue and certain headforms. High-strength epoxy resin (Falland-Cheung et al., 2017; Ondruschka et al., 2019), synthetic bone materials sold through commercial enterprises (Brown et al., 2019), and additive manufacturing (Plaisted et al., 2015) are some of the materials and methods presented in the literature to model the skull. However, these materials or methods may not be easily accessible or cost-effective approaches toward simply fabricating a calvarium model to mimic mechanical response at fracture. There are also potential drawbacks in the circumstances in which these models have been validated. Previous studies have compared their surrogate model's mechanical properties against the properties of calvaria reported in different studies (Brown et al., 2019; Falland-Cheung et al., 2017; Roberts et al., 2013). However, this comparison may draw uncertainty mainly due to contrasting testing methodologies. This includes the type of mechanical testing performed (bending, compression, tension, quasi-static loading, and dynamic loading), the morphology of specimens, and the theorems or instrumentation to quantify mechanical properties. Testing surrogate models and calvaria within the same study or laboratory setting ensures there are negligible methodological differences when comparing biomechanical properties or response thereafter. Moreover, previous studies have mostly limited the testing of their surrogate skulls to quasi-static loading conditions but had not considered dynamic impact conditions (Delille et al.,

2007; Falland-Cheung et al., 2017; Ondruschka et al., 2019; Plaisted et al., 2015). Impact testing is the most applicable form of mechanical loading to real-world head impacts and must be considered to appropriately validate a fracture model of the calvarium (Roberts et al., 2013).

Indeed, continued efforts towards a surrogate model of the calvarium would be an important step to mimic the biomechanical response of the calvarium. However, it is vital to initially characterize the morphometry, geometry, and mechanical response of real calvarium in order to appropriately design and validate a surrogate. Apart from porosity, bone volume, and density, few studies have investigated the morphometry that exists within each layer of the calvarium (Alexander et al., 2019; Boruah et al., 2015; McElhaney et al., 1970; Peterson & Dechow, 2002). These properties along with trabecular thickness, trabecular separation or trabecular bone pattern factor may be of specific interest when developing detailed physical or computational models of the calvarium. Various methods have been proposed to determine the thickness of the skull, including the cortical tables (Alexander et al., 2019; Boruah et al., 2015; Hubbard, 1971; Lillie et al., 2015; Thulung et al., 2019), but the radius of curvature of the calvarium is also an important geometrical property that needs consideration to accurately emulate the curvature on a surrogate. The mechanical response and properties of the calvarium under flexural bending tests have been reported in the literature (Auperrin et al., 2014; Delille et al., 2007; Hubbard, 1971; Lee et al., 2019; Motherway et al., 2009; Rahmoun et al., 2014; Zwirner et al., 2021). However, many of those studies have not quantified the mechanical measurements of the calvarium on both its inner and outer cortical surfaces, nor have they determined the surface strain at which the calvarium fractures (Hubbard, 1971). In addition, most of the loading conditions have been limited to quasi-static 3-point bending, while only a few have characterized the calvarium in dynamic impact bending (Motherway et al., 2009; Zwirner et al., 2021). It is therefore

evident, that the characterization of the calvarium's morphology, geometry and mechanical response is further needed to aid the design and evaluation of a surrogate.

Given the current state of research surrounding the mechanics of skull fracture, there are four directions research should turn towards to pragmatically develop a surrogate that can model this injury. Firstly, determine the average morphometry, geometry and mechanical response of the human calvarium. Secondly, employ readily available and cost-effective materials and approaches to fabricate a surrogate. Thirdly, validate the surrogate's mechanical response to calvarium within the same study and testing conditions to draw meaningful comparisons and prevent the factoring in of cross-study variations. Lastly, incorporate the testing of surrogates under dynamic impact conditions that factor in strain rates most applicable to real-world head impact scenarios. All these directions were considered in this dissertation to develop surrogate prototypes of beam geometry to mimic the mechanical response of the calvarium at fracture.

DISSERTATION OBJECTIVES & SUB-OBJECTIVES

The Dissertation's Objective

The objective of this dissertation was to characterize the morphometry, geometry, and mechanical response of the human calvarium to guide the construction of preliminary surrogate prototypes of the calvarium to model its mechanical response at fracture.

The Dissertation's Sub - Objectives

It is not feasible to instantly produce a surrogate model of the calvarium without gaining foresight into the morphometry, geometry, and mechanical response of real human calvaria. In this thesis, morphometry is defined as the measurements that characterize the microarchitectural structure of the calvarium such as the calvarium's density, its trabecular thickness, trabecular separation, and trabecular bone pattern factor. Geometry is defined as the gross dimension or size of the calvarium that can simply be measured as the length of a calvarium specimen, thickness, or radius of curvature. Morphometry and geometry of the calvarium are important to determine since they can be referred to as guidance when physically fabricating a surrogate model of calvarium or designing one in silico. Secondly, it is important to determine the range of the calvarium's mechanical response at fracture during experimental testing to ensure the surrogate's response falls within that range. A surrogate model that exhibits mechanical response comparable to calvaria will be an important step forward in the model's effort toward biofidelity. Collectively, all this information on the calvarium is necessary to move forth in constructing prospective surrogate models with the intent to mimic mechanical response at fracture. Therefore, this dissertation was categorized into four sub-objectives to facilitate a step-by-step approach toward fabricating and achieving surrogate prototypes. Each of the four sub-objectives was discussed within their own respective chapters, collectively, they are all intertwined to ultimately achieve the dissertation's objective.

The sub-objectives are as follows:

Sub-objective 1: Determine the morphometry and geometry of the human calvarium.

This objective determined the morphometry and geometry of the human calvarium and identified if significant differences in morphometry were present between sex, location, and between layers of the calvarium.

Specific null hypotheses tested:

1) no significant interaction effects between sex and location on the diploë morphometric properties.

2) no significant interaction effects between the cortical layers, sex, and location on the cortical morphometric properties.

3) no significant main effects or simple main effects, in other words, no significant differences in diploë morphometric properties between male and female and between frontal and parietal locations.

Sub-objective 2: Determine which morphometric and geometric properties have a significant influence on the mechanical response of the human calvarium during 4-point quasi-static bending.

This objective identified which morphometric and geometric properties determined in sub-objective 1 were significant predictors of the mechanical response of the calvarium. A significant predictor was defined as a morphometric or geometric property that was associated with a statistically significant univariate linear regression model to predict mechanical response.

Specific null hypothesis tested:

1) The coefficient of the slope for each linear regression model was equal to 0.

Sub-objective 3: Determine the mechanical response of the human calvarium in 4-point dynamic impact bending.

This objective characterized the mechanical response of the human calvarium in 4-point dynamic impact bending conditions and determined if there were significant differences between male and female calvaria.

Specific null hypothesis tested:

1) No significant differences in mechanical response between male and female calvaria.

Sub-objective 4: Develop preliminary surrogate models of the human calvarium to mimic the calvarium's mechanical response at fracture.

This objective used the information gathered from sub-objectives 1 to 3 to develop preliminary surrogate models of the human calvarium to mimic the calvarium's mechanical response at fracture.

Specific null hypothesis tested:

1) No significant differences between human calvaria and each surrogate prototype.

DISSERTATION BREAKDOWN

This is an article-based dissertation, meaning the body of the dissertation mainly encompasses articles that have either been published or accepted for publication, are currently under review or have been submitted to a peer-reviewed journal. The body of this dissertation is composed of two major sections: 1) the review of the literature (Part II) and 2) four articles divided into 4 chapters that conducted the corresponding sub-objectives (Part III).

In Part II, the review of the literature composes of three sections. The first part of the literature review contains information on the basic anatomy of the human calvarium to understand its general composition and structure. The anatomy of the calvarium is then followed by the second section which discusses the biomechanics of the skull. In this section, a series of previous studies are conveyed to comprehend the mechanics of the skull. After the mechanics of the skull are appreciated, the section goes on to define the mechanism associated with a skull fracture and reviews the reported values on the mechanical properties of the calvarium under flexural bending tests. The final section of the literature review describes the previous efforts that have been made to develop a physical surrogate of the calvarium. In part III, the dissertation presents four articles. Article one-chapter 1 determined the morphometry and geometry of the calvarium, article two-chapter 2 determined which morphometric or geometric properties of the calvarium were significant predictors of mechanical response under 4-point quasi-static bending, article three-chapter 3 characterized the mechanical response of the calvarium under 4-point dynamic impact bending, and article four-chapter 4 gathered the findings from chapters 1 to 3 to develop surrogate models of the calvarium to mimic mechanical response at fracture.

The final part of the dissertation encompasses a global conclusion, a summary of the dissertation's contributions, and a summary of limitations and future recommendations (Part IV).

REFERENCES

- Adanty, K., Clark, J. M., Post, A., Hoshizaki, T. B., & Gilchrist, M. D. (2020). Comparing two proposed protocols to test the oblique response of cycling helmets to fall impacts. *International Journal of Crashworthiness*, 25(6), 648–663. <https://doi.org/10.1080/13588265.2019.1628479>
- Alexander, S. L., Rafaels, K., Gunnarsson, C. A., & Weerasooriya, T. (2019). Structural analysis of the frontal and parietal bones of the human skull. *Journal of the Mechanical Behavior of Biomedical Materials*, 90, 689–701. <https://doi.org/10.1016/j.jmbbm.2018.10.035>
- Auperrin, A., Delille, R., Lesueur, D., Bruyère, K., Masson, C., & Drazétic, P. (2014). Geometrical and material parameters to assess the macroscopic mechanical behaviour of fresh cranial bone samples. *Journal of Biomechanics*, 47(5), 1180–1185. <https://doi.org/10.1016/j.jbiomech.2013.10.060>
- Boruah, S., Paskoff, G. R., Shender, B. S., Subit, D. L., Salzar, R. S., & Crandall, J. R. (2015). Variation of bone layer thicknesses and trabecular volume fraction in the adult male human calvarium. *Bone*, 77, 120–134. <https://doi.org/10.1016/j.bone.2015.04.031>
- Brown, A. D., Walters, J. B., Zhang, Y. X., Saadatfar, M., Escobedo-Diaz, J. P., & Hazell, P. J. (2019). The mechanical response of commercially available bone simulants for quasi-static and dynamic loading. *Journal of the Mechanical Behavior of Biomedical Materials*, 90, 404–416. <https://doi.org/10.1016/j.jmbbm.2018.10.032>
- Carson, H. J. (2009). Brain trauma in head injuries presenting with and without concurrent skull fractures. *Journal of Forensic and Legal Medicine*, 16(3), 115–120. <https://doi.org/10.1016/j.jflm.2008.08.013>
- Chattopadhyay, S., & Tripathi, C. (2010). Skull fracture and haemorrhage pattern among fatal and nonfatal head injury assault victims – a critical analysis. *Journal of Injury and Violence Research*, 2(2), 99–103. <https://doi.org/10.5249/jivr.v2i2.46>
- Clark, J. M., Adanty, K., Post, A., Hoshizaki, T. B., Clissold, J., McGoldrick, A., Hill, J., Annaidh, A. N., & Gilchrist, M. D. (2020). Proposed injury thresholds for concussion in equestrian sports. *Journal of Science and Medicine in Sport*, 23(3), 222–236. <https://doi.org/10.1016/j.jsams.2019.10.006>
- Crandall, J. R., Bose, D., Forman, J., Untaroiu, C. D., Arregui-Dalmases, C., Shaw, C. G., & Kerrigan, J. R. (2011). Human surrogates for injury biomechanics research. *Clinical Anatomy*, 24(3), 362–371. <https://doi.org/10.1002/ca.21152>
- Cripton, P. A., Dressler, D. M., Stuart, C. A., Dennison, C. R., & Richards, D. (2014). Bicycle helmets are highly effective at preventing head injury during head impact: Head-form accelerations and injury criteria for helmeted and unhelmeted impacts. *Accident; Analysis and Prevention*, 70, 1–7. <https://doi.org/10.1016/j.aap.2014.02.016>

- Daughton, S. (1990). Head Injury in the Workplace. *AAOHN Journal*, 38(10), 497–501. <https://doi.org/10.1177/216507999003801008>
- Delille, R., Lesueur, D., Potier, P., Drazetic, P., & Markiewicz, E. (2007). Experimental study of the bone behaviour of the human skull bone for the development of a physical head model. *International Journal of Crashworthiness*, 12(2), 101–108. <https://doi.org/10.1080/13588260701433081>
- Delye, H., Verschuere, P., Depreitere, B., Verpoest, I., Berckmans, D., Vander Sloten, J., Van Der Perre, G., & Goffin, J. (2007). Biomechanics of frontal skull fracture. *Journal of Neurotrauma*, 24(10), 1576–1586. <https://doi.org/10.1089/neu.2007.0283>
- Fahlstedt, M., Abayazid, F., Panzer, M. B., Trotta, A., Zhao, W., Ghajari, M., Gilchrist, M. D., Ji, S., Kleiven, S., Li, X., Annaidh, A. N., & Halldin, P. (2021). Ranking and Rating Bicycle Helmet Safety Performance in Oblique Impacts Using Eight Different Brain Injury Models. *Annals of Biomedical Engineering*, 49(3), 1097–1109. <https://doi.org/10.1007/s10439-020-02703-w>
- Falland-Cheung, L., Waddell, J. N., Chun Li, K., Tong, D., & Brunton, P. (2017). Investigation of the elastic modulus, tensile and flexural strength of five skull simulant materials for impact testing of a forensic skin/skull/brain model. *Journal of the Mechanical Behavior of Biomedical Materials*, 68, 303–307. <https://doi.org/10.1016/j.jmbbm.2017.02.023>
- Félizet, G. (1844-1909) A. du texte. (1873). *Recherches anatomiques et expérimentales sur les fractures du crâne / par le Dr G. Félizet,...* <https://gallica.bnf.fr/ark:/12148/bpt6k5740393g>
- Gurdjian, E. S., & Lissner, H. R. (1947). Deformations of the skull in head injury as studied by the “stresscoat” technic. *The American Journal of Surgery*, 73(2), 269–281. [https://doi.org/10.1016/0002-9610\(47\)90321-8](https://doi.org/10.1016/0002-9610(47)90321-8)
- Gurdjian, E. S., Roberts, V. L., & Thomas, L. M. (1966). Tolerance curves of acceleration and intracranial pressure and protective index in experimental head injury. *The Journal of Trauma*, 6(5), 600–604. <https://doi.org/10.1097/00005373-196609000-00005>
- Gurdjian, E. S., Webster, J. E., & Lissner, H. R. (1950). The Mechanism of Skull Fracture. *Journal of Neurosurgery*, 7(2), 106–114. <https://doi.org/10.3171/jns.1950.7.2.0106>
- Habicht, J. L., Kiessling, C., & Winkelmann, A. (2018). Bodies for Anatomy Education in Medical Schools: An Overview of the Sources of Cadavers Worldwide. *Academic Medicine*, 93(9), 1293–1300. <https://doi.org/10.1097/ACM.0000000000002227>
- Halldin, P., & Aare, M. (2003). A New Laboratory Rig for Evaluating Helmets Subject to Oblique Impacts. *Traffic Injury Prevention*, 4, 240–248.
- Hoshizaki, T. B., & Brien, S. E. (2004). The science and design of head protection in sport. *Neurosurgery*, 55(4), 956.
- Hoshizaki, T. B., Post, A., Kendall, M., Cournoyer, J., Rousseau, P., Gilchrist, M. D., Brien, S., Cusimano, M., & Marshall, S. (2017). The development of a threshold curve for the understanding of concussion in sport. *Trauma*, 19(3), 196–206. <https://doi.org/10.1177/1460408616676503>

- Hubbard, R. P. (1971). Flexure of layered cranial bone. *Journal of Biomechanics*, 4(4), 251–263. [https://doi.org/10.1016/0021-9290\(71\)90031-5](https://doi.org/10.1016/0021-9290(71)90031-5)
- Hubbard, R. P., & McLeod, D. G. (1974). Definition and Development of A Crash Dummy Head. *SAE Transactions*, 83, 3836–3851.
- Jankovic, J., Mazziotta, J. C., & Pomeroy, S. L. (2021). *Bradley and Daroff's Neurology in Clinical Practice, 2-Volume Set*. Elsevier Health Sciences.
- Karton, C., Blaine Hoshizaki, T., & Gilchrist, M. D. (2020). A novel repetitive head impact exposure measurement tool differentiates player position in National Football League. *Scientific Reports*, 10(1), Article 1. <https://doi.org/10.1038/s41598-019-54874-9>
- Kleiven, S. (2013). Why Most Traumatic Brain Injuries are Not Caused by Linear Acceleration but Skull Fractures are. *Frontiers in Bioengineering and Biotechnology*, 1. <https://doi.org/10.3389/fbioe.2013.00015>
- Knowles, B. M., & Dennison, C. R. (2017). Predicting Cumulative and Maximum Brain Strain Measures From HybridIII Head Kinematics: A Combined Laboratory Study and Post-Hoc Regression Analysis. *Annals of Biomedical Engineering*, 45(9), 2146–2158. <https://doi.org/10.1007/s10439-017-1848-y>
- Komisar, V., Dojnov, A., Yang, Y., Shishov, N., Chong, H., Yu, Y., Bercovitz, I., Cusimano, M. D., Becker, C., Mackey, D. C., & Robinovitch, S. N. (2022). Injuries from falls by older adults in long-term care captured on video: Prevalence of impacts and injuries to body parts. *BMC Geriatrics*, 22(1), 343. <https://doi.org/10.1186/s12877-022-03041-3>
- Kremer, C., Racette, S., Dionne, C.-A., & Sauvageau, A. (2008). Discrimination of Falls and Blows in Blunt Head Trauma: Systematic Study of the Hat Brim Line Rule in Relation to Skull Fractures. *Journal of Forensic Sciences*, 53(3), 716–719. <https://doi.org/10.1111/j.1556-4029.2008.00725.x>
- Lee, J. H. C., Ondruschka, B., Falland-Cheung, L., Scholze, M., Hammer, N., Tong, D. C., & Waddell, J. N. (2019). An Investigation on the Correlation between the Mechanical Properties of Human Skull Bone, Its Geometry, Microarchitectural Properties, and Water Content. *Journal of Healthcare Engineering*, 2019, 1–8. <https://doi.org/10.1155/2019/6515797>
- Li, Y., Ouellet, S., Vette, A. H., Raboud, D., Martin, A., & Dennison, C. R. (2021). Evaluation of the Kinematic Biofidelity and Inter-Test Repeatability of Global Accelerations and Brain Parenchyma Pressure for a Head–Brain Physical Model. *Journal of Biomechanical Engineering*, 143(9). <https://doi.org/10.1115/1.4050752>
- Lillie, E. M., Urban, J. E., Weaver, A. A., Powers, A. K., & Stitzel, J. D. (2015). Estimation of skull table thickness with clinical CT and validation with microCT. *Journal of Anatomy*, 226(1), 73–80. <https://doi.org/10.1111/joa.12259>

- Macpherson, B. C. M., Macpherson, P., & Jennett, B. (1990). CT evidence of intracranial contusion and haematoma in relation to the presence, site and type of skull fracture. *Clinical Radiology*, 42(5), 321–326. [https://doi.org/10.1016/S0009-9260\(05\)82145-2](https://doi.org/10.1016/S0009-9260(05)82145-2)
- Marks, P. (2005). HEAD TRAUMA | Pediatric and Adult, Clinical Aspects. In J. Payne-James (Ed.), *Encyclopedia of Forensic and Legal Medicine* (pp. 461–472). Elsevier. <https://doi.org/10.1016/B0-12-369399-3/00186-5>
- McElhaney, J. H., Fogle, J. L., Melvin, J. W., Haynes, R. R., Roberts, V. L., & Alem, N. M. (1970). Mechanical properties of cranial bone. *Journal of Biomechanics*, 3(5), 495–511. [https://doi.org/10.1016/0021-9290\(70\)90059-X](https://doi.org/10.1016/0021-9290(70)90059-X)
- McGrath, A., & Taylor, R. S. (2022). Pediatric Skull Fractures. In *StatPearls*. StatPearls Publishing. <http://www.ncbi.nlm.nih.gov/books/NBK482218/>
- Motherway, J. A., Verschueren, P., Van der Perre, G., Vander Sloten, J., & Gilchrist, M. D. (2009). The mechanical properties of cranial bone: The effect of loading rate and cranial sampling position. *Journal of Biomechanics*, 42(13), 2129–2135. <https://doi.org/10.1016/j.jbiomech.2009.05.030>
- Ondruschka, B., Lee, J. H. C., Scholze, M., Zwirner, J., Tong, D., Waddell, J. N., & Hammer, N. (2019). A biomechanical comparison between human calvarial bone and a skull simulant considering the role of attached periosteum and dura mater. *International Journal of Legal Medicine*, 133(5), 1603–1610. Scopus. <https://doi.org/10.1007/s00414-019-02102-4>
- Osmond, M. H., Klassen, T. P., Wells, G. A., Correll, R., Jarvis, A., Joubert, G., Bailey, B., Chauvin-Kimoff, L., Pusic, M., McConnell, D., Nijssen-Jordan, C., Silver, N., Taylor, B., & Stiell, I. G. (2010). CATCH: A clinical decision rule for the use of computed tomography in children with minor head injury. *CMAJ: Canadian Medical Association Journal*, 182(4), 341–348. <https://doi.org/10.1503/cmaj.091421>
- Pellman, E. J., Viano, D. C., Tucker, A. M., Casson, I. R., & Waeckerle, J. F. (2003). Concussion in Professional Football: Reconstruction of Game Impacts and Injuries. *Neurosurgery*, 53(4), 799–814. <https://doi.org/10.1227/01.NEU.0000083559.68424.3F>
- Peterson, J., & Dechow, P. C. (2002). Material properties of the inner and outer cortical tables of the human parietal bone. *The Anatomical Record*, 268(1), 7–15. <https://doi.org/10.1002/ar.10131>
- Plaisted, T. A., Gardner, J. M., & Gair, J. L. (2015). *Characterization of a Composite Material to Mimic Human Cranial Bone*. 12.
- Puvanachandra, P., & Hyder, A. A. (2009). *THE BURDEN OF TRAUMATIC BRAIN INJURY IN ASIA: A CALL FOR RESEARCH*. 4, 6.
- Rafaels, K. A., Cutcliffe, H. C., Salzar, R. S., Davis, M., Boggess, B., Bush, B., Harris, R., Rountree, M. S., Sanderson, E., Campman, S., Koch, S., & ‘Dale’ Bass, C. R. (2015). Injuries of the Head from Backface Deformation of Ballistic Protective Helmets Under Ballistic Impact. *Journal of Forensic Sciences*, 60(1), 219–225. <https://doi.org/10.1111/1556-4029.12570>

- Rahmoun, J., Auperrin, A., Delille, R., Naceur, H., & Drazetic, P. (2014). Characterization and micromechanical modeling of the human cranial bone elastic properties. *Mechanics Research Communications*, 60, 7–14. <https://doi.org/10.1016/j.mechrescom.2014.04.001>
- Roberts, J. C., Merkle, A. C., Carneal, C. M., Voo, L. M., Johannes, M. S., Paulson, J. M., Tankard, S., & Uy, O. M. (2013). Development of a Human Cranial Bone Surrogate for Impact Studies. *Frontiers in Bioengineering and Biotechnology*, 1. <https://doi.org/10.3389/fbioe.2013.00013>
- Sharma, V. K., Rango, J., Connaughton, A. J., Lombardo, D. J., & Sabesan, V. J. (2015). The Current State of Head and Neck Injuries in Extreme Sports. *Orthopaedic Journal of Sports Medicine*, 3(1), 2325967114564358. <https://doi.org/10.1177/2325967114564358>
- Shields, B. J., Burkett, E., & Smith, G. A. (2011). Epidemiology of balcony fall–related injuries, United States, 1990–2006. *The American Journal of Emergency Medicine*, 29(2), 174–180. <https://doi.org/10.1016/j.ajem.2009.08.023>
- Stables, G., Quigley, G., Basu, S., & Pillay, R. (2005). An unusual case of a compound depressed skull fracture after an assault with a stiletto heel. *Emergency Medicine Journal*, 22(4), 303–304.
- Thali, M. J., Kneubuehl, B. P., Zollinger, U., & Dirnhofer, R. (2002). The “Skin–skull–brain model”: A new instrument for the study of gunshot effects. *Forensic Science International*, 125(2), 178–189. [https://doi.org/10.1016/S0379-0738\(01\)00637-5](https://doi.org/10.1016/S0379-0738(01)00637-5)
- Thulung, S., Ranabhat, K., Bishokarma, S., & Gongal, D. N. (2019). Morphometric Measurement of Cranial Vault Thickness: A Tertiary Hospital Based Study. *JNMA: Journal of the Nepal Medical Association*, 57(215), 29–32. <https://doi.org/10.31729/jnma.3949>
- Versace, J. (1971). *A Review of the Severity Index* (SAE Technical Paper No. 710881). SAE International. <https://doi.org/10.4271/710881>
- Viano, D. C., Withnall, C., & Halstead, D. (2012). Impact Performance of Modern Football Helmets. *Annals of Biomedical Engineering*, 40(1), 160–174. <https://doi.org/10.1007/s10439-011-0384-4>
- Vorst, M. V., Stuhmiller, J., Ho, K., Yoganandan, N., & Pintar, F. (2003). Statistically and Biomechanically Based Criterion for Impact-Induced Skull Fracture. *Annual Proceedings / Association for the Advancement of Automotive Medicine*, 47, 363–381.
- Weisenbach, C. A., Logsdon, K., Salzar, R. S., Chancey, V. C., & Brozoski, F. (2018). Preliminary Investigation of Skull Fracture Patterns Using an Impactor Representative of Helmet Back-Face Deformation. *Military Medicine*, 183(suppl_1), 287–293. <https://doi.org/10.1093/milmed/usx210>
- Yoganandan, N., Pintar, F. A., Sances, A., Walsh, P. R., Ewing, C. L., Thomas, D. J., & Snyder, R. G. (1995). Biomechanics of skull fracture. *Journal of Neurotrauma*, 12(4), 659–668. <https://doi.org/10.1089/neu.1995.12.659>
- Zhang, L., Yang, K. H., & King, A. I. (2004). A Proposed Injury Threshold for Mild Traumatic Brain Injury. *Journal of Biomechanical Engineering*, 126(2), 226–236. <https://doi.org/10.1115/1.1691446>

Zwirner, J., Ondruschka, B., Scholze, M., Workman, J., Thambyah, A., & Hammer, N. (2021). The dynamic impact behavior of the human neurocranium. *Scientific Reports*, *11*(1), 11331. <https://doi.org/10.1038/s41598-021-90322-3>

PART II

BACKGROUND: REVIEW OF LITERATURE

Basic Anatomy: Human Calvarium.

The human skull is the skeletal region of the head that conforms to the human's facial features. It is surrounded externally by layers of the scalp (skin) and encloses the soft tissue of the brain (Figure 1a). The two sectors of the skull are the cranial vault and the facial bones (Hombach-Klonisch et al., 2019). The cranial vault is referred to as the calvarium or neurocranium and it consists of the frontal, parietal, temporal, sphenoid and occipital bones (Figure 1b). Like all bones, the calvarium is a hard tissue composed of 40% inorganic matter – hydroxyapatite (e.g. $\text{Ca}_{10}(\text{PO}_4)_6(\text{OH})_2$), 25% water, and 35% organic components (e.g. 90% collagen and 10% non-collagen proteins) (Feng, 2009). The bones of the calvarium are categorized as flat bones that protect the brain against external forces that could otherwise inflict a brain injury (Hombach-Klonisch et al., 2019).

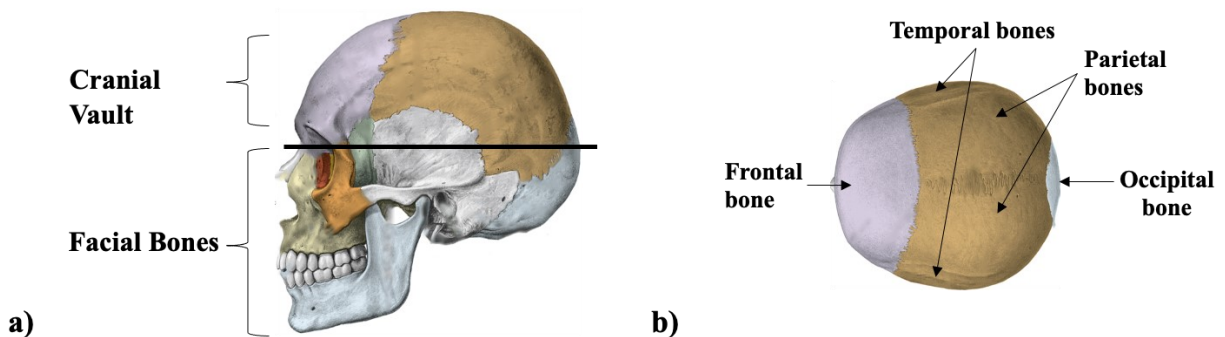


Figure 1. a) The subdivisions of the skull. b) The human calvarium. Image source: (Hombach-Klonisch et al., 2019). Copyright permissions from Elsevier Books have been granted (license number: 5477711430803), edited by the author. This article/chapter was published in Elsevier Books, vol 1, Sabine Hombach-Klonisch, Jason Peeler, Thomas Klonisch. Sobotta Clinical Atlas of Human Anatomy, 423-479, Copyright Elsevier, (2019).

Sutures are fibrous bands of tissue that formulate between the edges of the bones of the skull (Pritchard et al., 1956). The purpose of a suture is to permit skull growth as the head and brain expand during growth and development. The parietal bone consists of the sagittal suture that

connects the left and right parietal bone, it is visible on the superior aspect of the calvarium and runs anterior-posterior (Figure 2). The frontal bone consists of the metopic suture that runs superior-inferior and is most visible in a newborn infant (Gosling et al., 2017). The frontal and parietal bones are connected by the coronal suture that runs parallel to the coronal plane (Figure 2). The parietal and temporal bones are connected by the squamosal suture and are located on the lateral aspects of the calvarium (Figure 2). The occipital and parietal bone are joined by the lambdoid suture, and it is located on the posterior aspect of the calvarium (Figure 2). Finally, the sphenosquamosal suture vertically articulates between the sphenoid and temporal bone (Figure 2).

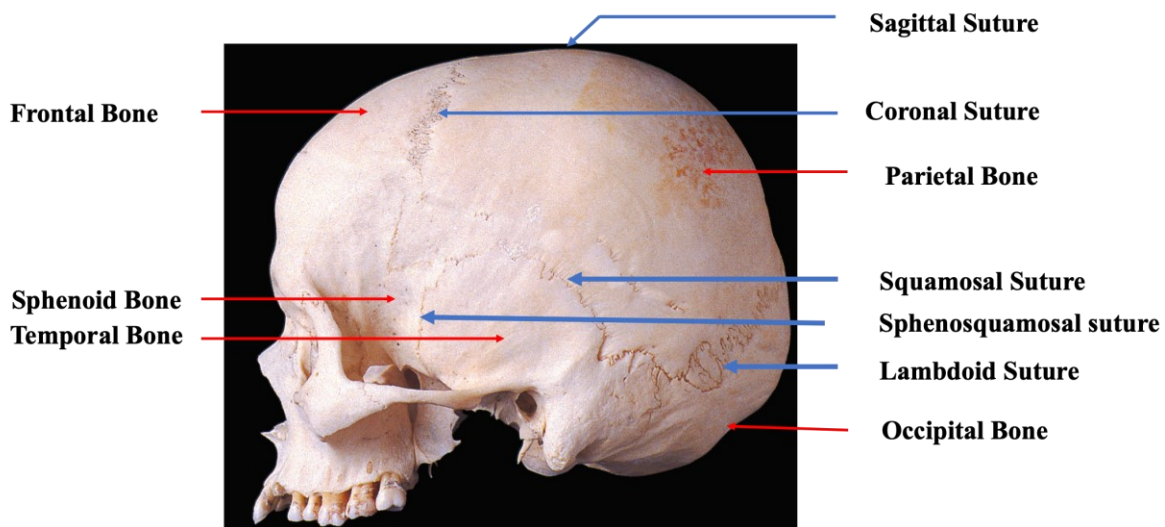


Figure 2. A lateral view of the human skull displays the sutures of the calvarium. **Image source:** (Gosling et al., 2017). Copyright permissions from Elsevier Books have been granted (license number: 5477710519339), edited by the author. This article/chapter was published in Elsevier Books, 6th edition, J.A. Gosling, P.F. Harris, J.R. Humpherson, I. Whitmore, P.L.T. Willan. Human Anatomy, Color Atlas and Textbook, 321-392, Copyright Elsevier, (2017).

The human calvarium is a three-layer structure that comprises a lattice-like network of bone (trabeculae) termed the diploë, compacted between two cortical layers (compact bone), the outer and inner cortical tables (Figure 3). The cortical tables are a high-density bone region harvested with osteons (microscopic units of bone); each osteon contains a central canal consisting of the cortical bone's blood supply (Hombach-Klonisch et al., 2019). The diploë, a low-density

region, houses a network of randomly distributed trabecular struts. The pores separating the struts contain a supply of red bone marrow which is required for blood cell formation within the diploë. The overall blood supply for the skull originates from the external carotid artery that branches off from the common carotid arteries. The unique structural design of the calvarium has been previously cited as analogous to layered panels used in an aircraft (Hubbard, 1971). The panels are sandwich structures that feature inner and outer high-stiffness faces divided by a low-stiffness core, parallel to the layered structure of the calvarium (Hubbard, 1971; Ueng, 2003). The sandwich structure is attributed to its low overall density, high-strength-to-weight ratio, and absorption capabilities during impact (Ueng, 2003).

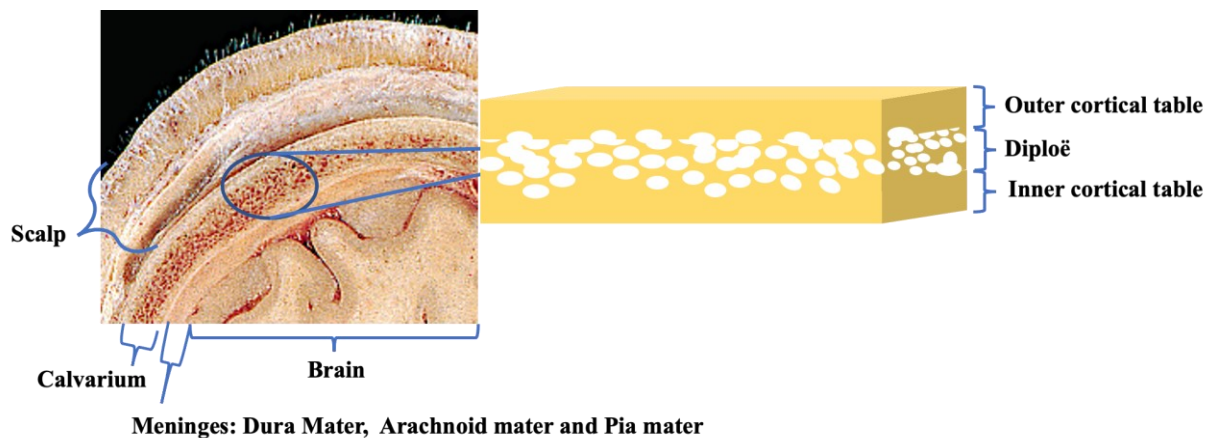


Figure 3. *The three-layered structure of the calvarium. Image source: (Gosling et al., 2017). Copyright permissions from Elsevier Books have been granted (license number: 5477710519339), edited by the author. This article/chapter was published in Elsevier, 6th edition, J.A. Gosling, P.F. Harris, J.R. Humpherson, I. Whitmore, P.L.T. Willan. Human Anatomy, Color Atlas and Textbook, 321-392, Copyright Elsevier, (2017).*

Skull Biomechanics

The advancements in brain injury models are apparent in the biomechanical literature (Ji et al., 2022). However, the skull remains the natural hard tissue that acts as the protective armour to the brain and deserves progressive biomechanical research to understand its mechanics and protect it

from injury. This can lead to a holistic refinement of head models that can predict the mechanical response of all types of head injuries with improved accuracy.

The Biomechanics of the Human Skull

The earliest documented study that quantified the mechanical response of the human skull occurred in 1880 by Messerer (Messerer, 1880). Quasi-static lateral compression tests were delivered to male and female unembalmed (fresh) cadaver heads. Fracture forces ranged from 400 to 600 kg (3924 to 5886 N) for males and 300 to 800 kg (2943 to 7848 N) for females. Male and female skulls deformed by 4.3 mm and 5.7 mm on average respectively just before skull fracture. It was also established that the human skull was more deformable in the lateral loading direction than in the frontal-posterior direction. Although, it is not entirely clear how the heads were positioned in the test bed when conducting these early experiments. Messerer's work accounts for earlier studies in the mid-1800s on mechanical tests (vise-grip compression, drop impacts, forceps compressions) of intact human heads for adults and pediatrics. However, the intent of these studies was limited to qualitative observations such as noting alterations in skull diameter and implications of elasticity (Messerer, 1880).

Gurdjian and colleagues established the mechanism of a skull fracture in the 1940s (Gurdjian et al., 1950; Gurdjian & Lissner, 1947a). Though, it was not until the 1950s to the 1960s that research on quantifying skull mechanics began to gain significant traction. This is because the interest concerning head injury shifted toward understanding the mechanism of brain injuries including TBIs and concussions, therefore, it was assumed brain injuries were associated with skull fractures. In a 1953 preliminary report, Gurdjian et al. documented linear, comminuted, and depressed fractures of the skull when anesthetized mongrel dogs were diagnosed with minimal to severe degrees of concussion as a result of ball peen hammer blows (Gurdjian et al., 1953). The

average peak head acceleration (in gravitational units) in which a fracture occurred was $438 \pm 188g$ and ranging between 230 and 780g (Gurdjian et al., 1953). Human cadavers were subject to frontal head impacts in which peak linear head acceleration and the durations of the head impacts were documented (Gurdjian, 1975; Gurdjian et al., 1953, 1955). Accelerometers were mounted on the inside (inner cortical surface) of the skull with metal fasteners. Cadaveric frontal head drops onto steel slabs demonstrated that average accelerations of 112 to 200g for a duration of 4 ms were associated with linear fractures. Whereas, no serious injuries were detected at 42g over a duration of several milliseconds (Gurdjian et al., 1966). With the accumulation of experimental testing on mongrel dogs and human cadavers (Gurdjian et al., 1953, 1955, 1964, 1966), Gurdjian and colleagues devised a head acceleration-time tolerance curve as a guide for establishing a head injury criterion, the curve soon revolutionized into what is commonly known as the Wayne State Tolerance Curve (WSTC), see Figure 5 (Gurdjian et al., 1953, 1955, 1966).

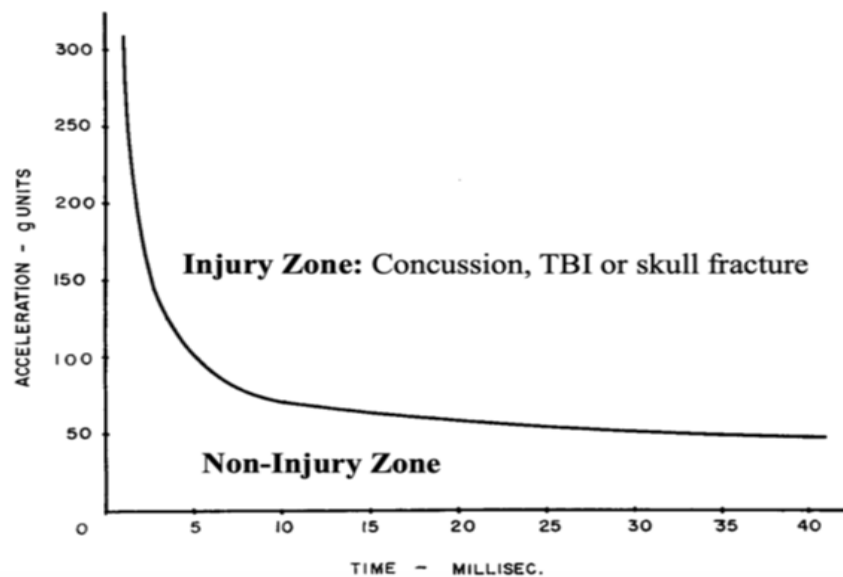


Figure 4. A head acceleration-time tolerance curve adopted by Gurdjian and colleagues. **Image source:** (Gurdjian et al., 1966) Copyright permissions from Wolters Kluwer Health, Inc. have been granted (license number: 5396600267734).

Subsequent to work by Gurdjian and colleagues, the intent of many skull fracture studies was to quantify the force at fracture and stiffness of the skull. Human calvaria (whole skull cap) were rigidly mounted in circular molds made of Castone and were impacted by steel penetrators of different diameters (0.43 to 0.61 inches) and impact velocities (0-20 mph) (Melvin et al., 1969). These resulted in localized penetrations with average failure loads ranging from 1030 to 1710 lbs of force (4581.65 to 7606.42 N) for the frontal region and 780 to 1290 lbs (3469.60 to 5738.18 N) for the parietal region. Nahum and colleagues conducted impacts on the frontal and parietal regions of embalmed and unembalmed human skulls using a controlled circular impacting mass (25.4 mm diameter) (Nahum et al., 1968). The frontal region experienced average forces at fracture between 4893 N with a range of 2600 to 8000 N (Nahum et al., 1968). The parietal region experienced average forces at fracture between 3300 N with a range of 2000 to 6000 N (Nahum et al., 1968). They also noted that embalming did not appear to affect their force results (Nahum et al., 1968). Hodgson and Thomas applied drop impacts of embalmed cadaver heads onto rigid and 60-durometer rubber and of various radii (Hodgson & Thomas, 1972). For rigid surface impacts, fractures mostly occurred at drop heights of 10 in (38.10 cm) to 30 in (76.20 cm) and at forces ranging from 3000 to 10,800 N for frontal impacts and from 5300 to 20,000 N for side impacts (Hodgson & Thomas, 1972). Accelerometers mounted on the side of the heads documented head acceleration between 150 to 410g for frontal impacts (Hodgson & Thomas, 1972). The cadavers tolerated greater fracture forces ranging from 5300 to 15,000 N with the compliant rubber surface and accelerations ranging from 115 to 360g (Hodgson & Thomas, 1972). Allsop and colleagues determined frontal stiffnesses of 20 mm diameter bar impacts at 1000 N/mm, 1800 N/mm for the temporoparietal (impact area of 6.45 cm²), and 4200 N/mm for the parietal (impact area of 50 cm²) (Allsop et al., 1988, 1991). Yoganandan et al. conducted a series of quasi-static and dynamic

loading of cadaveric unembalmed heads severed at the occipital-cervical 1 (C1)-cervical 2 (C2) junction of the body (Yoganandan et al., 1995). A hemispherical anvil (radius: 48 mm) was dropped at a rate of 2.54 mm/s for quasi-static loading and 7.1 to 8.0 m/s for dynamic loading (Yoganandan et al., 1995). Force-deflection curves exhibited a nonlinear behaviour, failure forces for quasi-static loading and dynamic loading ranged from 4500 to 11,900 N and 8800 to 14,100 N respectively (Yoganandan et al., 1995). Displacements of the anvil ranged from 7.8 mm to 16.6 mm for quasi-static loading and 3.4 to 9.8 mm for dynamic loading (Yoganandan et al., 1995). Stiffnesses ranged from 467 N/mm to 1290 N/mm for quasistatic loading and from 2462 N/mm to 5867 N/mm for dynamic loading (Yoganandan et al., 1995). Linear, depressed, circular, and multiple fractures were reported with wider fracture lines occurring away from the loading site - a phenomenon consistent with observations by Gurdjian et al.'s mechanism of a skull fracture (Gurdjian et al., 1947, 1950; Yoganandan et al., 1995).

Collectively, the described biomechanical studies on the human skull and head have demonstrated a mutual consistency in the forces, displacement, and stiffness measurements under mechanical loading. There remains a plethora of studies that have conducted comparable experiments and yielded consistent results (McIntosh et al., 1993; Ono et al., 1985; Schneider & Nahum, 1972; Van Lierde et al., 2003; Yoganandan et al., 1994). The limitation concerning intact human skull impacts is that it is challenging to relate the irregular geometry of the whole human skull with constitutive equations to estimate stress or modulus of elasticity. Therefore, recent studies have applied materials testing of calvarium specimens in compression, tension and bending to determine mechanical properties of the skull aside from force and displacement properties. Nevertheless, the described studies in this section are beneficial for those who wish to validate computational or physical models of the whole human skull.

The Mechanism of a Skull Fracture

Many of the historical studies on the mechanism of a skull fracture were qualitatively reported in the mid-19th century (Bruns, n.d.; Félizet, 1873). The common notion implied by these early studies was that skull fractures tend to occur due to an inward bending of the calvaria and that fracture commenced at the point of impact. By 1950, the mechanism of a skull fracture received further attention, largely in part due to work from Gurdjian, Webster, and Lissner (Gurdjian et al., 1950; Gurdjian & Lissner, 1947a). Stresscoat (strain-sensitive lacquer) was applied on freshly dry human skulls and dropped onto a solid steel slab. The stresscoat was only sensitive to detecting tensile strains, therefore, compressive strains could not be envisioned. It was established that at the point of impact, the surface of the calvarium's inner table experiences inbending – the calvarium bends toward the brain (Figure 4). In some cases, the calvaria may rebound (elastic behaviour) immediately after impact to its original position if the impact force was not sufficient to cause a fracture (Figure 4). As a result of the rebound, peripheral regions away from the point of impact experience outbending – the calvarium bends away from the brain (Figure 4) causing the outer cortical surface to experience what is known as a linear fracture (Figure 4). The linear fracture propagates a short or long distance from the peripheral region toward the point of impact because of the peak tensile stress concentration at the surface of the impact point after the rebound (Figure 4).

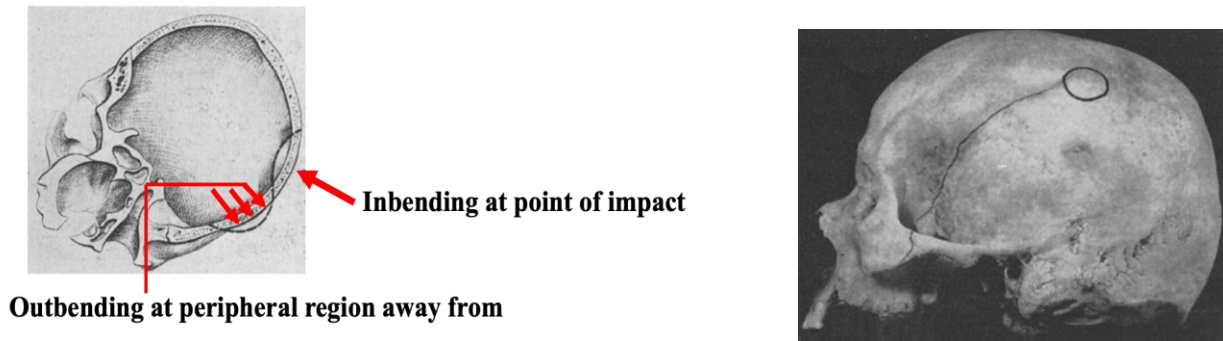


Figure 5. An illustration of the inbending-outbending effect (left image) resulting in a linear fracture that propagates towards the point of impact (black circle) (right image). **Image source:** (Gurdjian et al., 1950), edited by author. **Non-exclusive copyright permissions from American Association of Neurological Surgeons have been granted.**

If the impact force on the skull is sufficient, such as a high-velocity impact, the inner cortical surface reaches its maximum deformation from bending leading to what is known as a depressed fracture (Gurdjian et al., 1950; Gurdjian & Lissner, 1947b). With a depressed fracture, it is possible to observe brain contusions and lacerations (Gurdjian et al., 1955). In a subsequent study, stresscoat was applied to both the inner cortical and the outer cortical surface of the skull (Gurdjian et al., 1947). It was determined that the skull was weak in tension since crack patterns originated from the inner cortical surface where tension occurred. In these simple drop tests performed by Gurdjian and colleagues, it was identified that inbending of the calvarium caused by a blunt impact is the main mechanism of a skull fracture (Gurdjian et al., 1947, 1950; Gurdjian & Lissner, 1947a). In addition, it was documented that the outer surface of the calvarium can experience outbending or tensile straining leading to linear fractures at peripheral regions from the point of impact. Gurdjian et al. further remarked that deformation of the skull may cause compression of the underlying brain matter and thus increase the intracranial pressure within the brain (Gurdjian et al., 1955). In areas where a linear fracture develops, dura (the adhesive tissue between the skull and brain) may separate from the skull due to outbending resulting in an epidural hematoma (Gurdjian, 1975).

The Flexural Biomechanics of Calvarium Specimens

Since the mechanism of a skull fracture involves inward bending of the calvarium at the point of impact, it will be relevant to discuss those studies that have performed flexural bending tests on calvarium specimens to determine mechanical bending properties. In flexural testing, a beam experiences both compressive and tensile stresses at the outer fibres where the load is applied and on the inner fibres where the fracture originates, respectively (Figure 6). It is important to determine the measurements and properties of the human calvarium for a number of reasons, including validating the biofidelity of computational and physical surrogate models of the calvarium under similar loading conditions. Compression and tensile tests of calvarium specimens are well-documented in the literature (Boruah et al., 2013; Evans & Lissner, 1957; McElhaney et al., 1970; Robbins & Wood, 1969; Wood, 1971; Zhai et al., 2020).

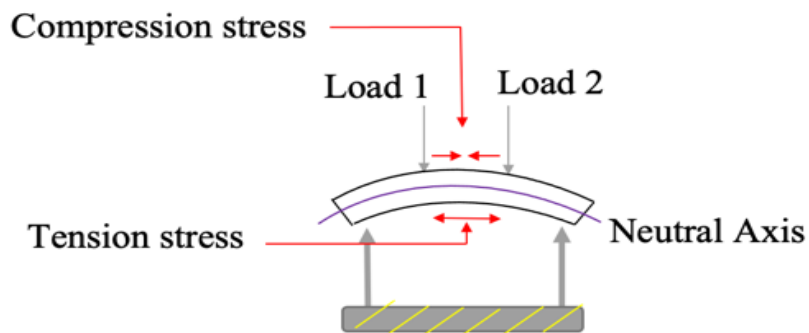


Figure 6. A beam under 4-point bending experiences its fibres under compression (shortening) from the beam's neutral axis to its outer surface where the load is applied, and fibres under tension (lengthening) from the beam's neutral axis to its inner surface.

The earliest study performed quasi-static three-point and four-point bending of eight embalmed parietal calvaria to relate the material properties and structural geometry of the layered calvaria to its flexural response (Hubbard, 1971). Each specimen in their study underwent three-point bending from which a compliance parameter (quotient of mid-span deflection/applied load) as a function of span length was plotted and fitted with a third-order polynomial (Hubbard, 1971).

The bending stiffness was related to the third power of span length and shearing stiffness was related to the first power of the span length (Kelsey et al., 1958). An experimental modulus of elasticity, E , was determined by dividing the bending stiffness by the specimen's cross-sectional second moment of inertia. The average experimental E for the eight specimens was 9.69 GPa (range from 7.79 to 15.31 GPa) (Hubbard, 1971). In this study, specimens were tested in a normal orientation where the load was applied on the outer table surface and an inverted orientation where the load was applied on the inner table (Hubbard, 1971). It was not cited why the unconventional inverted orientation was investigated, however, the fact that a linear fracture occurs due to outbending may be one reason for incorporating this orientation (Gurdjian et al., 1950). Six out of the 8 specimens tested in three-point bending also underwent four-point bending until failure (Hubbard, 1971). Strain gauges were mounted on the inner and outer table surfaces of the calvaria, however, only the tensile strain from the inner table was reported. The average tensile strain at failure was 0.51% (range from 0.33 to 0.76%) (Hubbard, 1971).

Delille et al. performed quasi-static three-point bending (10 mm/min) on over 300 unembalmed calvarium specimens (Delille et al., 2007). Their intent was to discover a resin with similar bending properties to model the human skull in a physical head model (Delille et al., 2007). They reported an average right parietal, left parietal, frontal, and temporal modulus of 5.00, 4.90, 3.80, and 11.30 GPa respectively (Delille et al., 2007). Their parietal modulus was less compared to the 9.69 GPa reported by Hubbard (Hubbard, 1971) and this may be due to the preservation method of the bone (embalmed vs unembalmed), morphology differences between specimens, and rate of loading (Delille et al., 2007). Auperrin and colleagues performed a similar experimental task as Delille et al. (Delille et al., 2007) on three-point bending (10 mm/min) of fresh calvarium specimens (Auperrin et al., 2014). They reported an apparent elastic modulus of 3.81, 5.00, and

9.70 GPa for the frontal, parietal, and temporal bones respectively which is consistent with Delille et al.'s study (Auperrin et al., 2014; Delille et al., 2007). Rahmoun et al. also performed three-point bending tests on calvarium specimens at a maximum displacement of 0.4 mm at a controlled velocity of 10 mm/min (Rahmoun et al., 2014). The average elastic modulus was in line with work by Delille et al. (Delille et al., 2007) and Auperrin et al. (Auperrin et al., 2014) which were 3.28, 4.53, 3.74, 6.00, 5.22, and 2.04 GPa for the frontal, left parietal, right parietal, left temporal, right temporal, and coronal suture respectively (Rahmoun et al., 2014). The average stiffness was 639, 463, 491, 277, 265, and 524 N/mm for the same order of calvarium locations (Rahmoun et al., 2014). Lee and colleagues performed quasi-static three-point (10mm/min) bending of human calvarium specimens with and without the periosteum attached for two embalmed cadaveric skulls (Lee et al., 2019). The skull bone with no periosteum attached had an average bending modulus and strength of 1.70 GPa and 42.00 MPa, respectively, and the other had averages of 2.74 GPa and 53.00 MPa, respectively (Lee et al., 2019). The skull bone with the periosteum attached had an average bending modulus and strength of 2.28 GPa and 68.00 MPa respectively, while another skull bone had 3.96 GPa and 99.00 MPa (Lee et al., 2019). They found that the periosteum had a significant effect on the mechanical properties they sought except for the bending strength of the skull with no periosteum. In addition, they disclosed their mechanical properties including bending modulus were lower than that reported by Auperrin et al. and Rahmoun et al. (Auperrin et al., 2014; Lee et al., 2019; Rahmoun et al., 2014).

Quasi-static loading is beneficial for obtaining a baseline characterization of the mechanical properties of the calvarium. In addition, the inertial effects experienced by the specimen are relatively low and can be ignored during this type of loading. Although, many real-world head injuries arise from dynamic head impacts with strain rates occurring in the range of 1-

10^3s^{-1} (Hosseini Farid et al., 2019; Zhai et al., 2020). To date, there are two reported studies that have characterized the mechanical properties of calvarium specimens under dynamic impact bending experiments (Motherway et al., 2009; Zwirner et al., 2021). Measurements and properties derived from impact testing are relevant to validate surrogates that intend to model skull fractures due to dynamic head impact scenarios. Motherway and colleagues performed three-point impact bending on male and female adult fresh frozen calvarium specimens (Motherway et al., 2009). Strain rates ranged from 21 to 26 s^{-1} , 26 to 30 s^{-1} , and 103 to 109 s^{-1} for the dynamic speeds of 0.5, 1, and 2.5 m/s respectively. The average range of the maximum force, elastic modulus, rupture stress, and energy absorbed until fracture for the 1 m/s impact speeds were 584 to 1035 N, 4.87 to 17.69 GPa, 78.15 to 102.60 MPa, and 76.06 to 193.19 kN m/m^3 respectively (Motherway et al., 2009). The strengths of the calvaria reported by Motherway et al. (82.13 to 126.91 MPa) are slightly greater than those derived from Lee et al.'s quasi-static derived strength values (42 to 99 MPa) which may be due to greater strain rates exhibited by Motherway et al.'s specimens (Lee et al., 2019; Motherway et al., 2009). In addition, the range of elastic moduli from Motherway et al.'s study (4.35 to 18.12 GPa) appears to fall in the range of moduli reported in the literature (1.30 GPa to 11.30 GPa) (Auperrin et al., 2014; Delille et al., 2007; Motherway et al., 2009). Zwirner and colleagues also performed dynamic three-point bending tests at impact velocities of 2.5, 3.0, and 3.5 m/s (Zwirner et al., 2021). At 2.5 m/s their embalmed calvarium specimens (frontal, parietal, occipital, and temporal regions) resisted 716 N of force on average and 1264 N for the 3.5 m/s group (Zwirner et al., 2021). Isolated temporal regions reported 638 N and 1136 N at 2.5 m/s and 3.5 m/s respectively (Zwirner et al., 2021). Across all regions, bending strengths of 98, 119, and 130 MPa were established for impact velocities at 2.5, 3.0, and 3.5 m/s respectively (Zwirner et al., 2021). In addition, they conveyed negative correlations with age (3 weeks to 94 years old) and

positive correlations with calvarium thickness (2 to 8 mm) when plotted against bending strength and force (Zwirner et al., 2021). Moreover, at 2.5 m/s, Zwirner et al.'s average force (716 N) collapsed across all regions and age groups was less than the force values presented in Motherway et al.'s study at the same impact velocity (1161.9 to 1315.9 N) (Motherway et al., 2009; Zwirner et al., 2021). This may be attributed to Zwirner et al.'s sample which mostly contained the temporal region and the mean age (48 years old) of their cadavers was lower compared to Motherway et al.'s study (81 years old) (Motherway et al., 2009; Zwirner et al., 2021).

The mechanical properties documented for calvarium specimens at quasi-static and dynamic bending tests are summarized in Table 1. This table demonstrates how the mechanical properties and measures compare across studies and accounts for the type of calvarium specimens that were tested in each. There remains only one study on the adult calvarium that performed 4-point bending and that study was limited to quasi-static bending (Hubbard, 1971). There also remain only two studies to have performed dynamic impact tests (Motherway et al., 2009; Zwirner et al., 2021), two studies to have documented force at fracture (Motherway et al., 2009; Zwirner et al., 2021), and only one study to document bending moment and strain at fracture (Hubbard, 1971). Therefore, it is evident from this summary (Table 1) that additional bending tests on adult calvarium specimens are required to obtain an appropriate range of mechanical properties and measurements attributed to the calvarium. The calvarium is also a heterogeneous structure that can be characterized by many morphometric properties such as density, porosity, and trabecular or cortical morphometry (Adanty et al., 2021). In addition to obtaining the mechanical properties of the calvarium, it is important to establish which morphometric properties have a significant effect on the mechanical response of the calvarium. This can influence one's approach to designing a surrogate model of the calvarium by tailoring the construction of their model according to relevant

morphometry and geometry associated with mechanical properties. Many studies have performed mechanical testing on pediatric specimens (Coats & Margulies, 2006; Davis et al., 2012; Igo et al., 2021; Kriewall, 1982; Kriewall et al., 1981; Margulies & Thibault, 2000; McPherson & Kriewall, 1980), however, this literature review will exclude the discussion on pediatric studies since the purpose of this thesis was to ultimately construct surrogate prototypes of the adult calvarium.

Table 1. The bending test results on adult calvaria reported in the literature prior to the presentation of this thesis.

Authors	Q=quasi-static Or D=dynamic Impacts	E=embalmed Or UE = unembalmed	M=male or F=female	Age	Loading Rate (LR) & Strain Rate (SR)	Regions sampled	Force (N)	Bending Moment (N.m)	Stress (MPa)	Strain (%)	Modulus (GPa)
Hubbard (1971)	Q, 3-point Q, 4-point	E	-	-	SR: 0.01s ⁻¹	P	-	4-point: 3.08	-	4-point: 0.51	3-point: 9.69
Delille et al. (2007)	Q, 3-point	UE	M, F	70.95	LR: 10 mm/min	F, P, T	-	-	-	-	RP: 5.00 LP: 4.90 F: 3.80 T:11.30
Auperrin et al. (2014)	Q, 3-point	UE	M	74.8	LR: 10 mm/min	F, P, T	-	-	-	-	P: 5.00 F: 3.81 T: 9.70
Rahmoun et al. (2014)	Q, 3-point	N/A	M	88	LR: 10 mm/min	F, P, T coronal suture	-	-	-	-	RP: 3.74 LP: 4.53 F: 3.28 RT: 5.22 LT: 6.00 Coronal Suture: 2.04
Lee et al. (2019)	Q, 3-point	E	M	M=61 F=86	LR: 10 mm/min	F, P, T, O	-	-	Bare bone skull 1 & 2: 42 & 53 Bone with periosteum attached Skull 1 & 2: 68 & 99	-	Bare bone skull 1 & 2: 1.70 & 2.74 Bone with periosteum attached Skull 1 & 2: 2.28 & 3.95
Motherway et al. (2009)	D, 3-point	UE	M, F	81	LR: 0.5, 1, 2.5 m/s SR at 0.5 m/s: 19-22s ⁻¹ SR at 1 m/s: 25-31s ⁻¹ SR at 2.5 m/s: 102-110s ⁻¹	F, P	0.5 m/s at RP, LP and F: 734.6, 721.7, 1062.3 1 m/s at RP, LP and F: 793.6, 584.3, 1035.9 0.5 m/s at RP, LP and F: 1161.9, 1228.6, 1315.9	-	0.5 m/s at RP, LP and F: 84.50, 82.13, 90.80 1 m/s at RP, LP and F: 82.98, 78.15, 102.60 0.5 m/s at RP, LP and F: 123.12, 133.61, 126.91	-	0.5 m/s at RP, LP and F: 10.33, 5.70, 4.35 1 m/s at RP, LP and F: 9.44, 17.69, 4.87 0.5 m/s at RP, LP and F: 12.80, 18.12, 16.34
Zwirner et al. (2021)	D, 3-point	E	M,F	48	LR:2.5, 3.0, 3.5 m/s	F, P, T, O	2.5 m/s: 716 3.5 m/s: 1264 2.5 m/s at T: 638 3.5 m/s at T: 1136	-	2.5 m/s: 98 3.0 m/s: 119 3.5 m/s: 130	-	-

RP: right parietal, LP: left parietal, P: Parietal, RT: right temporal, LT: left temporal, T: temporal, F: frontal, O: occipital

Proposed Physical Surrogate Models of the Calvarium

Cadaveric head models and headform dummies are employed to understand the mechanisms of trauma-related head injuries (i.e., skull fractures) and for testing protective gear (i.e., helmets). However, cadaveric tissue's mechanical properties and geometry are greatly variable across subjects, cadavers are also difficult to obtain, and the selection of cadaveric tissue is susceptible to sampling bias, mainly among older subjects (Yoganandan et al., 1995). Headform dummies are comprised of rigid material that may be necessary to perform a series of multiple impacts, but they typically lack an important biofidelic characteristic which is the frangibility required to investigate skull fractures. Therefore, to lessen the limitations concerning cadaveric head models and headform dummies, physical models of the calvarium to mimic fracture and mechanical response have been documented in the literature. Many of these surrogate models' mechanical response measures have been compared to previous studies that have delivered impacts to the human skull and calvarium specimens subject to bending, compression, and tensile testing.

For the study of the mechanisms related to cranial injuries by gunshots, Thali et al. developed a physical "skin-skull-brain model" (Thali et al., 2002). The purpose of this model was to allow for the reconstruction of characteristics related to gunshot trauma. The artificial skull was modelled as a sphere made of polyurethane material. The skull was also structurally layered with an internal and external table that sandwiched a porous region, however, important details on how this was layered were not provided. The model was also equipped with a periosteum made of latex that enveloped the skull to prevent the scattering of the bone fragments. Their model demonstrated realistic fracture lines and entrance and exit wounds during ballistic loading. Furthermore, a depressed internal table during glancing gunshots also showed bone fragments to lacerate their

surrogate brain tissue. Overall, their qualitative findings were consistent with previous experimental studies on bullet wounds on real skull tissue.

To replace the Hybrid III headform (originally designed for vehicle crash testing) with a more biofidelic headform, Delille and colleagues created a dummy head prototype consisting of a resin-based skullcap (Figure 7) (Delille et al., 2007). The resin they chose was not mentioned, however, they insisted that any chosen resin should have an identical average Young's modulus as they determined for human skull bone in quasi-static 3-point bending. Their skullcap was impacted at 5.56 to 6.00 m/s which was consistent with Nahum et al.'s work on dynamic head impacts delivered to post-mortem human subjects (PMHS) (Nahum et al., 1977). Their head prototype with and without a skin showed a comparable amplitude in the force-time response curve to the Hybrid III headform but the duration of impact was greater for the head prototype (Figure 7). When compared to Nahum et al.'s results in terms of duration (4.40 ms), the head prototype's duration with skin (3.96 ms) was comparable, however, the PMHS's peak force response was greater by about 2 kN (Figure 7).

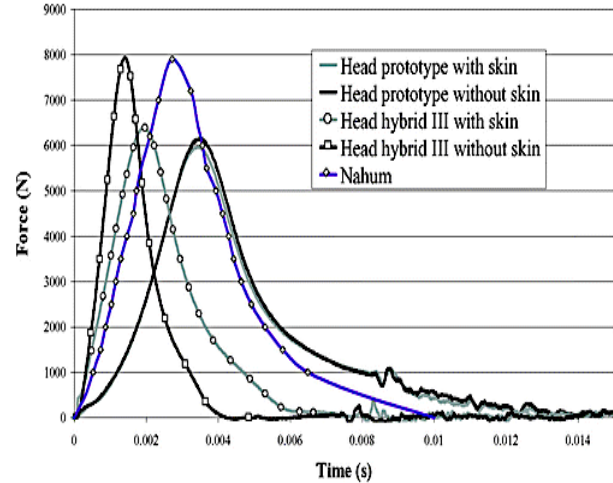
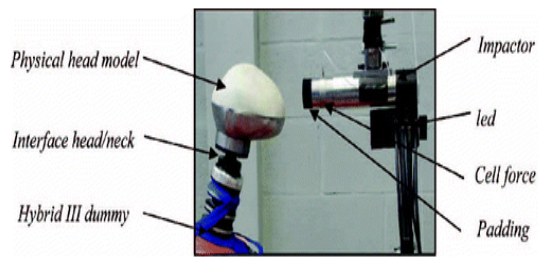


Figure 7. Delille et al.'s physical head model (left image) and force-time response compared to the Hybrid III headform and Nahum et al.'s PMHS study (right image). **Image source:** (Delille et al., 2007) Copyright permissions from Taylor and Francis have been granted. Experimental study of the bone behaviour of the human skull bone for the development of a physical head model, R Delille, D Lesueur, P Potier, P Drazetic, E Markiewicz, International Journal of Crashworthiness, © copyright (2007), reprinted by permission of Informa UK Limited, trading as Taylor & Taylor & Francis Group, <http://www.tandfonline.com>.

In 2013, Roberts et al. developed 3-layered cranial surrogate bones of flat geometry that were tested under quasi-static 3-point bending (Figure 8) (Roberts et al., 2013). Additionally, surrogate cranial tables were assessed in fracture toughness tests and tensile loading. Cranial tables were fabricated from epoxy resins (EPON 815C/EPIKURE 3234 or EPON 862/EPIKURE 3274 provided by Miller-Stephenson Chemical Co.) in which some tables were also mixed with randomly oriented glass fibres. The diplöe was modelled as one of three two-part urethane foams (U.S 16#, modified US 16#, and TC-812). The fracture toughness of the epoxy resin mixed with a percent of glass fibres used to model the cortical tables ($2.5 \text{ KIC MPa}\sqrt{\text{m}}$) was comparable with the average cortical bone of the femur ($3.07 \pm 1.75 \text{ KIC MPa}\sqrt{\text{m}}$). For cortical tables of epoxy plus 35% and 40% milled glass fibre, tensile strengths were 53.8 MPa and 52.43 MPa respectively, which were aligned with cortical bone of the human cranium tested in tensile loading (67.73 MPa) (Wood, 1971). The flat surrogate samples consisted of 2 or 2.2 mm cortical tables and a diplöe thickness of 4 or 3.8 mm which resulted in a total thickness of 8 mm, this total thickness falls in

the greater end of the range for calvarium (3-13 mm) depending on the region (Adanty et al., 2021). Nevertheless, under 3-point loading (Figure 8), the bending strength of cranial surrogates with US Foam 16# was 67.3 MPa and with TC-812 was 68.4 MPa. Roberts et al. concluded these values were aligned with the cranial bending strength of human cranial bone (82 MPa) (Hubbard, 1971). However, this comparison must be assessed with caution since bending strength was not reported by Hubbard (Hubbard, 1971), rather Roberts and colleagues may have manually computed it using geometrical properties reported by Hubbard. The average bending modulus of the surrogate cranial samples (2.98 GPa) was less than human cranial samples (11.73 GPa) reported by Hubbard (Hubbard, 1971). The cranial surrogates were then fabricated into flat panels made of epoxy plus 30% glass for the cranial tables plus either of the three types of urethane foams mentioned earlier to model the diplöe. Each of the flat panels was then subjected to drop tower impacts at an impact velocity of 3-5 m/s. The average force to fracture of the flat panels was 1650 N which was notably less than the range of force to fracture for impacts on intact human skulls reported in the section “The Biomechanics of the Human Skull”.

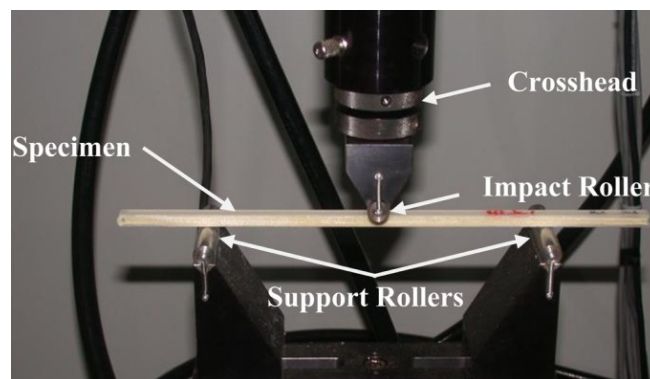


Figure 8. An image of a three-layered surrogate produced by Roberts et al. in a three-point bending test. Image source: (Roberts et al., 2013) This image was sourced from an open-access article, therefore distribution or reproduction provided the original author(s) or licensor are credited are permitted.

Plaisted et al. introduced a photocurable synthetic material of high-loading ceramic particulate reinforcement as a potential material to mimic cranial bone (Plaisted et al., 2015). This

material was produced through stereolithographic (SLA) additive manufacturing. Quasi-static tensile testing was performed on the synthetic material which resulted in strain rates of 10^{-4}s^{-1} to 10^{-2}s^{-1} . At similar strain rates, the tensile strength of their synthetic materials (60.4 to 78.1 MPa) was within one standard deviation of the tensile strength of cranial cortical tables (72.3 ± 14.4 MPa) (Wood, 1971). Furthermore, strain to failure (0.72 % to 0.98 %) and tensile modulus (9.5 GPa to 10.5 GPa) was also within one standard deviation of cranial cortical tables (0.69 ± 0.11 % and 12.8 ± 1.6 GPa).

Ondruschka et al. and Falland-Chueng et al. developed skull simulants using MasterFlow 622 (Degussa, Hanau, Germany), which has been described as a high-strength epoxy resin (Figure 9) (Falland-Cheung et al., 2017; Ondruschka et al., 2019). Ondruschka et al. performed quasi-static 3-point bending (10 mm/min) and reported statistically comparable bending modulus, maximum force, strain at peak force and deflection at peak force between their simulants and cranial tissue. However, their simulant's bending strength was significantly less at 43 MPa compared to their cranial tissue tested under similar conditions (55 MPa without the periosteum attached and 75 MPa with the periosteum attached). Falland-Chueng and colleagues performed 3-point bending at 5 mm/min on simulants made of the same high-strength epoxy resin (Masterflow 622) (Falland-Cheung et al., 2017). Their average bending strengths were 59.84 MPa which is greater than Ondruschka et al.'s simulant (43 MPa) and are closer to the bending stress values of cranial tissue reported in the literature (Table 1) (Lee et al., 2019; Motherway et al., 2009; Zwirner et al., 2021). Noteworthy was that the elastic modulus (6.65 GPa) in Falland-Cheung et al.'s findings was greater than Ondruschka et al.'s modulus (2 - 4 GPa), however, both these values fall in the range of moduli reported for calvaria since there is a considerable variance in the human data reported in the literature (see Table 1). In addition to the high-strength epoxy resin (Masterflow 622),

Falland-Cheung et al. used the following materials as potential surrogate models for the skull: fibre-filled epoxy resin (FFER) (Sawbones, Vashon, Washington, USA), polyethylene terephthalate glycol-modified (PETG), polylactic acid – 3D printing filament (PLA) and a self-cure acrylic denture base resin (Falland-Cheung et al., 2017). FFER exhibited a bending strength and modulus of 209.93 MPa and 17.96 GPa respectively, 41.24 MPa and 1.68 GPa for PETG, 92.76 MPa and 3.03 GPa for PLA and 79.60 MPa and 2.38 GPa for self-cure acrylic. Their study concluded that the high-strength epoxy (Masterflow 622) and the FFER simulants were comparable to the average modulus of the calvarium (8.51 GPa) and therefore, were suitable candidates to simulate the elastic properties of the calvarium. However, for simulating blunt force trauma at dynamic impact rates, the PLA's flexural strength was most suitable since its bending strength was closer to cranial bone tested in dynamic impacts (Motherway et al., 2009; Zwirner et al., 2021).



Figure 9. *A calvarium specimen (top image) and its high-strength epoxy resin (Masterflow 622) model (bottom image). Image source: (Ondruschka et al., 2019) Copyright permissions from Springer Nature has been granted (license number: 5397140998245). Benjamin Ondruschka, Jik Hang Clifford Lee, Mario Scholze, Johann Zwirner, Darryl Tong, John Neil Waddell, Niels Hammer, A biomechanical comparison between human calvarial bone and a skull simulant considering the role of attached periosteum and dura mater, International Journal of Legal Medicine, 133, 1603-1610, 2019, Springer Nature.*

In a recent article, Brown and colleagues studied three commercially available bone surrogates (Synbone, Sawbone and BoneSim) under a quasi-static compression condition and a dynamic compression condition using a Split-Hopkinson Pressure bar system (Brown et al., 2019). Synbone

(Synbone AG, Pacific Research Labs, Inc) is made of a polyurethane-based foam material that contains different levels of porosity through its thickness to emulate the cortical tables and diploë. Sawbone is composed of epoxy mixed with glass fibres to mimic the cortical tables and rigid polyurethane foam to mimic the diploë. BoneSim is composed of a mixture of dry bovine cortical bone and cyanoacrylate adhesive (Figure 10). An extensive number of compressive properties were reported in this study due to the different orientations of loading (transverse and longitudinal) and the densities of surrogate material that were tested. But to summarize, Synbone and BoneSim Y experienced comparable compressive modulus (1.5 GPa) when loaded transversely to values reported in the literature for the human skull (Brown et al., 2019). In addition, BoneSim was generally the favourable candidate material to mimic the compressive young's modulus, yield strength, and ultimate strength of the human skull (Brown et al., 2019).



Figure 10. Three commercially available bone surrogates. A, B, X, Y correspond to different densities used by Brown et al. The red arrows correspond to the two different loading conditions applied, transverse (top arrow) and longitudinal (bottom arrow). **Image source: (Brown et al., 2019) Copyright permissions from Elsevier has been granted (license number: 5395490184561)¹**

¹ Reprinted from Journal of the Mechanical Behaviour of Biomedical Materials, Volume 90, A.D. Brown, J.B. Walters, Y.X. Zhang, M. Saadatfar, J.P. Escobedo-Diaz, P.J. Hazell, The mechanical response of commercially available bone simulates for quasi-static and dynamic loading, 404-416, Copyright (2019), with permission from Elsevier. (Formatted according to Elsevier General Terms Section 3).

Presented in this section were potential surrogate models of the human skull using synthetic material to mimic fracture. These models were designed to either represent the whole geometry of the skull (Delille et al., 2007; Thali et al., 2002) or were fabricated as beams and tensile or compressive samples to determine mechanical properties (Brown et al., 2019; Falland-Cheung et al., 2017; Ondruschka et al., 2019; Plaisted et al., 2015; Roberts et al., 2013). Some of the proposed models fell within the range of mechanical measurements and properties documented for the calvarium, thus, they have the potential to be alternatives to cadaveric skulls or non-frangible skull models within headforms. However, many of the methodologies and materials introduced to fabricate the calvarium models may not be easily accessible or cost-effective approaches to construct a simple calvarium model to mimic fracture. Roberts et al. used EPON (Miller-Stephenson) and glass fibres with the addition of a zirconium coupling agent and an anti-foam surfactant to create their cortical layer (Roberts et al., 2013). The heterogeneous mixture for this thin layer may be relatively complex and time-consuming and most of these materials are not readily available at local retail corporations. Ondruschka et al. and Falland-Cheung et al. employed a high-strength epoxy to fabricate their samples (Falland-Cheung et al., 2017; Ondruschka et al., 2019), but this material is also not readily available at local retail corporations and is typically used in heavy-duty building applications. Additionally, Synbone and Sawbone are primarily employed in applications for surgical training and bone anatomy demonstrations, but these products have no biomechanical parallels to calvarium (Brown et al., 2019). Sawbone has a line of composite bones which are said to mimic the properties of human bones, but their product list does not contain a calvarium. BoneSim by BoneSim Laboratories showed comparable compressive properties to the human skull (Brown et al., 2019), but it is also inaccessible for local retail purchase and has not been tested under bending conditions – a mechanism most associated with a skull fracture

(Gurdjian et al., 1950). Plaisted et al. utilized additive manufacturing technology to fabricate a potential ceramic-based model (Plaisted et al., 2015), however, the availability of additive manufacturing technology is limited and may be an expensive piece of equipment for those who have budget constraints.

Prior to this dissertation, no study had employed cost-effective methods and materials that were readily available from local retail corporations to develop a simple model of the calvarium to mimic mechanical response at fracture. A model by these means can be implemented in present headforms to test protective devices against a skull fracture and head injuries. Therefore, this dissertation initiated a step-by-step program towards the fabrication of surrogate models of the calvarium to mimic mechanical response at fracture using cost-effective materials and methods.

REFERENCES

- Adanty, K., Rabey, K. N., Doschak, M. R., Bhagavathula, K. B., Hogan, J. D., Romanyk, D. L., Adeeb, S., Ouellet, S., Plaisted, T. A., Satapathy, S. S., & Dennison, C. R. (2021). Cortical and trabecular morphometric properties of the human calvarium. *Bone*, *148*, 115931. <https://doi.org/10.1016/j.bone.2021.115931>
- Allsop, D. “L,” Perl, T. R., & Warner, C. Y. (1991). Force/Deflection and Fracture Characteristics of the Temporo-parietal Region of the Human Head. *SAE Transactions*, *100*, 2009–2018.
- Allsop, D. “L,” Warner, C. Y., Wille, M. G., Schneider, D. C., & Nahum, A. M. (1988). Facial Impact Response—A Comparison of the Hybrid III Dummy and Human Cadaver. *SAE Transactions*, *97*, 1224–1240.
- Auperrin, A., Delille, R., Lesueur, D., Bruyère, K., Masson, C., & Drazétic, P. (2014). Geometrical and material parameters to assess the macroscopic mechanical behaviour of fresh cranial bone samples. *Journal of Biomechanics*, *47*(5), 1180–1185. <https://doi.org/10.1016/j.jbiomech.2013.10.060>
- Boruah, S., Henderson, K., Subit, D., Salzar, R. S., Shender, B. S., & Paskoff, G. (2013). *Response of Human Skull Bone to Dynamic Compressive Loading*. 12.
- Brown, A. D., Walters, J. B., Zhang, Y. X., Saadatfar, M., Escobedo-Diaz, J. P., & Hazell, P. J. (2019). The mechanical response of commercially available bone simulants for quasi-static and dynamic loading. *Journal of the Mechanical Behavior of Biomedical Materials*, *90*, 404–416. <https://doi.org/10.1016/j.jmbbm.2018.10.032>
- Bruns, V. (n.d.). *Handbuch der praktischen Chirurgie für Aerzte und Wund~irzte* (Vol. 1). Tiibingen: H. Laupp,.
- Coats, B., & Margulies, S. S. (2006). Material properties of human infant skull and suture at high rates. *Journal of Neurotrauma*, *23*(8), 1222–1232. <https://doi.org/10.1089/neu.2006.23.1222>
- Davis, M. T., Loyd, A. M., Shen, H. H., Mulroy, M. H., Nightingale, R. W., Myers, B. S., & Bass, C. D. (2012). The mechanical and morphological properties of 6 year-old cranial bone. *Journal of Biomechanics*, *45*(15), 2493–2498. <https://doi.org/10.1016/j.jbiomech.2012.07.001>
- Delille, R., Lesueur, D., Potier, P., Drazetic, P., & Markiewicz, E. (2007). Experimental study of the bone behaviour of the human skull bone for the development of a physical head model. *International Journal of Crashworthiness*, *12*(2), 101–108. <https://doi.org/10.1080/13588260701433081>
- Evans, F. G., & Lissner, H. R. (1957). Tensile and compressive strength of human parietal bone. *Journal of Applied Physiology*, *10*(3), 493–497. Scopus. <https://doi.org/10.1152/jappl.1957.10.3.493>
- Falland-Cheung, L., Waddell, J. N., Chun Li, K., Tong, D., & Brunton, P. (2017). Investigation of the elastic modulus, tensile and flexural strength of five skull simulant materials for impact testing of a forensic skin/skull/brain model. *Journal of the Mechanical Behavior of Biomedical Materials*, *68*, 303–307. <https://doi.org/10.1016/j.jmbbm.2017.02.023>

- Félizet, G. (1873). *Recherches anatomiques et expérimentales sur les fractures du crâne* (Vol. 1). A. Delahaye (Paris).
- Feng, X. (2009). Chemical and Biochemical Basis of Cell-Bone Matrix Interaction in Health and Disease. *Current Chemical Biology*, 3(2), 189–196. <https://doi.org/10.2174/187231309788166398>
- Gosling, J., Harris, P., Humpherson, J., Whitmore, I., & Willian, P. (2017). *Human Anatomy, Color Atlas and Textbook* (6th ed.). Elsevier. <https://www.elsevier.ca/ca/product.jsp?isbn=9780723438274>
- Gurdjian, E. S. (1975). Re-evaluation of the biomechanics of blunt impact injury of the head. *Surgery, Gynecology & Obstetrics*, 140(6), 845–850.
- Gurdjian, E. S., Hodgson, V. R., Hardy, W. G., Patrick, L. M., & Lissner, H. R. (1964). EVALUATION OF THE PROTECTIVE CHARACTERISTICS OF HELMETS IN SPORTS. *Journal of Trauma and Acute Care Surgery*, 4(3), 309–324.
- Gurdjian, E. S., & Lissner, H. R. (1947a). Deformations of the skull in head injury as studied by the “stresscoat” technic. *The American Journal of Surgery*, 73(2), 269–281. [https://doi.org/10.1016/0002-9610\(47\)90321-8](https://doi.org/10.1016/0002-9610(47)90321-8)
- Gurdjian, E. S., & Lissner, H. R. (1947b). Deformations of the skull in head injury as studied by the “stresscoat” technic. *The American Journal of Surgery*, 73(2), 269–281. [https://doi.org/10.1016/0002-9610\(47\)90321-8](https://doi.org/10.1016/0002-9610(47)90321-8)
- Gurdjian, E. S., Lissner, H. R., Latimer, F. R., Haddad, B. F., & Webster, J. E. (1953). Quantitative determination of acceleration and intracranial pressure in experimental head injury; preliminary report. *Neurology*, 3(6), 417–423. <https://doi.org/10.1212/wnl.3.6.417>
- Gurdjian, E. S., Lissner, H. R., & Webster, J. E. (1947). The mechanism of production of linear skull fracture; further studies on deformation of the skull by the stresscoat technique. *Surgery, Gynecology & Obstetrics*, 85(2), 195–210.
- Gurdjian, E. S., Roberts, V. L., & Thomas, L. M. (1966). Tolerance curves of acceleration and intracranial pressure and protective index in experimental head injury. *The Journal of Trauma*, 6(5), 600–604. <https://doi.org/10.1097/00005373-196609000-00005>
- Gurdjian, E. S., Webster, J. E., & Lissner, H. R. (1950). The Mechanism of Skull Fracture. *Journal of Neurosurgery*, 7(2), 106–114. <https://doi.org/10.3171/jns.1950.7.2.0106>
- Gurdjian, E. S., Webster, J. E., & Lissner, H. R. (1955). Observations on the mechanism of brain concussion, contusion, and laceration. *Surgery, Gynecology & Obstetrics*, 101(6), 680–690.
- Hodgson, V. R., & Thomas, L. M. (1972). *BREAKING STRENGTH OF THE HUMAN SKULL VS. IMPACT SURFACE CURVATURE* (Final Rept). Article Final Rept. <https://trid.trb.org/view/112380>
- Hombach-Klonisch, S., Klonisch, T., & Peeler, J. (2019). *Sobotta clinical atlas of human anatomy* (1st edition.). <https://www.clinicalkey.com/dura/browse/bookChapter/3-s2.0-C20150000260>
- Hosseini Farid, M., Eslaminejad, A., Ramzanpour, M., Ziejewski, M., & Karami, G. (2019, January 15). *The Strain Rates of the Brain and Skull Under Dynamic Loading*. ASME 2018

International Mechanical Engineering Congress and Exposition.
<https://doi.org/10.1115/IMECE2018-88300>

Hubbard, R. P. (1971). Flexure of layered cranial bone. *Journal of Biomechanics*, 4(4), 251–263.
[https://doi.org/10.1016/0021-9290\(71\)90031-5](https://doi.org/10.1016/0021-9290(71)90031-5)

Igo, B. J., Cottler, P. S., Black, J. S., & Panzer, M. B. (2021). The mechanical and microstructural properties of the pediatric skull. *Journal of the Mechanical Behavior of Biomedical Materials*, 120, 104578. <https://doi.org/10.1016/j.jmbbm.2021.104578>

Ji, S., Ghajari, M., Mao, H., Kraft, R. H., Hajiaghamemar, M., Panzer, M. B., Willinger, R., Gilchrist, M. D., Kleiven, S., & Stitzel, J. D. (2022). Use of Brain Biomechanical Models for Monitoring Impact Exposure in Contact Sports. *Annals of Biomedical Engineering*. <https://doi.org/10.1007/s10439-022-02999-w>

Kelsey, S., Gellatly, R. A., & Clark, B. W. (1958). The Shear Modulus of Foil Honeycomb Cores. *Aircraft Engineering and Aerospace Technology*, 30(10), 294–302.
<https://doi.org/10.1108/eb033026>

Kriewall, T. J. (1982). Structural, mechanical, and material properties of fetal cranial bone. *American Journal of Obstetrics & Gynecology*, 143(6), 707–714. [https://doi.org/10.1016/0002-9378\(82\)90119-3](https://doi.org/10.1016/0002-9378(82)90119-3)

Kriewall, T. J., McPherson, G. K., & Tsai, A. Ch. (1981). Bending properties and ash content of fetal cranial bone. *Journal of Biomechanics*, 14(2), 73–79. [https://doi.org/10.1016/0021-9290\(81\)90166-4](https://doi.org/10.1016/0021-9290(81)90166-4)

Lee, J. H. C., Ondruschka, B., Falland-Cheung, L., Scholze, M., Hammer, N., Tong, D. C., & Waddell, J. N. (2019). An Investigation on the Correlation between the Mechanical Properties of Human Skull Bone, Its Geometry, Microarchitectural Properties, and Water Content. *Journal of Healthcare Engineering*, 2019, 1–8. <https://doi.org/10.1155/2019/6515797>

Margulies, S. S., & Thibault, K. L. (2000). Infant Skull and Suture Properties: Measurements and Implications for Mechanisms of Pediatric Brain Injury. *Journal of Biomechanical Engineering*, 122(4), 364–371. <https://doi.org/10.1115/1.1287160>

McElhaney, J. H., Fogle, J. L., Melvin, J. W., Haynes, R. R., Roberts, V. L., & Alem, N. M. (1970). Mechanical properties of cranial bone. *Journal of Biomechanics*, 3(5), 495–511.
[https://doi.org/10.1016/0021-9290\(70\)90059-X](https://doi.org/10.1016/0021-9290(70)90059-X)

McIntosh, A. S., Kallieris, D., Mattern, R., & Miltner, E. (1993). *Head and Neck Injury Resulting from Low Velocity Direct Impact* (SAE Technical Paper No. 933112). SAE International.
<https://doi.org/10.4271/933112>

McPherson, G. K., & Kriewall, T. J. (1980). The elastic modulus of fetal cranial bone: A first step towards an understanding of the biomechanics of fetal head molding. *Journal of Biomechanics*, 13(1), 9–16. [https://doi.org/10.1016/0021-9290\(80\)90003-2](https://doi.org/10.1016/0021-9290(80)90003-2)

Melvin, J. W., Fuller, P. M., Daniel, R. P., & Pavliscak, G. M. (1969). Human Head and Knee Tolerance to Localized Impacts. *SAE Transactions*, 78, 1772–1782.

- Messerer, O. (1880). *Über Elasticität und Festigkeit der Menschlichen Knochen*. Stuttgart, Germany.
- Motherway, J. A., Verschueren, P., Van der Perre, G., Vander Sloten, J., & Gilchrist, M. D. (2009). The mechanical properties of cranial bone: The effect of loading rate and cranial sampling position. *Journal of Biomechanics*, 42(13), 2129–2135. <https://doi.org/10.1016/j.jbiomech.2009.05.030>
- Nahum, A. M., Gatts, J. D., Gadd, C. W., & Danforth, J. (1968). *Impact Tolerance of the Skull and Face* (SAE Technical Paper No. 680785). SAE International. <https://doi.org/10.4271/680785>
- Nahum, A. M., Smith, R., & Ward, C. C. (1977). *Intracranial Pressure Dynamics During Head Impact* (SAE Technical Paper No. 770922). SAE International. <https://doi.org/10.4271/770922>
- Ondruschka, B., Lee, J. H. C., Scholze, M., Zwirner, J., Tong, D., Waddell, J. N., & Hammer, N. (2019). A biomechanical comparison between human calvarial bone and a skull simulant considering the role of attached periosteum and dura mater. *International Journal of Legal Medicine*, 133(5), 1603–1610. Scopus. <https://doi.org/10.1007/s00414-019-02102-4>
- Ono, K., Kikuchi, A., Kobayashi, H., & Nakamura, N. (1985). Human head tolerances to sagittal and lateral impacts—Estimation deduced from experimental dead injury using subhuman primates and human cadaver skulls. In *Head injury prevention past and present research*.
- Plaisted, T. A., Gardner, J. M., & Gair, J. L. (2015). *Characterization of a Composite Material to Mimic Human Cranial Bone*. 12.
- Pritchard, J. J., Scott, J. H., & Girgis, F. G. (1956). The structure and development of cranial and facial sutures. *Journal of Anatomy*, 90(Pt 1), 73-86.3.
- Rahmoun, J., Auperrin, A., Delille, R., Naceur, H., & Drazetic, P. (2014). Characterization and micromechanical modeling of the human cranial bone elastic properties. *Mechanics Research Communications*, 60, 7–14. <https://doi.org/10.1016/j.mechrescom.2014.04.001>
- Robbins, D. H., & Wood, J. L. (1969). Determination of mechanical properties of the bones of the skull. *Experimental Mechanics*, 9(5). <https://wblldb.lievers.net/10207541.html>
- Roberts, J. C., Merkle, A. C., Carneal, C. M., Voo, L. M., Johannes, M. S., Paulson, J. M., Tankard, S., & Uy, O. M. (2013). Development of a Human Cranial Bone Surrogate for Impact Studies. *Frontiers in Bioengineering and Biotechnology*, 1. <https://doi.org/10.3389/fbioe.2013.00013>
- Schneider, D. C., & Nahum, A. M. (1972). *Impact Studies of Facial Bones and Skull* (SAE Technical Paper No. 720965). SAE International. <https://doi.org/10.4271/720965>
- Thali, M. J., Kneubuehl, B. P., Zollinger, U., & Dirnhofer, R. (2002). The “Skin–skull–brain model”: A new instrument for the study of gunshot effects. *Forensic Science International*, 125(2), 178–189. [https://doi.org/10.1016/S0379-0738\(01\)00637-5](https://doi.org/10.1016/S0379-0738(01)00637-5)
- Ueng, C. E. S. (2003). Sandwich Composites. In R. A. Meyers (Ed.), *Encyclopedia of Physical Science and Technology (Third Edition)* (pp. 407–412). Academic Press. <https://doi.org/10.1016/B0-12-227410-5/00672-4>
- Van Lierde, C., Depreitere, B., Vander Sloten, J., Van Audekercke, R., Van Der Perre, G., & Goffin, J. (2003). Skull Biomechanics: The Energy Absorbability of the Human Skull Frontal

Bone during Fracture under Quasi-Static Loading. *Journal of Applied Biomaterials and Biomechanics*, 1(3), 194–199. <https://doi.org/10.1177/228080000300100306>

Wood, J. L. (1971). Dynamic response of human cranial bone. *Journal of Biomechanics*, 4(1), 1–12. [https://doi.org/10.1016/0021-9290\(71\)90010-8](https://doi.org/10.1016/0021-9290(71)90010-8)

Yoganandan, N., Pintar, F. A., Sances, A., Walsh, P. R., Ewing, C. L., Thomas, D. J., & Snyder, R. G. (1995). Biomechanics of skull fracture. *Journal of Neurotrauma*, 12(4), 659–668. <https://doi.org/10.1089/neu.1995.12.659>

Yoganandan, N., Sances, A., Pintar, F. A., Walsh, P. R., Ewing, C. L., Thomas, D. J., Snyder, R. G., Reinartz, J., & Droese, K. (1994). Biomechanical Tolerance of the Cranium. *SAE Transactions*, 103, 184–189.

Zhai, X., Nauman, E. A., Moryl, D., Lycke, R., & Chen, W. W. (2020). The effects of loading-direction and strain-rate on the mechanical behaviors of human frontal skull bone. *Journal of the Mechanical Behavior of Biomedical Materials*, 103, 103597. <https://doi.org/10.1016/j.jmbbm.2019.103597>

Zwirner, J., Ondruschka, B., Scholze, M., Workman, J., Thambyah, A., & Hammer, N. (2021). The dynamic impact behavior of the human neurocranium. *Scientific Reports*, 11(1), 11331. <https://doi.org/10.1038/s41598-021-90322-3>

PART III

Chapter 1: The Morphometry and Geometry of The Human Calvarium.

Chapter 1 characterized the morphometric and geometric properties of the human calvarium. The results of this chapter, specifically the geometrical properties, were relevant because they were used to guide the physical construction of the surrogate prototypes discussed in Chapter 4. Developing a surrogate model of the calvarium based on first-hand knowledge of the morphometry and geometry of real human calvarium is critical to replicating its response to loading. In this chapter, the length, thickness, and width were the geometrical properties characterized for the beam-shaped calvarium specimens. The morphometric properties, which are the microarchitectural structures of the calvaria, were characterized in this chapter using micro-computed tomography (CT) 3-D imaging analysis. This included density, trabecular thickness, and trabecular separation to name a few. The results of this chapter are valuable to both physical and computational modellers of the human skull who wish to construct a model of the human calvarium for head injury research or other relevant fields. The results of Chapter 1 fulfill *sub-objective 1: Determine the morphometry and geometry of the human calvarium.*

Chapter 1 is a peer-reviewed journal article that was published in *Bone*. The journal author rights are as follows in accordance with Elsevier, “Please note that, as the author of this Elsevier article, you retain the right to include it in a thesis or dissertation, provided it is not published commercially. Permission is not required, but please ensure that you reference the journal as the original source. For more information on this and on your other retained rights, please visit: <https://www.elsevier.com/about/our-business/policies/copyright#Author-rights>”. Chapter 1’s text and content match exactly with the article published in *Bone* with no modifications.

Reference:

Adanty, K., Rabey, K.N., Doschak, M.R., Bhagavathula, K.B., Romanyk, D., Adeeb, S., Hogan, J.D., Ouellet, S., Plaisted, T.A., Satapathy, S.S., Dennison, C.R. (2021). Cortical And Trabecular Morphometric Properties Of The Human Calvarium. *Bone*. 148 115931 DOI: 10.1016/j.bone.2021.115931.

Cortical and Trabecular Morphometric Properties of The Human Calvarium

ABSTRACT

There is currently a gap in the literature that quantitatively describes the complex bone microarchitecture within the diploë (trabecular bone) and cortical layers of the human calvarium. The purpose of this study was to determine the morphometric properties of the diploë and cortical tables of the human calvarium in which key interacting factors of sex, location on the calvarium, and layers of the sandwich structure were considered. Micro-computed tomography (micro-CT) was utilized to capture images at 18 μm resolution of male (n=26) and female (n=24) embalmed calvarium specimens in the frontal and parietal regions (N=50). All images were post-processed and analyzed using vendor bundled CT-Analyzer software to determine the morphometric properties of the diploë and cortical layers. A two-way mixed (repeated measures) analysis of variance (ANOVA) was used to determine diploë morphometric properties accounting for factors of sex and location. A three-way mixed ANOVA was performed to determine cortical morphometric properties accounting for factors of cortical layer (inner and outer table), sex, and location. The study revealed no two-way interaction effects between sex and location on the diploë morphometry except for fractal dimension. Trabecular thickness and separation in the diploë were significantly greater in the male specimens; however, females showed a greater number of trabeculae and fractal dimension on average. Parietal specimens revealed a greater porosity, trabecular separation, and deviation from an ideal plate structure, but a lesser number of trabeculae and connectivity compared to the frontal location. Additionally, the study observed a lower density and greater porosity in the inner cortical layer than the outer which may be due to clear distinctions between each layer's physiological environment. The study provides valuable insight into the quantitative morphometry of the calvarium in which finite element modellers of the skull can refer to when designing detailed heterogenous or subject-specific skull models to effectively predict

injury. Furthermore, this study contributes towards the recent developments on physical surrogate models of the skull which require approximate measures of calvarium bone architecture in order to effectively fabricate a model and then accurately simulate a traumatic head impact event.

Keywords: human calvarium, bone morphometry, diploë, cortical table, micro-computed tomography (micro-CT)

1. INTRODUCTION

The human calvarium, which is also referred to as the neurocranium, encases the brain to protect it against external forces. The calvarium is comprised of a unique three-layer sandwich structure that consists of a porous trabecular bone layer referred to as the diploë, compressed between two cortical bone layers, the outer and inner cortical tables. Recent efforts have been made to quantify the morphological and geometrical characteristics for each layer in the sandwich structure (Alexander et al., 2019; Boruah et al., 2015; Lee et al., 2019; Lillie et al., 2015; McElhaney et al., 1970; Motherway et al., 2009; Peterson and Dechow, 2002). However, the morphological properties of the calvarium conveyed in the literature frequently include density and porosity measurements only, which do not thoroughly entail the complex microarchitecture that defines the diploë (e.g. trabecular thickness, fractal dimension, and trabecular bone pattern factor). Moreover, limited studies have accounted for interacting characteristics such as sex and location on the calvarium which may have a substantial influence on morphometric measurements or conceivably the mechanical responses during a skull fracture (Lillie et al., 2015; Motherway et al., 2009; Peterson and Dechow, 2002). A comprehensive study on the morphometry of the calvarium along with interaction effects such as sex, location on calvarium, and each layer of the sandwich structure would be paramount towards the geometrical design of finite element (FE) (Boruah et al., 2015; De Kegel et al., 2019) and physical surrogate (fracture) models of the skull (Brown et al., 2019; Falland-Cheung et al., 2017; Roberts et al., 2013). With available geometric and morphometric properties of the skull, modelers would be able to model the architecture of the skull, and when coupled with approximate mechanical properties, can confidently predict injury or non-traumatic related events during simulation or experimental analysis (Adanty et al., 2020; Boruah et al., 2015; De Kegel et al., 2019).

Properties of the human calvarium such as density, layer thickness, and porosity profiles through the calvarium thickness have been well quantified in the literature (Alexander et al., 2019; Boruah et al., 2015; Lillie et al., 2015; McElhaney et al., 1970; Peterson and Dechow, 2002). Morphology of the diploë has been of particular emphasis due to its heterogeneous composition and degree of trabecular connectivity. Consequently, the consideration of morphometric properties beyond the density and porosity of the diploë has been marginally reported (Adanty et al., 2020; Lee et al., 2019). From micro-computed tomography (micro-CT) scans on male calvarium samples, Boruah and colleagues computed diploë bone volume fraction, a direct counterpart measure of porosity, and reported a median bone volume fraction of 0.47 (95% CI 0.18-0.90) equating to a median porosity of 53% (Boruah et al., 2015). Likewise, Alexander et al. examined the thickness porosity profiles of higher-resolution micro-CT scans at a range of 5.3 μ m to 6.7 μ m (Alexander et al., 2019). Their study reported average (standard deviation) porosities of 7.2 (3.3) %, 16.1 (5.0) %, and 58.0 (8.3) % for the outer table, inner table and diploë, respectively. Calvarium density has generally been calculated using the Archimedes principle or by various forms of destructive methods resulting in a percentage ash density (Auperrin et al., 2014; McElhaney et al., 1970; Peterson and Dechow, 2002). Few studies have utilized non-destructive methods such as CT-imaging techniques to quantify calvarium bone mineral density (BMD) or tissue mineral density (TMD) (Boruah et al., 2013). Aupperin et al reported a range of apparent densities between 1.684 g/cm³ to 1.782 g/cm³ for the frontal, parietal, and temporal bones (Auperrin et al., 2014). Peterson and Dechow established a significant difference between inner (1.813 g/cm³) and outer (1.869 g/cm³) table apparent densities for male and female subjects (Peterson and Dechow, 2002). Imperative morphometric parameters of diploë trabeculae such as trabecular thickness (Tb.Th), trabecular separation (Tb.Sp), and trabecular number (Tb.N) have

not been considered for the calvarium. Obtaining a sense of these parameters and how they can potentially alter with sex, location, and layers may unravel novel characteristics on the composite nature of the calvarium and thus provide a valuable dataset for skull modelling purposes and proxy measures for bone strength in clinical diagnosis (Chen et al., 2018; Wu et al., 2015).

Three-dimensional (3D) imaging, such as micro-CT, can distinguish soft from hard tissue and compute complex 3D morphological indices of bone (Bouxsein et al., 2010). Given the innovative capabilities of 3D imaging, key morphometric parameters can be resolved to describe the full structure of trabeculae. Tb.Th is defined as the average thickness of trabeculae; Tb.Sp is defined as the average separated distance between trabeculae; and Tb.N is the average number of trabecular bone per unit length (Bouxsein et al., 2010). These parameters fundamentally characterize trabecular bone and have been well quantified in load-bearing parts of the human body such as the vertebral spine, femur, and mandible (Chen et al., 2013; Gong et al., 2005; Greenwood et al., 2015; Zebaze et al., 2010). Load-bearing parts may frequently endure mechanical demands from physical activity, the shifting of body weight, and chewing; therefore, their mechanical strength may have an association with their trabecular morphometry (Chen et al., 2013; Gong et al., 2005; Greenwood et al., 2015; Zebaze et al., 2010). Indeed, the calvarium does not bear load or experience mechanical demands to the same degree as the vertebral bones, femur, and mandible. Though the biomechanical response of an injury such as a skull fracture may be immensely dependent on structural properties of the diploë, therefore, Tb.Th, Tb.Sp, and Tb.N must be quantified for the diploë (Adanty et al., 2020; De Kegel et al., 2019; McElhaney et al., 1970; Motherway et al., 2009).

The purpose of this study was to determine the morphometric properties for the male and female calvarium, as well as report on the potential interaction effects between sex, location

(frontal and parietal), and the layers of the sandwich structure. These may be essential geometrical factors to consider as generic FE models progress away from a simplified design of the skull geometry based on Visible Human Database (U.S National Library of Medicine, 2000), and surrogate skull models work towards structural and mechanical validity for experimental skull fracture assessment (De Kegel et al., 2019). FE head injury models, particularly subject-specific models, require knowledge on the morphometric properties of the calvarium at different levels of sex, age, and location to accurately model, predict, and assess a skull fracture or a traumatic head impact (De Kegel et al., 2019). In addition to density and porosity measurements, physical surrogate fracture models of the human skull would also benefit from detailed morphometric properties of the diploë such as Tb.Th, Tb.Sp, and Tb.N in order to fabricate a model that is geometrically comparable to a real human calvarium (Brown et al., 2019; Falland-Cheung et al., 2017; Roberts et al., 2013).

The null hypotheses for this study were: 1) no significant interaction effects between sex and location on the diploë morphometric properties, 2) no significant interaction effects between the cortical layers, sex, and location on the cortical morphometric properties, and 3) no significant main effects or simple main effects, in other words, no significant differences in diploë morphometric properties between male and female and between frontal and parietal locations. Given there are known morphological differences between sexes for other anatomical regions such as the spine, pelvis, and overall skull shape (Keen, 1950; Nieves et al., 2005), differences in morphometry of the calvarium between sexes were anticipated. Lastly, this study hypothesized significant differences in cortical morphometry between the outer and inner cortical tables since previous findings observed differences in density and porosity between the two cortical layers (Alexander et al., 2019; Peterson and Dechow, 2002).

2. MATERIAL AND METHODS

All of the methods and protocols attributed to this work were approved by the University of Alberta Research Ethics Board (ID: Pro00089218). All specimens came from individuals from the University of Alberta Anatomical Gift Program.

2.1 Specimen Extraction

Frontal and parietal calvarium specimens were extracted from 13 male and 12 female embalmed (formalin fixed) cadavers using a Mopec autopsy saw. This resulted in a total sample size of n=50 calvarium specimens (Figure 1). All cadavers are stored at the University of Alberta in unbuffered aqueous formaldehyde 37% embalming fluid, which is composed of 4% phenol, 4% formulin (37% concentration), 8% glycol, 8% ethyl alcohol (95% concentration), and 76% water. To extract the frontal specimens, we located the center of the coronal suture on each calvarium and measured a point approximately 1.5 cm inferior to the suture. At that point we used a rectangular template model (55 mm in length and 8 mm in width) to outline a rectangular boundary that was used as a guide to cut and extract the frontal specimen as displayed in Figure 1. Similarly, we located the center of the squamosal suture and measured a point approximately 1.5 cm superior to that suture. At that point we used the rectangular template model to outline the region that was used as a guide to cut and extract the parietal specimens as displayed in Figure 1.

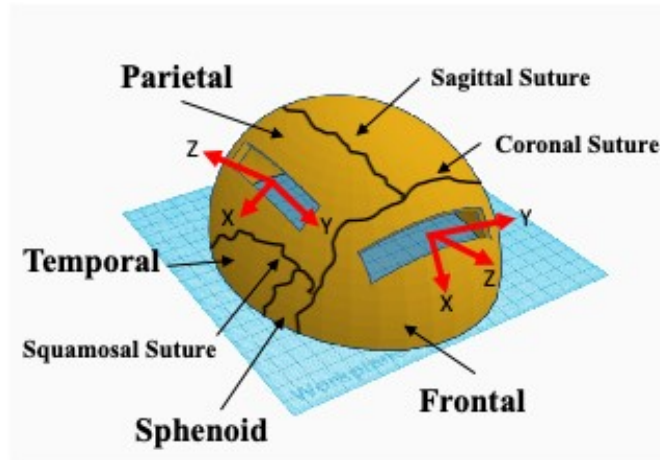


Figure 1. Schematic representation of a calvarium showing the frontal and parietal locations where specimens were extracted from each cadaver.

Furthermore, a selected number of specimens out of the 50 were additionally cut using a Buehler Isomet 4000-equipped with a water-based coolant (Cool 3) to ensure all specimens had approximately equal dimensions of length and width. Thickness varied across the specimens as expected. Figure 2 presents example images of the frontal and parietal calvarium for one male and one female subject. A summary of the subjects' average age and specimen dimensions for each sex are presented in Table 1. All subjects were examined for pre-existing bone pathology to ensure no pathological factors had influenced the subsequent morphometry results.



Figure 2. Example images of a male frontal (a.), male parietal (b.), female frontal (c.), and female parietal (d) calvarium specimen. *L*, *W* (into the page) and *T* correspond to the location of where length, width, and thickness dimensions were measured respectively at the center of each specimen using digital calipers.

Table 1. The average age and dimensions of the calvarium specimens.

Averages	Male subjects (n=13)	Female subjects (n=12)	All subjects (n=25)
Age	83.6 ± 8.9 years old	88.0 ± 9.0 years old	85.7 ± 9.0 years old
Frontal length	50.61 ± 2.63 mm	51.46 ± 1.83 mm	51.02 ± 2.28 mm
Parietal length	55.91 ± 2.31 mm	54.91 ± 2.47 mm	55.43 ± 2.39 mm
Frontal width	8.58 ± 0.43 mm	8.97 ± 1.57 mm	8.77 ± 1.17 mm
Parietal width	8.55 ± 0.40 mm	8.54 ± 0.57 mm	8.55 ± 0.49 mm
Frontal thickness	6.97 ± 1.54 mm	7.58 ± 1.94 mm	7.26 ± 1.78 mm
Parietal thickness	6.00 ± 1.49 mm	7.00 ± 1.24 mm	6.49 ± 1.46 mm

2.2 Micro-CT Scanning of Specimens

2.2.1 Image Acquisition

Prior to micro-CT imaging, all specimens were stored in immersed aqueous embalming fluid at room temperature. At the time of scanning, fully hydrated specimens were removed and positioned on pre-cut foam supports within 50 ml centrifugal tubes to inhibit movement (Figure 3a), and the local humid environment sealed with the air-tight screw cap to avoid specimen dehydration during the scanning process.

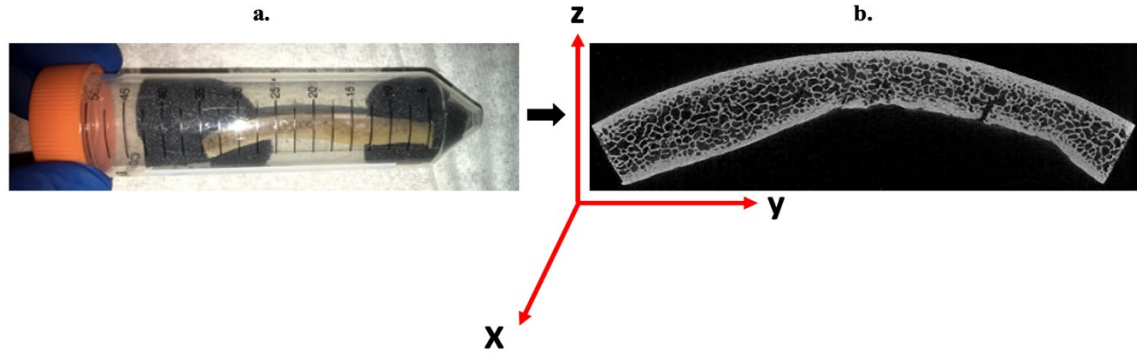


Figure 3. Example of a specimen stabilized in a centrifugal tube (a.) and the resulting reconstructed and filtered micro- CT image of the specimen (b.).

The tubes were then loaded into the micro-CT scanner (Bruker-Skyscan 1176) with each specimen scanned at a resolution (isotropic voxel size) of 18 μm . All micro-CT images were acquired at the following scanning parameters: 90 kV X-ray tube voltage (peak), 278 μA X-ray current, 1mm Al filter to remove low energy photons, 300 ms integration time, frame average of $n=3$, and 0.7° angular rotation step. Each specimen length required 4 multi-part field of view scans, through 180 degrees of rotation, that were subsequently joined using the post-alignment pre-processing software feature NRecon (version 1.6.3.3).

Following the scanning of the calvarium specimens, two vendor-sourced cylindrical calibration phantoms, each 4 mm in diameter and composed of known concentrations of calcium hydroxyapatite (HA) in epoxy resin were scanned under identical scanning parameters and resolution as the calvarium specimens (Phantom 1 BMD: 0.250 g HA/cm^3 and Phantom 2 BMD: 0.750 g HA/cm^3). A linear relationship for BMD as a function of micro-CT attenuation coefficients (AC) for the phantoms voxels was established resulting in equation 1. A negative and positive BMD corresponds to a non-bone voxel and a bone voxel, respectively.

$$BMD (\text{g HA/cm}^3) = 67.1939 (AC) - 0.3493 \quad (1)$$

2.2.2 Post-scanning Image Processing

Two-dimensional shadow projections in TIFF file formats (8-bit) were the product from each micro-CT scanned specimen. The shadow projections were then reconstructed into 3D voxel slices (BMP file format) by way of a modified Feldkamp algorithm using NRecon software package (Bruker-Skyscan). Prior to image segmentation, reconstructed scans for each specimen were filtered using a Gaussian blur (Radius=1) to reduce image noise. This radius of the Gaussian blur was chosen because it maintained image sharpness and reduced image noise without degrading the original reconstructed scans (Bouxsein et al., 2010). The result for one reconstructed and filtered micro-CT scanned specimen is presented in Figure 3b.

Segmentation of the filtered scans was performed on vendor bundled CT-Analyzer (version 1.10) software. The segmentation process initially involved delineating the diploë layer of the calvarium from the inner and outer cortical tables (Figure 4a). The contouring used to delineate the diploë layer was achieved manually on a slice-by-slice basis.

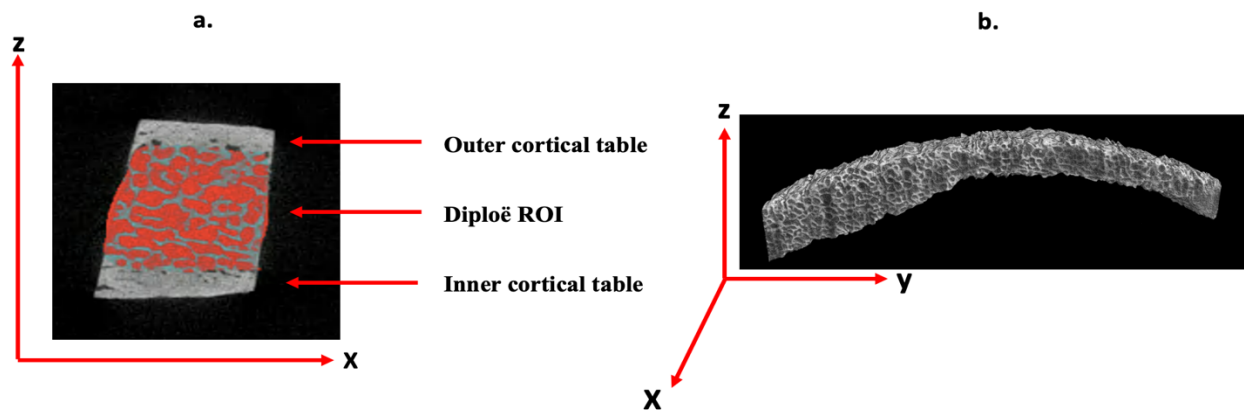


Figure 4. Diploë region of interest (ROI) shaded in red for a single cross-section of a calvarium specimen (a.). Resultant diploë VOI to be used for image analysis (b.)

As displayed in Figure 4, the region of interest (ROI), shaded red, is the diploë outlined with an irregular anatomic contour adjacent to the inside surfaces of the inner and outer cortical tables. This process was completed for each cross-section of the calvarium resulting in a digitally extracted volume of interest (VOI) of the diploë (Figure 4b). An equivalent contouring was employed to delineate the inner and outer cortical tables from the diploë, resulting in VOIs for each cortical table (Figure 5a, 5b). Supplementary Material A provides proof that the manual contouring to acquire the VOI for each specimen was a repeatable method in the current study. To finalize the segmentation, a global threshold was applied to the diploë and cortical tables VOIs in order to clearly distinguish non-bone voxels from bone voxels. A fixed value of 0.499 g HA/cm³ was the set threshold value for the diploë layer and a fixed value of 0.594 g HA/cm³ was used for the cortical tables. There is no agreed upon threshold value for bone in the literature (Bouxsein et al., 2010), however, the threshold values formally stated was sufficient to distinguish non-bone voxels and bone voxels for a majority of the cross-sections in a specimen for this study.

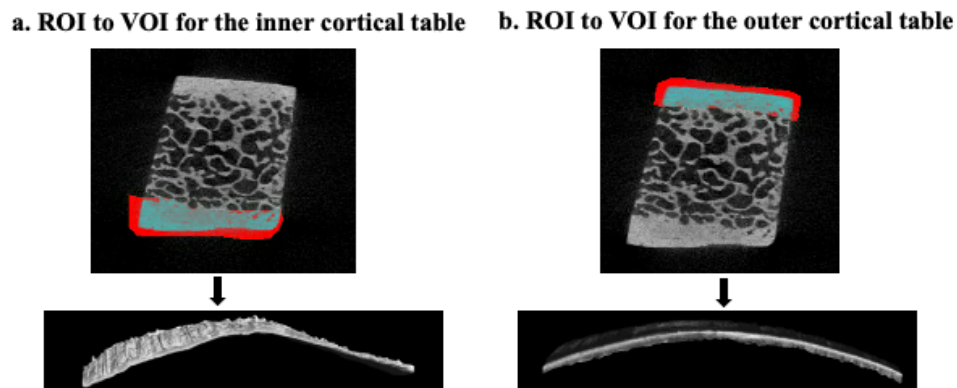


Figure 5. The ROI for the inner (a.) and outer (b.) cortical table and their resulting VOIs to be used for image analysis.

2.2.3 Image Analysis

Morphometric properties were determined for the diploë and cortical tables for each scanned specimen using the CT-Analyzer software. Table 2 outlines the morphometric properties of the diploë and cortical tables that were computed, along with how each property was defined in this study.

Table 2. Definitions of the morphometric properties measured in this study along with their unit of measure.

Diploë morphometry	Unit	Definition
BMD: bone mineral density	g HA/cm ³	Average density of bone and non-bone voxels
Porosity	%	Ratio of closed and open pores volume to total VOI volume
Tb.Th: trabecular thickness	mm	Average thickness of trabeculae
Tb.Sp: trabecular separation	mm	Average separation or distance between trabeculae
Tb.N: trabecular number	1/mm	Average number of trabeculae per mm
Tb.Pf: trabecular bone pattern factor	1/mm	A representative measure of trabecular connectivity or the ratio of convex to concave surface curvature. A high connectivity and structural integrity of trabecular bone is indicated by greater concave surfaces (lower or negative values).
uPi: un-plate index	Dimensionless	The ratio of a specimen's Tb.Th derived in 3D to the Tb.Th derived in 2D, an increasing uPi indicates departure from an ideal plate morphology.
FD: fractal dimension	Dimensionless unit between 2 and 3	A measure that describes trabecular bone surface complexity, where a number closer to 3 indicates a greater surface complexity
Cortical morphometry	Unit	Definition
TMD: tissue mineral density	g HA/cm ³	Average density of bone voxels exclusively
Porosity	%	Ratio of closed and open pores volume to total VOI volume

The calibration process completed during the image acquisition allowed for mean BMD and TMD measurements to be calculated based on the conversion of AC values to physical density (g HA/cm³) values for each bone voxel and non-bone voxel within the specimen VOI. BMD pertains to the density values attributed to the bone mineral content (bone voxels) and the pores (non-bone voxels) within the VOI. TMD pertains to the density of the bone mineral content in the VOI, excluding the pores. 3D based algorithms (built-in the software) were used by CT-Analyser to calculate Tb.Th, Tb.Sp and Tb.N. Tb.Th was determined using a sphere-fitting method. It involved the use of spheres which were optimized to completely encase all the voxels of trabeculae structure within the diploë VOI (Bouxsein et al., 2010; Hildebrand and Rüegsegger, 1997). The maximum diameters for all the spheres that were fitted for each trabeculae structure were averaged to approximate an average thickness of trabeculae (Figure 6). The same method was applied to calculate Tb.Sp, where in this case the spheres were fitted in the spaces between trabeculae (Figure 6).

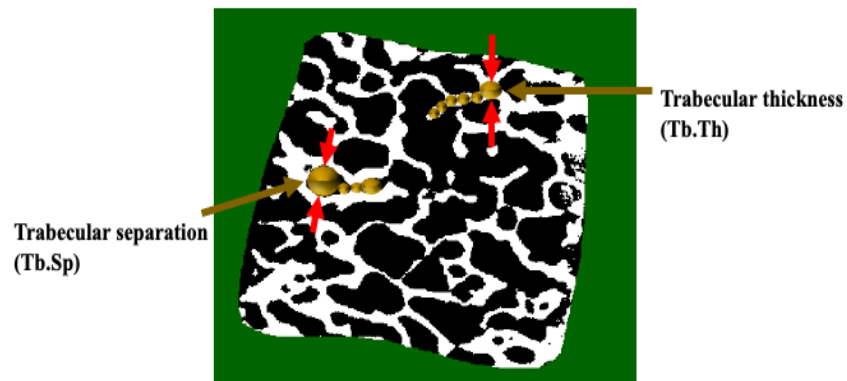


Figure 6. An example of a binarized diploë cross-section illustrating the sphere (gold circles) method to compute Tb.Th and Tb.Sp.

Tb.N was calculated by way of a parallel plate method in 3D (Parfitt et al., 1987). This method takes the ratio of bone volume (bone voxels in the VOI) to tissue volume (bone and non-

bone voxels in the VOI) in the diploë and divides it by Tb.Th, resulting in an average Tb.N (Bouxsein et al., 2010; Parfitt et al., 1987; Salmon, 2009). Tb.Pf has been considered a proxy measure of trabecular connectivity and is thought to be linearly dependent on percent bone volume (Kivell, 2016; Salmon, 2020). This parameter is calculated using equation 2, where BS and BV refer to bone surface and bone volume respectively, and 1 and 2 refer to before and after an image dilation procedure respectively (Hahn et al., 1992). An image dilation is a computer based thickening of the trabecular bone through the addition of pixels to the boundaries of the trabecular bone (Hahn et al., 1992). BS is the surface area of all the bone voxels within the VOI. It was computed in 3D using a marching cube algorithm that creates triangulations of the bone surface to determine surface area (Lorensen and Cline, 1987). BV is the volume of all the bone voxels within the VOI, it was computed using volumetric marching cubes in CT-Analyzer (Lorensen and Cline, 1987).

$$Tb.Pf = (BS_1 - BS_2) / (BV_1 - BV_2) \quad (2)$$

uPi is computed using equation 3. uPi is considered an alternative parameter to structural model index (SMI) but avoids out of range values (negative values) which may indicate concave surfaces occurring from porosity (Salmon, 2020).

$$uPi = (Tb.Th \times BS) / (2 \times BV) \quad (3)$$

As the uPi value increases, trabecular bone increases its departure from an ideal plate morphology (Salmon, 2020). A plate is considered an ideal morphology for trabecular bone because its structure is mechanically stronger compared to rods (Salmon et al., 2015). This can be understood by observing Figure 7, where plates can be described as wider regions of trabecular bone, whereas rods can be illustrated as elongated, thin, and cylindrical (Salmon et al., 2015) (Figure 7).

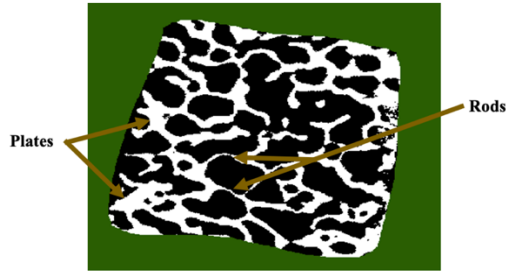


Figure 7. An example of a binarized diploë cross-section illustrating rods and plates within the trabecular region.

The diploë is a complex network of irregular and disorganized trabecular struts and therefore fractal dimension (FD) was another morphometric property considered in this study that measured the surface complexity of the diploë (Chappard et al., 2001; Chen et al., 2018). It is also an investigative property for bone strength indication and osteoporosis diagnosis (Chen et al., 2018; Wu et al., 2015). A box-counting algorithm was used to compute FD in 3D by CT-Analyser.

2.3 Statistical Analysis

The study's main objective was to determine morphometric properties of the diploë and cortical tables with the consideration of key interacting factors (sex, location, and layers of the sandwich structure), therefore, two and three-way mixed (repeated measures) analysis of variance (ANOVA) tests were performed. The dependent variables in this study were the diploë and cortical morphometric properties outlined in Table 2. The independent variables in this study were the: (1) two levels of sex: male and female, (2) two levels of calvarium location: frontal and parietal, and (3) two cortical layers of the calvarium: outer and inner cortical table.

2.3.1 Two-way mixed (repeated measures) ANOVA: Diploë

For each diploë morphometric property a two-way mixed ANOVA was conducted in which the independent variables were (1) sex and (2) calvarium location. Sex was treated as a between-specimen factor due to their independent levels (male and female) and calvarium location was

treated as a within-specimen factor (repeated measure) since their levels (frontal and parietal locations) originated from the same calvarium. The interaction term that was investigated for the two-way mixed ANOVA was sex*calvarium location.

2.3.2 Three-way mixed (repeated measures) ANOVA: Cortical

For each cortical morphometric property a three-way mixed ANOVA was conducted in which all three independent variables were included in the analysis. Sex was treated as a between-specimen factor but calvarium location and cortical layer were considered within-specimen factors (repeated measure) since their levels (frontal/parietal locations and inner/outer cortical layers, respectively) originated from the same calvarium. The interaction terms that were investigated for the three-way mixed ANOVA was sex*calvarium location*cortical layer, sex*cortical layer, and calvarium location*cortical layer.

A power analysis was performed to ensure our probability of committing a type two error was no more than 20% for the hypothesis testing of the main effects and simple main effects (multiple comparison tests). The authors referred to morphometry means and standard deviations (percent porosity and percent bone volume) from a previous study to determine the minimal sample size required to observe 80% power ($\beta=0.20$) (Motherway et al., 2009). This particular study was preferred to perform the power analysis since their morphometry analysis originated from 63 calvarium specimens from both sex and frontal and parietal locations, a parallel description of the samples used in the current study. Using calculation methods described by Eng (2003), a computed total sample size of 35 specimens were required to observe an 80% power (Eng, 2003). Therefore, 50 calvarium samples was a sufficient sample size for this study. All statistical tests yielded averages and 95% confidence intervals (CI) for each morphometric property and accounted for possible interaction effects between independent variables or main

effects. Statistical analysis was carried out using IBM SPSS version 25 (IBM Inc, Armonk, NY, USA). Bonferroni post-hoc tests were carried out to perform multiple comparison analyses when significant main effects were detected. The alpha level was set at 0.05 with a p-value less than 0.05 considered statistically significant.

3. RESULTS

3.1 Diploë Morphometry

All diploë morphometric variables satisfied normality, $p > 0.05$ (Shapiro-Wilk test) and homogeneity of variance, $p > 0.05$ (Levene's test), excluding the male parietal group which violated normality for Tb.Th ($p = 0.043$). Two-way mixed ANOVA tests were carried out despite this single violation, as the ANOVA is tolerant to deviations from normality. No statistically significant two-way interactions were reported between sex and calvarium location for all diploë morphometric properties except for FD (Table 3). Significant simple main effects established that FD was greater in females compared to males for each calvarium location on average (Table 4). Significant main effects established that Tb.Th and Tb.Sp were greater for male diploë compared to female, and Tb.N was significantly greater for female diploë compared to male (Table 5). Significant main effects established that Tb.N and Tb.Pf were greater for frontal specimens compared to parietal specimens, and parietal specimens reported a greater porosity, Tb.Sp, and uPi (Table 5).

Table 3. The statistical results for the interaction terms investigated for the diploë morphometry and cortical morphometry. The degree of freedom for each statistic was 1.

Sex*Calvarium location		
Diploë morphometry	p-value	F-statistic
BMD	0.353	0.900
Porosity	0.385	0.783
Tb.Th	0.454	0.580
Tb.Sp	0.078	3.406
Tb.N	0.923	0.010
Tb.Pf	0.951	0.004
uPi	0.208	1.681
FD*	0.046	4.441

Sex*Calvarium location*Cortical layer		
Cortical morphometry	p-value	F-statistic
TMD	0.159	2.320
Porosity	0.247	1.513

Sex*Cortical layer		
	p-value	F-statistic
TMD	0.892	0.019
Porosity*	0.021	7.436

Calvarium location*Cortical layer		
	p-value	F-statistic
TMD	0.603	0.288
Porosity	0.407	0.748

*Statistically significant ($p < 0.05$).

Table 4. Simple main effects: Averages [95% CIs] for FD with respect to sex, location, and all 50 specimens.

Diploë Morphometry	Calvarium location				All specimens
	Frontal		Parietal		
	Male	Female	Male	Female	
FD	2.60 * [2.56,2.69]	2.65 [2.62,2.69]	2.56* [2.53, 2.60]	2.67 [2.63, 2.71]	2.620 [2.599, 2.640]

*Statistically significant difference between male and female (p<0.05).

Table 5. Main effects: Averages [95% CIs] for diploë morphometry with respect to sex, location and all 50 specimens.

Diploë morphometry	Sex		Calvarium location		All specimens n=50
	Male	Female	Frontal	Parietal	
BMD (g HA/cm ³)	0.46 [0.40, 0.51]	0.44 [0.39, 0.50]	0.46 [0.42, 0.51]	0.44 [0.40, 0.48]	0.45 [0.42, 0.48]
Porosity (%)	52.6 [47.1, 58.1]	54.0 [48.3, 59.7]	51.2* [46.8, 55.6]	55.4 [51.2, 59.5]	53.3 [50.3, 56.2]
Tb.Th (mm)	0.29* [0.26, 0.32]	0.24 [0.21, 0.27]	0.26 [0.24, 0.28]	0.27 [0.25, 0.29]	0.27 [0.25, 0.28]
Tb.Sp (mm)	0.65* [0.58, 0.72]	0.52 [0.45, 0.59]	0.55* [0.50, 0.60]	0.62 [0.56, 0.68]	0.59 [0.54, 0.63]
Tb.N (mm ⁻¹)	1.65* [1.51, 1.78]	1.93 [1.79, 2.07]	1.89* [1.78, 1.99]	1.69 [1.58, 1.80]	1.78 [1.70, 1.87]
Tb.Pf (mm ⁻¹)	-10.92 [-13.41, -8.43]	-11.96 [-14.55, -9.37]	-13.28* [-15.47, -11.09]	-9.60 [-11.45, -7.76]	-11.42 [-12.88, -9.97]
uPi	1.60 [1.53, 1.66]	1.59 [1.52, 1.65]	1.56* [1.52, 1.60]	1.62 [1.56, 1.68]	1.59 [1.55, 1.63]

*Statistically significant difference between male and female or between frontal and parietal (p<0.05).

3.2 Cortical Morphometry

Normality was satisfied for TMD ($p > 0.05$), however it was violated for porosity in the male ($p < 0.001$) and female ($p = 0.025$) outer cortical table groups. Three-way mixed ANOVA tests were carried out despite these violations as ANOVA is tolerant from deviations of normality. No statistically significant three-way interaction effects and two-way interaction effects (sex*cortical layer and calvarium location*cortical layer) were reported for TMD (Table 3). Significant main effects established that the outer cortical table TMD was significantly greater than the inner cortical table (Table 6). No statistically significant three-way interaction effects were reported for porosity, however, a two-way interaction effect was established between sex and calvarium layer (Table 6). For each sex and location, the porosity of the inner cortical table was significantly greater than the outer cortical table (Table 6). Additionally, female cortical porosity was significantly greater compared to male at each cortical layer.

Table 6. Averages [95% CIs] for cortical morphometry with respect to sex, calvarium location, and cortical layer.

Cortical layers					
Cortical morphometry	Inner table		Outer table		All cortical layers
TMD (g HA/cm ³)	0.98 [0.97, 0.99]	*	1.03 [1.01, 1.04]		1.01 [1.00, 1.02]
Frontal location			Parietal location		
	Male	Female	Male	Female	
Porosity (%)	Inner table: 6.5 [4.5, 8.6] *	Inner table: 9.8 [7.9, 11.7] *	Inner table: 8.1 [6.1, 10.1] *	Inner table: 13.7 [10.6, 16.7] *	7.1 [6.3, 8.0]
	Outer table: 3.2 [1.6, 4.9]	Outer table: 5.3 [4.0, 6.6]	Outer table: 4.6 [3.0, 6.1]	Outer table: 7.1 [5.6, 8.5]	

* Statistically significant difference (p<0.05).

The Supplementary Material B provides histograms for all diploë and cortical morphometric properties.

4. DISCUSSION

4.1 Diploë morphometry

In the present study, diploë morphometry was quantified across sex and calvarium location using non-destructive micro-CT imaging-based methods. Apart from FD, there were no interaction effects that occurred between sex and location to influence the resultant diploë morphometry. Alternatively, significant differences of morphometry were mainly found between the levels of sex and the levels of location. BMD between the sexes were statistically equivalent and as expected, this result was also observed with porosity since a linear relationship was previously established between porosity and density (McElhaney et al., 1970). However, porosity was notably greater among the parietal specimens compared to the frontal specimens. This difference may be associated with the significantly greater Tb.Sp and uPi that were also reported. For the diploë to encompass greatly separated trabecular struts, along with deviations from a plate (wide) structure toward a rod (thin) structure, it can be speculated that pore space and thus porosity should increase accordingly. Therefore, it is plausible to infer that a relationship exists between morphometric parameters such as porosity, Tb.Sp, and uPi that could motivate future work to investigate. To the authors' knowledge, BMD and porosity measurements exclusively for the diploë using micro-CT imaging has not been adopted in the literature to date, and so the authors believe the current work represents a valued contribution. Utilizing micro-CT imaging-based methods, Boruah and colleagues presented a histogram of BMD measurements consisting of the whole calvarium sandwich structure (Boruah et al., 2013). Furthermore, destructive methods were applied to quantify apparent density for calvarium specimens by McElhaney et al (McElhaney et al., 1970). Although BMD was defined for the overall calvarium structure in these studies, the diploë region specifically was not investigated. The current study exclusively reported on average diploë BMD

and porosity, along with 95% CIs and distribution curves for future reference (see section on Supplementary Material B).

To verify that the diploë morphometric properties reported in this study were aligned with rational values of human trabeculae, the results were compared against trabecular morphometry values of different human bones reported in past findings (Alexander et al., 2019; Boruah et al., 2015; Kersh et al., 2013; Kim and Henkin, 2015; Reisinger et al., 2011). The ranges of BMD reported in this study are within the ranges of trabecular BMD values for the human mandible ($0.382 \pm 0.118 \text{ g HA/cm}^3$) and maxilla ($0.214 \pm 0.095 \text{ g HA/cm}^3$) (Kim and Henkin, 2015) which are bone regions that make up the skull and located inferior to the calvarium. Furthermore, diploë porosities reported in the current study are consistent with previous findings despite distinctions in scanning resolution and the physical sizes of tested specimens (Alexander et al., 2019; Boruah et al., 2015). With the present study finding no clear differences in the density of the diploë between sexes and calvarium regions, FE models or physical surrogates may conclude on a single value of each parameter for a skull diploë model (Brown et al., 2019; De Kegel et al., 2019; Falland-Cheung et al., 2017; Roberts et al., 2013). Conversely, slight location distinctions in morphometric properties such as porosity, Tb.Sp and uPi would need to be accounted for within subject-specific skull models in order to obtain accurate predictions on mechanical response at fracture (De Kegel et al., 2019).

Tb.Th, Tb.Sp and Tb.N were estimated in this study using a sphere fitting method. It was found that on average, Tb.Th and Tb.Sp were greater in male diploë, however, Tb.N was greater in female diploë. In other words, the results indicate that male trabecular struts are thicker and significantly separated from one another, yet the quantity of trabeculae is lower compared to that observed in females. One may hypothesize that thicker trabecular struts or a significant number of

trabeculae would enhance the mechanical strength of the diploë. However, a thorough study on the relationship between morphometry and mechanical strength that accounts for sex is required to confirm this hypothesis. Future work investigating this relationship would allow for computational mechanical modelers and researchers developing skull surrogates to determine appropriate design considerations for morphometry properties most attributing to a fracture.

The present study is the first to document trabecular properties for the diploë with a unique acknowledgement for sex and location interactions, therefore, it was challenging to refer to previous studies for possible comparison. In addition to BMD, Kim and Henkin reported Tb.Th (0.10 ± 0.02 mm), Tb.Sp (0.63 ± 0.18 mm), and Tb.N (2.07 ± 0.80 per mm) for the human maxilla and were comparable to the results reported in the current study (Kim and Henkin, 2015). Van Dessel et al likewise reported an average Tb.Pf of -8.54 ± 4.4 per mm for the human mandible (Van Dessel et al., 2016). This equates to a range of -12.94 to -4.14 per mm for one standard deviation and thus aligns with the Tb.Pf values reported in the current study (Van Dessel et al., 2016). It is important to recognize the negative value of Tb.Pf in the current study as this signifies a high connectivity and concave surface which is ideal for trabecular bone. Salmon (2020) first introduced the uPi parameter and calculated a range of average uPi between 1.50 and 1.75 for the tibia and femur of rats (Salmon, 2020). Salmon used Tb.Th, BS, and BV parameters from Tivesten et al's study to calculate the uPi (Tivesten et al., 2004). The average uPi reported in the present study falls within this range (Salmon, 2020; Tivesten et al., 2004). Unfortunately, to our best knowledge, there are no original articles that have documented the uPi parameter in human bone to date. One potential reason for this is because the alternative measure, SMI, is the most commonly used parameter that also identifies plate and rod structures (Salmon, 2020). Fortunately,

the uPi avoids the additional procedure required to compute SMI which is identifying out-of-range values corresponding to trabecular concave surfaces (Salmon, 2020).

The parietal location had a lower Tb.N and Tb.Pf compared to the frontal on average. Previously, it was noted that parietal specimens reported greater porosity due to significantly separated trabecular bone. As a result, undoubtedly, there should be less trabecular bone per unit length along with connectivity in the parietal, thus justifying the considerably lower Tb.N and Tb.Pf found in the parietal specimens. Furthermore, the parietal location deviated from an ideal plate structure (uPi parameter) significantly compared to the frontal bone. This indicates the parietal diploë consists of less plate like structures and more thin rod trabecular bone which could jeopardize the mechanical strength of the parietal diploë. At the present moment, there may not be a clear phenomenon to further explain this locational difference, however, the authors speculate it may provide reasoning for observed mechanical property differences between frontal and parietal regions as reported in previous studies (McElhaney et al., 1970; Motherway et al., 2009). The greater Tb.N and Tb.Pf, and the lower uPi in the frontal location may be the few diploë morphometric properties associated with the greater fracture force and energy absorption capabilities in frontal samples compared to the parietal as a recent study observed during 3-point impact loading on cranial bone (Motherway et al., 2009). By way of multiple or binary regression techniques, such an association would be worth investigating in the future in order to quantify the relationship between morphometric/geometric properties of the calvarium and mechanical responses (Adanty et al., 2020; De Kegel et al., 2019).

FD was also included in the analysis of diploë morphometry as it is widely regarded by clinical researchers as a good indicator for mechanical strength of bone as well as a complementary clinical diagnosis for osteoporosis (Chen et al., 2018; Feltrin et al., 2001; Wu et al., 2015). FD

simply describes the self-similar complexity of bone, particularly for porous structures, and when computed in 3D its dimension falls within 2 and 3 (Chen et al., 2018). A significantly greater FD in female diploë was evident in the present study, suggesting a greater surface complexity or a finer spatial resolution on self-similar imagery compared to male trabecular bone on average (Gonzales-Barron and Butler, 2005). Currently, there is inadequate evidence to confirm the true relationship between FD and other morphometric parameters such as porosity and BMD. From a study on trabecular bone samples of the human femoral head, a correlation beyond 0.80 was established between 2D computed FD and porosity (Pothuaud et al., 2000). Alternatively, FD was negatively associated with BMD (Harrar and Hamami, 2008), however that should be expected since the inverse relationship between BMD and porosity has been long-established (McElhaney et al., 1970). Based on these statistical relationships, the marginally lower BMD (greater porosity) revealed in the female specimens could be a contributing factor towards differences in FD among sex. More recently, FD was found to be positively correlated with bone stiffness during the compression of rodent bone using FE analysis (Wu et al., 2015). Although the relationship between diploë morphometry and the mechanical response of bone during computational and experimental loading is not fully established, it may provide critical inferences on which structural properties contribute greatly towards accurately modelling an injury.

4.2 Cortical Morphometry

The present study quantified TMD and porosity distinctions between the inner and outer cortical tables. Overall, the results entailed a clear morphometric difference between the two layers whereby the inner cortical table observed a lower TMD and greater porosity compared to the outer cortical table. These results were also evident in previous works (Alexander et al., 2019; Auperrin et al., 2014; Peterson and Dechow, 2002). Peterson and Dechow used a destructive method to

determine that the outer table was significantly denser than the inner table and suggested the inner table experiences a lower bone remodelling rate and a greater average of mineralization based on ash weight percentages to explain for the difference (Peterson and Dechow, 2002). This may hold as a reasonable inference because the inner table's surface is positioned in a unique biological environment consisting of the cerebral spinal fluid and the brain. Additionally, porosity was significantly greater in the inner table which may also help to explain for its significantly lower TMD. Indeed, many works including the present study have reported morphometric differences between the inner and outer cortical tables (Alexander et al., 2019; Auperrin et al., 2014; Peterson and Dechow, 2002). Regardless of cortical table or location, the female specimens averaged a greater porosity in comparison to the males. However, TMD was not sensitive to differences in sex which is rational given TMD is a function of solely bone voxels and therefore its relationship with porosity may not be necessarily consistent with the inverse relationship between BMD and porosity. It is recommended that these cortical differences are reflected in the material properties of the skull in existing FE head models to ensure validity of material properties and injury prediction (Horgan and Gilchrist, 2003; Kleiven and Hardy, 2002; Sahoo et al., 2014; Takhounts et al., 2008).

4.3 Future considerations and limitations

The study quantified the diploë and cortical morphometry of the human calvarium. From the set of morphometric indices investigated in this study, an appropriate step moving forward would be the determination of morphometric indices that can statistically predict mechanical properties during a skull fracture injury using statistical regression techniques (Adanty et al., 2020; De Kegel et al., 2019). An experimental design to consider for this step would consist of a bending mechanism on calvarium bone under quasi-static and dynamic impact loading conditions to induce

a skull fracture injury (Adanty et al., 2020; Hubbard, 1971; Lee et al., 2019; Motherway et al., 2009). This step would provide valuable information on which microarchitectural properties of the calvarium are relevant towards the design and development of a computational or surrogate fracture model. In return, the model would be able to confidently predict mechanical properties attributed to a skull fracture injury or other non-injurious events. The current study also quantified morphometry with respect to sex and location. Future work may investigate how mechanical properties during a skull fracture are influenced by morphometric properties along with sex and location. It was observed that most morphometric variables altered with both sex and location which may be an important factor to consider when assigning material properties such as density for subject-specific skull models.

First, all specimens from the cadaver subjects were sampled by convenience. In other words, the number of samples analyzed in this study was the maximum number of samples available to the authors during the time of extraction on the cadaver subjects. The morphometric results in this study are exclusively attributed to these 50 specimens and are by no means a fair generalization for the calvarium morphometry of the true human population. Despite the limitation on the number of calvarium samples used in this study, a power analysis was performed before testing to determine the minimum sample size required to observe an 80% power for the multiple comparisons test. Second, the study's specimens were sampled from the older age cohort within the province of Alberta, Canada, which suggests the results are biased towards a specific population. The authors were not given information on the ethnicity of the cadaver subjects. Future studies are encouraged to investigate morphology properties for younger age cohorts or the 50th percentile population. Third, the study used embalmed cadavers for specimen extraction because it was the only form of tissue available to the authors at the time. The authors acknowledge the

possibility of mechanical and material property differences between fresh, fresh-frozen and embalmed tissue (Ohman et al., 2008; Topp et al., 2012). However, to the authors best knowledge there is currently no agreed upon conclusion regarding morphometric differences between different forms or type of tissue. The authors suggest possible limitations regarding the use of micro-CT imaging for bone analysis. The study's density calibration was limited to two calibration phantoms with known densities of 0.250 g HA/cm³ and 0.750 g HA/cm³. As observed in previous studies, TMD biologically exceeds a density value of 1.00 g HA/cm³ and so the necessary extrapolation for density beyond this value is a probable source of error (Burghardt et al., 2008; Deuerling et al., 2010; Hildebrand and Rüegsegger, 1997). Certainly, manufacturing calibration phantoms exceeding 800 g HA/cm³ with epoxy resin is challenging, yet a few methods have been proposed to manufacture phantoms consisting of 1,200-3000 g HA/cm³ (Schweizer et al., 2007). Lastly, the authors acknowledge that the specimens were fixated in unbuffered aqueous formaldehyde 37% embalming fluid. Evidently, buffered formalin retards slight changes in pH when penetrating the bone tissue to prevent acidity (Thavarajah et al., 2012). Therefore, the authors recognize that this as a limitation of our fixation process.

5. CONCLUSION

This study revealed findings on the morphometric properties of the calvarium, whereby the consideration for interacting factors which included sex, location, and the 3-layers of the calvarium were investigated. With the exception of FD, the study found no significant interaction effects between sex and the calvarium location on diploë morphometry. On average, males had a greater Tb.Th and Tb.Sp; conversely, females had a greater Tb.N and FD compared to males. It was also found that the frontal location possessed a greater Tb.N and Tb.Pf, but the parietal location revealed greater levels of porosity, Tb.Sp, and uPi. Moreover, the inner cortical table revealed a significantly lower density and greater porosity which corroborates with previous findings (Alexander et al., 2019; Auperrin et al., 2014; Peterson and Dechow, 2002). The results in this study determined geometric measures on the diploë's complex structure and overall morphometry which can contribute towards the detailed geometric reconstruction of FE subject-specific skull models (De Kegel et al., 2019) as well as the fabrication of physical surrogate fracture models consisting of a 3-layer sandwich structure (Brown et al., 2019; Falland-Cheung et al., 2017; Roberts et al., 2013). The authors hope to embark on future experimental work geared towards statistically predicting the mechanical properties during a skull fracture using morphometric properties outlined in this study as potential predictors (Adanty et al., 2020).

ACKNOWLEDGEMENTS

The authors would like to acknowledge Hugh Barrett, Jason Papirny, and Dr. Daniel Livy of the University of Alberta's Division Anatomy for providing access to human cadavers and the necessary aid during dissection.

Funding: This research was sponsored by the Army Research Laboratory and was accomplished under Cooperative Agreement Number W911NF-19-2-0336. The views and conclusions contained in this document are those of the authors and should not be interpreted as representing the official policies, either expressed or implied, of the Army Research Laboratory or the U.S. Government. The U.S. Government is authorized to reproduce and distribute reprints for Government purposes notwithstanding any copyright notation herein.

DECLARATIONS OF INTEREST

None.

SUPPLEMENTARY MATERIAL A

The coefficient of variation for the manual acquisition of VOI

To determine if the method of manually acquiring the volume of interest (VOI) for each specimen was repeatable, coefficient of variations (CV) was computed for each morphometric parameter over two different VOIs completed by the same individual. The subset of specimens that were investigated was: 2 male frontal specimens, 2 female frontal specimens, 2 male parietal specimens, and 2 female parietal specimens, all of which were randomly selected. CV was expressed as a percent ratio of standard deviation (SD) to mean. The average CV was less than 5% for the presented specimens (Table 7 to 14) which is considered acceptable in clinical sciences (Campbell et al., 2010).

Table 7. CV (%) For A Male Frontal Specimen's Morphometry
Male Frontal Specimen 1

	VOI 1	VOI 2	Mean	SD	CV (%)
uPi	1.55	1.46	1.51	0.06	4.00
Tb.Pf (mm⁻¹)	-8.82	-8.52	-8.67	0.21	2.43
BMD (g HA/cm³)	0.52	0.52	0.52	0.00	0.00
Tb.N (mm⁻¹)	1.76	1.55	1.66	0.15	9.00
Tb.Th (mm)	0.29	0.33	0.31	0.03	8.54
Tb.Sp (mm)	0.61	0.64	0.62	0.02	3.14
Porosity (%)	48.72	49.09	48.90	0.26	0.53
FD	2.57	2.56	2.56	0.01	0.41
TMD-outer table (g HA/cm³)	1.04	1.04	1.04	0.00	0.01
Porosity-outer table (%)	2.44	2.46	2.45	0.01	0.58
TMD-inner table (g HA/cm³)	0.98	0.98	0.98	0.00	0.00
Porosity-inner table (%)	6.56	6.57	6.56	0.01	0.14
				Mean	2.40
				Max	9.00
				Min	0.00

Table 8. CV (%) For A Male Parietal Specimen's Morphometry
Male Parietal Specimen 1

	VOI 1	VOI 2	Mean	SD	CV (%)
uPi	1.54	1.47	1.51	0.05	3.16
Tb.Pf (mm⁻¹)	-7.19	-7.20	-7.19	0.01	0.12
BMD (g HA/cm³)	0.44	0.44	0.44	0.00	0.48
Tb.N (mm⁻¹)	1.73	1.55	1.64	0.13	7.89
Tb.Th (mm)	0.26	0.29	0.27	0.02	7.95
Tb.Sp (mm)	0.58	0.60	0.59	0.01	2.45
Porosity (%)	55.65	55.61	55.63	0.03	0.05
FD	2.59	2.57	2.58	0.01	0.31
TMD-outer table					
(g HA/cm³)	1.07	1.07	1.07	0.00	0.01
Porosity-outer table					
(%)	3.14	3.51	3.32	0.26	7.80
TMD-inner table					
(g HA/cm³)	1.05	1.05	1.05	0.00	0.06
Porosity-inner					
table (%)	6.81	6.91	6.86	0.07	1.06
				Mean	2.61
				Max	7.95
				Min	0.01

Table 9. CV (%) For A Male Frontal Specimen's Morphometry
Male Frontal Specimen 2

	VOI 1	VOI 2	Mean	SD	CV (%)
uPi	1.46	1.45	1.46	0.00	0.19
Tb.Pf (mm⁻¹)	-13.54	-14.15	-13.84	0.44	3.16
BMD (g HA/cm³)	0.53	0.53	0.53	0.00	0.87
Tb.N (mm⁻¹)	1.46	1.33	1.39	0.09	6.37
Tb.Th (mm)	0.38	0.37	0.37	0.01	2.95
Tb.Sp (mm)	0.68	0.71	0.70	0.02	2.91
Porosity (%)	44.30	43.93	44.12	0.26	0.59
FD	2.62	2.58	2.60	0.03	1.01
TMD-outer table					
(g HA/cm³)	1.01	1.01	1.01	0.00	0.26
Porosity-outer table (%)					
	3.06	3.50	3.28	0.31	9.36
TMD-inner table					
(g HA/cm³)	1.00	1.00	1.00	0.00	0.32
Porosity-inner table (%)					
	6.02	6.08	6.05	0.05	0.78
				Mean	2.40
				Max	9.36
				Min	0.26

Table 10. CV (%) For A Male Parietal Specimen's Morphometry
Male Parietal Specimen 2

	VOI 1	VOI 2	Mean	SD	CV (%)
uPi	1.54	1.34	1.44	0.15	10.19
Tb.Pf (mm⁻¹)	-11.19	-12.21	-11.70	0.72	6.15
BMD (g HA/cm³)	0.46	0.46	0.46	0.00	0.24
Tb.N (mm⁻¹)	1.34	1.23	1.28	0.07	5.71
Tb.Th (mm)	0.36	0.39	0.37	0.02	6.25
Tb.Sp (mm)	0.76	0.79	0.77	0.02	2.90
Porosity (%)	52.34	52.39	52.36	0.04	0.07
FD	2.61	2.58	2.59	0.02	0.71
TMD-outer table					
(g HA/cm³)	1.02	1.02	1.02	0.00	0.10
Porosity-outer table (%)	2.90	3.18	3.04	0.20	6.60
TMD-inner table					
(g HA/cm³)	0.99	0.99	0.99	0.00	0.03
Porosity-inner table (%)	8.20	8.32	8.26	0.08	1.01
				Mean	3.33
				Max	6.60
				Min	0.03

Table 11. CV (%) For A Female Frontal Specimen's Morphometry
Female Frontal Specimen 1

	VOI 1	VOI 2	Mean	SD	CV (%)
uPi	1.60	1.60	1.60	0.00	0.12
Tb.Pf (mm⁻¹)	-9.60	-9.62	-9.61	0.02	0.18
BMD (g HA/cm³)	0.41	0.43	0.42	0.02	3.92
Tb.N (mm⁻¹)	1.93	1.93	1.93	0.00	0.23
Tb.Th (mm)	0.21	0.21	0.21	0.00	0.22
Tb.Sp (mm)	0.56	0.56	0.56	0.00	0.33
Porosity (%)	59.81	59.55	59.68	0.18	0.31
FD	2.65	2.65	2.65	0.00	0.04
TMD-outer table					
(g HA/cm³)	1.00	1.00	1.00	0.00	0.00
Porosity-outer table (%)					
	5.11	5.11	5.11	0.00	0.00
TMD-inner table					
(g HA/cm³)	0.96	0.96	0.96	0.00	0.04
Porosity-inner table (%)					
	9.82	9.95	9.88	0.10	0.96
				Mean	0.53
				Max	3.92
				Min	0.00

Table 12. CV (%) For A Female Parietal Specimen's Morphometry
Female Parietal Specimen 1

	VOI 1	VOI 2	Mean	SD	CV(%)
uPi	1.63	1.52	1.58	0.07	4.71
Tb.Pf (mm⁻¹)	-6.46	-6.84	-6.65	0.27	4.02
BMD (g HA/cm³)	0.35	0.33	0.34	0.01	4.24
Tb.N (mm⁻¹)	1.55	1.38	1.46	0.12	7.88
Tb.Th (mm)	0.22	0.24	0.23	0.02	7.50
Tb.Sp (mm)	0.77	0.79	0.78	0.02	2.31
Porosity (%)	66.05	66.24	66.14	0.13	0.20
FD	2.61	2.59	2.60	0.01	0.32
TMD-outer table					
(g HA/cm³)	1.08	1.08	1.08	0.00	0.00
Porosity-outer table (%)					
	7.23	7.23	7.23	0.00	0.00
TMD-inner table					
(g HA/cm³)	1.02	1.02	1.02	0.00	0.01
Porosity-inner table (%)					
	12.76	12.81	12.78	0.03	0.26
				Mean	2.62
				Max	7.88
				Min	0.00

Table 13. CV (%) For A Female Frontal Specimen's Morphometry
Female Frontal Specimen 2

	VOI 1	VOI 2	Mean	SD	CV(%)
uPi	1.46	1.46	1.46	0.00	0.05
Tb.Pf (mm⁻¹)	-17.24	-16.12	-16.12	0.79	4.93
BMD (g HA/cm³)	0.67	0.69	0.69	0.01	1.95
Tb.N (mm⁻¹)	2.36	2.50	2.50	0.10	4.04
Tb.Th (mm)	0.30	0.32	0.32	0.01	3.09
Tb.Sp (mm)	0.30	0.32	0.32	0.02	5.98
Porosity (%)	28.44	28.27	28.27	0.12	0.43
FD	2.55	2.52	2.52	0.02	0.82
TMD-outer table					
(g HA/cm³)	1.02	1.02	1.02	0.00	0.00
Porosity-outer table (%)					
	3.51	3.51	3.51	0.00	0.00
TMD-inner table					
(g HA/cm³)	0.95	0.95	0.95	0.00	0.00
Porosity-inner table (%)					
	8.29	8.29	8.29	0.00	0.00
				Mean	1.77
				Max	5.98
				Min	0.00

Table 14. CV (%) For A Female Frontal Specimen's Morphometry

	VOI 1	VOI 2	Mean	SD	CV(%)
uPi	1.48	1.49	1.49	0.01	0.70
Tb.Pf (mm⁻¹)	-17.26	-16.51	-16.51	0.53	3.23
BMD (g HA/cm³)	0.58	0.61	0.61	0.02	3.87
Tb.N (mm⁻¹)	1.85	1.74	1.74	0.08	4.77
Tb.Th (mm)	0.33	0.32	0.32	0.01	2.32
Tb.Sp (mm)	0.41	0.41	0.41	0.00	0.42
Porosity (%)	39.33	35.95	35.95	2.40	6.66
FD	2.67	2.67	2.67	0.00	0.07
TMD-outer table					
(g HA/cm³)	1.01	1.01	1.01	0.00	0.07
Porosity-outer table (%)					
	5.14	5.08	5.11	0.04	0.87
TMD-inner table					
(g HA/cm³)	0.98	0.98	0.98	0.00	0.01
Porosity-inner table (%)					
	12.93	12.91	12.92	0.01	0.07
				Mean	1.92
				Max	6.66
				Min	0.01

SUPPLEMENTARY MATERIAL B

Distribution plots for each morphometric parameter.

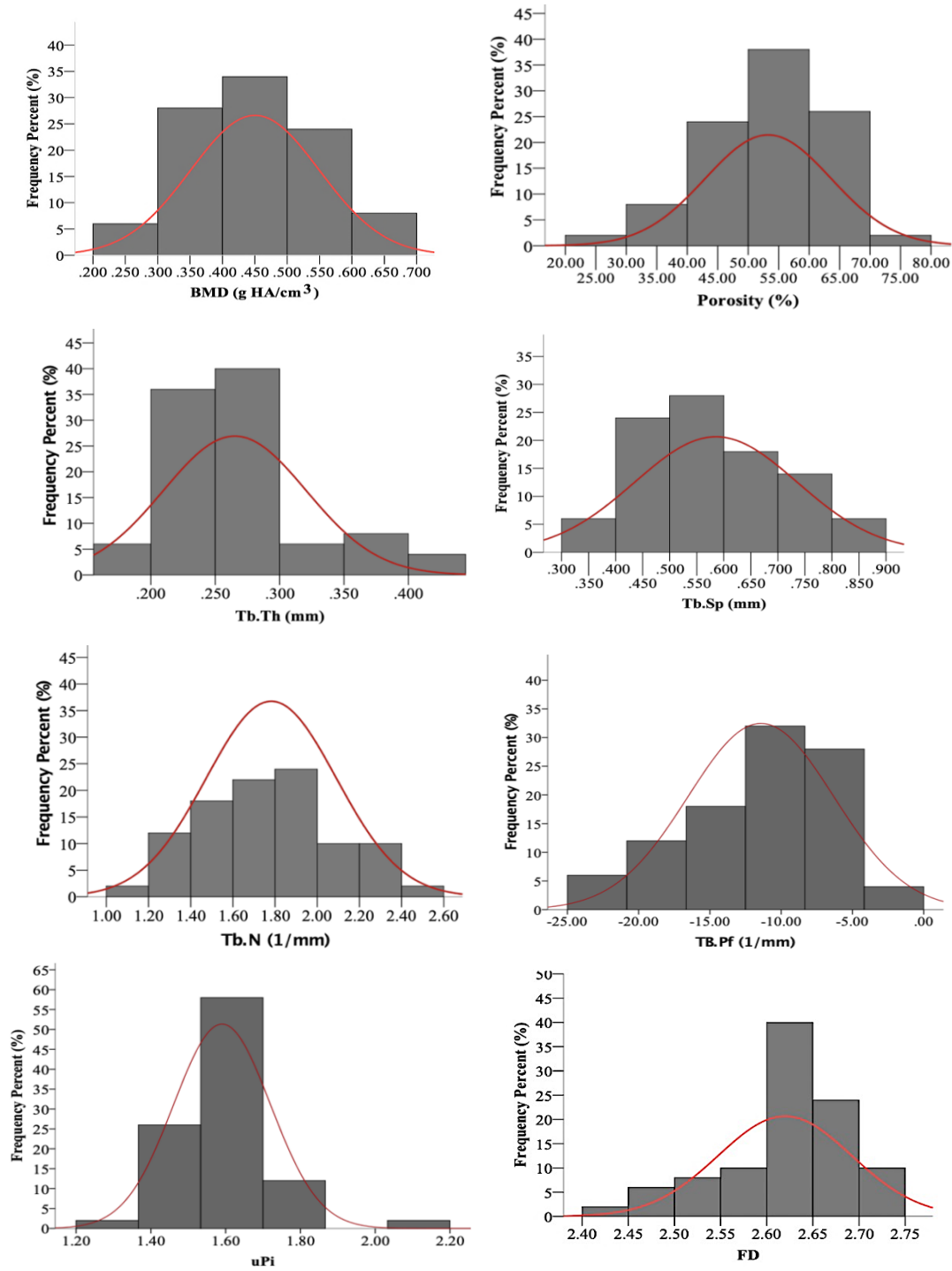


Figure 8. Distribution and normality curves (red) for each diploë morphometric property.

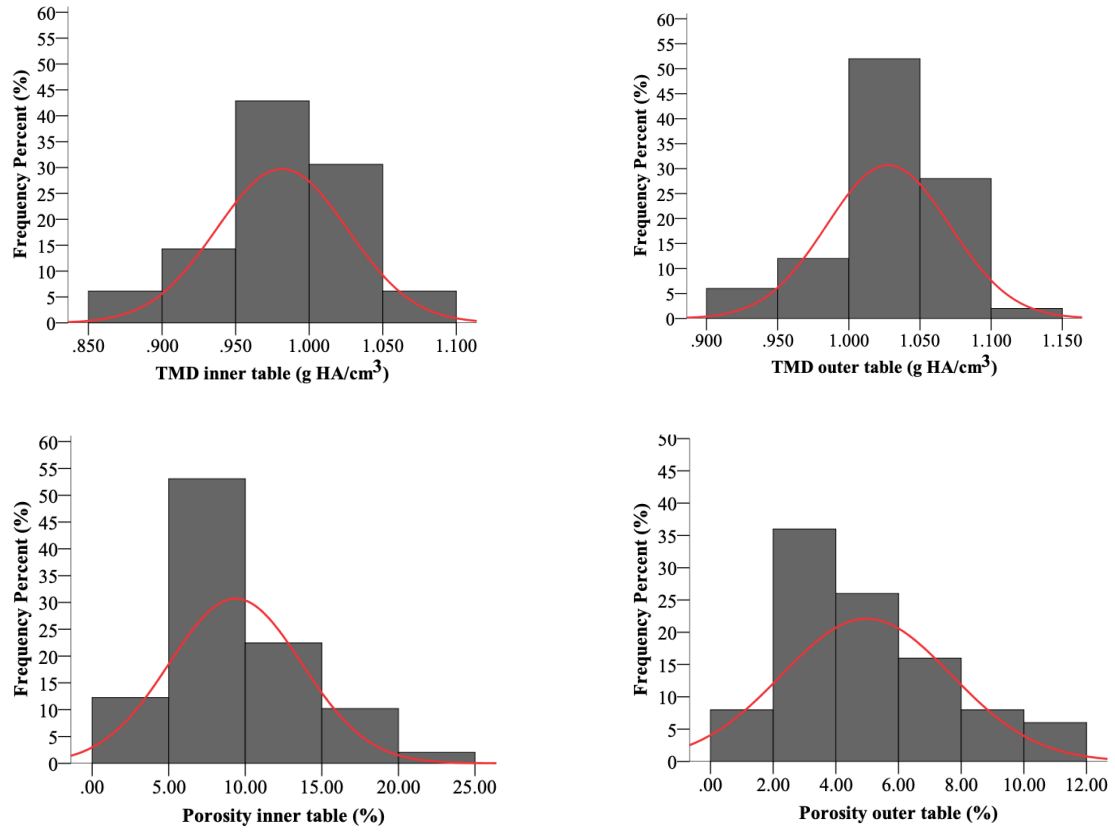


Figure 9. Distribution and normality curves (red) for each cortical morphometric property.

REFERENCES

- Adanty, K., Tronchin, O., Bhagavathula, K.B., Rabey, K.N., Doschak, M.R., Romanyk, D., Hogan, J.D., Ouellet, S., Plaisted, T.A., Satapathy, S.S., Dennison, C.R., 2020. On the Ability of Morphometric Indices of Skull Diploë to Explain Variation in Bone Fracture Force and Fracture Strain in Four-Point Bending: A Preliminary Step Toward A Simulant Fracture Model. *IRCOBI Conf.* 2020 821–822.
- Alexander, S.L., Rafaels, K., Gunnarsson, C.A., Weerasooriya, T., 2019. Structural analysis of the frontal and parietal bones of the human skull. *J. Mech. Behav. Biomed. Mater.* 90, 689–701. <https://doi.org/10.1016/j.jmbbm.2018.10.035>
- Auperrin, A., Delille, R., Lesueur, D., Bruyère, K., Masson, C., Drazétic, P., 2014. Geometrical and material parameters to assess the macroscopic mechanical behaviour of fresh cranial bone samples. *J. Biomech.* 47, 1180–1185. <https://doi.org/10.1016/j.jbiomech.2013.10.060>
- Boruah, S., Henderson, K., Subit, D., Salzar, R.S., Shender, B.S., Paskoff, G., 2013. Response of Human Skull Bone to Dynamic Compressive Loading 12.
- Boruah, S., Paskoff, G.R., Shender, B.S., Subit, D.L., Salzar, R.S., Crandall, J.R., 2015. Variation of bone layer thicknesses and trabecular volume fraction in the adult male human calvarium. *Bone* 77, 120–134. <https://doi.org/10.1016/j.bone.2015.04.031>
- Bouxsein, M.L., Boyd, S.K., Christiansen, B.A., Guldberg, R.E., Jepsen, K.J., Müller, R., 2010. Guidelines for assessment of bone microstructure in rodents using micro-computed tomography. *J. Bone Miner. Res.* 25, 1468–1486. <https://doi.org/10.1002/jbmr.141>
- Brown, A.D., Walters, J.B., Zhang, Y.X., Saadatfar, M., Escobedo-Diaz, J.P., Hazell, P.J., 2019. The mechanical response of commercially available bone simulants for quasi-static and dynamic loading. *J. Mech. Behav. Biomed. Mater.* 90, 404–416. <https://doi.org/10.1016/j.jmbbm.2018.10.032>
- Burghardt, A.J., Kazakia, G.J., Laib, A., Majumdar, S., 2008. Quantitative Assessment of Bone Tissue Mineralization with Polychromatic Micro-Computed Tomography. *Calcif. Tissue Int.* 83, 129–138. <https://doi.org/10.1007/s00223-008-9158-x>
- Campbell, M.J., Machin, D., Walters, S.J., 2010. *Medical Statistics: A Textbook for the Health Sciences.* John Wiley & Sons, Incorporated, New York, UNITED KINGDOM.
- Chappard, D., Legrand, E., Haettich, B., Chalès, G., Auvinet, B., Eschard, J.-P., Hamelin, J.-P., Baslé, M.-F., Audran, M., 2001. Fractal dimension of trabecular bone: comparison of three histomorphometric computed techniques for measuring the architectural two-dimensional complexity. *J. Pathol.* 195, 515–521. <https://doi.org/10.1002/path.970>
- Chen, H., Zhou, X., Fujita, H., Onozuka, M., Kubo, K.-Y., 2013. Age-Related Changes in Trabecular and Cortical Bone Microstructure. *Int. J. Endocrinol.* 2013. <https://doi.org/10.1155/2013/213234>

- Chen, Q., Bao, N., Yao, Q., Li, Z.-Y., 2018. Fractal dimension: A complementary diagnostic indicator of osteoporosis to bone mineral density. *Med. Hypotheses* 116, 136–138. <https://doi.org/10.1016/j.mehy.2018.05.006>
- De Kegel, D., Meynen, A., Famaey, N., Harry van Lenthe, G., Depreitere, B., Sloten, J.V., 2019. Skull fracture prediction through subject-specific finite element modelling is highly sensitive to model parameters. *J. Mech. Behav. Biomed. Mater.* 100, 103384. <https://doi.org/10.1016/j.jmbbm.2019.103384>
- Deuerling, J.M., Rudy, D.J., Niebur, G.L., Roeder, R.K., 2010. Improved accuracy of cortical bone mineralization measured by polychromatic microcomputed tomography using a novel high mineral density composite calibration phantom. *Med. Phys.* 37, 5138–5145. <https://doi.org/10.1118/1.3480507>
- Eng, J., 2003. Sample Size Estimation: How Many Individuals Should Be Studied?1. *Radiology*.
- Falland-Cheung, L., Waddell, J.N., Chun Li, K., Tong, D., Brunton, P., 2017. Investigation of the elastic modulus, tensile and flexural strength of five skull simulant materials for impact testing of a forensic skin/skull/brain model. *J. Mech. Behav. Biomed. Mater.* 68, 303–307. <https://doi.org/10.1016/j.jmbbm.2017.02.023>
- Feltrin, G.P., Macchi, V., Saccavini, C., Tosi, E., Dus, C., Fassina, A., Parenti, A., Caro, R.D., 2001. Fractal analysis of lumbar vertebral cancellous bone architecture. *Clin. Anat.* 14, 414–417. <https://doi.org/10.1002/ca.1076>
- Gong, H., Zhang, M., Yeung, H.Y., Qin, L., 2005. Regional variations in microstructural properties of vertebral trabeculae with aging. *J. Bone Miner. Metab.* 23, 174–180. <https://doi.org/10.1007/s00774-004-0557-4>
- Gonzales-Barron, U., Butler, F., 2005. A COMPARISON OF VISUAL ASSESSMENT AND DIGITAL FRACTAL TEXTURE ANALYSIS OF BREAD-CRUMB FEATURES, in: Cauvain, S.P., Salmon, S.S., Young, L.S. (Eds.), *Using Cereal Science and Technology for the Benefit of Consumers*, Woodhead Publishing Series in Food Science, Technology and Nutrition. Woodhead Publishing, pp. 395–400. <https://doi.org/10.1533/9781845690632.10.395>
- Greenwood, C., Clement, J.G., Dicken, A.J., Evans, J.P.O., Lyburn, I.D., Martin, R.M., Rogers, K.D., Stone, N., Adams, G., Zioupos, P., 2015. The micro-architecture of human cancellous bone from fracture neck of femur patients in relation to the structural integrity and fracture toughness of the tissue. *Bone Rep.* 3, 67–75. <https://doi.org/10.1016/j.bonr.2015.10.001>
- Hahn, M., Vogel, M., Pompesius-Kempa, M., Delling, G., 1992. Trabecular bone pattern factor—a new parameter for simple quantification of bone microarchitecture. *Bone* 13, 327–330. [https://doi.org/10.1016/8756-3282\(92\)90078-B](https://doi.org/10.1016/8756-3282(92)90078-B)
- Harrar, K., Hamami, L., 2008. The fractal dimension correlated to the bone mineral density. *WSEAS Trans. Signal Process.* 4, 110–126.

- Hildebrand, T., Rügsegger, P., 1997. A new method for the model-independent assessment of thickness in three-dimensional images. *J. Microsc.* 185, 67–75. <https://doi.org/10.1046/j.1365-2818.1997.1340694.x>
- Horgan, T.J., Gilchrist, M.D., 2003. The creation of three-dimensional finite element models for simulating head impact biomechanics. *Int. J. Crashworthiness* 8, 353–366. <https://doi.org/10.1533/ijcr.2003.0243>
- Hubbard, R.P., 1971. Flexure of layered cranial bone. *J. Biomech.* 4, 251–263. [https://doi.org/10.1016/0021-9290\(71\)90031-5](https://doi.org/10.1016/0021-9290(71)90031-5)
- Keen, J.A., 1950. A study of the differences between male and female skulls. *Am. J. Phys. Anthropol.* 8, 65–80. <https://doi.org/10.1002/ajpa.1330080113>
- Kersh, M.E., Zysset, P.K., Pahr, D.H., Wolfram, U., Larsson, D., Pandey, M.G., 2013. Measurement of structural anisotropy in femoral trabecular bone using clinical-resolution CT images. *J. Biomech.* 46, 2659–2666. <https://doi.org/10.1016/j.jbiomech.2013.07.047>
- Kim, Y.J., Henkin, J., 2015. Micro-computed tomography assessment of human alveolar bone: bone density and three-dimensional micro-architecture. *Clin. Implant Dent. Relat. Res.* 17, 307–313. <https://doi.org/10.1111/cid.12109>
- Kivell, T.L., 2016. A review of trabecular bone functional adaptation: what have we learned from trabecular analyses in extant hominoids and what can we apply to fossils? *J. Anat.* 228, 569–594. <https://doi.org/10.1111/joa.12446>
- Kleiven, S., Hardy, W.N., 2002. Correlation of an FE Model of the Human Head with Local Brain Motion--Consequences for Injury Prediction. *Stapp Car Crash J.* 46, 123–144.
- Lee, J.H.C., Ondruschka, B., Falland-Cheung, L., Scholze, M., Hammer, N., Tong, D.C., Waddell, J.N., 2019. An Investigation on the Correlation between the Mechanical Properties of Human Skull Bone, Its Geometry, Microarchitectural Properties, and Water Content. *J. Healthc. Eng.* 2019, 1–8. <https://doi.org/10.1155/2019/6515797>
- Lillie, E.M., Urban, J.E., Weaver, A.A., Powers, A.K., Stitzel, J.D., 2015. Estimation of skull table thickness with clinical CT and validation with microCT. *J. Anat.* 226, 73–80. <https://doi.org/10.1111/joa.12259>
- Lorensen, W.E., Cline, H.E., 1987. Marching cubes: A high resolution 3D surface construction algorithm. *ACM SIGGRAPH Comput. Graph.* 21, 163–169. <https://doi.org/10.1145/37402.37422>
- McElhaney, J.H., Fogle, J.L., Melvin, J.W., Haynes, R.R., Roberts, V.L., Alem, N.M., 1970. Mechanical properties of cranial bone. *J. Biomech.* 3, 495–511. [https://doi.org/10.1016/0021-9290\(70\)90059-X](https://doi.org/10.1016/0021-9290(70)90059-X)
- Motherway, J.A., Verschueren, P., Van der Perre, G., Vander Sloten, J., Gilchrist, M.D., 2009. The mechanical properties of cranial bone: The effect of loading rate and cranial sampling position. *J. Biomech.* 42, 2129–2135. <https://doi.org/10.1016/j.jbiomech.2009.05.030>

- Nieves, J.W., Formica, C., Ruffing, J., Zion, M., Garrett, P., Lindsay, R., Cosman, F., 2005. Males Have Larger Skeletal Size and Bone Mass Than Females, Despite Comparable Body Size. *J. Bone Miner. Res.* 20, 529–535. <https://doi.org/10.1359/JBMR.041005>
- Ohman, C., Dall'Ara, E., Baleani, M., Jan, S.V.S., Viceconti, M., 2008. The effects of embalming using a 4% formalin solution on the compressive mechanical properties of human cortical bone. *Clin. Biomech.* <https://doi.org/10.1016/j.clinbiomech.2008.07.007>
- Parfitt, A.M., Drezner, M.K., Glorieux, F.H., Kanis, J.A., Malluche, H., Meunier, P.J., Ott, S.M., Recker, R.R., 1987. Bone histomorphometry: standardization of nomenclature, symbols, and units. Report of the ASBMR Histomorphometry Nomenclature Committee. *J. Bone Miner. Res. Off. J. Am. Soc. Bone Miner. Res.* 2, 595–610. <https://doi.org/10.1002/jbmr.5650020617>
- Peterson, J., Dechow, P.C., 2002. Material properties of the inner and outer cortical tables of the human parietal bone. *Anat. Rec.* 268, 7–15. <https://doi.org/10.1002/ar.10131>
- Pothuau, L., Benhamou, C.L., Porion, P., Lespessailles, E., Harba, R., Levitz, P., 2000. Fractal Dimension of Trabecular Bone Projection Texture Is Related to Three-Dimensional Microarchitecture. *J. Bone Miner. Res.* 15, 691–699. <https://doi.org/10.1359/jbmr.2000.15.4.691>
- Reisinger, A.G., Pahr, D.H., Zysset, P.K., 2011. Principal stiffness orientation and degree of anisotropy of human osteons based on nanoindentation in three distinct planes. *J. Mech. Behav. Biomed. Mater., Special Issue Soft Tissues* 4, 2113–2127. <https://doi.org/10.1016/j.jmbbm.2011.07.010>
- Roberts, J.C., Merkle, A.C., Carneal, C.M., Voo, L.M., Johannes, M.S., Paulson, J.M., Tankard, S., Uy, O.M., 2013. Development of a Human Cranial Bone Surrogate for Impact Studies. *Front. Bioeng. Biotechnol.* 1. <https://doi.org/10.3389/fbioe.2013.00013>
- Sahoo, D., Deck, C., Willinger, R., 2014. Development and validation of an advanced anisotropic visco-hyperelastic human brain FE model. *J. Mech. Behav. Biomed. Mater., Forensic Biomechanics* 33, 24–42. <https://doi.org/10.1016/j.jmbbm.2013.08.022>
- Salmon, P., 2020. Application of Bone Morphometry and Densitometry by X-Ray Micro-CT to Bone Disease Models and Phenotypes, in: Orhan, K. (Ed.), *Micro-Computed Tomography (Micro-CT) in Medicine and Engineering*. Springer International Publishing, Cham, pp. 49–75. https://doi.org/10.1007/978-3-030-16641-0_5
- Salmon, P., 2009. MORPHOMETRIC PARAMETERS IN CT_ANALYSER 36.
- Salmon, P.L., Ohlsson, C., Shefelbine, S.J., Doube, M., 2015. Structure Model Index Does Not Measure Rods and Plates in Trabecular Bone. *Front. Endocrinol.* 6. <https://doi.org/10.3389/fendo.2015.00162>
- Schweizer, S., Hattendorf, B., Schneider, P., Aeschlimann, B., Gauckler, L., Müller, R., Günther, D., 2007. Preparation and characterization of calibration standards for bone density determination by micro-computed tomography. *Analyst* 132, 1040–1045. <https://doi.org/10.1039/B703220J>

Takhounts, E.G., Ridella, S.A., Hasija, V., Tannous, R.E., Campbell, J.Q., Malone, D., Danelson, K., Stitzel, J., Rowson, S., Duma, S., 2008. Investigation of traumatic brain injuries using the next generation of simulated injury monitor (SIMon) finite element head model. *Stapp Car Crash J.* 52, 1–31.

Thavarajah, R., Mudimbaimannar, V.K., Elizabeth, J., Rao, U.K., Ranganathan, K., 2012. Chemical and physical basics of routine formaldehyde fixation. *J. Oral Maxillofac. Pathol. JOMFP* 16, 400–405. <https://doi.org/10.4103/0973-029X.102496>

Tivesten, A., Movérare-Skrtic, S., Chagin, A., Venken, K., Salmon, P., Vanderschueren, D., Sävendahl, L., Holmång, A., Ohlsson, C., 2004. Additive protective effects of estrogen and androgen treatment on trabecular bone in ovariectomized rats. *J. Bone Miner. Res. Off. J. Am. Soc. Bone Miner. Res.* 19, 1833–1839. <https://doi.org/10.1359/JBMR.040819>

Topp, T., Müller, T., Huss, S., Kann, P.H., Weihe, E., Ruchholtz, S., Zettl, R.P., 2012. Embalmed and fresh frozen human bones in orthopedic cadaveric studies: which bone is authentic and feasible? *Acta Orthop.* 83, 543–547. <https://doi.org/10.3109/17453674.2012.727079>

U.S National Library of Medicine, 2000. Department of Health and Human Services: Visible Human Database.

Van Dessel, J., Nicolielo, L.F.P., Huang, Y., Slagmolen, P., Politis, C., Lambrichts, I., Jacobs, R., 2016. Quantification of bone quality using different cone beam computed tomography devices: Accuracy assessment for edentulous human mandibles. *Eur. J. Oral Implantol.* 9, 411–424.

Wu, Y., Adeeb, S., Doschak, M.R., 2015. Using Micro-CT Derived Bone Microarchitecture to Analyze Bone Stiffness – A Case Study on Osteoporosis Rat Bone. *Front. Endocrinol.* 6. <https://doi.org/10.3389/fendo.2015.00080>

Zebaze, R.M., Ghasem-Zadeh, A., Bohte, A., Iuliano-Burns, S., Mirams, M., Price, R.I., Mackie, E.J., Seeman, E., 2010. Intracortical remodelling and porosity in the distal radius and post-mortem femurs of women: a cross-sectional study. *The Lancet* 375, 1729–1736. [https://doi.org/10.1016/S0140-6736\(10\)60320-](https://doi.org/10.1016/S0140-6736(10)60320-)

Chapter 2: The Effect of Morphometric and Geometric Indices of The Human Calvarium On Mechanical Response.

In Chapter 2, the mechanical response of the human calvarium was quantified under 4-point quasi-static bending conditions. Subsequently, Chapter 2 identified which morphometric and geometric properties derived from Chapter 1 were significant predictors or influencers of the calvarium's mechanical response. Determining this established the structure-function relationship of the calvarium and established the key predictors or influencers of mechanical response so that physical and computational modellers of the calvarium could integrate the select predictors within their model to achieve the desired response. In addition, the mechanical response of the 4-point bending tests was used for comparison against the surrogate prototypes, and the cortical layers' thicknesses, diploë thickness and inner and outer radius of curvature were determined to assist with the geometrical construction of the surrogate prototypes. The findings of this chapter fulfill *sub-objective 2: Determine which morphometric and geometric properties have a significant influence on the mechanical response of human calvarium during 4-point quasi-static bending*. Chapter 2 is under review for publication in *Clinical Biomechanics*.

The Effect of Morphometric and Geometric Indices of The Human Calvarium On Mechanical Response

ABSTRACT

When developing a surrogate model of the human skull, there is a multitude of complex morphometric and geometric properties that one may choose from to include within their model. To simplify this approach, it is important to identify only the properties that have a significant influence on the mechanical response of the skull. The objective of this study was to identify which morphometric and geometric properties of the human calvarium were significant predictors of mechanical response. A significant predictor was defined as a morphometric or geometric property that was associated with a statistically significant univariate linear regression model to predict mechanical response. Calvarium specimens (N=24) from male and female human cadavers were micro-computed tomography (μ CT) scanned at a resolution of 18 μ m to determine morphometric and geometric properties. The specimens were assumed to be Euler-Bernoulli beams and were subject to 4-point quasi-static bending (2 mm/min) to determine mechanical response. Linear regressions were performed with Bonferroni adjustments, the morphometric and geometric properties were independent or predictor variables and the mechanical response variables were dependent or outcome variables. Nine significant linear regression models ($p < 0.05$) were established, they included output variables of either force and bending moment at the occurrence of fracture, compressive modulus, and tensile strain rate. In the diploë, the trabecular bone pattern factor was the single significant predictor of mechanical response. The inner cortical table of the calvarium had more significant predictors (inner cortical thickness, inner cortical tissue mineral density, and inner cortical porosity) compared to the outer cortical table and diploë. The morphometric and geometric properties that have a key influence on mechanical response were

established. These properties can aid the design of surrogate models of the skull that seek to mimic its mechanical response during simulated head impacts.

Keywords: Human Calvaria; Morphometry; Mechanical Response, Predictive Capabilities, Micro-CT

1. INTRODUCTION

1.1 Problem statement

Head injury models are employed when studying the injury biomechanics of the human head during the reconstruction of civilian activities such as falls and automobile collisions (Fahlstedt et al. 2021; Hubbard and McLeod 1974; Li et al. 2021). Head models are of particular significance in helmet testing to make inferences on their protective capabilities against head and brain injuries (Adanty, Clark, et al. 2020; Rowson, Rowson, and Duma 2015; Azar et al. 2019). Head injury models can be represented as either a simple or multifaceted physical surrogate and/or computational head model (Ghajari, Hellyer, and Sharp 2017; Hubbard and McLeod 1974; Mao et al. 2013). As we continue to structurally advance head models, we must consider whether the morphometric variability of the human head influences the mechanical response of the head leading to injury (Adanty et al. 2021). Identifying the relevant morphometric indices that demonstrate robust relationships and predictive capabilities on mechanical response can guide our approach to designing surrogate and computational models to effectively enhance biofidelity and model injury. The human skull is the first line of defence when a human is met with a direct impact to the head to protect the brain, therefore, as a first step, it is sensible to investigate the relationship between the skull's morphometry and mechanical properties before exploring the complex intricacies of the brain.

The calvarium is a distinct structure of the human skull that is structurally composed of flat bones to protect the brain against direct contact from a head impact (Anderson, Kortz, and Al Kharazi 2021). What further defines the distinct composition of the calvarium is its three-layered sandwich structure that consists of two thin cortical bone layers (outer table and inner table) separated by a thick diploë layer. The diploë comprises a random assembly of trabecular bone that

is separated with varying degrees of pore sizes. The cortical tables encompass a layer of dense bone, however, it is proven that the cortical tables have an average porosity between 3.2 to 13.7 %, and on average, porosity is greater in the inner table compared to the outer table (Adanty et al. 2021). Indeed, there is a vast array of properties that characterizes the morphometry within each distinct layer of the calvarium aside from porosity alone (Adanty et al. 2021). However, from a mechanical standpoint, it is unknown whether a subset of morphometric properties are significant predictors of mechanical response. Describing the effect calvarium morphometry has on mechanical response may help to explain the observed variation of modulus, stress, and strain values of crania reported between different studies (Hubbard 1971; Margulies and Thibault 2000; Delille et al. 2007; Motherway et al. 2009; Davis et al. 2012; Auperrin et al. 2014; Lee et al. 2019; Adanty et al. 2022; Zwirner et al. 2021). Furthermore, establishing the significant predictors of morphometry and mechanical properties can inform physical and computational modellers of the skull on which physical properties to prioritize when designing a skull model to simulate real-world head injuries in civilian activities, sports, and military scenarios (De Kegel et al. 2019; Adanty et al. 2021).

Studies that have investigated the correlation and regression between the morphometry of calvarium and its mechanical properties have limited their morphometric indices of interest to density and porosity. McElhaney et al. performed linear regression analyses of crania and reported coefficients of determination (R^2) between 0.60 and 0.65 between dry weight density and compressive properties such as strength and modulus (McElhaney et al. 1970). Motherway et al. established a modest correlation between percent bone volume and both elastic modulus and maximum stress for crania in three-point bending (Motherway et al. 2009). However, a correlation analysis is limited in its interpretation since the statistical test only establishes if a linear association

exists between variables. It cannot describe the effect, or the variation one variable can explain for another, and it cannot provide an equation or model to predict mechanical response. The calvarium is a relatively complex structure and its morphometry can be quantified by more than just density and porosity. Trabecular thickness (Tb.Th), trabecular separation (Tb.Sp), and trabecular bone pattern factor (Tb.Pf) are a few out of many morphometric properties that describe the microarchitecture of diploë (Adanty et al. 2021; Salmon 2020). Adanty et al. established regression models of diploë morphometry (density, porosity, Tb.Th, Tb.Sp, and trabecular number (Tb.N)) and mechanical measurements (force and strain at fracture) (Adanty, Tronchin, et al. 2020). Their regression models yielded non-significant R^2 values of 0.30 to 0.42. While a limited set of diploë morphometry and mechanical properties were explored by Adanty et al., there remains an immense list of diploë and cortical morphometry in which their effect on mechanical response has not been established. Thus, the current study presents a deeper investigation by which univariate linear regression models for additional morphometric and geometric properties and mechanical variables were determined.

1.2 Purpose and relevance of this study

This work applied univariate linear regression analyses to determine which morphometric and geometrical properties from the diploë and cortical layers of the calvarium were significant predictors of mechanical response during quasi-static 4-point bending. Quantifying the predictive capabilities of morphometry and geometry on mechanical response can influence one's approach to designing a surrogate or computational model of the skull. In other words, if one has knowledge that porosity and Tb.Th of the diploë are key influencers or significant predictors of stress at skull fracture, then one would tailor the construction of their model according to those morphometric

properties that matter. The null hypothesis tested per linear regression test was that *the coefficient of the slope for the linear regression model was equal to 0.*

2. MATERIALS AND METHODS

All the methods and protocols that pertained to this study were approved by the University of Alberta Research Ethics Board (ID: Pro00089218). All the human specimens collected for this study originated from individuals (85.8 ± 9.0 years old) registered in the University of Alberta Anatomical Gift Program. Each individual was screened for pre-existing bone pathologies to ensure there were no pathological factors that could affect the results.

A full comprehensive description of the method for the extraction of specimens (described in *section 2.1*), the μ CT scanning of human calvaria (described in *section 2.2*), and how each diploë and cortical morphometric property was computed (described in *section 2.3*) can be read in a previous report (Adanty et al. 2021).

2.1 The Specimens

The present study was allocated 24 embalmed human cadavers by the University of Alberta's Division of Anatomy. Of those 24 cadavers, 13 were male (83.6 ± 9.0 years old) and 11 were female (88.4 ± 9.0 years old) subjects. A Mopec autopsy saw was used to sever one beam-shaped specimen from the frontal or parietal region of the cadavers' calvarium (N=24) (Figure 1) (Adanty et al. 2021). The frontal specimens were acquired by marking a point approximately 1.5 cm inferior to the coronal suture and then tracing a rectangular beam model at that mark (55 mm in length and 8 mm in width) to cut and obtain the frontal specimen (Adanty et al. 2021) (Figure 1). The center of the squamosal suture was located and a point was marked approximately 1.5 cm superior to that suture to obtain the parietal specimens (Adanty et al. 2021). Some specimens were further cut along the y-axis-direction and x-axis-direction to ensure the width and length of the specimens were uniform across all specimens respectively (Adanty et al. 2021). The length (L), centre width (W), and centre thickness (T) of each specimen were measured using digital callipers (Figure 1b)

(Adanty et al. 2021). Table 1 summarizes the geometric properties of the specimens. Prior to testing, the specimens were stored at room temperature in unbuffered aqueous formaldehyde 37% embalming fluid, which is composed of 4% phenol, 4% formalin (37% concentration), 8% glycol, 8% ethyl alcohol (95% concentration), and 76% water to preserve hydration (Adanty et al. 2021).

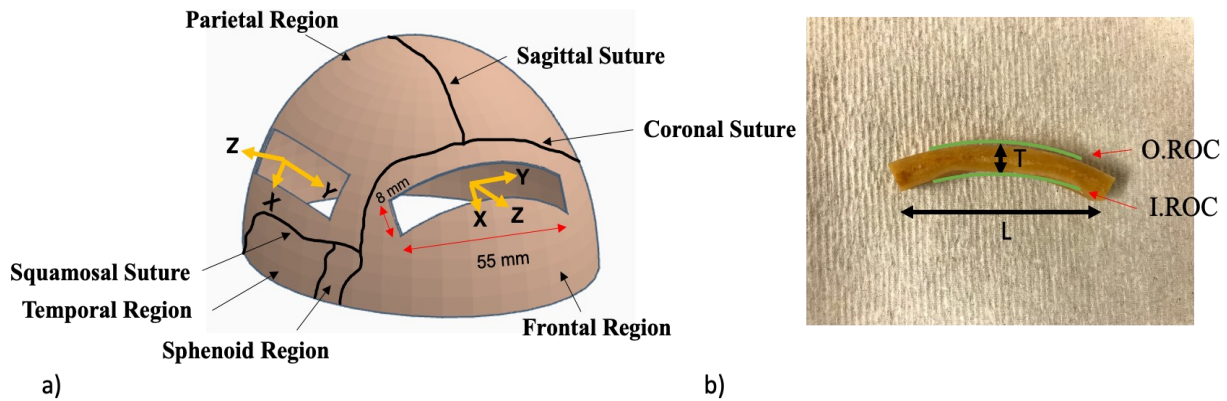


Figure 1. a) A simplified model of the human calvarium presenting the regions from which the frontal and parietal specimens were obtained. b) A human calvarium specimen, where L =length and T =thickness were measured at the center of the specimen. O.ROC=outer radius of curvature and I.ROC=inner radius of curvature was determined in Geomagic software (2014) by 3-Dimensional (3D) Systems (Rock Hill, South Carolina).

Table 1. The average geometrical properties of the specimens with 95% confidence intervals.

Geometric Properties	$I_x (m^4)$	$L (mm)$	$W (mm)$	$T (mm)$	$O.ROC (mm)$	$I.ROC (mm)$
Male Specimens (n=13)	1.95E-10 (1.12E-10, 2.78E-10)	55.69 (53.88, 57.50)	8.57 (8.38, 8.76)	6.27 (5.47, 7.06)	93.54 (72.54, 114.54)	83.46 (59.85, 107.08)
Female Specimens (n=11)	2.78E-10 (2.35E-11, 5.32E-10)	55.38 (53.48, 57.29)	8.75 (8.09, 9.41)	7.00 (5.49, 8.59)	72.08 (63.07, 81.09)	62.52 (51.85, 73.19)
Male & Female (N=24)	2.33E-10 (1.18E-10, 3.48E-10)	55.55 (54.34, 56.76)	8.65 (8.35, 8.95)	6.62 (5.84, 7.40)	83.70 (71.56, 95.85)	73.86 (60.38, 87.35)

N: total number of samples, n: number of samples per sex, I_x : second moment of inertia, L: length, W: width, T: thickness, O.ROC and I.ROC: outer cortical and inner cortical radius of curvature, respectively.

2.2 Micro-Computed Tomography (μ CT)

The specimens were separately loaded into a Bruker-Skyscan 1176 and μ CT scanned at a resolution of 18 μ m (Adanty et al. 2021). The resulting images from each scan were shadow projections (TIFF files) which were then reconstructed and filtered (Gaussian blur, radius=1) using NRecon (version 1.6.3.3, Bruker-Skyscan) to obtain 3D voxel slices in bitmap (BMP) file format (Figure 2) (Adanty et al. 2021). The BMP files for each specimen were loaded into BoneJ (an ImageJ plugin for bone image analysis) software (Doube et al. 2010) and was used to compute the second moment of inertia (I_x) (Table1) at a cross-section that was located approximately at the center of each specimen. The I_x computed in BoneJ was also verified using secondary software. (Computed Tomography (CT)-Analyzer, version 1.10, Bruker-Skyscan). The BMP files for each specimen were then converted into an STL file using Materialise MIMICS (Materialise NV 24.0).

These STL files were then uploaded into Geomagic software (2014) by 3-Dimensional (3D) Systems (Rock Hill, South Carolina) to determine the outer and inner cortical radius of curvature (O.ROC and I.ROC) (Figure 1b). The average second moment of inertia and ROC for the specimens are presented in Table 1.

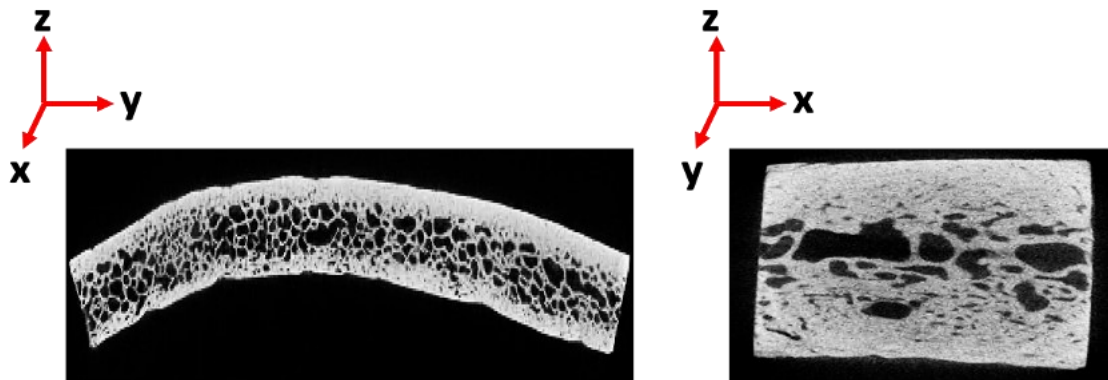


Figure 2. An example of a reconstructed μ CT BMP image at two different cross-sections for a calvarium specimen.

2.3 Morphometric and Geometrical Properties

The reconstructed images for each specimen were further processed in CT-Analyzer where segmentation (Figure 3) was performed to delineate the diploë layer and cortical tables (Adanty et al. 2021). The type of segmentation performed was manual contouring on a slice-by-slice base, this contour method was chosen to capture the irregular nature and non-uniform layers between each cross-section of the calvarium. To precisely delineate the diploë or the region of interest (ROI), an irregular anatomic contour adjacent to the inner surfaces of the inner and outer cortical tables was applied on the cross-section of a specimen (Bouxsein et al. 2010; Adanty et al. 2021). CT-Analyzer then performed semi-automated contouring for the remaining cross-sections by performing an extrapolation based on the first contour made. Each cross-section was reviewed by the operator to ensure the semi-automated contour properly outlined all areas of the ROI, in this case, the diploë. Once all the contours were reviewed by the operator, CT-Analyzer accumulated

all the ROIs to form a volume of interest (VOI) of the diploë (Figure 4). The irregular anatomic contour method was then applied to the inner and outer cortical tables (Figure 4). A global threshold was then applied to each VOI to differentiate non-bone voxels from bone voxels (Adanty et al. 2021). Outer cortical thickness, inner cortical thickness, and diploë thickness were measured in CT-Analyzer (Figure 4).

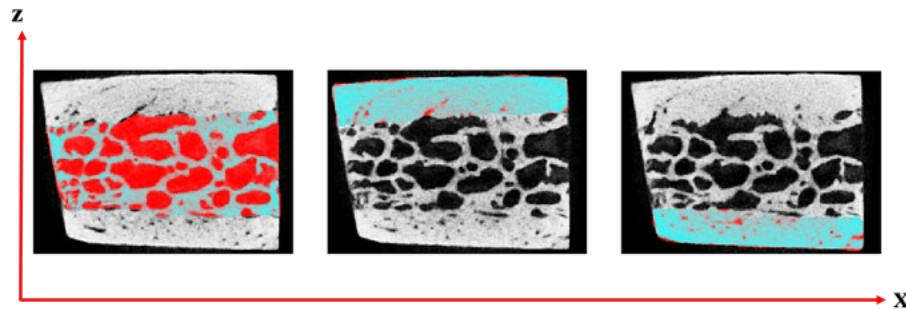


Figure 3. In this example of a reconstructed μ CT BMP cross-section, the ROI of the diploë is encapsulated with an irregular anatomic contour shown in red (left image). The irregular anatomic contour (in red) is also applied to the ROI on the outer cortical table (middle image) and inner cortical table (right image).

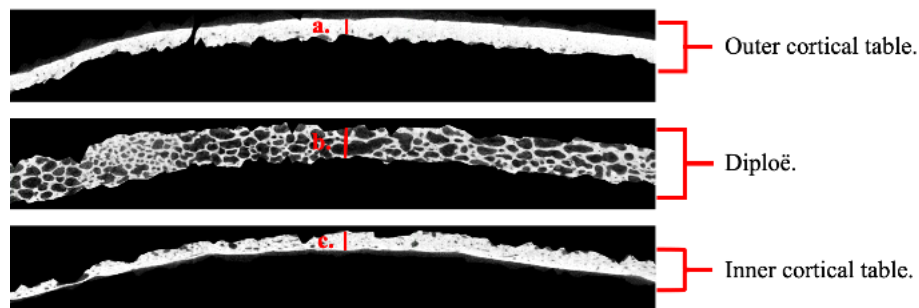


Figure 4. Reconstructed μ CT BMP images of the segmented layers for this calvarium. Top image: the VOI for a segmented outer cortical layer (note the possible vascular foramen perforating the outer cortical layer in this section). Middle image: the VOI for a segmented diploë. Bottom image: the VOI for a segmented inner cortical layer. At the approximate center of each layer, **a.** represents the outer cortical thickness, **b.** represents the diploë thickness, and **c.** represents the inner cortical thickness.

After segmentation and thresholding, morphometric and geometric properties were determined for the diploë, inner cortical, and outer cortical regions of each specimen in CT-Analyzer (Adanty et al. 2021). Table 2 presents a list of diploë morphometric properties that were used in this study for regression analyses along with a complete definition for each property. Initially, up to 8 morphometric parameters were determined for the diploë, however, an earlier pilot study revealed strong correlations between porosity and bone mineral density ($r=0.95$), Tb.N and Tb.Sp ($r=0.83$), fractal dimension and Tb.Sp ($r=0.71$) and fractal dimension and Tb.N ($r=0.70$). The consideration of morphometric parameters with strong correlations amongst one another would result in a repetition of statistical findings when performing regression analyses. Therefore, we reduced our final list of diploë morphometric properties to analyze in this study to those presented in Table 2 since these properties demonstrated correlations less than 0.70 which can be considered at the most moderate associations (Mukaka 2012). Nevertheless, a full description of the diploë morphometry that was excluded (fractal dimension, bone mineral density, and Tb.N) from this study's analysis can be found in a recent article (Adanty et al. 2021). Table 2 also presents a list of cortical morphometric and geometric properties that were determined in CT-Analyzer, though we did not find strong associations between these properties. All the morphometric and geometric properties were chosen in this study because they all quantify unique structures within the calvarium and have been quantified for the human skull in previous studies (Kim and Henkin 2015; Alexander et al. 2019; Boruah et al. 2015; Adanty et al. 2021).

Table 2. Diploë and cortical morphometric and geometric properties computed in this work. The properties here are defined in accordance with work by Adanty et al. (Adanty et al. 2021).

Diploë morphometric properties
Trabecular thickness (Tb.Th) (mm): <i>Defined as the mean thickness of trabeculae in the diploë.</i>
Trabecular separation (Tb.Sp) (mm): <i>Defined as the average separating distance between trabeculae in the diploë.</i>
Un-plate index (uPi): <i>A dimensionless parameter that typically falls between 1 and 2 (Adanty et al. 2021; Salmon 2020). Defined as the ratio of Tb.Th quantified in 3D to the Tb.Th quantified in 2D where an increasing uPi (towards 2) indicates trabeculae is departing from an ideal plate morphology to a rod morphology in the diploë.</i>
Porosity (%): <i>Defined as the ratio of closed pores and open pores volume to the total volume of the diploë.</i>
Trabecular bone pattern factor (Tb.Pf) (1/mm): <i>Defined as the trabecular connectivity or the ratio of convex to concave surface curvature of trabeculae in the diploë. A high connectivity and structural integrity of trabecular bone is indicated by greater concave surfaces (lower or negative values).</i>
Diploë thickness (mm) (Fig 4): <i>Defined as the distance from the top of the diploë to the bottom of the diploë at the approximate center of the calvaria.</i>
Cortical morphometry and geometric properties
Inner cortical thickness (mm) (Fig 4): <i>Defined as the thickness of the inner cortical layer at the approximate center of the calvaria.</i>
Outer cortical thickness (mm) (Fig 4): <i>Defined as the thickness of the outer cortical layer at the approximate center of the calvaria.</i>
Inner cortical tissue mineral density (TMD) (g HA/cm³): <i>Average density of the bone voxels exclusively in the inner cortical layer.</i>
Outer cortical tissue mineral density (TMD) (g HA/cm³): <i>Average density of the bone voxels exclusively in the outer cortical layer.</i>
Inner cortical porosity (%): <i>Ratio of closed and open pores volume to total volume in the inner cortical layer.</i>
Outer cortical porosity (%): <i>Ratio of closed and open pores volume to total volume in the outer cortical layer.</i>

2.4 The Preparation of Specimens for Mechanical Testing

Before mechanical testing, each specimen was attached with fiber Bragg gratings (FBGs) on the inner and outer cortical surfaces of the specimen to measure surface strain (Figure 5). All the FBGs in this study were manufactured by Technica Optical Components, LLC (Beijing, China). A single FBG of 1 mm in length was built into the core of a glass optical fiber (Figure 5). Tensile or compressive strain acting on the FBG can be quantified due to a relative change in the Bragg wavelength ($\Delta\lambda_B$) from the FBG (Dennison and Wild 2008; Dennison et al. 2010; Nelson et al. 1998). The light source that is supplied to an optical fiber with an FBG to record the $\Delta\lambda_B$ is called an optical sensing interrogator and the one used in this study was a MicronOptics (MO) Interrogator (SM130 Optical Sensing Interrogator, Micron Optics, Atlanta, USA). The acquisition rate for the MO interrogator was set at its maximum of 2 kHz, this was an adequate sampling rate to acquire the surface strain data in this study. The FBGs' strain or gauge factor to convert $\Delta\lambda_B$ to strain was 1.2 pm/ $\mu\epsilon$. FBGs have been employed in previous work to quantify surface strains of calvaria (Adanty et al. 2022). Additionally, FBGs were used to quantify periodontal ligament strains in *ex vivo* swine models (Houg et al. 2021) and to quantify force/stress and fluid pressure in intact cadaveric human hips (Dennison et al. 2010).

For the FBGs to remain bonded to the specimens' surfaces during testing, cyanoacrylate (Loctite® Instant Adhesive 401™) was used as an adhesive between the FBG and the specimens' surfaces. To accelerate the drying process of the cyanoacrylate, Scotch Tape (3M) was applied on the surface after applying the cyanoacrylate followed by 10-15 seconds of low heat at 100°F using a heat gun. To ensure the cyanoacrylate was fully cured for proper adhesion between the FBGs and specimens' surfaces, the cyanoacrylate was allowed to dry for no more than 10 hours at room temperature. The scotch tape was then removed from the surface of the specimen for mechanical

testing to immediately commence. Adhesives such as cyanoacrylate or epoxy have been shown to not affect the sensitivity of FBGs when measuring strain (Tian et al. 2019).

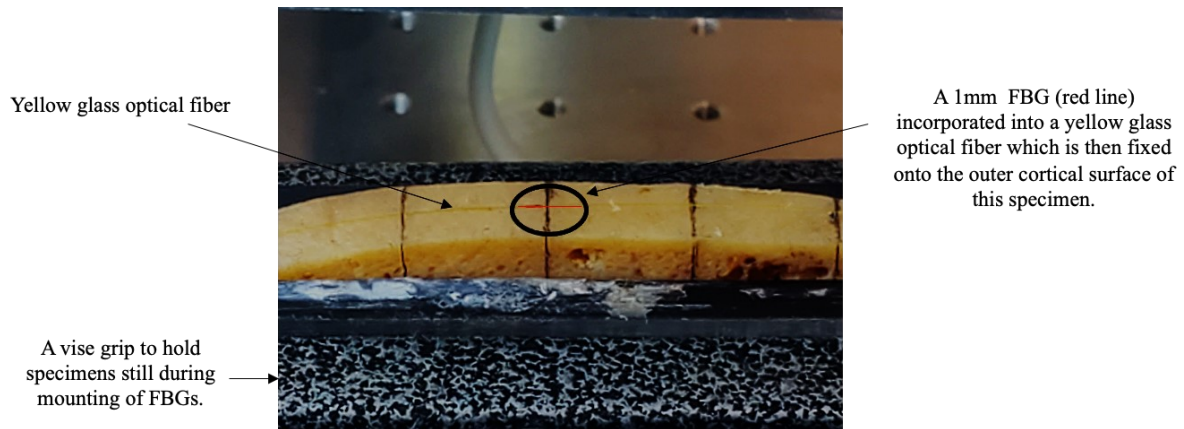


Figure 5. An example of a calvarium implemented with an FBG on its outer cortical surface. Note the red line representing the FBG is enhanced for illustrative purposes.

2.5 Mechanical Testing: 4-Point Quasi-Static Bending Testing

The specimens fitted with the FBGs were then placed in an Instron E3000 (ElectroPuls E3000 Test Instrument) to perform 4-point quasi-static bending until fracture (Figures 6 and 7). The 4-point bending arrangement generates a pure bending mode at the mid-region of the specimens with minimal shear stress, thus this bending arrangement was selected for this study. In addition, the specimens were not horizontally constrained on the bottom supports of the Instron to reduce any possibility of horizontal shearing effects within the specimen. The custom inner fixtures (Figure 6) were adjusted along the vertical direction to compensate for the naturally uneven surface of the calvaria. This allowed both inner fixtures to rest equally on the specimen so that forces delivered to the calvaria were evenly applied. All tests were displacement controlled at 2 mm/min until fracture. The moment of specimen fracture was established at the peak force endured by the specimen immediately before the instant halting of the Instron.

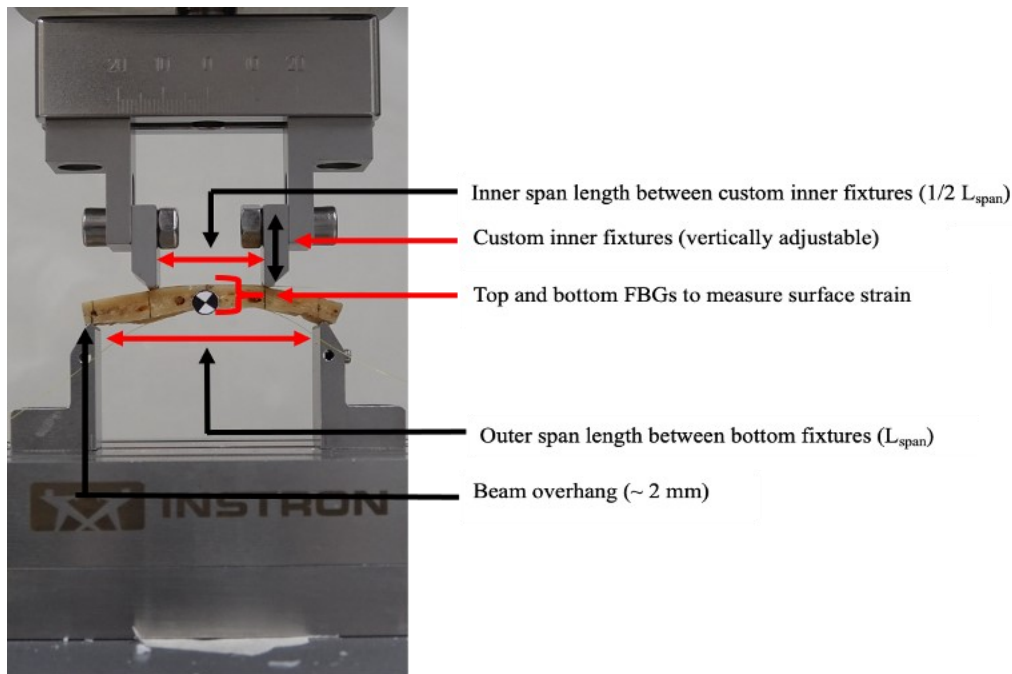


Figure 6. An example of a calvarium specimen in the Instron E3000 for quasi-static 4-point bending. All specimens were positioned such that the inner cortical table was in contact with the bottom fixtures.

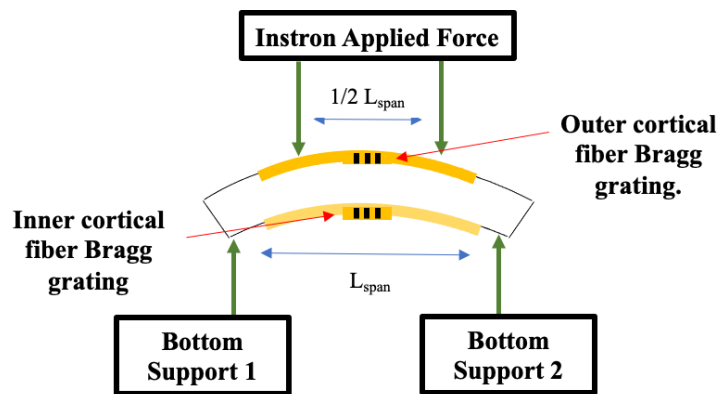


Figure 7. A 2D diagram of the known forces acting on the specimen during quasi-static 4-point bending. The outer cortical FBG quantifies the outer cortical surface strain (compressive strain) and the inner cortical FBG quantifies the inner cortical surface strain (tensile strain).

2.6 Mechanical Response Variables

The mechanical response variables determined in this study were 1) force at fracture (N)-defined as the force at the instance of fracture, 2) bending moment at fracture (N.m)-defined as the bending moment at the instance of fracture, and 3-4) tensile (inner cortical) and compressive (outer cortical)

surface strain rate (s^{-1})- the FBGs sensed a fairly linear strain-time association through the duration of the test, therefore the slope at the initial linear portion of the strain-time plot was used to compute strain rate (Figure 8), 5-6) the inner cortical and outer cortical surface strain at fracture (%)-defined as the surface strain at the instance of fracture, 7-8) tensile (inner cortical) and compressive (outer cortical) bending stress at fracture (MPa)-defined as the bending stress at the instance of fracture (Figure 9), and 9-10) tensile (inner cortical) and compressive (outer cortical) effective bending modulus (GPa)-defined as the slope of the stress-strain plot (Figure 10) that corresponds to the interval of strain used to compute strain-rate (Figure 8). In Figure 9, the centroid was computed in BoneJ when determining I_x . *Effective* implies that the modulus was a bulk estimate assuming the composite structure of the calvarium to be uniform. Each specimen was assumed to be a Euler-Bernoulli beam to apply the Euler-Bernoulli theorem. The Euler-Bernoulli beam theorem was used to approximate the bending stress of the calvaria (equation 1) (Roark, Young, and Budynas 2002).

The variables were chosen to characterize mechanical response at fracture and before fracture (bending modulus and strain rate). For the 4-point bending of the calvarium in quasi-static loading, most of the mechanical response variables mentioned have not been quantified for the inner and outer surfaces of the calvarium in the literature (Adanty et al. 2022). All these measurements can be relevant when taking a step-by-step approach to validate a physical or computational surrogate model of the calvarium.

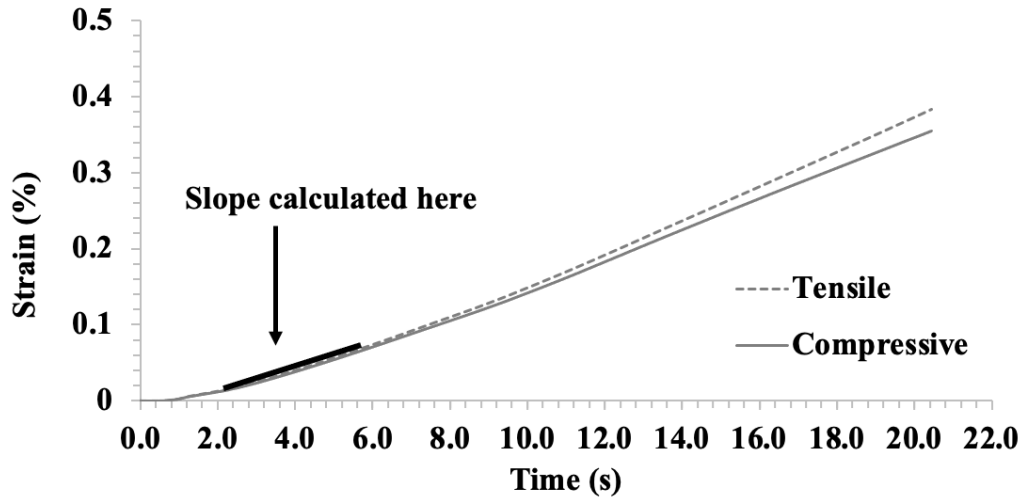


Figure 8. Tensile and compressive strain rate was determined as the initial linear portion of the strain-time plot.

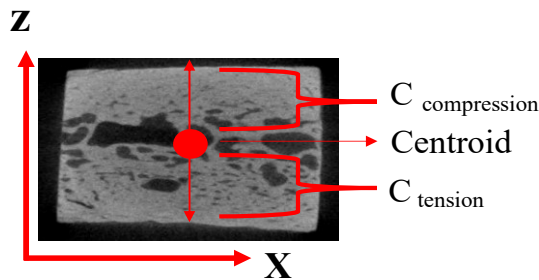


Figure 9. A cross-section of a calvaria specimen annotated with parameters required to compute bending stress (equations 1).

$$\sigma_{tensile\ or\ compressive} = \frac{M(C_{tension\ or\ compression})}{I_x} \quad (1)$$

Where, σ = Stress (Pa)
 M = Bending moment (N.m)
 I_x = Second moment of inertia (m^4)
 $C_{tension\ or\ compression}$ = Distance from centroid to the inner cortical surface or outer cortical surface (m)

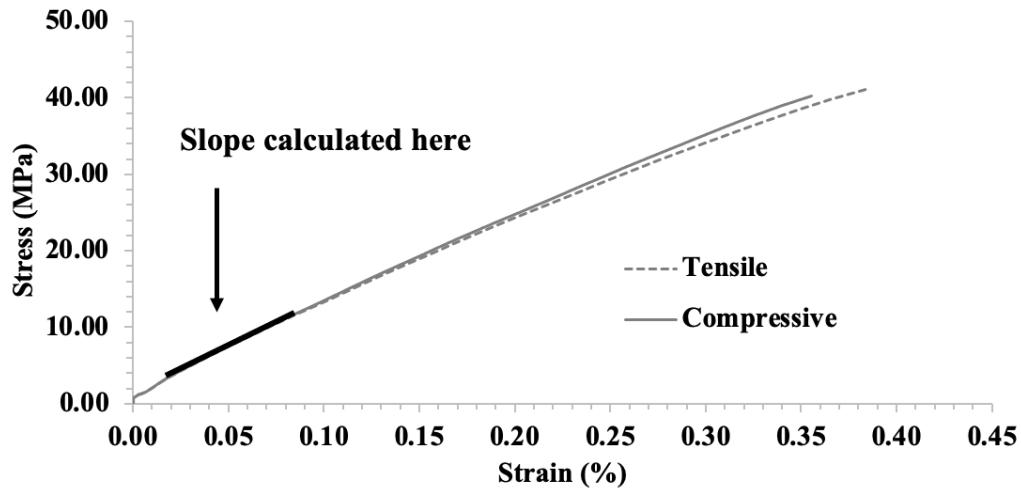


Figure 10. Tensile and compressive effective bending modulus was determined as the initial linear slope of the stress-strain plot.

2.7 Statistical Analysis

A univariate linear regression analysis was considered to study the relationship and influence of morphometric and geometric properties on mechanical response. A regression infers if an independent variable has a significant effect on the dependent variable, it quantifies the effect or the variation the dependent variable can be explained by the independent variable, and it provides a linear model or equation that includes the independent variable to estimate or predict the dependent variable (Laerd Statistics 2015).

The independent variables or predictor variables (6) were: Tb.Th, Tb.Sp, uPi, porosity, Tb.Pf, and diploë thickness for the diploë morphometry and geometry. Inner cortical thickness, outer cortical thickness, inner cortical TMD, outer cortical TMD, inner cortical porosity, and outer cortical porosity were the independent variables (6) for the cortical morphometry and geometry. The dependent variables (10) were inner cortical surface strain and outer cortical surface strain at fracture, force and bending moment at fracture, tensile and compressive stress at fracture, tensile and compressive effective bending modulus, and tensile and compressive strain rate. A multivariable regression analysis that would include region, sex, or multiple independent variables

was not considered since a sample size estimation (for a power of 0.8) of 43 was required which was not possible to obtain in this study (Milton 1986). In a similar manner, a step-wise linear regression that can sequentially add or remove predictor variables to yield a significant predictive model was not considered since it too requires a sufficient sample size in order to accommodate two or more predictor variables. Therefore, given the number of cranial tissue samples that were available for this study, the linear regression analysis was the appropriate statistical method chosen. Regardless of region and sex, the samples were pooled together to perform the linear regression analysis. The statistical significance for each model was reported with the alpha level set at 0.05. R^2 and adjusted R^2 were reported for each regression model, these coefficients represent the proportion of variances in each dependent variable that can be explained by the independent variable for the sample and population respectively. A significant predictor variable was defined as a morphometric or geometric property that was associated with a statistically significant linear regression model to predict mechanical response. To decrease the risk of making a Type 1 error since we carried out a series of linear regression analyses for the independent variables in the diploë (6), we performed a Bonferroni correction where we adjusted the resulting p-values for each statistical model by multiplying it by 6 since there were 6 diploë independent variables. However, for the cortical morphometry, we adjusted the resulting p-value by multiplying it by 3 since the inner cortical and outer cortical layers' morphometry were independent of each other. All statistical analyses were carried out using IBM SPSS version 25 (IBM Inc., Armonk, NY, USA).

3. RESULTS

Nine statistically significant linear regression models to predict mechanical response were determined (Table 3). Five morphometric or geometric properties were significant predictors of mechanical response (Table 3). Each significant model was graphically represented as a scatterplot that included regression-fitted lines with their respective 95% confidence intervals or bands (Figures 11a and 11b). In addition, we reported on the means for all morphometric and geometric properties and mechanical response variables in Table 4. Tb.Pf was the single diploë morphometry that was a significant predictor of force and bending moment at fracture. Out of all the morphometric and geometrical properties presented in this study, the linear regression model for Tb.Pf had the greatest adjusted R^2 , which was 0.53 for force and bending moment at fracture. The inner cortical layer had 3 significant predictors (inner cortical thickness, inner cortical tissue mineral density, and inner cortical porosity) of mechanical response with 4 significant linear regression models. The diploë had 1 significant predictor (Tb.Pf) with 2 significant linear regression models and the outer cortical layer had 1 significant predictor (outer cortical TMD) and 3 significant linear regression models.

Table 3. Linear regression models for significant ($p<0.05$) predictors of mechanical response.

Linear regression model equation	95% CI of the slope for the linear regression model	Bonferroni adjusted p-values	F-values	R² values and adjusted R² values
Force at fracture = 17.04 - 31.70*(Tb.Pf)	-19.02, -44.38	p<0.001	26.90	0.55 and 0.53
Bending moment at fracture = 0.30-0.18*(Tb.Pf)	-0.11, -0.25	p<0.001	26.85	0.55 and 0.53
Force at fracture = 1.04E2+1.72E2*(Inner cortical thickness)	63.21, 280.60	p=0.009	10.76	0.33 and 0.30
Bending moment at fracture = 0.87+0.89*(Inner cortical thickness)	0.27, 1.52	p=0.021	8.91	0.29 and 0.26
Compressive modulus = -38.07+50.36*(Inner cortical TMD)	22.52, 78.20	p=0.003	14.08	0.39 and 0.36
Force at fracture = 3.73E3-3.27E3*(Outer cortical TMD)	-1091.63, -5438.63	p=0.015	9.71	0.31 and 0.28
Bending moment at fracture = 20.59-17.83*(Outer cortical TMD)	-5.67, -29.99	p=0.018	9.25	0.30 and 0.26
Compressive modulus = -30.31+40.68*(Outer cortical TMD)	11.18, 70.18	p=0.027	8.18	0.27 and 0.24
Tensile strain rate = 6.96E-5+1.59E-5*(Inner cortical porosity)	6.00E-6, 2.60E-5	p=0.012	10.26	0.32 and 0.29

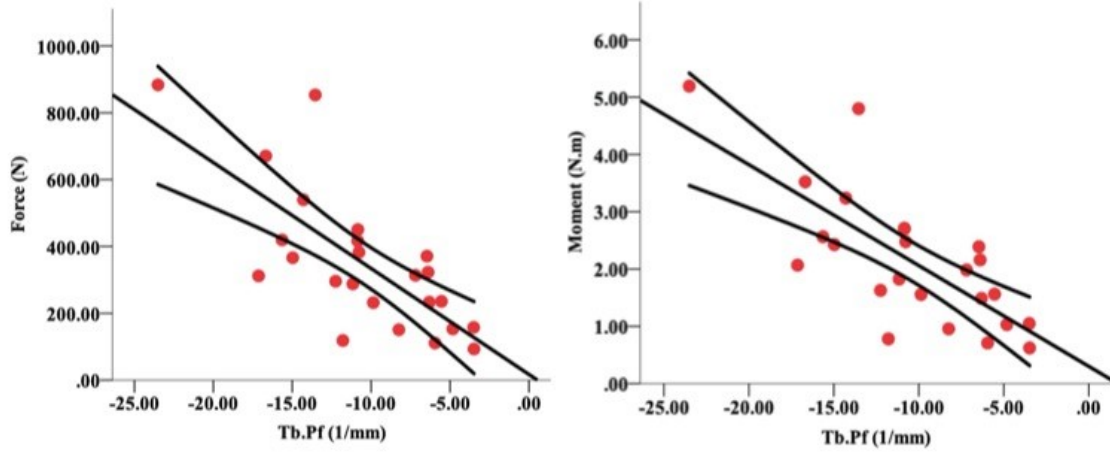


Figure 11 a). Scatterplots with linear regression fitted lines and 95% CIs (two curved lines) for Tb.Pf. The 95% CI indicates that there is a 95% probability that the true or population regression line is within the confidence bands.

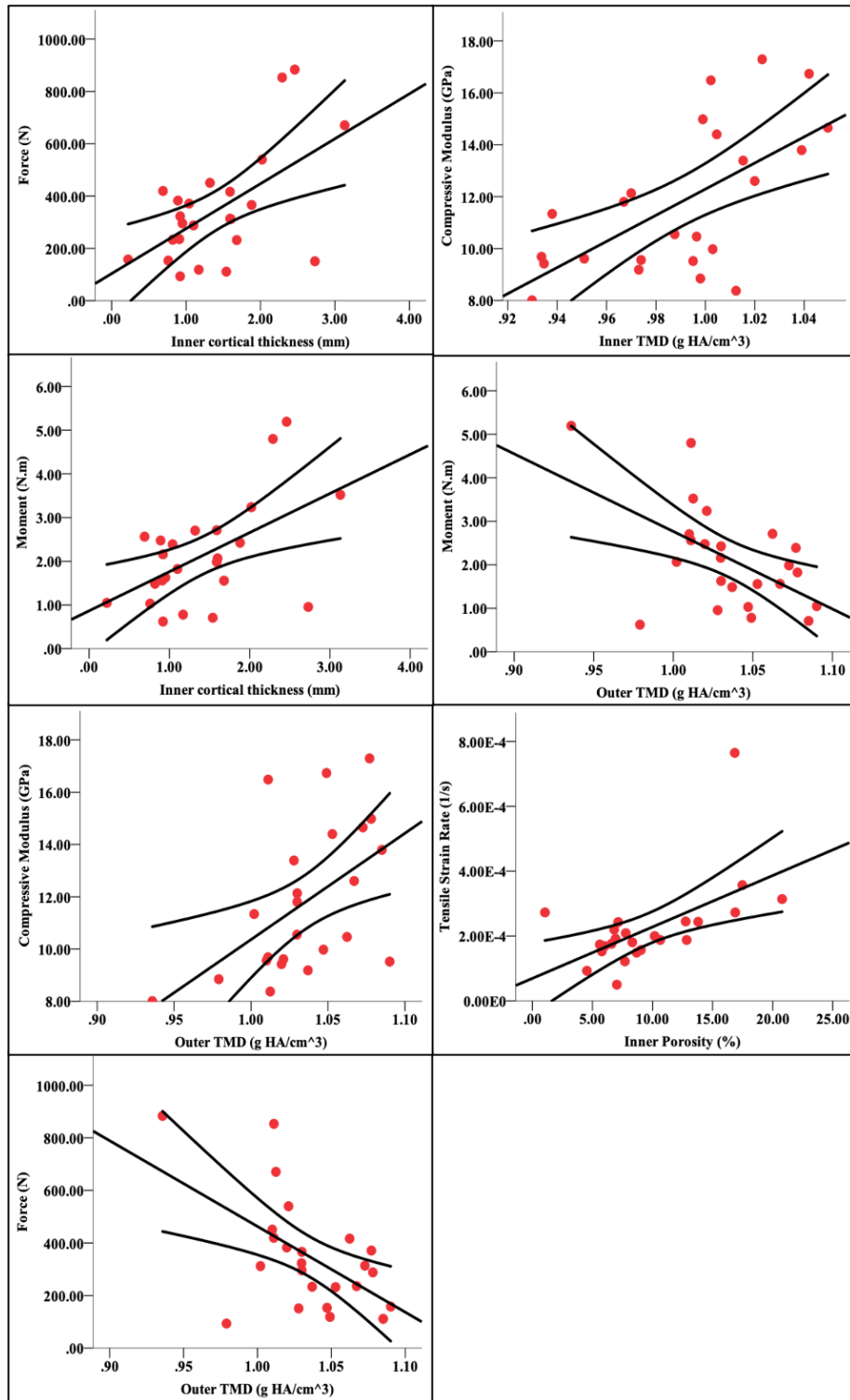


Figure 11 b). Scatterplots with linear regression fitted lines and 95% CIs (two curved lines) for cortical morphometry and geometric properties. The 95% CI indicates that there is a 95% probability that the true or population regression line is within the confidence bands.

Table 4. The means for all morphometric and geometric properties and mechanical response variables.

Morphometric and geometrical properties	Mean and 95% CIs
Tb.Th (mm)	0.26 ± 0.05 and 0.24, 0.29
Tb.Sp (mm)	0.62 ± 0.05 and 0.55, 0.69
uPi	1.61 ± 0.16 and 1.54, 1.67
Diploë Porosity (%)	55.79 ± 10.93 and 51.17, 60.41
Tb.Pf (1/mm)	-10.47 ± 4.98 and -12.57, -8.36
Diploë Thickness (mm)	3.82 ± 1.72 and 3.09, 4.54
Inner cortical thickness (mm)	1.43 ± 0.71 and 1.13, 1.73
Outer cortical thickness (mm)	1.62 ± 0.50 and 1.41, 1.84
Inner cortical TMD (g HA/cm ³)	0.99 ± 0.03 and 0.98 to 1.00
Outer cortical TMD (g HA/cm ³)	1.03 ± 0.04 and 1.02 to 1.05
Inner cortical porosity (%)	9.63 ± 4.76 and 7.62 to 11.64
Outer cortical porosity (%)	5.19 ± 2.60 and 4.09 to 6.29
Mechanical response variables	Mean and 95% CIs
Inner cortical surface strain at fracture (%)	0.38 ± 0.20 and 0.30, 0.46
Outer cortical surface strain at fracture (%)	0.32 ± 0.11 and 0.27, 0.37
Force at fracture (N)	348.79 ± 212.77 and 258.94, 438.63
Bending moment at fracture (N.m)	2.14 ± 1.18 and 1.64, 2.64
Tensile stress at fracture (MPa)	38.53 ± 12.52 and 33.24, 43.82
Compressive stress at fracture (MPa)	37.39 ± 13.00 and 32.01, 42.96
Tensile effective bending modulus (GPa)	11.15 ± 3.57 and 9.64, 12.66
Compressive effective bending modulus (GPa)	11.78 ± 2.82 and 10.59, 12.93
Tensile strain rate (s ⁻¹)	2.20E-4 ± 1.34E-4 and 1.7E-4, 2.8E-4
Compressive strain rate (s ⁻¹)	1.80E-4 ± 5.4E-5 and 1.6E-4, 2.0E-4

4. DISCUSSION

The present study identified which diploë and cortical morphometric properties were significant predictors of the mechanical response of calvaria subjected to quasi-static 4-point bending. Tb.Pf was the significant predictor of force and bending moment at fracture in the diploë. Inner and outer cortical morphometric and geometric properties were significant predictors of force and bending moment at fracture, strain rate, and effective bending modulus.

The mechanical response reported in Table 4 is briefly compared to previous studies that also performed bending on calvaria. The tensile (38.53 MPa) and compressive (37.39 MPa) stress in the present study is close to Lee et al.'s average bending stress on calvaria (42 and 53 MPa) (Lee et al. 2019). However, the present study's stress response is noticeably less compared to Motherway et al.'s (82.13 to 133.61 MPa) and Zwirner et al.'s (98 to 130 MPa) bending stress but slightly greater compared to Adanty et al.'s findings (23.34 to 30.45 MPa) (Motherway et al. 2009; Zwirner et al. 2021; Adanty et al. 2022). For effective bending modulus, the present study's findings (average tensile: 11.15 GPa and average compressive: 11.78 GPa) are comparable with Hubbard's bending modulus of 9.69 GPa, Motherway et al.'s reported bending modulus (4.35 to 18.12 GPa) and Adanty et al.'s bending modulus (7.25 to 20.75 GPa) (Hubbard 1971; Motherway et al. 2009; Adanty et al. 2022). Delille et al., Auperrin et al., and Rahmoun et al. reported average bending moduli between 2.04 to 5.22 GPa at frontal and parietal regions of the calvarium which is lower than the present study's bending modulus (Delille et al. 2007; Auperrin et al. 2014; Rahmoun et al. 2014). In summary, the present study's stress and effective bending modulus are consistent with previous findings. Delille et al., Auperrin et al., Rahmoun et al. and Lee et al. performed 3-point quasi-static bending at a greater displacement rate (10 mm/min) than the present study which performed 4-point bending at 2 mm/min (Auperrin et al. 2014; Lee et al. 2019;

Rahmoun et al. 2014; Delille et al. 2007). Motherway et al. and Zwirner et al. performed 3-point dynamic impact bending at numerous dynamic rates while Adanty et al. performed 4-point dynamic impact bending (Motherway et al. 2009; Zwirner et al. 2021; Adanty et al. 2022). Hubbard performed both 3-point and 4-point quasi-static bending but did not report stress or modulus for 4-point bending (Hubbard 1971). Rather Hubbard's average bending moment (3.08 N.m) and strain at fracture (0.51 %) in 4-point bending are consistent with the present study's results. The various types of loading (3-point and 4-point bending), loading rates (quasi-static and dynamic), the loading mass, specimen morphology, age, and specimen treatment (fresh, fresh-frozen and embalmed) are all factors that can contribute to the slight differences in mechanical response across the present study and previous findings.

4.1 Diploë morphometry and mechanical response

Tb.Pf is a morphometric property quantifying the connectivity of trabeculae in the diploë volume (Hahn et al. 1992). Hahn and colleagues were the first group to develop this histomorphometric parameter which was measured in the iliac crest of 192 human subjects (Hahn et al. 1992). A high connectivity of trabeculae is characterized by a high number of concave surfaces of trabeculae creating a well-connected porous lattice (Hahn et al. 1992). However, a high number of secluded trabeculae results in a low and poor connectivity between trabeculae and convex surfaces of the trabeculae (Hahn et al. 1992). Figure 12 supplements this explanation of Tb.Pf with an image scheme from Hahn et al.'s study (Hahn et al. 1992).

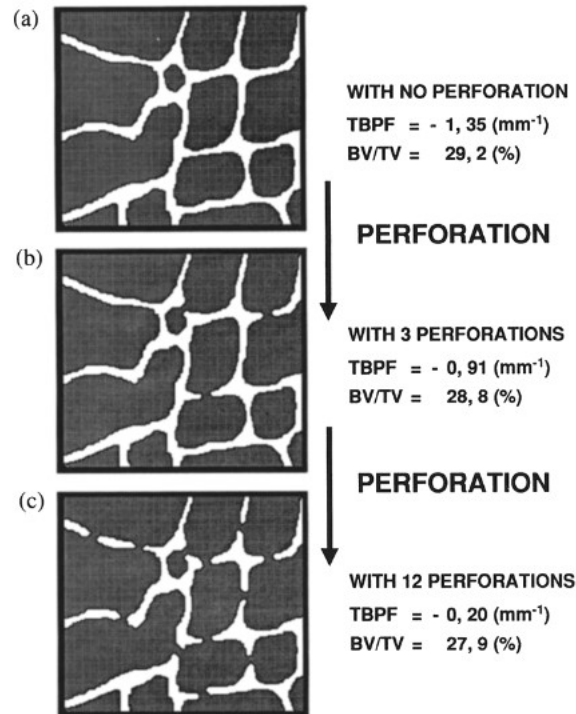


Figure 12. An image scheme reproduced from Hahn et al. to explain Tb.Pf. The highest connectivity in (a) has a Tb.Pf that is more negative or further left on the number line (-1.35 mm^{-1}) and the lowest connectivity in (c) has a Tb.Pf value that is less negative or further right on the number line (-0.20 mm^{-1})².

From the linear regression analyses, it was found that approximately 53 % of the variation for both force and bending moment at fracture was explained by Tb.Pf. Based on the description of Tb.Pf, this implies a high number of concave surfaces and thus well-connected trabeculae may considerably explain for greater force and bending moment at fracture (Hahn et al. 1992). Detailed calvarium surrogate models that wish to include a diploë should then consider the connectivity of trabeculae to assure forces and moments are aligned with that of the human calvaria. While the relationship between bone connectivity and force makes mechanical sense, the remaining morphometric variables of the diploë were not significant predictors of mechanical response. One

² Reprinted from Bone, Volume 13, M Hahn, M Vogel, M Pompesius-Kempa, G Delling, Trabecular Bone Pattern Factor-A New Parameter for Simple Quantification of Bone Microarchitecture, 372-330, Copyright (1992), with permission from Elsevier.

would presume a low porosity, thicker trabeculae-Tb.Th, and plate-like trabeculae-uPi for a porous structure would significantly explain the variation of the mechanical response of that structure. However, given the composite three-layered structure of calvarium, the diploë morphometry has competing morphometry from the surrounding cortical layers in affecting mechanical response as observed in this study. One can speculate that if the diploë were tested as an isolated structure, Tb.Th, Tb.Sp, porosity, and uPi may play a greater role in explaining the variance of mechanical response, however, additional studies are required to confirm this suggestion.

4.2 Cortical morphometry and mechanical response

According to Hubbard, since the inner cortical and outer cortical layers of the calvarium are stiffer and denser compared to the diploë, forces in the cortical layers are much greater during bending deformation compared to the diploë (Hubbard 1971). Theoretically, this inference is accurate because the stress in a beam is at its maximum on the outer surfaces of the beam during bending (surfaces of the inner cortical and outer cortical layers) and its minimum near the beam's neutral axis (located in the diploë) (Roark, Young, and Budynas 2002). With this understanding, the cortical layer morphometry was expected to have a greater number of significant predictors of mechanical response. Thirty percent and 26% of the variation for force and bending moment at fracture were dictated by inner cortical thickness, respectively. Thus, an increase in inner table thickness may estimate greater forces and bending moments at fracture. Hubbard performed quasi-static 4-point bending on 5 calvarium specimens, a proportional relationship between peak bending moments (2.03 to 3.42 N.m) and inner table thickness (1.27 to 1.73 mm) was observed (Hubbard 1971). TMD for the inner table and outer table explained 36 % and 24 % of the variation for the compressive effective bending modulus, respectively. The relationship between cranial density and modulus has been established in previous literature (McElhaney et al. 1970; Motherway et al.

2009). McElhaney et al. performed compression on cubed-shaped calvaria and then subsequent regression analyses between modulus of elasticity and dry weight density (McElhaney et al. 1970). They established significant linear and non-linear regression equations between modulus and density with moderate to strong R^2 s (0.62-0.86) (McElhaney et al. 1970). In addition, one study found that percentage bone volume, a proxy measure of density and porosity, to be directly proportional to elastic modulus (Motherway et al. 2009). Though, what distinguishes the previous findings from the present study's findings is that the latter identifies the cortical tables' densities to be the exclusive layers of the calvaria that are significant predictors of modulus as opposed to the density of the whole calvarium (all layers considered) (McElhaney et al. 1970; Motherway et al. 2009). Our finding may suggest that it is important for the cortical densities of layered calvarium models to closely match those of the human calvarium to achieve a desired modulus.

The present study found inner cortical porosity to be a significant predictor of tensile strain rate. Previous studies have demonstrated that an increase in porosity weakens the structural integrity of cranial tissue resulting in lower strength and modulus values (McElhaney et al. 1970; Motherway et al. 2009; Adanty, Tronchin, et al. 2020). Thus, the calvarium should deform at a faster rate with greater porosity, especially at the inner cortical layer. The findings of the present work demonstrate that the inner cortical table had the most significant predictors (thickness, TMD, and porosity) of mechanical response in this work. Conversely, outer cortical TMD was the single morphometry of the outer cortical layer to explain the variation of force at fracture (adjusted $R^2 = 0.28$), bending moment at fracture (adjusted $R^2 = 0.26$), and compressive effective modulus (adjusted $R^2 = 0.24$). Noteworthy here is that an increasing outer cortical TMD results in a decrease in force and bending moment at fracture (Figure 11 b). Indeed, this finding is challenging to explain given previous studies had noted an increase in cranial density to be significantly associated with

an increase in properties such as strength and modulus (McElhaney et al. 1970). As previously stated, the inner cortical table had the most predictors (thickness, TMD, and porosity) of mechanical response while the outer cortical layer had just one, TMD. From a theoretical aspect, beams that are typically loaded in bending experience fracture initiation and growth originating from the tensile surface (Roark, Young, and Budynas 2002; Mott and Untener 2018), which for the calvarium would be the surface of the inner cortical table. This notion may implicate why the inner cortical table had the most morphometric and geometric properties as significant predictors of mechanical response compared to the outer cortical table in this study. Yet, it is recommended that modellers of the calvarium not overlook the outer cortical TMD, if overall, they wish to obtain appropriate forces, moments, and compressive modulus during bending.

4.3 Limitations

The present work sampled the calvarium specimens by convenience, meaning the specimens obtained were the greatest number of samples available to perform this research. The human donors were restricted to an older age population who resided in one geographical province. Future work should maximize sample size by including samples from multiple age groups, and sampling across a greater geographical area to expand the generalization of the study's findings. The specimens were extracted from embalmed human donors; however, the effect embalming has on the mechanical response of cranial tissue exclusively remains undetermined. Previous studies have demonstrated no significant differences in mechanical properties amongst fresh-frozen and embalmed human femora and calcanea (Topp et al. 2012; Mick et al. 2015; Zech et al. 2006). Although one study showed that formalin fixation significantly affected the loss and dynamic modulus during cyclic loading of murine femurs and vertebrae (Nazarian et al. 2009). In addition, Ohman et al. showed that the long-term preservation of formalin-fixated human cortical bone of

the femoral diaphysis significantly affected its Young's modulus, yield strain and ultimate strain (Ohman et al. 2008). Future work is encouraged to determine how material and mechanical properties may be altered between fresh, fresh-frozen, and embalmed cranial tissue so that limitations can be established when using each form of tissue. An irregular anatomic contour method was the type of manual segmentation used in this study. Manual segmentation is regarded as the gold standard for image segmentation, but its limitations are that it is a time-consuming procedure since each cross-section is investigated, and it is sensitive to intra and interobserver variability (Starmans et al. 2020; Bouxsein et al. 2010). The specimens were kept under room conditions for no more than 10 hours to allow proper curing of the cyanoacrylate, however, the potential for drying effects on mechanical response may be a limitation. The present work limited statistical analyses to a series of linear regressions that are associated with a single independent or predictor variable. Although, Bonferroni adjustments were applied to reduce the chances of committing a Type I error. With an adequate sample size, the authors recommend future research to perform a multivariable regression analysis to factor in all potential predictor variables, age, sex, and location in one equation to determine if a linear or non-linear model can significantly predict mechanical response. Furthermore, a step-wise linear regression can apply an automated procedure to efficiently include within one model only the multiple predictor variables that have a significant effect on the calvarium's mechanical behaviour. The specimens were assumed to be Euler-Bernoulli beams to apply the Euler-Bernoulli theorem. We acknowledge the limitations that the calvarium is indeed a curved beam and it is a heterogenous structure due to its three-layer composition and porous diploë region. Therefore, the specimens violate some of the assumptions of the Euler-Bernoulli theorem (Roark, Young, and Budynas 2002). However, we proceeded with applying the theorem since the mean I.ROC (73.86 mm) and O.ROC (83.70 mm) were at least 10

times the mean thickness (6.62 mm) of all specimens to assume a straight beam (Table 1) and the strains experienced by the specimens were small (<0.5%). Lastly, the study limited its mechanical testing to quasi-static loading resulting in quasi-static strain rates of 10^{-4}s^{-1} . However, dynamic impact loading conditions are most associated with applications observed in real-world head impacts (Hosseini Farid et al. 2019; Zhai et al. 2020). Therefore, as a next step, it is prudent for future studies to investigate the relationship between calvarium morphometry and mechanical response variables derived from impact bending resulting in dynamic strain rates.

5. CONCLUSION

More than one morphometric and geometrical property was a significant predictor of mechanical response for calvaria under 4-point quasi-static bending. Tb.Pf was the single diploë morphometry that was a significant predictor of force and bending moment at fracture. The inner cortical layer had the most morphometric and geometric properties as significant predictors of mechanical response particularly the inner cortical thickness, inner cortical TMD, and inner cortical porosity. To the authors' best knowledge, this is the first study to conduct a series of linear regressions between the calvarium's mechanical response and the calvarium's morphometry and geometry in all three of its structural layers. The findings from this work implicate which morphometric and geometric properties surrogate or computational modellers should emphasize when fabricating a three-layered skull model to accurately simulate injury.

ACKNOWLEDGEMENTS

Acknowledgement is given to Hugh Barrett, Jason Papirny, and Dr. Daniel Livy of the University of Alberta's Division of Anatomy for their efforts in providing the human cadavers and performing dissections necessary for this study.

Funding: This research was sponsored by the US Army Combat Capabilities Development Command - Army Research Laboratory and the International Technical Center Americas under Cooperative Agreement Number W911NF-19-2-0336. The views and conclusions contained in this document are those of the authors and should not be interpreted as representing the official policies, either expressed or implied, of the Army Research Laboratory or the U.S. Government. The U.S. Government is authorized to reproduce and distribute reprints for Government purposes notwithstanding any copyright notation herein. The authors declare that the roles of this study's sponsor included the financial resources to complete the study, the analysis and interpretation of data, the writing of the manuscript, and the decision to submit the manuscript for publication.

REFERENCES

- Adanty, Kevin, Kapil Bharadwaj Bhagavathula, Olivia Tronchin, David X Li, Karyne N. Rabey, Michael R Doschak, Samer Adeeb, et al. 2022. “The Mechanical Characterization and Comparison of Male and Female Calvaria Under Four-Point Bending Impacts.” *Journal of Biomechanical Engineering*, December, 1–47. <https://doi.org/10.1115/1.4056459>.
- Adanty, Kevin, James Michio Clark, Andrew Post, Thomas Blaine Hoshizaki, and Michael D. Gilchrist. 2020. “Comparing Two Proposed Protocols to Test the Oblique Response of Cycling Helmets to Fall Impacts.” *International Journal of Crashworthiness* 25 (6): 648–63. <https://doi.org/10.1080/13588265.2019.1628479>.
- Adanty, Kevin, Karyne N. Rabey, Michael R. Doschak, Kapil B. Bhagavathula, James D. Hogan, Dan L. Romanyk, Samer Adeeb, et al. 2021. “Cortical and Trabecular Morphometric Properties of the Human Calvarium.” *Bone* 148 (July): 115931. <https://doi.org/10.1016/j.bone.2021.115931>.
- Adanty, Kevin, Olivia Tronchin, Kapil B. Bhagavathula, Karyne N. Rabey, Michael R. Doschak, Daniel Romanyk, James D. Hogan, et al. 2020. “On the Ability of Morphometric Indices of Skull Diploë to Explain Variation in Bone Fracture Force and Fracture Strain in Four-Point Bending: A Preliminary Step Toward A Simulant Fracture Model.” *IRCOBI Conference 2020*, 821–22.
- Alexander, Stephen L., Karin Rafaels, C. Allan Gunnarsson, and Tusit Weerasooriya. 2019. “Structural Analysis of the Frontal and Parietal Bones of the Human Skull.” *Journal of the Mechanical Behavior of Biomedical Materials* 90 (February): 689–701. <https://doi.org/10.1016/j.jmbbm.2018.10.035>.
- Anderson, Bradley W., Michael W. Kortz, and Khalid A. Al Kharazi. 2021. “Anatomy, Head and Neck, Skull.” In *StatPearls*. Treasure Island (FL): StatPearls Publishing. <http://www.ncbi.nlm.nih.gov/books/NBK499834/>.
- Auperrin, Audrey, Rémi Delille, Denis Lesueur, Karine Bruyère, Catherine Masson, and Pascal Drazétic. 2014. “Geometrical and Material Parameters to Assess the Macroscopic Mechanical Behaviour of Fresh Cranial Bone Samples.” *Journal of Biomechanics* 47 (5): 1180–85. <https://doi.org/10.1016/j.jbiomech.2013.10.060>.
- Azar, Austin, Kapil Bharadwaj Bhagavathula, James Hogan, Simon Ouellet, Sikhanda Satapathy, and Christopher R. Dennison. 2019. “Protective Headgear Attenuates Forces on the Inner Table and Pressure in the Brain Parenchyma During Blast and Impact: An Experimental Study Using a Simulant-Based Surrogate Model of the Human Head.” *Journal of Biomechanical Engineering* 142 (4). <https://doi.org/10.1115/1.4044926>.
- Boruah, Sourabh, Glenn R. Paskoff, Barry S. Shender, Damien L. Subit, Robert S. Salzar, and Jeff R. Crandall. 2015. “Variation of Bone Layer Thicknesses and Trabecular Volume Fraction in the Adult Male Human Calvarium.” *Bone* 77 (August): 120–34. <https://doi.org/10.1016/j.bone.2015.04.031>.

- Bouxsein, Mary L., Stephen K. Boyd, Blaine A. Christiansen, Robert E. Guldberg, Karl J. Jepsen, and Ralph Müller. 2010. "Guidelines for Assessment of Bone Microstructure in Rodents Using Micro-Computed Tomography." *Journal of Bone and Mineral Research* 25 (7): 1468–86. <https://doi.org/10.1002/jbmr.141>.
- Davis, Matthew T., Andre M. Loyd, Han-yu Henry Shen, Maura H. Mulroy, Roger W. Nightingale, Barry S. Myers, and Cameron Dale Bass. 2012. "The Mechanical and Morphological Properties of 6 Year-Old Cranial Bone." *Journal of Biomechanics* 45 (15): 2493–98. <https://doi.org/10.1016/j.jbiomech.2012.07.001>.
- De Kegel, Dries, Alexander Meynen, Nele Famaey, G. Harry van Lenthe, Bart Depreitere, and Jos Vander Sloten. 2019. "Skull Fracture Prediction through Subject-Specific Finite Element Modelling Is Highly Sensitive to Model Parameters." *Journal of the Mechanical Behavior of Biomedical Materials* 100 (December): 103384. <https://doi.org/10.1016/j.jmbbm.2019.103384>.
- Delille, R., D. Lesueur, P. Potier, P. Drazetic, and E. Markiewicz. 2007. "Experimental Study of the Bone Behaviour of the Human Skull Bone for the Development of a Physical Head Model." *International Journal of Crashworthiness* 12 (2): 101–8. <https://doi.org/10.1080/13588260701433081>.
- Dennison, Christopher R., and Peter M. Wild. 2008. "Enhanced Sensitivity of an In-Fibre Bragg Grating Pressure Sensor Achieved through Fibre Diameter Reduction." *Measurement Science and Technology* 19: 11pp.
- Dennison, Christopher R, Peter M Wild, David R Wilson, and Michael K Gilbert. 2010. "An In-Fiber Bragg Grating Sensor for Contact Force and Stress Measurements in Articular Joints." *Measurement Science and Technology* 21 (11): 115803. <https://doi.org/10.1088/0957-0233/21/11/115803>.
- Doube, Michael, Michał M. Kłosowski, Ignacio Arganda-Carreras, Fabrice P. Cordelières, Robert P. Dougherty, Jonathan S. Jackson, Benjamin Schmid, John R. Hutchinson, and Sandra J. Shefelbine. 2010. "BoneJ: Free and Extensible Bone Image Analysis in ImageJ." *Bone* 47 (6): 1076–79. <https://doi.org/10.1016/j.bone.2010.08.023>.
- Fahlstedt, Madelen, Fady Abayazid, Matthew B. Panzer, Antonia Trotta, Wei Zhao, Mazdak Ghajari, Michael D. Gilchrist, et al. 2021. "Ranking and Rating Bicycle Helmet Safety Performance in Oblique Impacts Using Eight Different Brain Injury Models." *Annals of Biomedical Engineering* 49 (3): 1097–1109. <https://doi.org/10.1007/s10439-020-02703-w>.
- Ghajari, Mazdak, Peter J Hellyer, and David J Sharp. 2017. "Computational Modelling of Traumatic Brain Injury Predicts the Location of Chronic Traumatic Encephalopathy Pathology." *Brain* 140 (2): 333–43. <https://doi.org/10.1093/brain/aww317>.
- Hahn, M., M. Vogel, M. Pompesius-Kempa, and G. Delling. 1992. "Trabecular Bone Pattern Factor—a New Parameter for Simple Quantification of Bone Microarchitecture." *Bone* 13 (4): 327–30. [https://doi.org/10.1016/8756-3282\(92\)90078-B](https://doi.org/10.1016/8756-3282(92)90078-B).

Hosseini Farid, Mohammad, Ashkan Eslaminejad, Mohammadreza Ramzanpour, Mariusz Ziejewski, and Ghodrat Karami. 2019. "The Strain Rates of the Brain and Skull Under Dynamic Loading." In . American Society of Mechanical Engineers Digital Collection. <https://doi.org/10.1115/IMECE2018-88300>.

Houg, Kathryn P., Leigh Armijo, Michael R. Doschak, Paul W. Major, Tracy Popowics, Christopher R. Dennison, and Dan L. Romanyk. 2021. "Experimental Repeatability, Sensitivity, and Reproducibility of Force and Strain Measurements from within the Periodontal Ligament Space during Ex Vivo Swine Tooth Loading." *Journal of the Mechanical Behavior of Biomedical Materials* 120 (August): 104562. <https://doi.org/10.1016/j.jmbbm.2021.104562>.

Hubbard, Robert P. 1971. "Flexure of Layered Cranial Bone." *Journal of Biomechanics* 4 (4): 251–63. [https://doi.org/10.1016/0021-9290\(71\)90031-5](https://doi.org/10.1016/0021-9290(71)90031-5).

Hubbard, Robert P., and Donald G. McLeod. 1974. "Definition and Development of A Crash Dummy Head." *SAE Transactions* 83: 3836–51.

Kim, Yoon Jeong, and Jeffrey Henkin. 2015. "Micro-Computed Tomography Assessment of Human Alveolar Bone: Bone Density and Three-Dimensional Micro-Architecture." *Clinical Implant Dentistry and Related Research* 17 (2): 307–13. <https://doi.org/10.1111/cid.12109>.

Laerd Statistics. 2015. "Simple Linear Regression Using SPSS Statistics." *Statistical Tutorials and Software Guides*. <https://statistics.laerd.com/>.

Lee, Jik Hang Clifford, Benjamin Ondruschka, Lisa Falland-Cheung, Mario Scholze, Niels Hammer, Darryl Chan Tong, and John Neil Waddell. 2019. "An Investigation on the Correlation between the Mechanical Properties of Human Skull Bone, Its Geometry, Microarchitectural Properties, and Water Content." *Journal of Healthcare Engineering* 2019 (May): 1–8. <https://doi.org/10.1155/2019/6515797>.

Li, Yizhao, Simon Ouellet, Albert H. Vette, Don Raboud, Ashton Martin, and Christopher R. Dennison. 2021. "Evaluation of the Kinematic Biofidelity and Inter-Test Repeatability of Global Accelerations and Brain Parenchyma Pressure for a Head–Brain Physical Model." *Journal of Biomechanical Engineering* 143 (9). <https://doi.org/10.1115/1.4050752>.

Mao, Haojie, Liying Zhang, Binhui Jiang, Vinay V. Genthikatti, Xin Jin, Feng Zhu, Rahul Makwana, et al. 2013. "Development of a Finite Element Human Head Model Partially Validated With Thirty Five Experimental Cases." *Journal of Biomechanical Engineering* 135 (11). <https://doi.org/10.1115/1.4025101>.

Margulies, Susan S., and Kirk L. Thibault. 2000. "Infant Skull and Suture Properties: Measurements and Implications for Mechanisms of Pediatric Brain Injury." *Journal of Biomechanical Engineering* 122 (4): 364–71. <https://doi.org/10.1115/1.1287160>.

McElhaney, James H., John L. Fogle, John W. Melvin, Russell R. Haynes, Verne L. Roberts, and Nabih M. Alem. 1970. "Mechanical Properties of Cranial Bone." *Journal of Biomechanics* 3 (5): 495–511. [https://doi.org/10.1016/0021-9290\(70\)90059-X](https://doi.org/10.1016/0021-9290(70)90059-X).

- Mick, E., H. Steinke, T. Wolfskämpf, J. Wieding, N. Hammer, M. Schulze, R. Souffrant, and R. Bader. 2015. "Influence of Short-Term Fixation with Mixed Formalin or Ethanol Solution on the Mechanical Properties of Human Cortical Bone." *Current Directions in Biomedical Engineering* 1 (1): 335–39. <https://doi.org/10.1515/cdbme-2015-0083>.
- Milton, Sande. 1986. "A Sample Size Formula for Multiple Regression Studies on JSTOR." *The Public Opinion Quarterly* 50 (1): 112–18.
- Motherway, Julie A., Peter Verschueren, Georges Van der Perre, Jos Vander Sloten, and Michael D. Gilchrist. 2009. "The Mechanical Properties of Cranial Bone: The Effect of Loading Rate and Cranial Sampling Position." *Journal of Biomechanics* 42 (13): 2129–35. <https://doi.org/10.1016/j.jbiomech.2009.05.030>.
- Mott, Robert L., and Joseph A. Untener. 2018. *Applied Strength of Materials, Sixth Edition SI Units Version*. 6th ed. Taylor and Francis Group.
- Mukaka, MM. 2012. "A Guide to Appropriate Use of Correlation Coefficient in Medical Research." *Malawi Medical Journal : The Journal of Medical Association of Malawi* 24 (3): 69–71.
- Nazarian, Ara, Bryan J. Hermannsson, John Muller, David Zurakowski, and Brian D. Snyder. 2009. "Effects of Tissue Preservation on Murine Bone Mechanical Properties." *Journal of Biomechanics* 42 (1): 82–86. <https://doi.org/10.1016/j.jbiomech.2008.09.037>.
- Nelson, Drew V., Alberto Makino, Craig M. Lawrence, John M. Seim, Whitten L. Schulz, and Eric Udd. 1998. "Determination of the K-Matrix for the Multiparameter Fiber Grating Sensor in AD072 Fibercore Fiber" 3489 (September): 79–85. <https://doi.org/10.1117/12.323418>.
- Ohman, Caroline, Enrico Dall'Ara, Massimiliano Baleani, Serge Van Sint Jan, and Marco Viceconti. 2008. "The Effects of Embalming Using a 4% Formalin Solution on the Compressive Mechanical Properties of Human Cortical Bone." *Clinical Biomechanics*. <https://doi.org/10.1016/j.clinbiomech.2008.07.007>.
- Rahmoun, J., A. Auperrin, R. Delille, H. Naceur, and P. Drazetic. 2014. "Characterization and Micromechanical Modeling of the Human Cranial Bone Elastic Properties." *Mechanics Research Communications* 60 (September): 7–14. <https://doi.org/10.1016/j.mechrescom.2014.04.001>.
- Roark, Raymond J., Warren C. Young, and Richard G. Budynas. 2002. *Roark's Formulas for Stress and Strain*. 7th ed. New York: McGraw-Hill.
- Rowson, Bethany, Steven Rowson, and Stefan M. Duma. 2015. "Hockey STAR: A Methodology for Assessing the Biomechanical Performance of Hockey Helmets." *Annals of Biomedical Engineering* 43 (10): 2429–43. <https://doi.org/10.1007/s10439-015-1278-7>.
- Salmon, Phil. 2020. "Application of Bone Morphometry and Densitometry by X-Ray Micro-CT to Bone Disease Models and Phenotypes." In *Micro-Computed Tomography (Micro-CT) in Medicine and Engineering*, edited by Kaan Orhan, 49–75. Cham: Springer International Publishing. https://doi.org/10.1007/978-3-030-16641-0_5.

Starmans, Martijn P. A., Sebastian R. van der Voort, Jose M. Castillo Tovar, Jifke F. Veenland, Stefan Klein, and Wiro J. Niessen. 2020. "Chapter 18 - Radiomics: Data Mining Using Quantitative Medical Image Features." In *Handbook of Medical Image Computing and Computer Assisted Intervention*, edited by S. Kevin Zhou, Daniel Rueckert, and Gabor Fichtinger, 429–56. The Elsevier and MICCAI Society Book Series. Academic Press. <https://doi.org/10.1016/B978-0-12-816176-0.00023-5>.

Tian, Heng, Dong-guang Liu, Yan-ping Wang, and Qing-lin Wang. 2019. "Effect of Adhesive Type on the Sensitivity Coefficient of FBG Sensor Bonded on the Surface of CFRP." *Optoelectronics Letters* 15 (4): 264–68. <https://doi.org/10.1007/s11801-019-8183-5>.

Topp, Tobias, Thorben Müller, Sebastian Huss, Peter Herbert Kann, Eberhard Weihe, Steffen Ruchholtz, and Ralph Peter Zettl. 2012. "Embalmed and Fresh Frozen Human Bones in Orthopedic Cadaveric Studies: Which Bone Is Authentic and Feasible?" *Acta Orthopaedica* 83 (5): 543–47. <https://doi.org/10.3109/17453674.2012.727079>.

Zech, Stefan, Thomas Goesling, Stefan Hankemeier, Karsten Knobloch, Jens Geerling, Kristof Schultz-Brunn, Christian Krettek, and Martinus Richter. 2006. "Differences in the Mechanical Properties of Calcaneal Artificial Specimens, Fresh Frozen Specimens, and Embalmed Specimens in Experimental Testing." *Foot & Ankle International* 27 (12): 1126–36. <https://doi.org/10.1177/107110070602701220>.

Zhai, Xuedong, Eric A. Nauman, Dana Moryl, Roy Lycke, and Weinong W. Chen. 2020. "The Effects of Loading-Direction and Strain-Rate on the Mechanical Behaviors of Human Frontal Skull Bone." *Journal of the Mechanical Behavior of Biomedical Materials* 103 (March): 103597. <https://doi.org/10.1016/j.jmbbm.2019.103597>.

Zwirner, Johann, Benjamin Ondruschka, Mario Scholze, Joshua Workman, Ashvin Thambyah, and Niels Hammer. 2021. "The Dynamic Impact Behavior of the Human Neurocranium." *Scientific Reports* 11 (1): 11331. <https://doi.org/10.1038/s41598-021-90322-3>.

CONFLICT OF INTEREST STATEMENT

The authors declare that they have no known competing financial interests or personal relationships that could have appeared to influence the work reported in this paper.

Chapter 3: The Mechanical Characterization and Comparison of Male and Female Calvaria Under Four-Point Bending Impacts.

In Chapter 3, the calvarium specimens were characterized under 4-point dynamic impact bending conditions to determine mechanical response at fracture which expands upon the quasi-static results from Chapter 2. Most real-world head impact cases occur at dynamic loading and strain rates. Therefore, employing a dynamic impact testing configuration is pertinent to characterize the calvarium. The combined findings from Chapters 2 and 3 provided averages and 95% confidence intervals for mechanical response variables of the calvarium. These measurements and properties were necessary to assess how well the surrogate prototypes introduced in Chapter 4 compared with human calvarium. The results of Chapter 3 complete *sub-objective 3: Determine the mechanical response of human calvarium in 4-point dynamic impact bending.*

Chapter 3 is a peer-reviewed journal article that was published in the *Journal of Biomechanical Engineering – The American Society of Mechanical Engineers (ASME)*. Chapter 3's text and content match exactly with the published article. Permission to reproduce the article in this dissertation has been granted by ASME.

Reference:

Adanty, K., Bhagavathula, K.B., Tronchin, O., Li, D., Rabey, K.N., Adeeb, S., Hogan, J.D., Ouellet, S., Plaisted, T.A., Satapathy, S.S., Romanyk, D., Dennison, C.R. (2023). The Mechanical Characterization and Comparison of Male and Female Calvaria Under Four-Point Bending Impacts. *ASME Journal of Biomechanical Engineering* 145(5): 051009. DOI: 10.1115/1.4056459.

The Mechanical Characterization and Comparison of Male and Female Calvaria Under Four-Point Bending Impacts

ABSTRACT

The circumstances in which we mechanically test and critically assess human calvarium tissue would find relevance under conditions encompassing real-world head impacts. These conditions include, among other variables, impact velocities, and strain rates. Compared to quasi-static loading on calvaria, there is less reporting on the impact loading of the calvaria and consequently, there are relatively fewer mechanical properties on calvaria at relevant impact loading rates available in the literature. The purpose of this work was to report on the mechanical response of 23 human calvarium specimens subjected to dynamic 4-point bending impacts. Impacts were performed using a custom-built 4-point impact apparatus at impact velocities of 0.86 to 0.89 m/s resulting in surface strain rates of 2-3/s – representative of strain rates observed in vehicle collisions and blunt impacts. The study revealed comparable effective bending moduli (11-15 GPa) to the limited work reported on the impact mechanics of calvaria in the literature, however, fracture bending stress (10-47 MPa) was relatively less. As expected, surface strains at fracture (0.21-0.25%) were less compared to studies that performed quasi-static bending. Moreover, the study revealed no significant differences in mechanical response between male and female calvaria. The findings presented in this work are relevant to many areas including validating surrogate skull fracture models in silico or laboratory during impact and optimizing protective devices used by civilians to reduce the risk of a serious head injury.

Keywords: Human Calvarium; Calvarium Biomechanics; Skull Fracture; Impact Loading; Sex Differences

1. INTRODUCTION

Establishing the mechanical response of the human calvarium is required to quantify the onset of a traumatic head injury such as a skull fracture. Knowledge of such onsets allows helmet and automobile industries to then make informed decisions on enhancing protection against skull fractures in applications such as military and sports (Delaney, 2004; Weisenbach et al., 2018). Furthermore, defining the mechanical onset of a skull fracture allows one to confidently validate physical surrogate and computational models to accurately simulate a fracture. As we explore novel testing methodologies on skull and brain tissue to determine mechanical properties (Melvin & Yoganandan, 2015), we must ensure the manner of testing contains conditions most pertinent to real-world head impacts. These conditions can include appropriate impact speeds and strain rates. With this direction of testing, engineers and scientists can be assured that subsequent mechanical properties used to verify surrogate models are derived from impact characteristics associated with real-world head injuries. The testing on full surrogate or cadaveric head models in large-scale impact testing equipment such as a linear drop tower, pendulum, pneumatic linear impactor, and oblique testing apparatuses have been well documented in the literature to simulate real-world head impacts (Aare & Halldin, 2003; Adanty, Clark, et al., 2020; Karton et al., 2020; Knowles & Dennison, 2017; Li et al., 2021; Melvin & Yoganandan, 2015). This work performed controlled and small-scale impacts on human calvarium tissue with resulting strain rates applicable to rates observed in real-world head impacts (Hosseini Farid et al., 2019; Zhai et al., 2020).

The quasi-static bending of calvaria has been documented in the literature to investigate skull fracture mechanics (Adanty, Tronchin, et al., 2020; Auperrin et al., 2014; Delille et al., 2007; Hubbard, 1971). Work by Hubbard (1971) was one of the earliest studies to perform 3 and 4-point bending on adult parietal specimens at quasi-static deformation rates with strain rates within 0.01/s

(Hubbard, 1971). Similarly, Delille et al. and Auperrin et al. performed 3-point quasi-static bending at displacement rates of 10 mm/min for fresh-frozen frontal and parietal specimens (Auperrin et al., 2014; Delille et al., 2007). More recently, in a short communication, Adanty et al. performed 4-point quasi-static bending on embalmed calvaria at displacement rates of 2 mm/min resulting in strain rates of 10^{-4} /s (Adanty, Tronchin, et al., 2020). While these findings have been appropriate contributions to understanding skull fracture mechanics, quasi-static loading conditions are not associated with the sudden head impact conditions observed in real-world traumatic head impacts. Indeed, the typical strain rates observed from these studies were less than 1/s and though this rate may be appropriate to carefully note the fracture patterns of the skull and quantify mechanical properties, these strain rates are significantly less than the rates observed in real-world head impacts (Hosseini Farid et al., 2019; Zhai et al., 2020). Most real-world head impacts during ballistics, falls, sports, and vehicle accidents endure intermediate to high strain rates of 1- 10^3 /s to the skull (Hosseini Farid et al., 2019; Zhai et al., 2020). It is at these high-loading rates where we require further quantification of mechanical properties of skull tissue to accurately validate surrogate or computational skull models and then optimize helmet and protective devices accordingly.

The primary focus of this paper was to quantify the mechanical response of the calvarium related to impact, however, the effect of sex on mechanical response comes into question. To our knowledge, the comparison of mechanical response between sexes for the bending of calvaria has not been reported in the literature to date. Most surrogate and computational human head models utilized in injury biomechanics are typically validated from experimental data of the 50th percentile male population. This limits the conclusions of the mechanical outputs for these models to the male population as opposed to the general population consisting of males and females. Indeed, an

initial understanding of any potential differences in mechanical response between sex may inform if sex-specific skull models are necessary for future design paradigms.

The purpose of this study was to report on the mechanical response of human calvaria in dynamic 4-point bending impacts. A baseline understanding of skull mechanics during dynamic bending impacts can provide a critical direction towards 1) advancing helmet protection to prevent skull injuries and 2) an initial point of reference to validate physical surrogate or computational skull models to simulate fracture. In addition, the following null hypothesis was tested in this study: *no significant differences in mechanical response between male and female calvaria.*

2. METHODS

The methods and protocols associated with this work were approved by the University of Alberta Research Ethics Board (ID: Pro00089218). All specimens came from individuals in the University of Alberta Anatomical Gift Program. All individuals were examined for pre-existing bone pathology based on provided medical records to ensure no pathological factors had influenced the subsequent results.

2.1 Specimens

Calvarium specimens of curved beam geometry were extracted from the frontal or parietal regions of 23 male (n=11) and female (n=12) embalmed calvaria using an autopsy saw (Fig. 1). To obtain the frontal specimens, a point was landmarked approximately 1.5 cm inferior to the coronal suture and then a rectangular beam model (55 mm in length and 8 mm in width) was used to outline and extract one frontal specimen (Fig. 1) (Adanty et al., 2021).

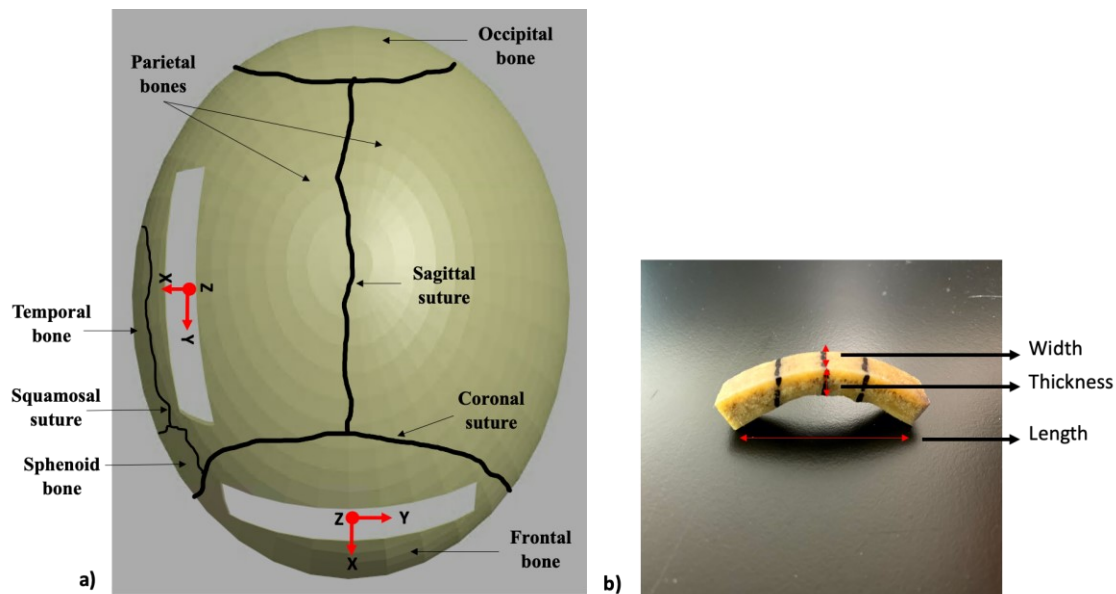


Figure 1. a) A top-view model of the human calvarium displaying the outline which the frontal and parietal specimens were extracted from. b) An example of a beam-shaped human calvarium specimen.

To obtain the parietal specimens, we located the center of the squamosal suture and landmarked a point approximately 1.5 cm superior to the suture to extract one specimen (Adanty et al., 2021). The orientation in which the specimens were extracted (Fig. 1) was preferred to avoid the coronal and sagittal sutures on the skull, as well as to avoid the challenges of cutting the specimens at regions with excessive curvature. Excessive curvature can be observed at bony prominences of the skull such as the metopic ridge, parietal eminence, frontal eminence, and particularly towards the supraorbital ridge and temporal ridge. Due to sample size constraints, one specimen, as opposed to multiple specimens, was extracted per calvarium. In addition, one specimen extracted per calvarium over multiple specimens avoids the challenge of cutting at regions of excessive curvature as discussed and avoids the potential effect of intra-specimen variation on the mechanical response. The specimens were then scanned using micro-computed tomography (CT) at a resolution of 18 μm (Bruker-Skyscan 1176, Kontich, BE). Scanning parameters included a 90 kV X-ray tube voltage, 278 μA X-ray current, 1 mm Al filter, 300 ms integration time, frame average of $n = 3$, and 0.7° angular rotation step (Adanty et al., 2021). Using the micro-CT scanned images for each specimen, the second moment of inertia (I) and the half-thickness (Fig. 2a) at the approximate center of the specimen was computed by way of third-party software (BoneJ-an ImageJ plugin) (Doube et al., 2010) and verified using a secondary software (Computed Tomography (CT)-Analyzer-version 1.10, Bruker-Skyscan). The surface radius of curvature (ROC) was computed in Geomagic software by 3-Dimensional (3D) Systems (Rock Hill, South Carolina) (Fig. 2b). Table 1 provides a geometric description of the specimens. Specimen width, thickness, and 2nd moment of inertia were determined to estimate bending stress. Specimen ROC was computed to ensure ROC was 10 times the thickness of the specimens on average to assume a straight beam when applying the Euler-Bernoulli beam theorem to compute

bending stress (Roark et al., 2002). Before testing and for the maintenance of hydration, the specimens were stored in unbuffered aqueous formaldehyde 37% embalming fluid, which is composed of 4% phenol, 4% formalin (37% concentration), 8% glycol, 8% ethyl alcohol (95% concentration), and 76% water. Additional details on the method of extraction and micro-CT imaging and analysis of calvaria are published in a recent article by the present authors (Adanty et al., 2021).

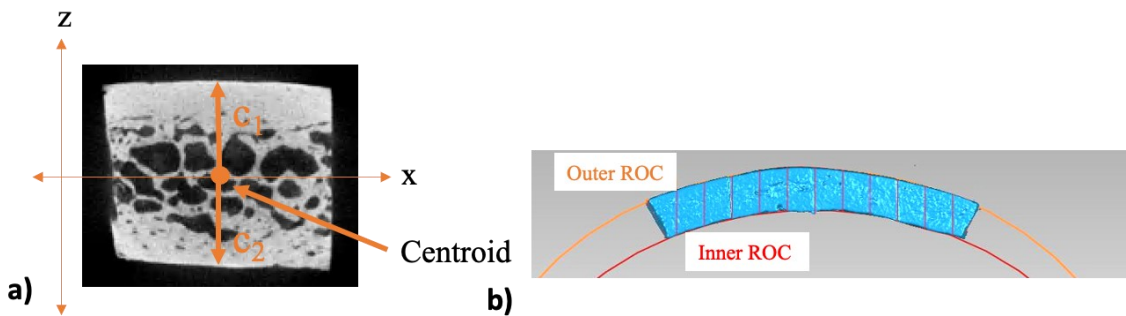


Figure 2. a) A cross-sectional micro-CT scanned image from a calvarium specimen, where c_1 and c_2 represent the half-thickness of the specimen from the centroid to the outer cortical and inner cortical surface, respectively. b) An STL model of a calvarium specimen in Geomagic software to compute outer ROC and inner ROC.

Table 1. The mean age and geometric properties of the calvaria (95% confidence interval).

Age and Geometry	Male (n=11)	Female (n=12)	All specimens (n=23)
Age	84.6 (78.2, 90.9)	88.0 (82.3, 93.7)	86.4 (82.4, 90.3)
Length (mm)	51.68 (50.02, 53.34)	52.12 (50.83, 53.38)	51.90 (50.95, 52.85)
Width (mm)	8.46 (8.16, 8.75)	8.76 (7.80, 9.71)	8.61 (8.13, 9.09)
Thickness (mm)	6.79 (5.62, 7.96)	7.42 (6.81, 8.02)	7.12 (6.52, 7.72)
2 nd moment of inertia (I) (m ⁴)	2.18E-10 (1.51E-10, 2.85E-10)	2.74E-10 (2.09E-10, 3.38E-10)	2.47E-10 (2.02E-10, 2.91E-10)
Outer surface ROC (mm)	69.04 (63.25, 74.83)	62.16 (56.77, 67.56)	65.45 (61.53, 69.37)
Inner surface ROC (mm)	74.98 (26.13, 123.82)*	47.7 (37.46 to 57.97)	60.75 (38.17, 83.33)

*one male specimen had an inner ROC of 291.39 mm which is a major outlier. With this outlier removed, the average inner surface ROC for the males is 53.33 mm (95% CI 46.09, 60.57).

2.2 Specimen Preparation

Preceding the commencement of mechanical testing, fibre Bragg gratings (FBGs) were adhered to the outer cortical and inner cortical surfaces of each specimen to quantify surface strains during testing (Fig. 3a). The FBGs were glued to the cortical surfaces using cyanoacrylate to ensure the FBGs remained intimately bonded to the surface. Scotch Tape (3M) was applied on the glued surface followed by low heat from a heat gun (100°F for 15 seconds) to facilitate the drying of the cyanoacrylate. After 10 h, the cyanoacrylate was fully dried, and the Scotch Tape (3M) was removed to begin mechanical testing. The purpose of waiting at least 10 h was to ensure the cyanoacrylate was fully cured so that the FBGs remained securely bonded to the specimens for accurate measurements of strain during testing. Preliminary examinations on adhering FBGs to swine scapula found that the cyanoacrylate did not fully cure when waiting 5 hours or less after

investigating FBG bonding resilience. FBGs are 1mm strain transducers in length (Fig. 3a) implemented in optical fibres and perturbations on the FBG, such as surface strain, can be quantified based on proportional changes in a Bragg wavelength ($\Delta\lambda_B$) (Dennison & Wild, 2008). The sensitivity of the FBG is 1.2 pm/ $\mu\epsilon$. The application of cyanoacrylate on FBGs has demonstrated minimal effects on the FBGs' ability to quantify strain (Tian et al., 2019). FBGs has been used in biomedical applications for invasive biosensing in humans and animals (Al-Fakih et al., 2012; Houg et al., 2021).

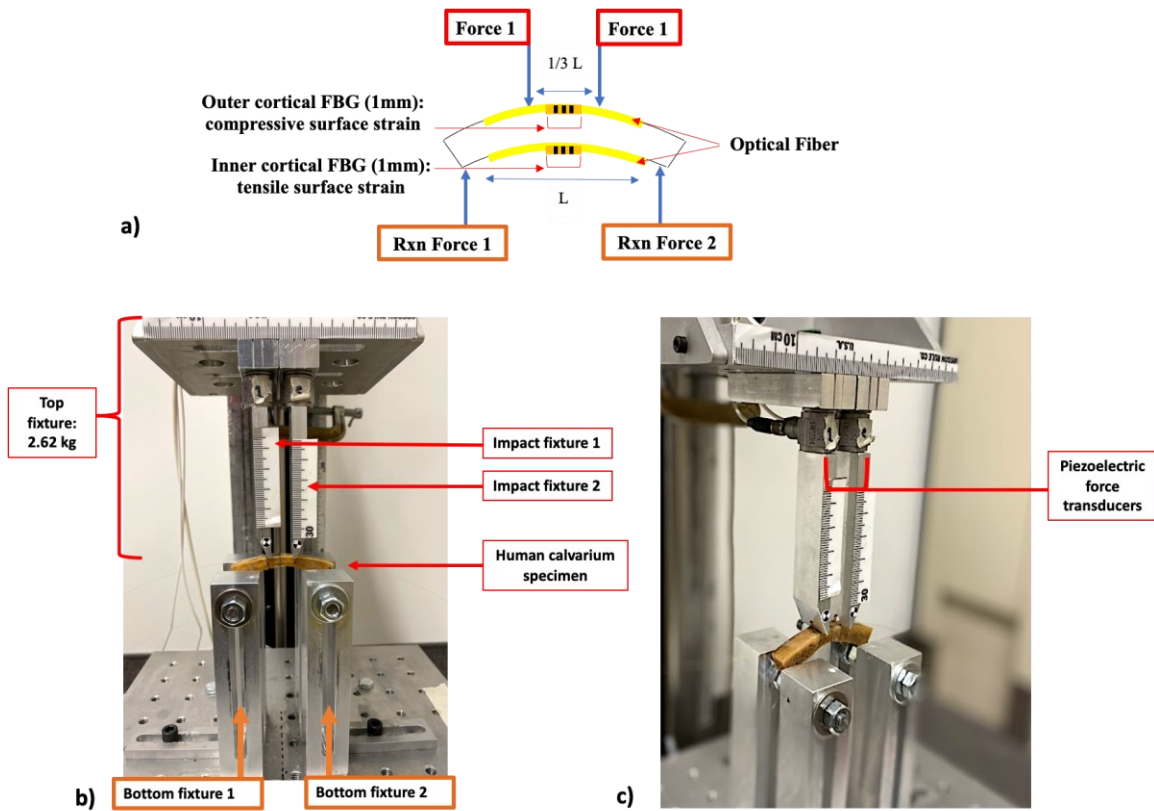


Figure 3. a) A 2D schematic of the 4-point bending impact and where the FBGs were placed on the surface of the calvaria. b) A frontal view of the custom-built 4-point impact apparatus. c) An isometric view of the custom-built 4-point impact apparatus.

2.3 Mechanical Testing: 4-Point Dynamic Bending Impacts

The specimens were placed in a guided custom-built 4-point testing apparatus to perform impacts (Fig. 3b and 3c). The 4-point bending configuration was chosen because this configuration

produces as close as possible a state of pure bending at the mid-region of the specimens. Therefore, failure was mainly attributed to bending stress and less so with a complex stress-state encompassing bending and shear that can arise in 3-point bending. The velocities of the top impact fixture ranged between 0.86-0.89 m/s just prior to impact. These velocities were captured using a high-speed camera at 5,000 frames per second (Phantom v61-1280 x 800 CMOS sensor) and verified using Phantom Multicam Software. Given the mass of the top impact fixture attached to the guide rail was 2.62 kg (Fig. 3b), the impact kinetic energy was 0.97-1.04 joules. The instrumentation for the guided top impact fixture included two inertially compensated piezoelectric force transducers (PCB model 208C05) for each impact fixture (Fig. 3c). Each specimen was set on the bottom fixtures and was free to move horizontally to avoid horizontal shear stresses within the specimen as much as possible during bending deformation. The free horizontal movement of the specimens holds no clinical relevance regarding injury, rather the intention was to carry out testing conditions related to pure bending and ensure fracture was associated with bending stress.

Table 2. Mechanical response variables determined for each test.

Mechanical Response Variables	Description
Force at fracture (N)	The force measured at time of fracture.
Bending moment at fracture (N.m)	The calculated bending moment endured by the specimen at time of fracture.
Tensile surface strain at fracture (%)	The surface strain of the specimen at the time of fracture, measured using FBGs. Tensile strain was quantified on the inner cortical surface and compressive strain was quantified on the outer cortical surface (Fig. 3a).
Compressive surface strain at fracture (%)	
Tensile bending stress at fracture (MPa)	The calculated bending stress endured by the specimen at the time of fracture, estimated using the Euler-Bernoulli Beam theorem by assuming specimens were homogenous and of simple beam geometry (Roark et al., 2002):
Compressive bending stress at fracture (MPa)	
	$\sigma_{tensile} = \frac{M(c_2)}{I}$ $\sigma_{compression} = \frac{M(c_1)}{I}$ <p>Where, σ = stress (MPa) M= fracture moment (N.m) I=second moment of inertia (m⁴) c= half-thickness- the distance from the centroid to the surface of the specimen (See Fig. 2a)</p>
Tensile effective bending modulus (GPa)	The slope of the stress-strain plot (Fig. 4) associated with initial linear region of the strain-time plot. The term <i>effective</i> signifies that the calvaria are indeed three-layer composite structures and that the modulus is a bulk estimate assuming the specimen is homogenous (Roark et al., 2002).
Compressive effective bending modulus (GPa)	
Tensile strain rate (1/s)	The slope at the initial linear region for each strain-time plot (See Fig. 4).
Compressive strain rate (1/s)	

The mechanical response variables determined for each bend test are outlined in Table 2. All fracture properties of the specimens were documented at the observation of fracture initiation, where initiation of fracture was determined visually from instant playback video recorded from the high-speed camera. The authors applied the Euler-Bernoulli beam theory to make a simplified

gross estimation of the stress-state of the calvaria (Roark et al., 2002). One major assumption when applying the theorem is that the specimens are straight and if curved the specimen must have a thickness of 10 times the ROC— the average specimens in our work satisfied this assumption for both inner and outer ROC thus the specimens were assumed to be straight (Table 1) (Roark et al., 2002). A second major assumption is that plane sections of the specimens remain perpendicular to the neutral axis before deformation and remain perpendicular to the neutral axis during deformation (Adeeb, 2011; Roark et al., 2002). A third major assumption is that the strains the specimens experience are small (Adeeb, 2011; Roark et al., 2002). Both these assumptions were met since the specimens fractured at small strains of less than 0.5% (Hayes et al., 2015) and we did not observe any noticeable changes in geometry during deformation just as observed with other brittle materials. Indeed, the calvarium is a heterogeneous structure, of nonuniform cross-sections, and anisotropic, which provide some limitations to the use of the beam theory (Roark et al., 2002). Though, previous studies have applied the beam theorem to make parallel assumptions to estimate stress and thus draw comparisons between studies (Auperrin et al., 2014; Davis et al., 2012; Delille et al., 2007; Igo et al., 2021; J. H. C. Lee et al., 2019; Margulies & Thibault, 2000). The FBGs detected a linear relationship between surface strain and time following the application of the force from the impact prongs on the outer cortical surface of the specimens (Fig. 4). At the initial stages of the impact where the impact prongs first came into sudden contact with the specimen, surface strain remained in an unstrained state and several milliseconds later strain increased linearly with time. Therefore, strain rates and effective bending moduli-slope of the stress-strain plot (Fig. 4) were reported for all the specimens at corresponding linear strain-time variations.

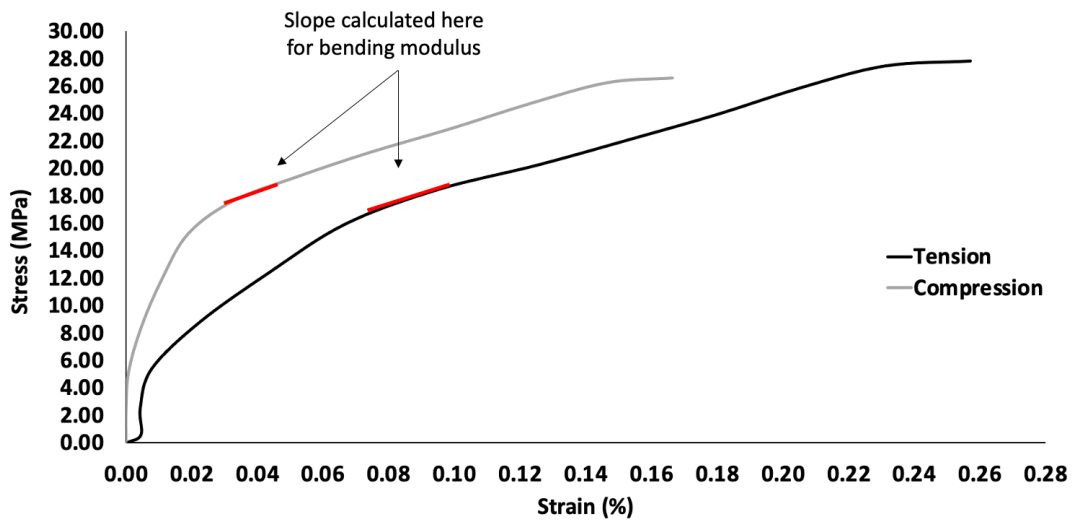
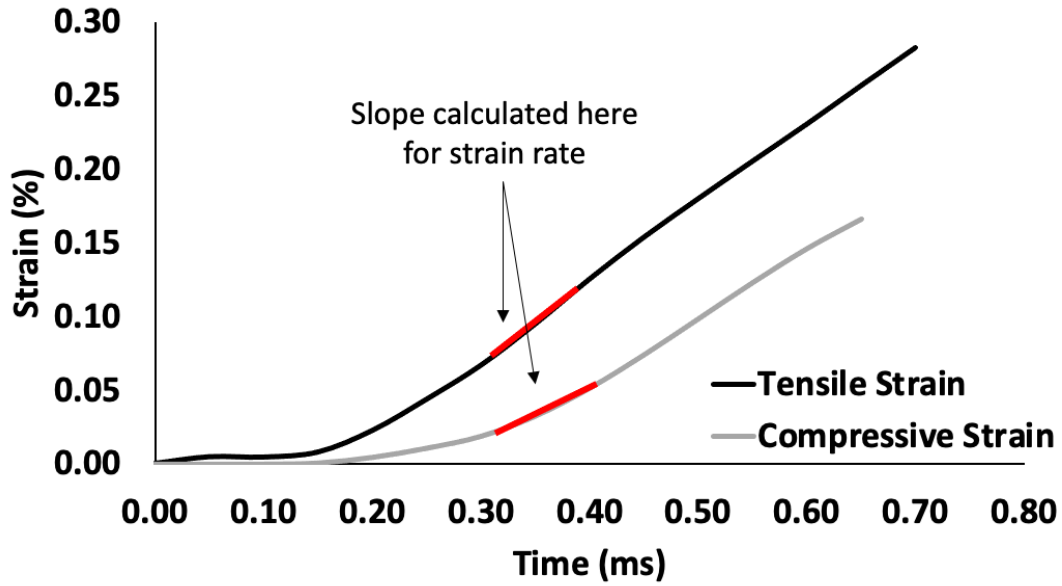


Figure 4. An example of a strain-time plot (top graph) and its corresponding stress-strain plot (bottom graph) for a calvarium presenting where the slope was computed to obtain strain-rate and effective bending modulus respectively. The indicated slope on the stress-strain plot (bottom graph) to determine the effective bending modulus corresponds to the strain-rate (slope) in the strain-time plot (top graph).

2.4 Statistical Analysis

Descriptive statistics on the mechanical response variables were reported. To test the following null hypothesis: *no significant differences in mechanical response between male and female calvaria*, an independent-samples t-test was performed using IBM SPSS version 25 (IBM Inc., Armonk, NY, USA). The independent variables were male and female and the dependent variables were the mechanical response variables (Table 2). When a dependent variable was not normally distributed (verified using a Shapiro-Wilk Test) for an independent variable a Mann-Whitney U test was performed. Therefore, the null hypothesis tested for this non-parametric test was *no significant differences in distributions or medians in mechanical response between male and female calvaria*. Using preliminary data from a pilot project, a power analysis determined a total minimum sample size of N=12 specimens to ensure the probability of committing a type 2 error was 20% (Eng, 2003). The alpha level was set at 0.05 where a p-value less than 0.05 was statistically significant.

Given the present study was limited to 23 specimens, the frontal (n=18) and parietal (n=5) regions were grouped together as one region. Therefore, to justify omitting region as a second independent variable, an additional statistical test was performed to test the following null hypothesis: *no significant differences in mechanical response between frontal and parietal regions*. Due to an uneven sample size between the two regions, parametric and non-parametric tests were performed to test the null hypothesis.

3. RESULTS

The descriptive statistics of the mechanical response with respect to sex are presented in Table 3. In addition, descriptive statistics of the mechanical response averaged across both sexes are presented in Table 4.

Table 3. Descriptive statistics of the mechanical response variables according to sex.

Mechanical Response Variables	Male (M) and Female (F) Mean	95% CI	Male (M) and Female (F) Median
Force at fracture (N)	M:224.75 ± 83.82 F:222.93 ± 79.71	M:168.43, 281.06 F: 172.28, 273.58	M:200.76 F: 217.62
Bending moment at fracture (N.m)	M:1.70 ± 0.56 F:1.70 ± 0.64	M:1.32, 2.08 F:1.29, 2.11	M:1.51 F:1.65
Tensile surface strain at fracture (%)	M:0.24 ± 0.08 F:0.25 ± 0.09	M:0.19, 0.30 F:0.19, 0.31	M:0.26 F:0.25
Compressive surface strain at fracture (%)	M:0.22 ± 0.10 F:0.20 ± 0.11	M:0.15, 0.28 F:0.13, 0.27	M:0.25 F:0.20
Tensile bending stress at fracture (MPa)	M:29.89 ± 9.10 F:24.29 ± 7.01	M:23.77, 36.00 F:19.84, 28.74	M:29.60 F:24.21
Compressive bending stress at fracture (MPa)	M:29.73 ± 9.78 F:23.54 ± 7.72	M:23.16, 36.31 F:18.63, 28.45	M:28.47 F:23.45
Tensile effective bending modulus (GPa)	M:11.74 ± 11.07 F:11.03 ± 8.39	M:4.30, 19.17 F:5.71, 16.37	M:8.58 F:7.52
Compressive effective bending modulus (GPa)	M:10.83 ± 6.09 F:18.27 ± 18.09	M:6.74, 14.92 F:6.78, 29.76	M:10.15 F:11.14
Tensile strain rate (1/s)	M:3.27 ± 2.56 F:2.93 ± 1.40	M:1.55, 4.99 F:2.04, 3.82	M:3.50 F:3.10
Compressive strain rate (1/s)	M:2.89 ± 2.14 F:1.87 ± 1.39	M:1.46, 4.33 F:0.98, 2.75	M:2.75 F:1.43

Table 4. Descriptive statistics of the mechanical response variables across both sexes.

Mechanical Response Variables	Mean	95% CI	Median
Force at fracture (N)	223.80 ± 79.82	189.28, 258.32	208.41
Bending moment at fracture (N.m)	1.70 ± 0.59	1.45, 1.96	1.60
Tensile surface strain at fracture (%)	0.25 ± 0.08	0.21 to 0.28	0.25
Compressive surface strain at fracture (%)	0.21 ± 0.10	0.16 to 0.25	0.21
Tensile bending stress at fracture (MPa)	26.97 ± 8.39	23.34, 30.60	24.84
Compressive bending stress at fracture (MPa)	26.50 ± 9.13	22.55, 30.45	25.73
Tensile effective bending modulus (GPa)	11.37 ± 9.54	7.25, 15.50	7.95
Compressive effective bending modulus (GPa)	14.71 ± 13.96	8.68, 20.75	10.21
Tensile strain rate (1/s)	3.09 ± 2.00	2.23, 3.96	3.40
Compressive strain rate (1/s)	2.35 ± 1.82	1.57, 3.15	2.09

No significant differences were reported in mechanical response between sex. All tests performed using a t-test are displayed as bar charts (Fig. 5). All tests performed using a Mann-Whitney U Test are displayed as histograms to present the distribution of the mechanical variables concerning sex (Fig. 6). By visual inspection, the distributional shapes between male and female compressive effective bending modulus were not comparable (Fig. 6). Thus, mean ranks were assessed between males (mean rank: 10.91) and females (mean rank: 13.00) for compressive effective bending modulus ($p=0.49$). Distributional shapes between male and female tensile effective bending modulus were comparable, therefore, medians were assessed between males (8.58 GPa) and females (7.52 GPa). No significant differences between sex were reported for the geometric properties (Table 5). Table 6 provides a comprehensive comparison between the present

study's findings to the quasi-static and dynamic bending results of adult calvaria reported in the literature. From independent-sample t-tests and Mann-Whitney U tests, the differences in mechanical response between regions (frontal and parietal) were not significant ($p > 0.05$), thus, including region as a second independent variable was not necessary for this study.

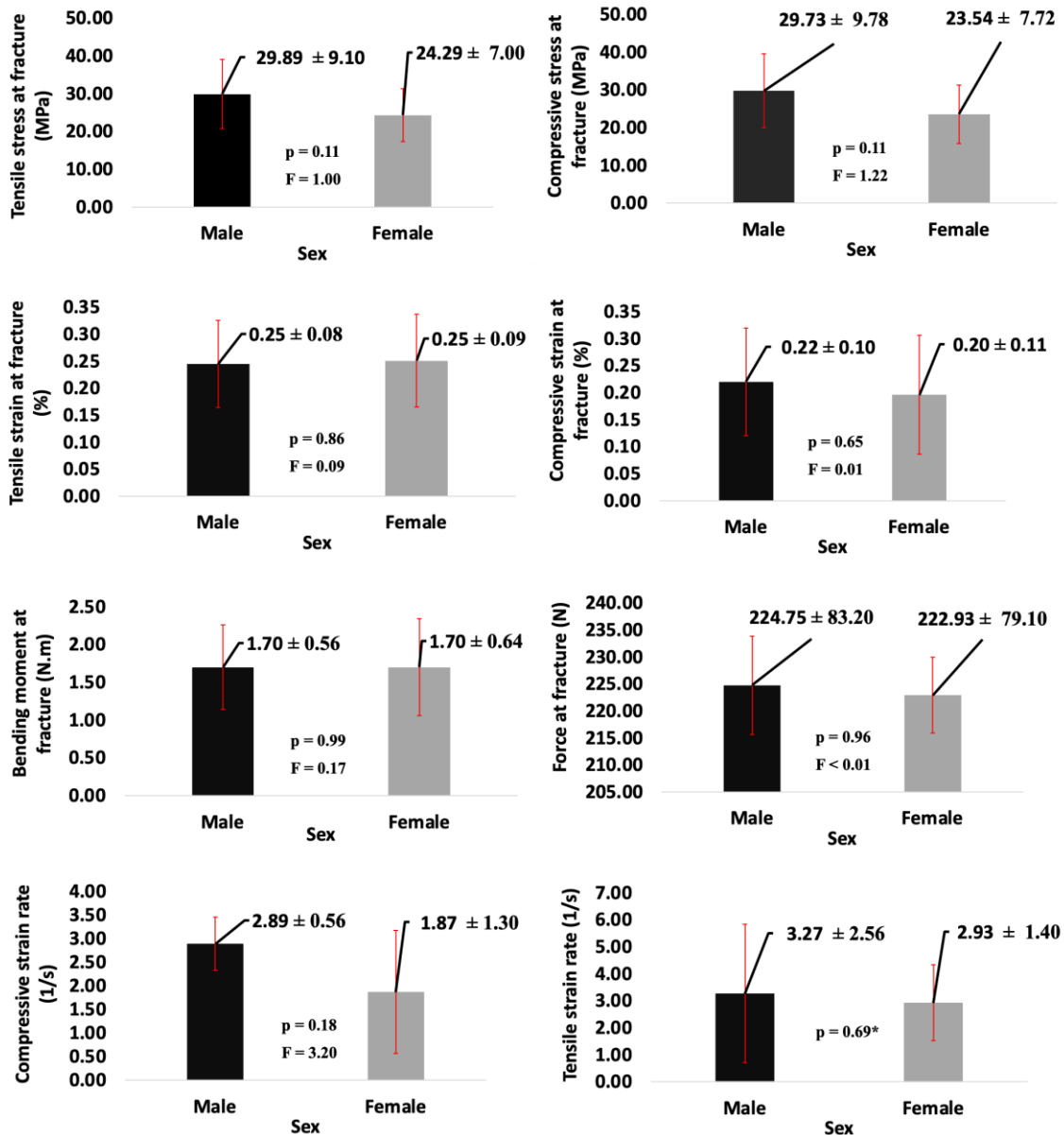


Figure 5. Bar charts comparing the mechanical response between male and female. * indicates a Welch t-test was performed for violating homogeneity of variance.

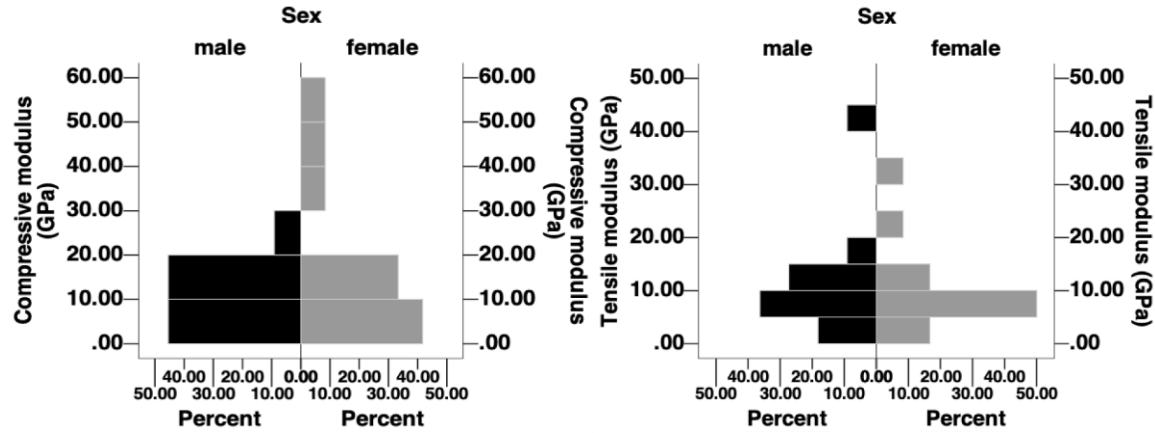


Figure 6. Histograms for compressive modulus and tensile modulus with respect to sex.

Table 5. Statistical report for the geometry of the calvaria presented in Table 1 where no significant differences in geometry were reported between sexes ($p > 0.05$).

Geometry	p-value	F-statistic
Length (mm)	0.65	0.32
Width (mm)	0.83*	-
Thickness (mm)	0.31**	-
2 nd moment of inertia (I) (m^4)	0.20	<0.01
Outer surface ROC (mm)	0.07	0.12
Inner surface ROC (mm)	0.13*	-

*Mann-Whitney U Test exact p-value. **Welch T-Test for violating homogeneity of variance.

Table 6. A comparison between the present study's 4-point bending impact results to bending test results on adult calvaria reported in the current literature. F, P, T, and O are frontal, parietal, temporal and occipital respectively. R and L refer to right and left respectively.

Authors	Q=quasi-static Or D=dynamic Impacts	E= embalmed Or UE = unembalmed	M=male or F=female	Age	Loading Rate (LR) & Strain Rate (SR)	Regions sampled	Force (N)	Bending Moment (N.m)	Stress (MPa)	Strain (%)	Modulus (GPa)
Hubbard (1971)	Q, 3-point Q, 4-point	E	-	N/A	SR: 0.01 s ⁻¹	P	-	4-point: 3.08	-	4-point: 0.51	3-point: 9.69
Delille et al. (2007)	Q, 3-point	UE	M, F	70.95	LR: 10 mm/min	F, P, T	-	-	-	-	<ul style="list-style-type: none"> RP: 5.00 LP: 4.90 F: 3.80 T: 11.30
Auperrin et al. (2014)	Q, 3-point	UE	M	74.8	LR: 10 mm/min	F, P, T	-	-	-	-	<ul style="list-style-type: none"> P: 5.00 F: 3.81 T: 9.70
Rahmoun et al. (2014)	Q, 3-point	-	M	88	LR: 10 mm/min	F, P, T coronal suture	-	-	-	-	<ul style="list-style-type: none"> RP: 3.74 LP: 4.53 F: 3.28 RT: 5.22 LT: 6.00 Coronal Suture: 2.04
Lee et al. (2019)	Q, 3-point	E	M	M=61 F=86	LR: 10 mm/min	F, P, T, O	-	-	<ul style="list-style-type: none"> Bare bone skull 1 & 2: 42 & 53 Bone with periosteum attached Skull 1 & 2: 68 & 99 	-	<ul style="list-style-type: none"> Bare bone skull 1 & 2: 1.70 & 2.74 Bone with periosteum attached skull 1 & 2: 2.28 & 3.95
Motherway et al. (2009)	D, 3-point	UE	M, F	81	<ul style="list-style-type: none"> LR: 0.5, 1, 2.5 m/s SR at 0.5 m/s: 19-22 s⁻¹ SR at 1 m/s: 25-31 s⁻¹ SR at 2.5 m/s: 102-110 s⁻¹ 	F, P	<ul style="list-style-type: none"> 0.5 m/s at RP, LP and F: 734.6, 721.7, 1062.3 1 m/s at RP, LP and F: 793.6, 584.3, 1035.9 0.5 m/s at RP, LP and F: 1161.9, 1228.6, 1315.9 	-	<ul style="list-style-type: none"> 0.5 m/s at RP, LP and F: 84.50, 82.13, 90.80 1 m/s at RP, LP and F: 82.98, 78.15, 102.60 0.5 m/s at RP, LP and F: 123.12, 133.61, 126.91 	-	<ul style="list-style-type: none"> 0.5 m/s at RP, LP and F: 10.33, 5.70, 4.35 1 m/s at RP, LP and F: 9.44, 17.69, 4.87 0.5 m/s at RP, LP and F: 12.80, 18.12, 16.34
Zwirner et al. (2021)	D, 3-point	E	M, F	48	LR: 2.5, 3.0, 3.5 m/s	F, P, T, O	<ul style="list-style-type: none"> 2.5 m/s: 716 3.5 m/s: 1264 2.5 m/s at T: 638 3.5 m/s at T: 1136 	-	<ul style="list-style-type: none"> 2.5 m/s: 98 3.0 m/s: 119 3.5 m/s: 130 	-	-
Present Study (2022)	D, 4-point	E	M, F	86.4, (82.4, 90.3)	<ul style="list-style-type: none"> LR: 0.86-0.89 m/s SR: Tensile = 3.09 s⁻¹ (2.23, 3.96) SR: Compressive = 2.35 s⁻¹ (1.57, 3.15) 	F, P	223.80 (189.28, 258.32)	1.70 (1.45, 1.96)	<ul style="list-style-type: none"> Tensile: 26.97 (23.34, 30.60) Compression: 26.50 (22.55, 30.45) 	<ul style="list-style-type: none"> Tensile: 0.25 (0.21, 0.28) Compression: 0.21 (0.16, 0.25) 	<ul style="list-style-type: none"> Tensile: 11.37 (7.25, 15.50) Compression: 14.71 (8.68, 20.75)

Verified through playback of high-speed video, fracture initiation originated at the tensile (inner cortical) surface and then propagated through the diploë and finally through the compressive (outer cortical) surface of the specimens as expected. Fracture did not always initiate at the location of the FBGs (center of the specimen) but rather anywhere between the two points of loading which was expected in 4-point bending since bending moment is constant and maximum between the two points of loading. As a result of this, the strain response imposed on the FBGs when a fracture occurred elsewhere was measured.

4. DISCUSSION

To our knowledge, this is the first set of works to study the mechanics of calvaria in a 4-point bending impact modality. The mechanical response of 23 calvaria at strain rates (2 to 3/s on average) associated with real-world head impacts was reported (Hosseini Farid et al., 2019; Zhai et al., 2020). No significant differences in mechanical response between sex were revealed.

An examination of the literature (see Table 6) disclosed two studies that conducted bending impacts on cranial specimens in a 3-point configuration (Motherway et al., 2009; Zwirner et al., 2021). Motherway et al. did not clarify their approach in computing strain rates but reported a range between 20-100/s for impact velocities between 0.5 and 2.5 m/s (Motherway et al., 2009). Zwirner et al. conducted impacts at 2.5, 3.0, and 3.5 m/s but failed to disclose strain rates (Zwirner et al., 2021). Nonetheless, at 2.5 m/s, Motherway et al. recorded greater fracture forces of 1161 N to 1315 N compared to Zwirner et al.'s findings which averaged 716 N (Motherway et al., 2009; Zwirner et al., 2021). In addition, Motherway et al.'s fracture forces at 1.0 m/s (584 N to 1035 N) (Motherway et al., 2009) were greater compared to the present study which documented an average of 223 N at 0.86-0.89 m/s. There is no single factor to explain the variation of fracture forces between the present work and the literature, however, there are a few characteristics from each study that may contribute to differences in mechanical properties (Motherway et al., 2009; Zwirner et al., 2021). The first characteristic is the difference in bending configuration between the present and previous works (Motherway et al., 2009; Zwirner et al., 2021). In the 3-point configuration, the peak stress is located directly below the single point of impact on the specimen, whereas the peak stress is distributed over the distance between two points of impact in the 4-point configuration. Additionally, in the 4-point configuration, the greater number of pores located in the specimens' diploë distributed between the two points of impact may contribute to reducing

overall bending strength compared to 3-point loading (McElhaney et al., 1970). This notion may be a contributing factor for observing lower stresses between the present work's findings at 27 MPa for 4-point loading and previous findings at 78 to 103 MPa in 3-point loading (Motherway et al., 2009). Two studies that examined polymer and wood-based materials found that 3-point bending yielded greater bending strength compared to 4-point bending (Chitchumnong et al., 1989; Hein et al., 2018). An additional consideration worth noting is that the kinetic energy ($0.5 \cdot m \cdot v^2$) and geometry of the impacting mass may be distinct across studies despite similar impact velocities. This may also influence mechanical outcomes such as force and stress. A second characteristic between studies is morphometry, donor age, and treatment of specimens (Adanty et al., 2021). In the present study, specimens were extracted from the frontal and parietal regions in which density, porosity, and diploë or cortical morphometry may be distinctive to temporal and occipital specimens employed by Zwirner et al. (Adanty et al., 2021; Zwirner et al., 2021). Zwirner et al. also sampled specimens from cadavers with an average age of 48 years old over a range of 3 weeks to 94 years old, however, the present work sampled from donors at an average age of 86 years old and Motherway et al. from 81 years old (Motherway et al., 2009). Age may influence the biomechanical response of the calvarium and warrants further investigation (Motherway et al., 2009; Zwirner et al., 2021). Concerning tissue treatment, the present study extracted embalmed tissue, Zwirner et al. extracted samples at a median of 70-h post-mortem with a freeze-thaw procedure prior to testing, and Motherway et al. obtained samples from fresh-frozen cadavers (Motherway et al., 2009; Zwirner et al., 2021). According to previous studies, different tissue treatments or preservation methods may or may not significantly affect the mechanical response of bone (Burkhart et al., 2010; Carothers et al., 1949; Crandall, 1994; Evans, 1973; K. E. Lee & Pelker, 1985; Mick et al., 2015; Nahum et al., 1968; Nazarian et al., 2009; Pelker et al., 1984; Topp

et al., 2012; Wilke et al., 1996), nevertheless, future work should investigate if fresh, fresh-frozen, and embalmed tissue influence the calvarium's mechanical response.

Despite differing characteristics between the present work and previous findings, one optimistic observation is that the bending moduli from Motherway et al.'s work (5-19 GPa) are in the range of effective bending moduli reported in the present work (7.25-20.75 GPa), see Table 6. Conversely, and as shown in Table 6, the average bending moduli derived from 3-point quasi-static bending (1.70-11.30 GPa) (Auperrin et al., 2014; Hubbard, 1971; J. H. C. Lee et al., 2019; Rahmoun et al., 2014) falls in the lower end of the spectrum for the range of bending moduli presented in this study (7.25-20.75 GPa) and Motherway et al.'s findings (5-19 GPa) (Motherway et al., 2009). This can simply be attributed to contrary loading and strain rates between the dynamic and quasi-static testing which also verifies the viscoelastic nature of biological specimens - strain rate dependent. In any case, one must cautiously compare information gathered from quasi-static and impact testing. In quasi-static loading, the force applicator is pre-loaded on the specimen, the load is applied in a way that inertial effects of the specimen can be ignored, and strain rates remain relatively constant until fracture. Conversely, as observed in the present study, the force applicator is not pre-loaded on the specimen resulting in a sudden impact. As shown in Figure 4, the strain-time curve for one sample exhibits a non-linear behaviour until about 0.05 %, this could be the region where the impact prongs are first adapting to full contact with the specimen. After about 0.05% the strain then begins a gradual linear response as well as its corresponding stress-strain curve. It was in this linear region modulus was determined such that the strain-rate remained constant (Figure 4). Since such a sudden impact is a defining characteristic of real-world head impacts, future work should consider the effect of inertial response such as the specimen acceleration during impact on mechanical properties. The present study is the first set of works to

document strains on both the inner cortical and outer cortical surfaces of calvaria using FBGs. The strains at fracture in the present study are marginally less (0.21-0.25%) than the tensile surface strains reported in quasi-static bending by Hubbard (0.33-0.76%) and Adanty et al. (mean: 0.31 %) (Adanty, Tronchin, et al., 2020; Hubbard, 1971). This may suggest that greater strain rates observed during impact bending can initiate a fracture at lower strains compared to specimens subjected to quasi-static bending at lower strain rates (Ural et al., 2011). To support this suggestion, a study on tensile loading of human cranial bone found a negative linear regression coefficient deemed significant between breaking strain and strain rate (Wood, 1971). Therefore, from a logical standpoint, the strain at fracture attributed to a strain rate of $2\text{-}3\text{ s}^{-1}$ in the present study should be less than the strain reported by Hubbard that yielded a strain rate of 0.01 s^{-1} .

There was no evidence to reject the null hypothesis: *no significant differences in mechanical response between male and female calvaria*. Likewise, recent work by Zwirner et al. produced sex-independent force and stress measurements (Zwirner et al., 2021). Compared to work on load-bearing bones in humans, there is scarce literature differentiating the mechanical properties of male and female crania (Nieves et al., 2005). One probable factor for observing no differences was the comparable geometry in specimens between sex since specimen thickness and second moment of inertia are associated with the computation of bending stress and modulus. Similarly, surface strain is a measure proportional to the specimen geometry (Hubbard, 1971). Since the calvarium is a three-layered composite structure, Hubbard demonstrated that surface strain on the cortical layer is a function of calvarium thickness and bending stiffness, where stiffness is related to second moment of inertia and elastic modulus (Hubbard, 1971). For surrogate and computational modellers, the present work's findings on sex-independent mechanical response may infer that future calvarium models irrespective of sex are appropriate to model injury

for the general population. However, a greater sample size across different age groups and greater impact speeds are required to support the present work's findings.

5. LIMITATIONS

5.1 Specimens

The findings from the present study are biased towards an older age population in the province of Alberta, Canada, therefore, future work is encouraged to perform testing on a younger age cohort or a specific population more vulnerable to head injury. Despite performing a power analysis, the authors of this work acknowledge limitations on the sample size. The specimens in this work were sampled by convenience, meaning it was the maximum number of specimens accessible to the authors at the time of the study. The authors limited the extraction of the specimens on each calvarium in a horizontal orientation (parallel to sutures) at the frontal (medial to lateral) and parietal (anterior to posterior) regions as displayed in Figure 1. This is one orientation out of many in which the specimens could have been extracted, however, bony prominence regions can vary in size and geometry between individual calvaria. For example, extracting specimens in the vertical orientation at the frontal region would require carefulness when cutting through the metopic ridge and the frontal eminence as the curvature considerably changes when cutting superior to inferior or vice versa. The result of this would then be calvarium beam specimens with a complex curvature that would then be challenging to configure for impact in 4-point bending. Nonetheless, the authors suggest future studies consider harvesting specimens at multiple orientations to account for the anisotropic nature of bone during mechanical testing.

The current study employed embalmed calvarium specimens. In biomechanical research, tissue is preserved with embalming fluid for the following reasons: 1) if fresh tissue is inaccessible and sufficient sample size is required, 2) if additional time and care are necessary to apply instrumentation and prepare for mechanical testing, and 3) to prevent the transmission of infectious diseases such as AIDS (HIV), Hepatitis, and more recently SARS-CoV-2 virus (Crandall, 1994).

To determine the mechanical effects embalming may have on fresh tissue, we investigated a dissertation by Crandall (1994) that mechanically tested 150 bovine ribs (Crandall, 1994). Similar to the geometry of calvaria employed in the present study, the ribs were curved and comprised cortical and trabecular tissue. The ribs were also tested under bending conditions like the calvaria in the present study, except under 3-point quasi-static loading. The calvaria used in this study were subject to formaldehyde embalming fluid, similarly, two groups of ribs from Crandall's work were subject to formaldehyde solution by Michigan Anatomical Fluid and formaldehyde by University of Virginia Fluid (Crandall, 1994). Both groups of ribs treated with formaldehyde were found to have a less than 12% difference in elastic modulus, yield stress, ultimate stress, and ultimate strain compared to the fresh ribs which were not statistically significant (Crandall, 1994). Rather, the frozen group of ribs had up to a 25% and 28% difference compared to fresh and embalmed ribs respectively which were both statistically significant (Crandall, 1994). Meanwhile, previous studies cited by Crandall showed that the freezing process was an appropriate preservation technique that did not affect material properties (K. E. Lee & Pelker, 1985; Pelker et al., 1984). In addition to Crandall's findings, Nazarian et al. found that formalin altered the viscoelasticity of bone significantly, but bending stiffness, modulus of elasticity, yield displacement, yield load, yield strain, and yield strength was not significantly different between frozen, formalin-fixed, and fresh murine bone (Nazarian et al., 2009). Mick et al. and Topp et al. demonstrated that there were no significant differences between embalmed and fresh-frozen tissue of the human femur (Mick et al., 2015; Topp et al., 2012). Wilke et al. showed the range of motion for L1-L2 spinal segments from 16-week-old calves was significantly reduced in the embalmed group compared to the fresh group (Wilke et al., 1996). Earlier studies by Carothers et al. (1949) and Evans (1973) showed that formalin can significantly increase the strength of human long bones under tensile and bending

loading (Carothers et al., 1949; Evans, 1973). Burkhart et al. showed that the axial stiffness of human femora significantly increased by 14% in the embalmed group compared to the fresh group (Burkhart et al., 2010). In summary, embalming of tissue is indeed a limitation but its mechanical effect on fresh tissue is inconsistent across the literature and we cannot be certain on how much it influences calvarium exclusively. Therefore, when it comes to the human calvarium it is unknown how much of a biomechanical effect embalming has on fresh calvaria. We encourage future studies to explore different forms of tissue preservations and their mechanical effect on skull or calvarium tissue to formulate if the use of embalmed skull tissue is truly a viable source or not for biomechanical testing.

5.2 Mechanical Testing

As discussed earlier, most specimens experienced fracture initiation between the two points of loading, however, few specimens experienced fracture initiation under one of the two points of loading. One possible reason for this occurrence is because, at that point of loading, the specimen contained a considerable number of pores in the diploë that weakened the specimen at that area and thus initiated fracture at that point. This may not necessarily be a limitation with respect to the specimen's natural morphology, however, it may be a limitation to consider when using 4-point bending for impact on a nonhomogeneous structure. The pattern or shape of the fracture was not reported as this study was concerned with quantifying mechanical response at fracture. However, future work may consider documenting qualitative observations on fracture shapes and patterns - butterfly fracture, linear fracture, or oblique fracture as these are important characteristics to consider when developing models to mimic skull fracture. The authors acknowledge the limitations of modelling the specimens as a Euler-Bernoulli beam to estimate bending stress. The authors attempted to model the bending stress using the curved beam theorem based on equations

proposed by Roark and Young (2002) (Roark et al., 2002). The stress at fracture derived from the curved beam theorem had an average percent difference of 1.66 % in tensile stress at fracture and a difference of 2.13 % in compressive stress at fracture with respect to fracture stress derived from the Euler-Bernoulli beam theorem. This percent difference is less than the 4-5% error advised by Roark and Young (2002) when applying the Euler-Bernoulli beam theorem on a curved beam (Roark et al., 2002). One possible explanation for this small difference between the two theorems is that the calvarium specimens fractured at small strains of less than 0.5 % which satisfies the assumption of small deformation when applying the Euler-Bernoulli beam theorem.

6. CONCLUSION

To express the importance of testing human calvaria under conditions most applicable to real-world head impacts (strain rates $> 1s^{-1}$), the mechanical response of calvaria subjected to 4-point bending impacts was determined. The present study documented effective bending moduli that were in line with previous studies that performed 3-point impact bending on calvaria, however, fracture bending stress was less. Surface strains were relatively less compared to previous findings that quantified surface strains during quasi-static bending. No significant differences in mechanical response between male and female calvaria were established.

ACKNOWLEDGMENT

The authors would like to thank Hugh Barrett, Jason Papirny, and Dr. Daniel Livy of the University of Alberta's Division Anatomy for providing access to human cadavers and the necessary aid during dissection.

FUNDING

Funding: This research was sponsored by the US Army Combat Capabilities Development Command - Army Research Laboratory and the International Technical Center Americas under Cooperative Agreement Number W911NF-19-2-0336. The views and conclusions contained in this document are those of the authors and should not be interpreted as representing the official policies, either expressed or implied, of the Army Research Laboratory or the U.S. Government. The U.S. Government is authorized to reproduce and distribute reprints for Government purposes notwithstanding any copyright notation herein. The authors declare that the roles of this study's sponsor included the financial resources to complete the study, the analysis and interpretation of data, the writing of the manuscript, and the decision to submit the manuscript for publication.

REFERENCES

- Aare, M., & Halldin, P. (2003). A New Laboratory Rig for Evaluating Helmets Subject to Oblique Impacts. *Traffic Injury Prevention, 4*(3), 240–248. <https://doi.org/10.1080/15389580309879>
- Adanty, K., Clark, J. M., Post, A., Hoshizaki, T. B., & Gilchrist, M. D. (2020). Comparing two proposed protocols to test the oblique response of cycling helmets to fall impacts. *International Journal of Crashworthiness, 25*(6), 648–663. <https://doi.org/10.1080/13588265.2019.1628479>
- Adanty, K., Rabey, K. N., Doschak, M. R., Bhagavathula, K. B., Hogan, J. D., Romanyk, D. L., Adeeb, S., Ouellet, S., Plaisted, T. A., Satapathy, S. S., & Dennison, C. R. (2021). Cortical and trabecular morphometric properties of the human calvarium. *Bone, 148*, 115931. <https://doi.org/10.1016/j.bone.2021.115931>
- Adanty, K., Tronchin, O., Bhagavathula, K. B., Rabey, K. N., Doschak, M. R., Romanyk, D., Hogan, J. D., Ouellet, S., Plaisted, T. A., Satapathy, S. S., & Dennison, C. R. (2020). On the Ability of Morphometric Indices of Skull Diploë to Explain Variation in Bone Fracture Force and Fracture Strain in Four-Point Bending: A Preliminary Step Toward A Simulant Fracture Model. *IRCOBI Conference 2020*, 821–822.
- Adeeb, S. (2011). *Introduction to Solid Mechanics and Finite Element Analysis Using Mathematica* (1st ed.). Kendall Hunt. <https://he.kendallhunt.com/product/introduction-solid-mechanics-and-finite-element-analysis-using-mathematica>
- Al-Fakih, E., Osman, N. A. A., & Adikan, F. R. M. (2012). The Use of Fiber Bragg Grating Sensors in Biomechanics and Rehabilitation Applications: The State-of-the-Art and Ongoing Research Topics. *Sensors (Basel, Switzerland), 12*(10), 12890–12926. <https://doi.org/10.3390/s121012890>
- Auperrin, A., Delille, R., Lesueur, D., Bruyère, K., Masson, C., & Drazétic, P. (2014). Geometrical and material parameters to assess the macroscopic mechanical behaviour of fresh cranial bone samples. *Journal of Biomechanics, 47*(5), 1180–1185. <https://doi.org/10.1016/j.jbiomech.2013.10.060>
- Burkhart, K. J., Nowak, T. E., Blum, J., Kuhn, S., Welker, M., Sternstein, W., Mueller, L. P., & Rommens, P. M. (2010). Influence of formalin fixation on the biomechanical properties of human diaphyseal bone. *Biomedizinische Technik. Biomedical Engineering, 55*(6), 361–365. <https://doi.org/10.1515/BMT.2010.043>
- Carothers, C., Smith, F., & Calabrasi, P. (1949). *Naval Medical Research Report NM 001 056.02.13*.
- Chitchumnong, P., Brooks, S. C., & Stafford, G. D. (1989). Comparison of three- and four-point flexural strength testing of denture-base polymers. *Dental Materials, 5*(1), 2–5. [https://doi.org/10.1016/0109-5641\(89\)90082-1](https://doi.org/10.1016/0109-5641(89)90082-1)
- Crandall, J. R. (1994). *The preservation of human surrogates for biomechanical studies*. University of Virginia.

- Davis, M. T., Loyd, A. M., Shen, H. H., Mulroy, M. H., Nightingale, R. W., Myers, B. S., & Bass, C. D. (2012). The mechanical and morphological properties of 6 year-old cranial bone. *Journal of Biomechanics*, 45(15), 2493–2498. <https://doi.org/10.1016/j.jbiomech.2012.07.001>
- Delaney, J. S. (2004). Head Injuries Presenting to Emergency Departments in the United States From 1990 to 1999 for Ice Hockey, Soccer, and Football. *Clinical Journal of Sport Medicine*, 14(2), 80–87.
- Delille, R., Lesueur, D., Potier, P., Drazetic, P., & Markiewicz, E. (2007). Experimental study of the bone behaviour of the human skull bone for the development of a physical head model. *International Journal of Crashworthiness*, 12(2), 101–108. <https://doi.org/10.1080/13588260701433081>
- Dennison, C. R., & Wild, P. M. (2008). Enhanced sensitivity of an in-fibre Bragg grating pressure sensor achieved through fibre diameter reduction. *Measurement Science and Technology*, 19, 11pp.
- Doube, M., Kłosowski, M. M., Arganda-Carreras, I., Cordelières, F. P., Dougherty, R. P., Jackson, J. S., Schmid, B., Hutchinson, J. R., & Shefelbine, S. J. (2010). BoneJ: Free and extensible bone image analysis in ImageJ. *Bone*, 47(6), 1076–1079. <https://doi.org/10.1016/j.bone.2010.08.023>
- Eng, J. (2003). Sample Size Estimation: How Many Individuals Should Be Studied?1. *Radiology*. <https://pubs.rsna.org/doi/abs/10.1148/radiol.2272012051>
- Evans, F. G. (1973). *Mechanical Properties of Bone*. Charles C. Thomas.
- Hayes, M. D., Edwards, D. B., & Shah, A. R. (2015). 4—Fractography Basics. In M. D. Hayes, D. B. Edwards, & A. R. Shah (Eds.), *Fractography in Failure Analysis of Polymers* (pp. 48–92). William Andrew Publishing. <https://doi.org/10.1016/B978-0-323-24272-1.00004-0>
- Hein, P. R. G., Brancheriau, L., Hein, P. R. G., & Brancheriau, L. (2018). Comparison between three-point and four-point flexural tests to determine wood strength of Eucalyptus specimens. *Maderas. Ciencia y Tecnología*, 20(3), 333–342. <https://doi.org/10.4067/S0718-221X2018005003401>
- Hosseini Farid, M., Eslaminejad, A., Ramzanpour, M., Ziejewski, M., & Karami, G. (2019, January 15). *The Strain Rates of the Brain and Skull Under Dynamic Loading*. ASME 2018 International Mechanical Engineering Congress and Exposition. <https://doi.org/10.1115/IMECE2018-88300>
- Houg, K. P., Armijo, L., Doschak, M. R., Major, P. W., Popowics, T., Dennison, C. R., & Romanyk, D. L. (2021). Experimental repeatability, sensitivity, and reproducibility of force and strain measurements from within the periodontal ligament space during ex vivo swine tooth loading. *Journal of the Mechanical Behavior of Biomedical Materials*, 120, 104562. <https://doi.org/10.1016/j.jmbbm.2021.104562>
- Hubbard, R. P. (1971). Flexure of layered cranial bone. *Journal of Biomechanics*, 4(4), 251–263. [https://doi.org/10.1016/0021-9290\(71\)90031-5](https://doi.org/10.1016/0021-9290(71)90031-5)

- Igo, B. J., Cottler, P. S., Black, J. S., & Panzer, M. B. (2021). The mechanical and microstructural properties of the pediatric skull. *Journal of the Mechanical Behavior of Biomedical Materials*, *120*, 104578. <https://doi.org/10.1016/j.jmbbm.2021.104578>
- Karton, C., Blaine Hoshizaki, T., & Gilchrist, M. D. (2020). A novel repetitive head impact exposure measurement tool differentiates player position in National Football League. *Scientific Reports*, *10*(1), Article 1. <https://doi.org/10.1038/s41598-019-54874-9>
- Knowles, B. M., & Dennison, C. R. (2017). Predicting Cumulative and Maximum Brain Strain Measures From HybridIII Head Kinematics: A Combined Laboratory Study and Post-Hoc Regression Analysis. *Annals of Biomedical Engineering*, *45*(9), 2146–2158. <https://doi.org/10.1007/s10439-017-1848-y>
- Lee, J. H. C., Ondruschka, B., Falland-Cheung, L., Scholze, M., Hammer, N., Tong, D. C., & Waddell, J. N. (2019). An Investigation on the Correlation between the Mechanical Properties of Human Skull Bone, Its Geometry, Microarchitectural Properties, and Water Content. *Journal of Healthcare Engineering*, *2019*, 1–8. <https://doi.org/10.1155/2019/6515797>
- Lee, K. E., & Pelker, R. R. (1985). Effect of freezing on histologic and biomechanical failure patterns in the rabbit capital femoral growth plate. *Journal of Orthopaedic Research: Official Publication of the Orthopaedic Research Society*, *3*(4), 514–515. <https://doi.org/10.1002/jor.1100030415>
- Li, Y., Ouellet, S., Vette, A. H., Raboud, D., Martin, A., & Dennison, C. R. (2021). Evaluation of the Kinematic Biofidelity and Inter-Test Repeatability of Global Accelerations and Brain Parenchyma Pressure for a Head–Brain Physical Model. *Journal of Biomechanical Engineering*, *143*(9). <https://doi.org/10.1115/1.4050752>
- Margulies, S. S., & Thibault, K. L. (2000). Infant Skull and Suture Properties: Measurements and Implications for Mechanisms of Pediatric Brain Injury. *Journal of Biomechanical Engineering*, *122*(4), 364–371. <https://doi.org/10.1115/1.1287160>
- McElhaney, J. H., Fogle, J. L., Melvin, J. W., Haynes, R. R., Roberts, V. L., & Alem, N. M. (1970). Mechanical properties of cranial bone. *Journal of Biomechanics*, *3*(5), 495–511. [https://doi.org/10.1016/0021-9290\(70\)90059-X](https://doi.org/10.1016/0021-9290(70)90059-X)
- Melvin, J. W., & Yoganandan, N. (2015). Biomechanics of Brain Injury: A Historical Perspective. In N. Yoganandan, A. M. Nahum, & J. W. Melvin (Eds.), *Accidental Injury: Biomechanics and Prevention* (pp. 221–245). Springer. https://doi.org/10.1007/978-1-4939-1732-7_9
- Mick, E., Steinke, H., Wolfskämpf, T., Wieding, J., Hammer, N., Schulze, M., Souffrant, R., & Bader, R. (2015). Influence of short-term fixation with mixed formalin or ethanol solution on the mechanical properties of human cortical bone. *Current Directions in Biomedical Engineering*, *1*(1), 335–339. <https://doi.org/10.1515/cdbme-2015-0083>
- Motherway, J. A., Verschueren, P., Van der Perre, G., Vander Sloten, J., & Gilchrist, M. D. (2009). The mechanical properties of cranial bone: The effect of loading rate and cranial sampling position. *Journal of Biomechanics*, *42*(13), 2129–2135. <https://doi.org/10.1016/j.jbiomech.2009.05.030>

- Nahum, A. M., Gatts, J. D., Gadd, C. W., & Danforth, J. (1968). *Impact Tolerance of the Skull and Face* (SAE Technical Paper No. 680785). SAE International. <https://doi.org/10.4271/680785>
- Nazarian, A., Hermannsson, B. J., Muller, J., Zurakowski, D., & Snyder, B. D. (2009). Effects of tissue preservation on murine bone mechanical properties. *Journal of Biomechanics*, *42*(1), 82–86. <https://doi.org/10.1016/j.jbiomech.2008.09.037>
- Nieves, J. W., Formica, C., Ruffing, J., Zion, M., Garrett, P., Lindsay, R., & Cosman, F. (2005). Males Have Larger Skeletal Size and Bone Mass Than Females, Despite Comparable Body Size. *Journal of Bone and Mineral Research*, *20*(3), 529–535. <https://doi.org/10.1359/JBMR.041005>
- Pelker, R. R., Friedlaender, G. E., Markham, T. C., Panjabi, M. M., & Moen, C. J. (1984). Effects of freezing and freeze-drying on the biomechanical properties of rat bone. *Journal of Orthopaedic Research: Official Publication of the Orthopaedic Research Society*, *1*(4), 405–411. <https://doi.org/10.1002/jor.1100010409>
- Rahmoun, J., Auperrin, A., Delille, R., Naceur, H., & Drazetic, P. (2014). Characterization and micromechanical modeling of the human cranial bone elastic properties. *Mechanics Research Communications*, *60*, 7–14. <https://doi.org/10.1016/j.mechrescom.2014.04.001>
- Roark, R. J., Young, W. C., & Budynas, R. G. (2002). *Roark's formulas for stress and strain* (7th ed). McGraw-Hill.
- Tian, H., Liu, D., Wang, Y., & Wang, Q. (2019). Effect of adhesive type on the sensitivity coefficient of FBG sensor bonded on the surface of CFRP. *Optoelectronics Letters*, *15*(4), 264–268. <https://doi.org/10.1007/s11801-019-8183-5>
- Topp, T., Müller, T., Huss, S., Kann, P. H., Weihe, E., Ruchholtz, S., & Zettl, R. P. (2012). Embalmed and fresh frozen human bones in orthopedic cadaveric studies: Which bone is authentic and feasible? *Acta Orthopaedica*, *83*(5), 543–547. <https://doi.org/10.3109/17453674.2012.727079>
- Ural, A., Zioupos, P., Buchanan, D., & Vashishth, D. (2011). THE EFFECT OF STRAIN RATE ON FRACTURE TOUGHNESS OF HUMAN CORTICAL BONE: A FINITE ELEMENT STUDY. *Journal of the Mechanical Behavior of Biomedical Materials*, *4*(7), 1021–1032. <https://doi.org/10.1016/j.jmbbm.2011.03.011>
- Weisenbach, C. A., Logsdon, K., Salzar, R. S., Chancey, V. C., & Brozoski, F. (2018). Preliminary Investigation of Skull Fracture Patterns Using an Impactor Representative of Helmet Back-Face Deformation. *Military Medicine*, *183*(suppl_1), 287–293. <https://doi.org/10.1093/milmed/usx210>
- Wilke, H.-J., Krischak, S., & Claes, L. E. (1996). Formalin fixation strongly influences biomechanical properties of the spine. *Journal of Biomechanics*, *29*(12), 1629–1631. [https://doi.org/10.1016/S0021-9290\(96\)80016-9](https://doi.org/10.1016/S0021-9290(96)80016-9)
- Wood, J. L. (1971). Dynamic response of human cranial bone. *Journal of Biomechanics*, *4*(1), 1–12. [https://doi.org/10.1016/0021-9290\(71\)90010-8](https://doi.org/10.1016/0021-9290(71)90010-8)
- Zhai, X., Nauman, E. A., Moryl, D., Lycke, R., & Chen, W. W. (2020). The effects of loading-direction and strain-rate on the mechanical behaviors of human frontal skull bone. *Journal of the*

Mechanical Behavior of Biomedical Materials, 103, 103597.
<https://doi.org/10.1016/j.jmbbm.2019.103597>

Zwirner, J., Ondruschka, B., Scholze, M., Workman, J., Thambyah, A., & Hammer, N. (2021). The dynamic impact behavior of the human neurocranium. *Scientific Reports*, 11(1), 11331.
<https://doi.org/10.1038/s41598-021-90322-3>

Chapter 4: The Development of Preliminary Human Calvarium Surrogate Models to Mimic Mechanical Response at Fracture.

Chapter 4 obtained the geometrical properties of the calvarium accumulated through Chapters 1 to 3 to guide the fabrication of three preliminary surrogate models. The surrogate models were then statistically compared with the mechanical response variables of the calvarium specimens presented in Chapters 2 (quasi-static loading) and 3 (dynamic impact loading). The development of the surrogate models was not possible without characterizing the geometry, morphometry, and mechanical response of the calvarium reported in the previous chapters. To develop the surrogates, a simple approach using cost-effective and readily available materials was considered. The current chapter evaluated which surrogate model would be a suitable candidate for further development when mimicking the mechanical response of the calvarium at fracture. The findings from Chapter 4 fulfill *sub-objective 4: Develop preliminary surrogate models of the human calvarium to mimic the calvarium's mechanical response at fracture*. Chapter 4 has been submitted to *Annals of Biomedical Engineering*.

A Preliminary Step Towards A Physical Surrogate of The Human Calvarium To Model Fracture

ABSTRACT

A surrogate model of the human calvarium can be used to assess skull-fracture-related head injuries without continuously requiring post-mortem human skulls. Skull simulants developed in the literature often require sophisticated manufacturing procedures and/or materials not always practical when factoring in time or expense considerations. This study's objective was to fabricate three different exploratory surrogate models of the calvarium to mimic the calvarium's mechanical response at fracture using readily available and cost-effective materials, specifically epoxy and chalk. The surrogates and calvaria were subject to quasi-static and dynamic impact 4-point bending and their mechanical responses were compared statistically. Under quasi-static loading, all three surrogates showed a considerable number of significant differences in mechanical response variables to calvaria ($p < 0.05$). Under dynamic impact loading, an epoxy-chalk three-layered surrogate showed the most non-significant ($p > 0.05$) differences in mechanical response variables when compared to calvaria. This included force and bending moment at fracture, tensile strain at fracture, tensile and compressive stress at fracture, tensile modulus, and tensile strain rate. Our study illustrates that employing epoxy and chalk, which are readily available and cost-effective, and structuring them in a three-layered concept, similar to the calvarium, has the potential to mimic the mechanical response of calvaria in impact loading.

Key Terms: cost-effective, readily-available, pragmatic, biomechanical testing, epoxy, chalk

1. INTRODUCTION

If blunt force trauma delivered to the head is great enough, a skull fracture can occur. This type of head injury can be fatal and may result in a severe life-threatening brain injury (Macpherson et al., 1990). Recent reports show that a skull fracture is most commonly reported in motor-vehicle accidents and falls (Marks, 2005). A skull fracture may also arise from extreme sports, criminal assaults, and back-face deformation arising from ballistic-loaded military helmets (Chattopadhyay & Tripathi, 2010; Sharma et al., 2015; Weisenbach et al., 2018). Given the commonplace circumstances in which a skull fracture can occur, it is important to study the biomechanics of a skull fracture so that preventative measures can be proposed to reduce its likelihood of occurrence. To study the biomechanics of a skull fracture, a physical surrogate of the calvarium that is frangible and mimics the mechanical response at fracture of the calvarium is necessary for head impact experimentation. The surrogate can then be integrated with existing headforms to simulate skull fracture events and evaluate protective equipment.

Indeed, the ideal surrogate to conduct trauma-induced impacts to mimic fracture is the human skull or intact human head harvested from post-mortem human subjects (PMHS). Though, PMHSs are not easily obtainable due to factors such as financial costs, nationwide laws that may restrict research on PMHS, and complex logistic and storage methods for PMH tissue. In addition, variations in the biomechanical properties of PMH tissue are often large due to morphological distinctions across subjects. When tissue from PMHS is unobtainable but physiological conditions analogous to humans are required, live or sacrificed animal head models are used as alternative surrogates to model a skull fracture or injury (Gurdjian & Lissner, 1947; Hodgson & Thomas, 1972; Liu et al., 2012). However, their distinct Haversian system of bone, less discernment of cortical and trabecular separation compared to human calvaria, and the cost associated with

maintaining live animals introduce challenges in biomechanical research (Hillier & Bell, 2007). Some anthropomorphic test devices (ATDs) of the head have been developed to quantify and determine the potential for which a skull fracture may occur such as the ballistic load sensing headform (BLSH) (Anctil et al., 2008) or the National Institute of Justice (NIJ) clay-based headform (JAMES L. UNDERWOOD, n.d.). ATD headforms are necessary for acquiring repeatable and reproducible global head kinematic response over repeated trials. However, their stiff or over-compliant material composition prevents the true observation of skull deformation resulting in a fracture (Anctil et al., 2008; Hubbard & McLeod, 1974; JAMES L. UNDERWOOD, n.d.). Perhaps the introduction of a surrogate or test device that deforms and fractures in a similar nature to a real skull would allow for a realistic coupling between the impacting object and the head, and subsequently, a realistic coupling between the surrogate and the brain during skull deformation. Lastly, computational models of the skull developed through finite element methods (FEM) are also a convenient means to model fracture, particularly if physical models are inaccessible. Nonetheless, simulation time, model verification, element selection, boundary conditions, and assumptions regarding material behaviour all pose challenges when considering computational models. It may then be appropriate to turn towards readily available materials and cost-effective strategies to design a simple physical surrogate of the calvarium that can mimic its biomechanical response at fracture. Such a simplified approach would enable biomechanical researchers and forensic scientists to easily simulate fracture on a cost and time – effective bases.

Preliminary efforts have been made to develop a surrogate model of the skull (Thali et al., 2002) or calvarium (Delille et al., 2007). Alternatively, many have tested synthetic bone models to compare their surrogates' mechanical properties to calvarium (Brown et al., 2019; Falland-Cheung et al., 2017; Ondruschka et al., 2019; Plaisted et al., 2015; Roberts et al., 2013). Thali et

al. introduced a synthetic “skin-skull-brain model” to simulate gunshot wounds to the head (Thali et al., 2002). Their model consisted of a layered polyurethane skull that featured an internal and external tabula and a porous diploë sandwiched in between the tabula. The mechanical response of their model was not determined but it exhibited realistic linear fracture profiles arising from the entrance wounds of the ballistic projectiles (Thali et al., 2002). Delille et al. developed a new physical head model in an attempt to replace the standard Hybrid III headform (Delille et al., 2007). However, the type of resin chosen to construct their skull model was not specified. When investigating the force-time response of their model with respect to cadaveric results by Nahum et al. (Nahum et al., 1977), they suggested their overall model was more biofidelic in terms of impact duration than the Hybrid III headform (composed of steel and rubber) (Delille et al., 2007). Roberts et al. developed surrogates with commercial grade epoxy resin (EPON 815C or 862) mixed with 30% milled glass fibres to model the cortical tables of the calvarium, while the diploë was modelled with urethane foams (US Foam #16 and BJB-TC). Their surrogates yielded peak bending stresses within the range of calvarium, but their bending modulus was less compared to calvarium when undergoing quasi-static three-point bending. Moreover, the force to fracture for their surrogate plate models that underwent flat panel drop tests was less in comparison to impact testing on intact human skulls (Roberts et al., 2013). In two studies, high-strength epoxy resin (MasterFlow, Germany) used to model the calvarium was loaded in quasi-static three-point bending (Falland-Cheung et al., 2017; Ondruschka et al., 2019). Both studies reported high-strength epoxy resin to be within the range of calvarium for bending strength but, their modulus values fell in the lower end of the range of calvarium. Plaisted et al. (2015) used stereolithographic additive processing to produce composite structures consisting of a photocurable polymer and a high-loading ceramic to mimic fracture (Plaisted et al., 2015). Under quasi-static tensile loading,

their composite structures fell within the range of tensile strength and modulus of elasticity reported for calvaria (Plaisted et al., 2015). Brown et al. (2019) conducted high-rate compression testing on commercially available bone surrogates using a Split-Hopkinson Pressure bar system (Brown et al., 2019). Their bone surrogates (BoneSim, Synbone, and Sawbone) did not display the potential to mimic the brittle comportment of bone (Brown et al., 2019). In their study, Bonesim appeared to be the only viable material to align with compressive modulus, yield and ultimate strength of calvarium (Brown et al., 2019).

The purpose of this study was to present a simple and pragmatic approach toward the development of three preliminary surrogate models of the human calvarium with the intent to mimic the mechanical response of the calvarium at fracture. In addition, hypothesis testing was performed to compare the mechanical response at fracture, bending modulus and strain rates between the surrogates' and calvarium specimens. The present study's approach to modelling the calvarium was particularly unique to previous studies due to 3 main elements. First, cost-effective materials obtained from local retail corporations were readily available to fabricate the surrogates. Second, the surrogates were mechanically tested in both 4-point quasi-static and dynamic impact bending conditions. Thirdly, the surrogates' mechanical response was statistically compared against human calvaria which was tested in consistent laboratory settings and bending conditions as the surrogates.

2. MATERIALS AND METHODS

2.1 Surrogate Development – Prototype 1: Pure Epoxy

In this section, we discuss the fabrication of a pure epoxy prototype. Previous studies had employed construction-based epoxy normally intended for large-scale industrial applications that may not be accessible from local retail corporations for the simple development of a surrogate calvarium (Falland-Cheung et al., 2017; Ondruschka et al., 2019; Roberts et al., 2013). Indeed, epoxy has proven to be a prospective material to mimic the fracture response of the calvarium due to its unique ability to withstand significant forces prior to failure when subject to bending (Falland-Cheung et al., 2017; Ondruschka et al., 2019; Roberts et al., 2013). In addition, epoxy can be subjected to a variety of curing agents to alter its properties and improve its performance in future work. Therefore, to remain consistent with previous studies we selected LePage Speed Set Epoxy (Henkel, Düsseldorf, Germany) to fabricate prototype 1. This epoxy was readily available from local retail corporations and was cost-effective.

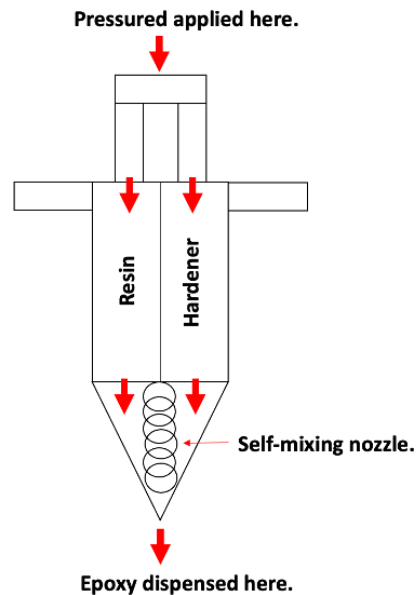


Figure 1. A schematic to illustrate the double-syringe self-mixing nozzle epoxy applicator.

The epoxy is composed of resin and hardener mixed in a 1:1 ratio through a self-mixing nozzle applicator (Figure 1) (Henkel, 2016). The epoxy was dispensed from the nozzle applicator into a pre-made silicone mold (Figure 2) that contained the imprints of curved beams. After 15 minutes of initial drying, the prototypes were removed from the mold and stored at ambient conditions until the time of testing.

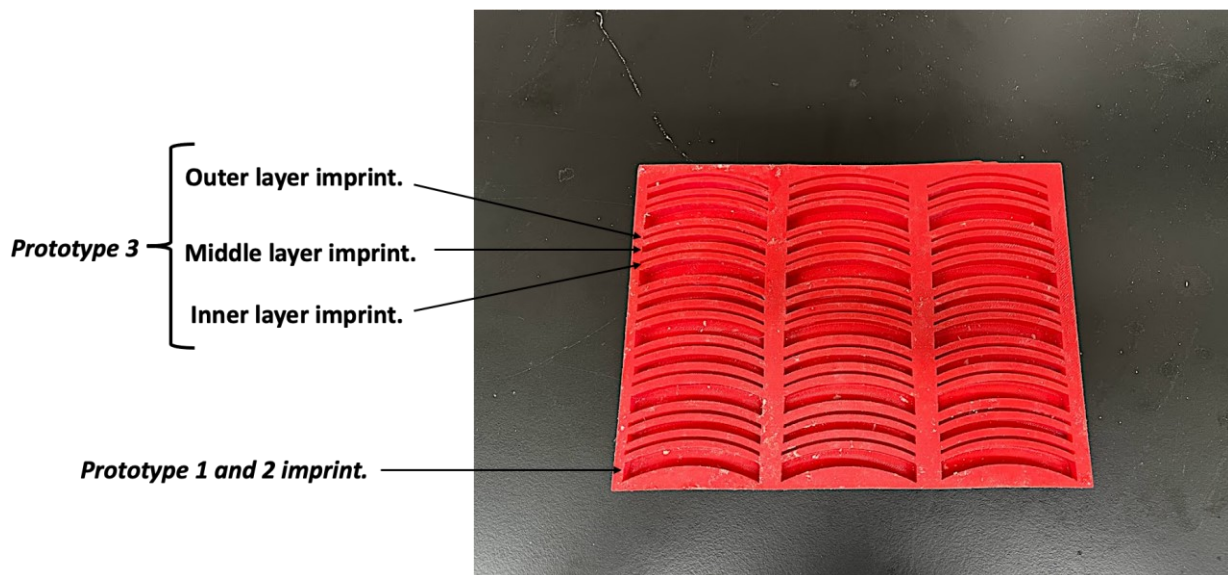


Figure 2. The silicone mold with each prototype's imprint.

2.2 Surrogate Development – Prototype 2: Epoxy-Chalk Mix

For prototype 2, chalk was incorporated with the epoxy. Although chalk alone may be a soft material that cannot withstand forces similar to the calvarium, it is considered a brittle material like the calvarium and can be an important characteristic to mimic a brittle response when combined with a high-strength material such as epoxy. Therefore, the purpose of chalk mixed with the epoxy was to induce some form of brittleness through impurities within the structure of the prototype, similar to the brittle behaviour of real bone when fractured. Like most bones in the human body, the calvarium's inorganic matter composes of a calcium phosphate material - hydroxyapatite ($\text{Ca}_{10}(\text{PO}_4)_6(\text{OH})_2$). Chalk is a type of limestone that is composed of calcite–natural

calcium carbonate (CaCO_3), therefore, chalk's calcium component makes it a potential candidate to mimic the brittle and inorganic nature of bone. In addition, chalk is a readily available and cost-effective material.

The chalk was crushed into a powdered form (2.31 g) and transferred into a mini reclosable clear plastic piping bag. 4.69 g of the epoxy was dispensed into the piping bag and mixed thoroughly with the chalk for 2 minutes. The mixture of epoxy and chalk was then dispensed from the piping bag into the silicone mold (Figure 2) and allowed to dry for 15 minutes. The prototype was then removed from the mold and stored at ambient conditions until the time of testing.

2.3 Surrogate Development – Prototype 3: Epoxy-Chalk Sandwich Layered

The calvarium is a three-layered structure that comprises an outer and inner cortical table that sandwiches a porous layer - diploë. Hence, the present study considered a three-layered structure for prototype 3. A previous study characterized the complex morphometric indices of the diploë and cortical tables using micro-computed tomography (CT) analysis (Adanty et al., 2021). But for simplicity, the diploë or middle layer for prototype 3 was modelled as a solid epoxy layer and the inner and outer cortical tables were modelled as a mixture of epoxy and chalk. The epoxy layer provided strength through the middle of the structure, while the epoxy-chalk cortical tables induced brittleness to facilitate a brittle fracture response at the inner cortical surface like calvaria (Adanty et al., 2022).

To construct the middle layer of prototype 3, the epoxy was dispensed into the silicone mold that contained the imprint of a 3 mm thick curved beam (Figure 2). To construct each of the inner and outer layers of prototype 3, 4.31 g of chalk and 5.00 g of epoxy were mixed in a piping bag for 2 minutes. The mixture was dispensed into the silicone mold that contained an imprint of a 2.00 mm thick outer and a 1.87 mm thick inner curved layer. All three layers were allowed to

dry for 15 minutes and were then adhered together using the epoxy to ensure a strong cohesion between layers. Prototype 3 was stored at ambient conditions until the time of testing.

2.4 Surrogate Geometry

Table 1 displays the physical characteristics of all three prototypes. The second moment of inertia (I_x) was computed for each prototype by assuming the cross-section of each prototype was a solid rectangular section and applying equation (1). It was ensured that no pores were visibly present for each prototype to assume a solid rectangular section. Any prototype with visible pores or unintended imperfections on its external surface that could introduce stress concentrations was discarded.

$$I_x = \frac{bh^3}{12} \quad (1)$$

Where, b = base or width and h = height or thickness.

The geometry of the prototypes was intended to be consistent with calvarium specimens that they were compared to during mechanical testing. When analyzing micro-CT images, on average, the calvarium has a slightly thicker outer cortical table than the inner cortical table (see Tables 2 and 3) which was accounted for in prototype 3. It was important to ensure the geometry of the inner and outer layers for prototype 3 were approximately matched with the calvarium since our preliminary findings have demonstrated that the inner and outer cortical tables' geometric properties can significantly influence the mechanical response of the calvarium.

Table 1. A schematic, composition, I_x and weight for each prototype.

Prototype	Schematic	Composition	$I (m^4)$	Weight (g)
Prototype 1		Pure epoxy	2.33E-10	3.51 ± 0.20
Prototype 2		Epoxy (4.69 g) + Chalk (2.31)	2.41E-10	3.93 ± 0.21
Prototype 3		Middle layer: pure epoxy Inner or outer layer: epoxy (5.00 g) + Chalk (4.31 g)	2.26E-10	3.89 ± 0.35

O.ROC = outer radius of curvature (ROC), I.ROC = Inner ROC, T=thickness, W=width, L=length, I=inner layer, O=outer layer.

2.5 Human Calvaria

All the methods pertaining to the human calvarium specimens were approved by the University of Alberta Research Ethics Board (ID: Pro 00089218). All specimens originated from individual embalmed cadavers supplied by the University of Alberta Anatomical Gift Program.

Human calvarium specimens were employed in this study to 1) ensure the surrogates' geometrical dimensions were consistent with the average geometrical properties of the calvarium

specimens and 2) for the statistical comparison of mechanical response against the surrogates prototypes. The morphometry, geometry and mechanical response of the calvarium specimens are reported in this study and in previous studies (Adanty et al., 2021, 2022). The calvarium specimens were obtained from male and female subjects in the frontal and parietal regions. The calvarium specimens were micro-CT scanned and analyzed using third-party imaging software to determine morphometric and geometrical properties (Adanty et al., 2021) (Figure 3). The length, width, and thickness were verified using digital calipers (Adanty et al., 2021) (Figure 3). The calvarium specimens were then subject to 4-point quasi-static bending (Group 1) specimens) and 4-point dynamic impact bending (Group 2) specimens) (Adanty et al., 2022). The average age of the donors and weight of the calvarium specimens for Group 1) were 85.8 ± 9.0 years old and 4.88 ± 0.15 g respectively, and for Group 2) was 86.4 ± 9.3 years old and 5.35 ± 1.23 g respectively. Note the geometrical properties of the calvarium specimens in Tables 2 and 3. For mechanical testing, the calvarium specimens were not grouped by region or sex but were rather pooled together. No significant differences in mechanical response between sex and regions in 4-point dynamic impact loading were established (Adanty et al., 2022).

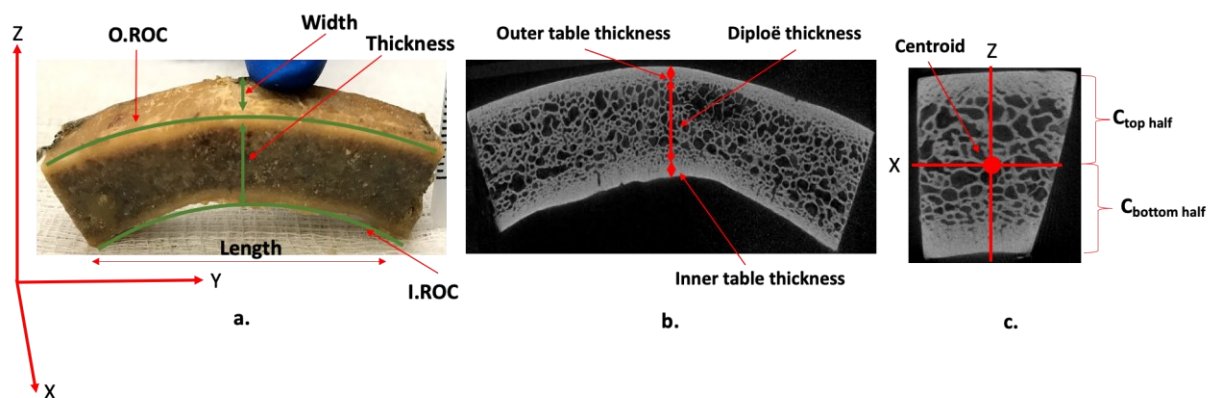


Figure 3. *a.* An example of a frontal calvarium specimen. *b.* A z-y micro-CT image of the calvarium. *c.* A z-x micro-CT image of the calvarium.

Table 2. Mean and 95% confidence intervals (CI) for geometrical properties of Group 1) specimens.

Geometry	I_x (m^4)	Length (mm)	Width (mm)	Thickness (mm)	O.ROC (mm)	I.ROC (mm)	Inner table thickness (mm)	Outer table thickness (mm)	Diploë thickness (mm)
Calvaria (n=24)	2.33E-10 (1.18E-10, 3.48E-10)	55.55 (54.34, 56.76)	8.65 (8.35, 8.95)	6.62 (5.84, 7.40)	83.70 (71.56, 95.85)	73.86 (60.38, 87.35)	1.43 (1.13, 1.73)	1.62 (1.41, 1.84)	3.82 (3.09, 4.54)

Table 3. Mean and 95% CIs for geometrical properties of Group 2) specimens.

Geometry	I_x (m^4)	Length (mm)	Width (mm)	Thickness (mm)	O.ROC (mm)	I.ROC (mm)	Inner table thickness (mm)	Outer table thickness (mm)	Diploë thickness (mm)
Calvaria (n=23)	2.47E-10 (2.02E-10, 2.91E-10)	51.90 (50.95, 52.85)	8.61 (8.13, 9.09)	7.12 (6.52, 7.72)	65.45 (61.53, 69.37)	60.75 (38.17, 83.33)	1.66 (1.44, 1.88)	1.87 (1.69, 2.05)	3.74 (3.06, 4.42)

2.6 Mechanical Testing Of The Surrogate Prototypes

The equipment and test parameters for the mechanical testing of the surrogate prototypes were consistent with the mechanical testing of calvarium specimens (Adanty et al., 2022). 4-point bending was performed on the surrogate prototypes and calvarium specimens. Quasi-static bending was chosen to characterize the mechanical response of the prototypes whereby the inertial effects are negligible during testing. However, most real-world head impacts are sudden and occur in dynamic circumstances that result in strain rates between $1s^{-1}$ and 10^3s^{-1} (Hosseini Farid et al., 2018). Therefore, dynamic impact bending was also performed on the prototypes.

Before testing, the prototypes were instrumented with fibre Bragg gratings (FBGs) at both the inner and outer surfaces using cyanoacrylate to quantify surface strain (%) during mechanical testing (Figure 4) (Adanty et al., 2022). All three prototypes were loaded in 4-point quasi-static bending until fracture at a displacement control rate of 2 mm/min. Figure 4a shows a schematic of

the 4-point quasi-static bending test and Figure 5 shows each prototype and a calvarium specimen undergoing 4-point quasi-static bending.

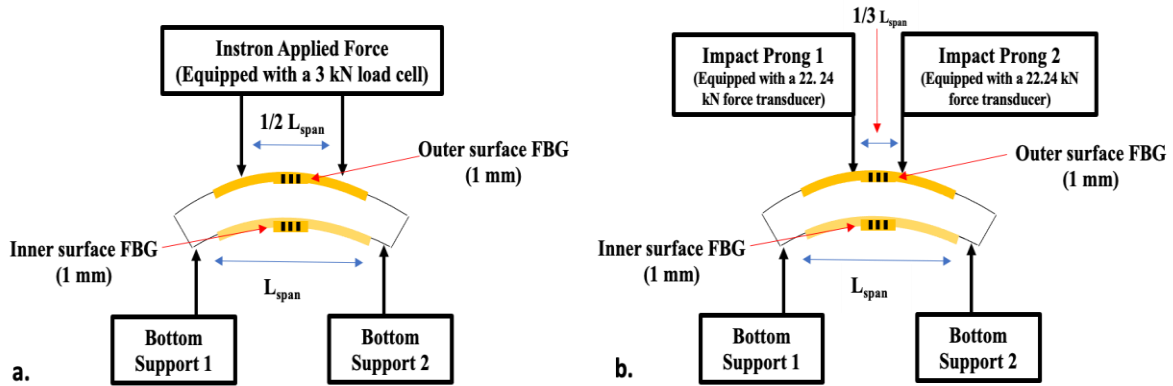


Figure 4. *a.* A schematic of the 4-point quasi-static bending test. *b.* A schematic of the 4-point dynamic impact bending test.

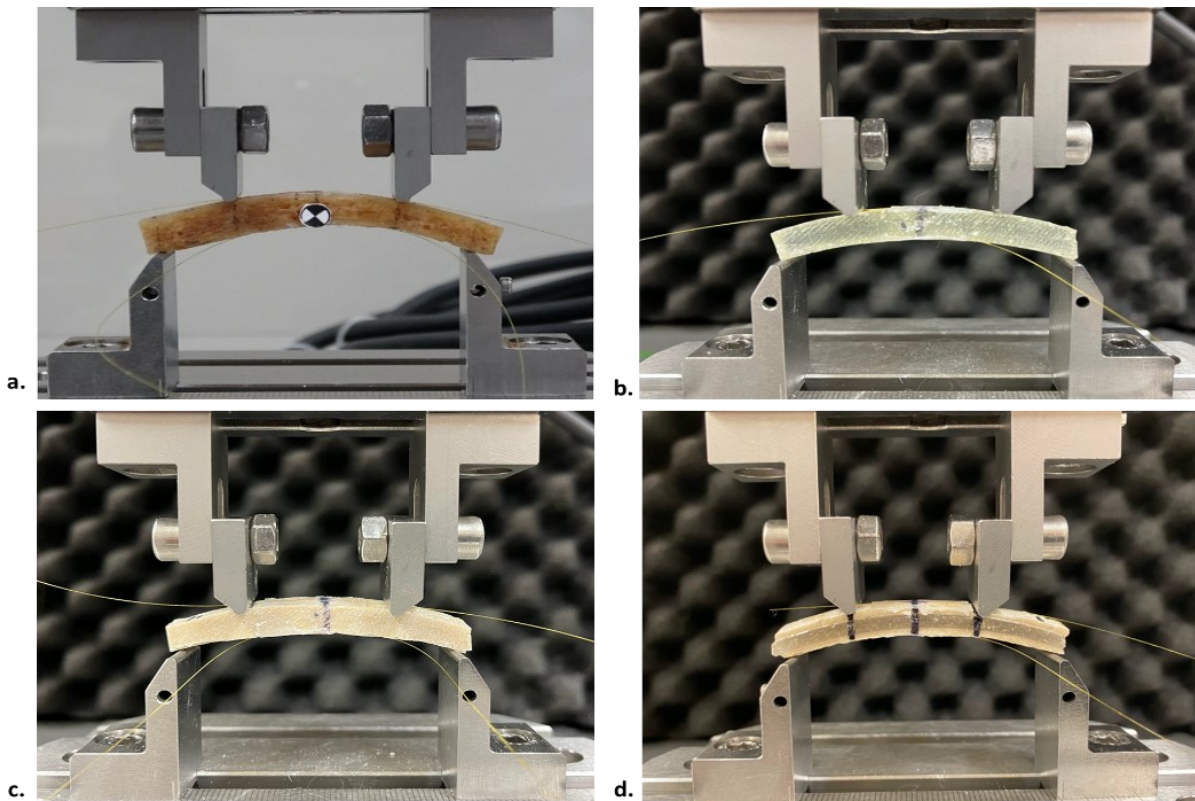


Figure 5. *a.* An example of a calvarium specimen, *b.* prototype 1, *c.* prototype 2 and *d.* prototype 3 under 4-point quasi-static bending in an Instron E3000.

All three prototypes were placed in a custom-built 4-point testing apparatus to perform dynamic impact bending until fracture. The apparatus consisted of a top fixture with two impacting prongs that were dropped from a consistent height and guided freely to impact the prototypes that rested on bottom fixtures (Adanty et al., 2022). The impact velocities were 0.86 to 0.89 m/s and was verified using a high-speed camera at a capturing rate of 5 kHz. Figure 4b shows a schematic of the 4-point dynamic impact bending test and Figure 6 shows each prototype and a calvarium specimen undergoing the 4-point dynamic impact bending test.

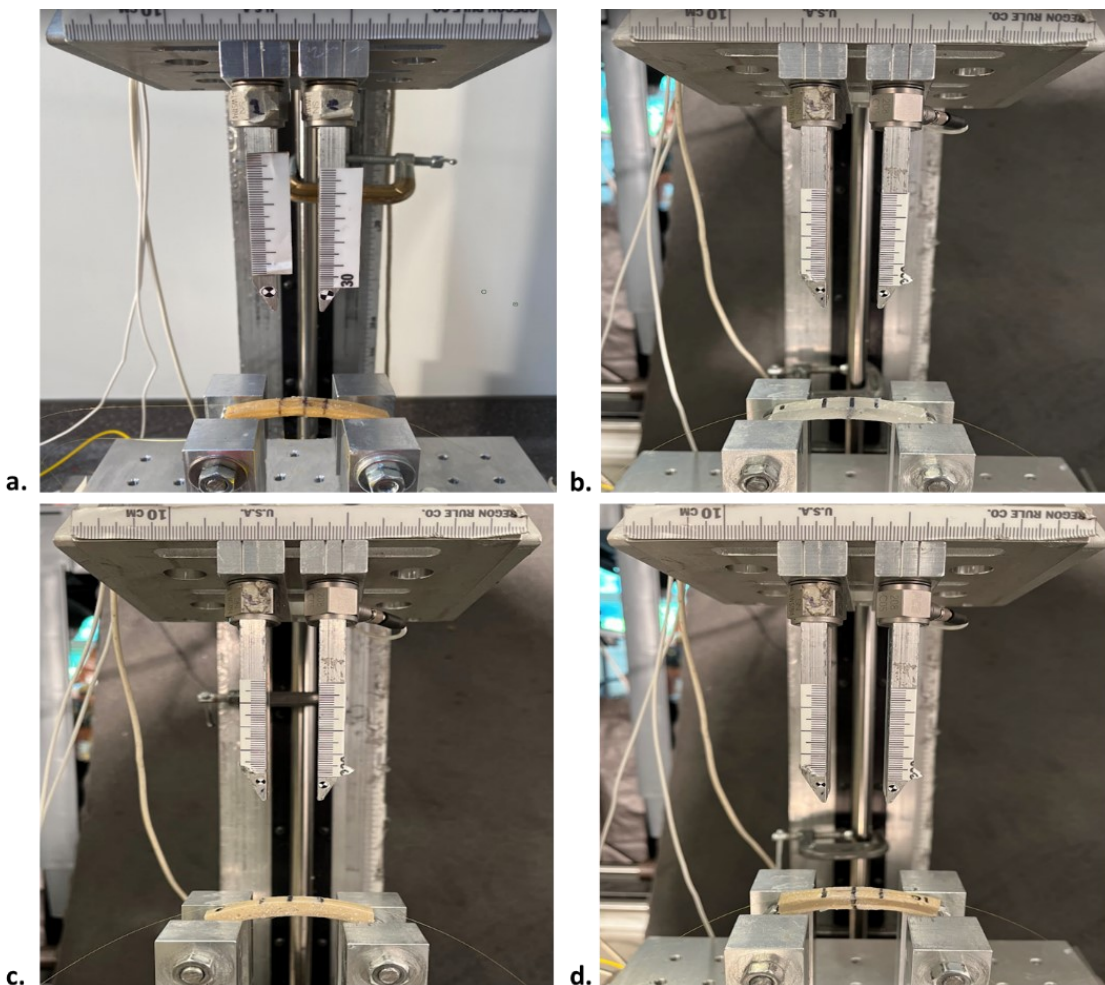


Figure 6. *a.* An example of a calvarium specimen, *b.* prototype 1, *c.* prototype 2 and *d.* prototype 3 under 4-point dynamic impact bending.

The mechanical response variables quantified at fracture included force (N), bending moment (Nm), the tensile (inner table) and compressive (outer table) surface strain (%), and tensile and compressive bending stress (MPa). The tensile and compressive strain rate (1/s) was considered a mechanical response variable since displacement rate (quasi-static) and impact velocities (dynamic loading) were controlled or pre-selected before testing. An effective bending modulus (GPa) was estimated at the initial linear slope of the stress-strain curve for the quasi-static test. For the dynamic impact bending test, an effective bending modulus was estimated at the slope of the stress-strain curve where a corresponding linear strain-time was established (Adanty et al., 2022). Bending stress was estimated by applying the Euler-Bernoulli beam theorem equation. This theorem was applied since the beam deformation was small (strain less than 5 %), and the ROC of the prototypes were close to 10 times their thickness on average to assume a straight beam (Adanty et al., 2022; Roark et al., 2002).

2.7 Statistics

For each dependent variable (mechanical response variable), a one-way analysis of variance (ANOVA) was applied (IBM SPSS version 25). The single independent variable applied in the analysis consisted of the beam models: calvarium specimens and each prototype. The null hypothesis tested was, *no significant differences between the calvarium specimens and each prototype*. A Tukey Honest Significant Difference (HSD) post-hoc-test was applied for pairwise comparison between the calvarium specimens and each prototype. If homogeneity of variance was violated, a Games-Howell nonparametric post-hoc-test was applied for the pairwise comparison. If normality was violated, a Kruskal-Wallis H test was applied for the comparison between the calvarium specimens and each prototype. The significance level was set at an alpha level of 0.05

for all tests. A minimum of $n=8$ for each prototype in comparison to the Group 1) specimens ($n=24$) and Group 2) specimens ($n=23$) resulted in an a priori power of 0.90.

3. RESULTS

3.1 Group 1) Specimens and Surrogate Prototypes

Table 4 presents the mechanical response for the Group 1 specimens and prototypes. The single p-values correspond to the Tukey HSD or Games-Howell test result. All p-values for the Kruskal-Wallis H test were less than 0.003. From Tukey HSD post-hoc-tests, there were no significant differences ($p>0.05$) in tensile strain rate between human calvaria and all prototypes and no significant differences in compressive strain rate between calvaria and prototype 3. From Games-Howell tests, there was no significant difference in force, bending moment, tensile stress, and compressive stress at fracture between calvaria and prototype 2. There was no significant difference in tensile strain and compressive strain at fracture between calvaria and prototype 3. Prototypes 1, 2 and 3 experienced 9, 5, and 6 significant differences in mechanical response variables compared to calvaria under quasi-static loading respectively.

3.2 Group 2) Specimens and Surrogate Prototypes

Table 5 presents the mechanical response for the Group 2 specimens (Adanty et al., 2022) and prototypes. The single p-values correspond to the Tukey HSD or Games-Howell test result. From Tukey HSD post-hoc tests, there were no significant differences ($p>0.05$) in bending moment, tensile stress, and compressive stress between calvaria and all prototypes. From Games-Howell tests, there was no significant difference in tensile modulus and tensile strain between calvaria and prototype 3. Prototypes 1, 2 and 3 experienced 6, 6, and 3 significant differences in mechanical response variables compared to calvaria under dynamic impact loading respectively.

Table 4. Mean \pm standard deviation (SD), 95% CIs, and median for Group 1) calvaria and each prototype in quasi-static loading.

Mechanical Response Variables	Calvaria (n=24)	Prototype 1 (n=8)	Prototype 2 (n=8)	Prototype 3 (n=8)
Force at fracture (N)	348.79 \pm 212.77 258.94, 438.63 312.81	^{^#} 531.09 \pm 79.27 464.82, 597.36 550.03 p<0.01	312.30 \pm 35.55 282.58, 342.03 317.31 p=0.94	^{^#} 180.49 \pm 29.03 156.23, 204.74 183.51 p<0.01
Bending moment at fracture (Nm)	2.14 \pm 1.18 1.64, 2.64 2.03	^{^#} 3.63 \pm 0.52 3.20, 4.07 3.78 p<0.01	2.15 \pm 0.24 1.94, 2.35 2.18 p=0.95	^{^#} 1.17 \pm 0.18 1.02, 1.31 1.11 p<0.01
Tensile strain at fracture (%)	0.38 \pm 0.20 0.30, 0.46 0.38	^{^#} 2.91 \pm 1.00 2.07, 3.75 2.94 p<0.01	^{^#} 0.98 \pm 0.15 2.07, 3.75 1.02 p<0.01	0.47 \pm 0.19 0.32, 0.63 0.46 p=0.94
Compressive strain at fracture (%)	0.32 \pm 0.11 0.27, 0.37 0.34	[^] 2.84 \pm 0.87 2.11, 3.56 2.91 p<0.01	[^] 0.82 \pm 0.10 0.73, 0.91 0.82 p<0.01	0.38 \pm 0.12 2.11, 3.56 0.39 p=0.98
Tensile stress at fracture (MPa)	38.53 \pm 12.52 33.24, 43.82 38.46	[^] 54.11 \pm 7.72 47.66, 60.56 54.79 p=0.02	32.26 \pm 5.25 27.87, 36.65 32.01 p=0.41	[^] 17.72 \pm 2.40 15.71, 19.73 17.40 p<0.01
Compressive stress at fracture (MPa)	37.39 \pm 13.00 32.01, 42.96 36.17	[^] 54.11 \pm 7.72 47.66, 60.56 54.79 p=0.01	32.26 \pm 5.25 27.87, 36.65 32.01 p=0.59	[^] 17.72 \pm 2.40 15.71, 19.73 17.40 p<0.01
Tensile Modulus (GPa)	11.15 \pm 3.57 9.64, 12.66 10.08	^{^#} 2.09 \pm 0.82 1.42, 2.77 1.75 p<0.01	^{^#} 3.84 \pm 0.59 3.40, 4.39 3.76 p<0.01	^{^#} 4.52 \pm 1.50 3.27, 5.77 4.66 p<0.01
Compressive Modulus (GPa)	11.78 \pm 2.82 10.59, 12.93 10.94	[^] 2.12 \pm 0.77 1.48, 2.77 1.88 p<0.01	[^] 4.09 \pm 0.57 3.61, 4.56 4.00 p<0.01	[^] 5.13 \pm 1.32 3.27, 5.77 4.66 p<0.01
Tensile Strain Rate (s ⁻¹)	2.2E-4 \pm 1.3E-4 1.7E-4, 2.8E-4 1.90E-4	3.3E-4 \pm 6.1E-4 2.8E-4, 3.8E-4 3.1E-4 p=0.10	2.6E-4 \pm 8.8E-5 1.8E-4, 3.3E-4 2.6E-4 p=0.87	2.6E-4 \pm 4.6E-4 2.2E-4, 2.9E-4 2.7E-4 p=0.88
Compressive Strain Rate (s ⁻¹)	1.8E-4 \pm 5.4E-5 1.6E-4, 2.0E-4 1.9E-4	[*] 3.2E-4 \pm 5.7E-5 2.7E-4, 3.7E-4 3.0E-4 p<0.01	[*] 2.6E-4 \pm 3.5E-5 2.3E-4, 2.9E-4 2.6E-4 p<0.01	2.2E-4 \pm 4.1E-5 1.9E-4, 2.5E-4 2.2E-4 p=0.22

* significantly different to calvaria, p<0.05 (Tukey HSD), [^] significantly different to calvaria, p<0.05 (Games-Howell), [#] significantly different to calvaria, p<0.05 (Kruskal-Wallis H test).

Table 5. Mean \pm SD, 95% CI, and median for Group 2) calvaria and each prototype in dynamic impact bending.

Mechanical Response Variables	Calvaria (n=24)	Prototype 1 (n=8)	Prototype 2 (n=8)	Prototype 3 (n=8)
Force at fracture (N)	223.80 \pm 79.82 189.30, 258.32 208.41	204.84 \pm 33.71 173.66, 236.02 215.44 p=0.83	192.89 \pm 29.04 162.41, 223.72 188.33 p=0.31	169.30 \pm 32.03 139.67, 198.93 169.37 p=0.67
Bending moment at fracture (Nm)	1.70 \pm 0.59 1.45, 1.96 1.60	1.82 \pm 0.31 1.53, 2.10 1.90 p=0.97	1.70 \pm 0.28 1.41, 2.00 1.68 p=0.99	1.46 \pm 0.29 1.19, 1.72 1.44 p=0.88
Tensile strain at fracture (%)	0.25 \pm 0.08 0.21, 0.28 0.25	[^] 0.55 \pm 0.14 0.42, 0.68 0.53 p<0.01	[^] 0.39 \pm 0.05 0.16, 0.25 0.21 P<0.01	0.37 \pm 0.19 0.19, 0.55 0.36 p=0.27
Compressive strain at fracture (%)	0.21 \pm 0.10 0.16, 0.25 0.21	*0.42 \pm 0.13 0.30, 0.53 0.36 p<0.01	*0.36 \pm 0.15 0.21, 0.52 0.32 p=0.02	*0.33 \pm 0.08 0.26, 0.40 0.32 p=0.02
Tensile stress at fracture (MPa)	26.97 \pm 8.39 23.34, 30.60 24.84	27.41 \pm 5.18 22.61, 32.20 27.51 p=0.99	25.76 \pm 5.09 20.41, 31.11 25.60 p=0.99	21.48 \pm 4.12 17.68, 25.28 20.89 p=0.64
Compressive stress at fracture (MPa)	26.50 \pm 9.13 22.55, 30.45 25.73	27.41 \pm 5.18 22.61, 32.20 27.51 p=0.99	25.76 \pm 5.09 20.41, 31.11 25.60 p=0.99	21.48 \pm 4.12 17.68, 25.28 20.89 p=0.74
Tensile Modulus (GPa)	11.37 \pm 9.54 7.25, 15.50 7.95	[^] 4.62 \pm 1.34 3.38, 5.87 5.06 p=0.01	[^] 5.00 \pm 1.34 3.59, 6.41 5.49 p=0.01	6.11 \pm 3.58 2.80, 9.42 5.29 p=0.15
Compressive Modulus (GPa)	14.71 \pm 13.96 8.68, 20.75 10.21	[^] 4.79 \pm 1.49 3.41, 6.17 5.05 p=0.01	[^] 5.00 \pm 1.34 3.59, 6.41 5.49 p=0.03	[^] 6.03 \pm 2.17 4.02, 8.04 5.76 p=0.04
Tensile Strain Rate (s ⁻¹)	3.09 \pm 2.00 2.23, 3.96 3.40	[^] 6.89 \pm 1.78 5.24, 8.54 7.35 p<0.01	[^] 6.07 \pm 0.76 5.27, 6.87 6.29 p<0.01	5.57 \pm 2.29 3.45, 7.70 5.43 p=0.11
Compressive Strain Rate (s ⁻¹)	2.35 \pm 1.82 1.57, 3.15 2.09	*7.24 \pm 1.93 5.45, 9.03 8.15 p<0.01	*5.91 \pm 2.29 3.51, 8.32 4.84 p=0.01	*5.73 \pm 1.79 4.08, 7.39 5.70 p=0.01

* significantly differently to calvaria, p<0.05 (Tukey HSD), [^] significantly differently to calvaria, p<0.05 (Games-Howell), # significantly differently to calvaria, p<0.05 (Kruskal-Wallis H test).

The prototypes' bending stress (Figure 7) and effective bending modulus (Figure 8) derived from quasi-static loading are presented in a bar chart with three previous studies that performed three-point quasi-static bending tests (10 mm/min) on simulant skull materials (Falland-Cheung et al., 2017; Ondruschka et al., 2019; Roberts et al., 2013). The prototypes' bending stress and effective bending modulus derived from dynamic impact loading were not charted with previous studies since to our knowledge, no study has performed dynamic impact bending on simulant skull materials.

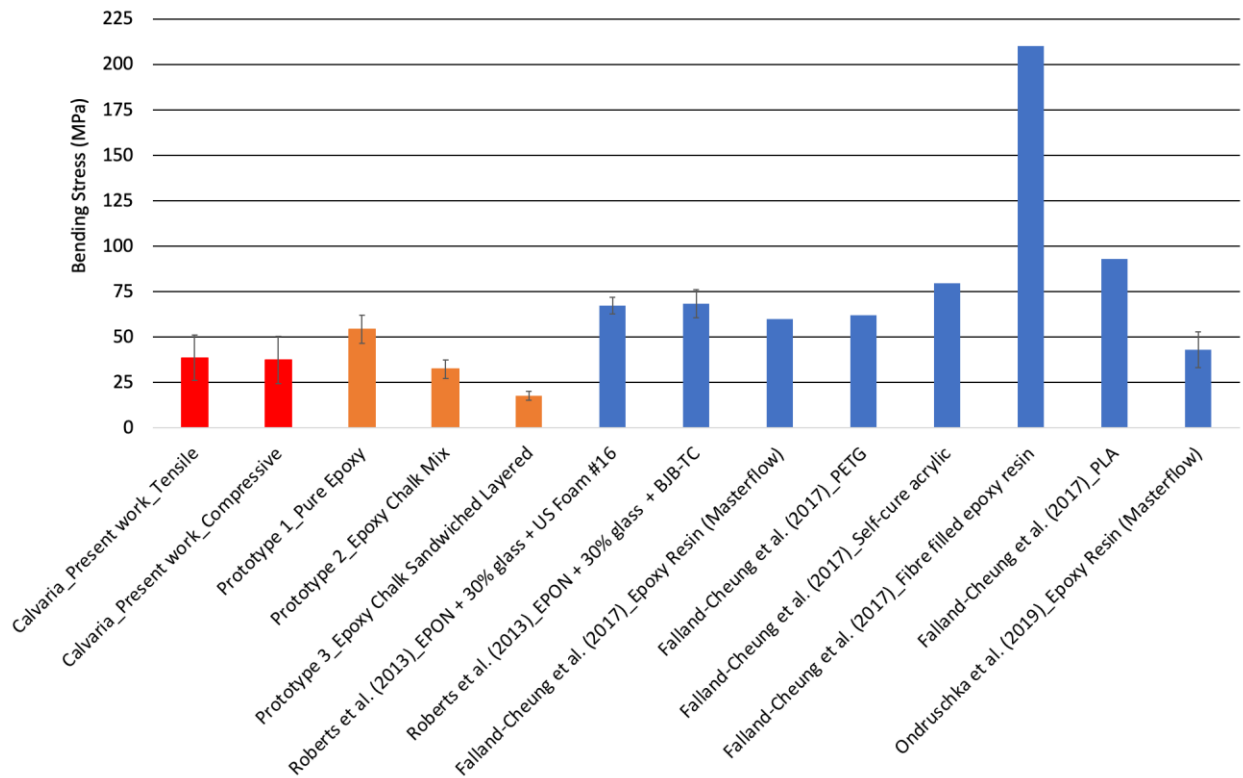


Figure 7. The bending stress of the calvaria (red), the surrogate prototypes (orange) and simulant skull materials (blue) from previous studies (Falland-Cheung et al., 2017; Ondruschka et al., 2019; Roberts et al., 2013) that tested in 3-point quasi-static bending at 10 mm/min. US Foam #16 and BJB-TC were two-part expanding urethane foam (Roberts et al., 2013), PETG was modified polyethylene terephthalate glycol (Falland-Cheung et al., 2017), the self-cure acrylic was denture base resin (Falland-Cheung et al., 2017), and the PLA was polylactic acid used as a 3-D printing filament (Falland-Cheung et al., 2017).

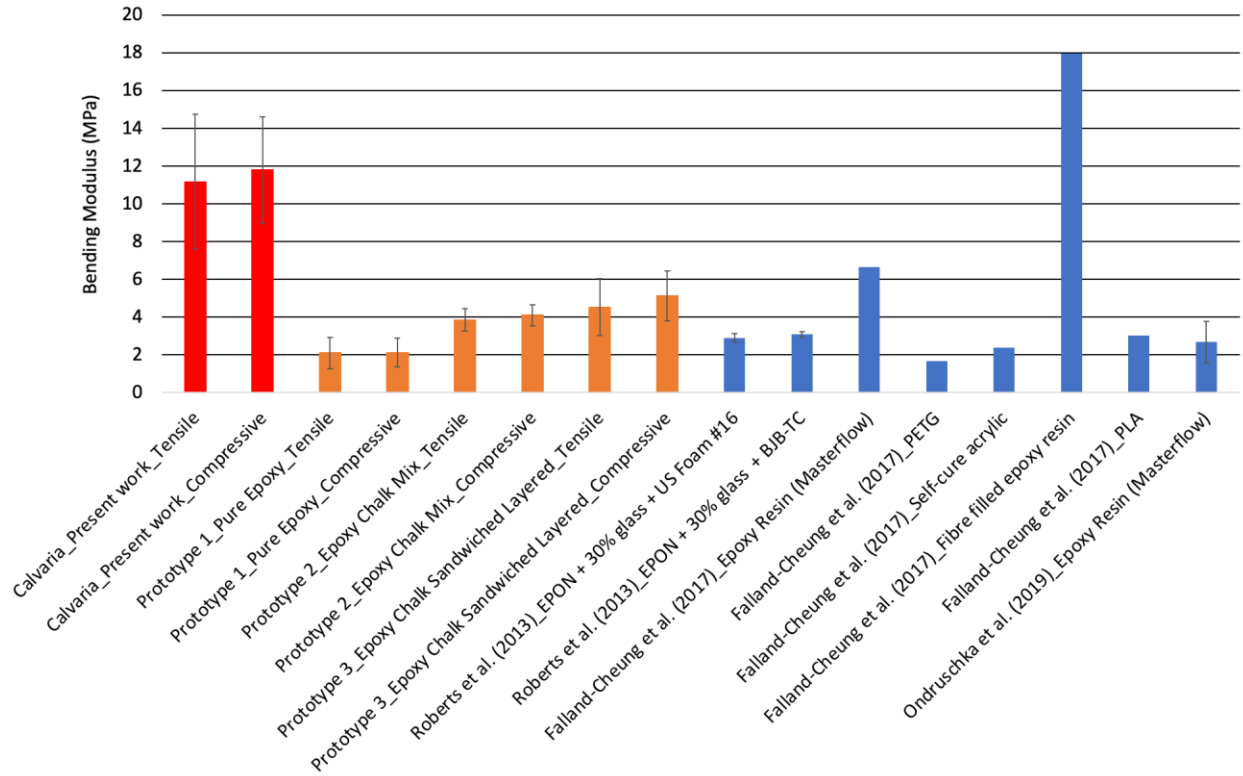


Figure 8. The bending modulus of the calvaria (red), the surrogate prototypes (orange) and simulant skull materials (blue) from the previous studies (Falland-Cheung et al., 2017; Ondruschka et al., 2019; Roberts et al., 2013) that tested in 3-point quasi-static bending at 10 mm/min.

4. DISCUSSION

For quasi-static and dynamic impact loading, the incorporation of chalk with the epoxy for prototypes 2 and 3 appeared to influence their mechanical response with respect to prototype 1. This is evident by the decrease in strain observed in prototype 3 which resulted in a comparable strain response to calvarium. For prototype 2, the addition of chalk was most impactful during dynamic impact loading where its mean strain was close to one standard deviation of the calvarium. These observations in prototypes 2 and 3 indicate that chalk may be a contributing factor in increasing the brittleness of the structure. As a result of the reduction in the strain at fracture with the addition of chalk, the bending modulus or stiffness increased in prototypes 2 and 3 compared to prototype 1 which can be visualized in Figure 8. Notably, the layered concept and the mixture of chalk in prototype 3 contributed to a tensile bending modulus that was within the 95% CI of the calvarium for dynamic impact loading. However, the calvarium's bending modulus remained greater than all prototypes. Despite the increase in bending modulus for prototypes 2 and 3, the strength as represented by the force, moment, and stress at fracture decreased with the addition of chalk, this can be visualized for stress by the orange bar plots in Figure 7. Overall, prototype 1 yielded greater stress at fracture during impact loading but a low bending modulus due to a high strain or deformation response in comparison to calvarium. This may implicate that prototype 1 retains a high strength but low bending modulus and that employing epoxy alone may not be feasible for mimicking the fracture response of the calvarium (Falland-Cheung et al., 2017; Ondruschka et al., 2019).

In dynamic impact loading, prototypes 1 and 3 were comparable to calvarium for more mechanical response variables than in quasi-static loading. Prototype 2 saw more significant differences in mechanical response variables to calvarium in dynamic impact loading, but its strain

response was closer to calvarium than pure epoxy, and its mechanical response at fracture including force, bending moment, tensile and compressive stress was not significantly different from calvaria (Table 5). These findings suggest that overall, the prototypes performed better in dynamic impact loading than quasi-static loading when comparing mechanical response to calvarium. This is an important observation since most real-world head injuries arise from dynamic impact loading where strain rates are generally 1s^{-1} or greater (Hosseini Farid et al., 2018). Therefore, a surrogate geared towards biomechanically modelling injury should be validated in dynamic impact loading conditions for improved biofidelity and not be limited solely to quasi-static loading as observed in previous studies (Falland-Cheung et al., 2017; Ondruschka et al., 2019; Roberts et al., 2013). Regarding strain rates, the prototypes experienced consistent strain rates in quasi-static loading with calvaria. Despite the prototypes and calvarias' similar geometry and coherent impact velocities, the prototypes' strain rates were generally greater than the calvaria in dynamic impact loading. The distinction in material composition between the calvarium's dense bone surface and the prototype's epoxy or epoxy-chalk mix surface can be a factor for strain-rate differences. Perhaps epoxy filler and additives to enhance its stiffness could decrease the prototypes' rate of strain or deformation, thereby decreasing its strain at fracture and increasing modulus.

In comparison to previous studies that have reported bending properties of simulant skull materials (Figure 7), prototype 1's bending stress at fracture (54.11 MPa) is comparable to Robert et al.'s two surrogates (67.3 and 68.4 MPa), and Falland-Cheung et al.'s (59.84 MPa) and Ondruschka et al.'s (42.9 MPa) epoxy resin (Masterflow) surrogates (Falland-Cheung et al., 2017; Ondruschka et al., 2019; Roberts et al., 2013). The epoxy resin (EPON-Miller-Stephenson Chemical Co.) employed by Robert et al. and the epoxy resin (Masterflow 622) employed by

Falland-Cheung et al. and Ondruschka et al. may not be readily available from local retail corporations compared to the type of epoxy used in this study (Falland-Cheung et al., 2017; Ondruschka et al., 2019; Roberts et al., 2013), yet, Figure 7 demonstrates that all epoxies generated consistent bending stress results. In terms of bending modulus (Figure 8), prototype 3's (4.52 GPa tensile and 5.13 GPa compressive) response was consistent with Falland-Cheung et al.'s epoxy resin (6.65 GPa) (Falland-Cheung et al., 2017). Rather, prototype 1's bending moduli (2.09 GPa tensile and 2.212 GPa compressive) were comparable to Robert et al.'s surrogates (2.89 GPa and 3.08 GPa), Falland -Cheung et al.'s PETG (1.68 GPa) and self-cure acrylic (2.38 GPa), and Ondruschka et al.'s epoxy resin (2.67 GPa) (Falland-Cheung et al., 2017; Ondruschka et al., 2019; Roberts et al., 2013). Overall, in quasi-static loading, the bending modulus from the three prototypes and the simulant skull materials in previous studies are less stiff compared to calvaria. To our knowledge, no study has performed dynamic impact bending on simulant or surrogate skulls to compare the dynamic behaviour of our prototypes. Dynamic impact loading is an essential testing configuration for potential surrogates to be engaged under real-world head impact testing circumstances.

To determine the best prototype for further development when simulating the mechanical response of the calvarium, the performance of the prototypes' mechanical response to calvarium was primarily assessed. As established earlier, the prototypes exhibited more differences in mechanical response variables to calvaria under quasi-static loading. Therefore, the surrogates may require design adjustments to improve their mechanical response under quasi-static loading. However, the dynamic impact conditions resulted in strain rates greater than 1s^{-1} which relates to real-world head impact circumstances (Hosseini Farid et al., 2018), thus, the results from the dynamic impacts are most relevant. Under dynamic impact conditions, prototype 3 only had three

mechanical response variables that were significantly different from calvaria which was compressive strain rate, modulus, and strain at fracture, whereas prototypes 1 and 2 yielded six significant differences. Therefore, under dynamic loading, prototype 3 is the optimal surrogate for further development when simulating the mechanical response of the calvarium at fracture. The 95% CI of tensile strain, modulus, and strain rate for prototype 3 was greater than prototypes 1 and 2 which may have contributed to prototype 3's statistical comparison to calvaria. Since the construction of prototype 3 required additional steps including the adhesion of three different layers, challenges in obtaining consistently built samples may be a factor for the greater 95% CI. Nonetheless, prototype 3's three-layered structure imitates the sandwich structure of calvarium as opposed to the single-layered fabricated for prototypes 1 and 2. The three-layered structure and the mixture of epoxy and chalk may be imperative factors that influenced prototype 3's comparable response to calvaria. Since the intent of this work was to introduce surrogates with a comparable mechanical response at fracture to calvarium, the most important variables would be all except for the effective bending modulus and strain rate since these were obtained before fracture. Therefore, prototypes 1 to 3 may be appropriate to assess response at fracture with the understanding that strain is the common variable that differs from calvaria. For non-fracture impact events, modulus and strain rate would be important variables to consider, thus prototype 3 would be the ideal option based on its results.

Future directions for prototype 3 can be explored to improve its proximity in mechanical response towards calvaria. To increase the brittleness or reduce the strain response of prototype 3 toward the calvarium's average, one may investigate various ratios of chalk to epoxy for the inner and outer layers. Alternatively, one may also investigate potential substitutes for chalk that retain brittle-like characteristics such as glass, ceramic, or graphite, or fillers and additives, however,

their cost and accessibility may not be comparable to chalk. One may also consider replacing the pure epoxy middle layer of prototype 3 with a micro-structure containing trabecular struts such as a honeycomb structure to better imitate the diploë. But theoretically, in a typical sandwich structure like the calvarium, where the middle layer or core is less stiff than the inner and outer layers or faces (Hubbard, 1971), the forces developed in the core are less critical. Therefore, pure epoxy may be appropriate to continue characterizing the middle layer of prototype 3 because it was demonstrated in the present study that pure epoxy alone (prototype 1) had a lower bending modulus or stiffness compared to the epoxy-chalk composites in prototypes 2 and 3.

The limitations of the methodology in this work are acknowledged by the authors. The prototypes' mechanical response was matched against calvarium specimens that were embalmed and extracted from senior-aged donors (Adanty et al., 2022). Fresh or fresh-frozen specimens from middle-aged donors should be a vital inclusion in future studies since the mechanical properties of the bone can be altered by age and tissue preservation methods (Nazarian et al., 2009) which can affect how we draw conclusions when comparing mechanical response to the prototypes. The prototypes were not micro-CT scanned for imaging analysis, therefore, the density, porosity, and more accurate measures of I_x compared to calvaria are unknown. Furthermore, with the absence of imaging analysis, there was no way to determine if imperfections or discontinuity existed within the internal structure of the prototypes such as the formation of bubbles or miniature air pockets. These factors may have influenced the mechanical response of the prototypes, thus micro-CT scanning followed by imaging analysis needs to be considered in future investigations before expanding the prototypes into a frontal or parietal region. Finally, despite the prototypes' gross geometry being in close alignment with calvaria, their weights were slightly less than calvaria. This may indicate the density of the prototypes may be less than the calvaria which can affect the

strength of the prototype. Different ratios of chalk to epoxy or if possible, cost-effective alternative materials that can match the density of calvaria should be explored as potential solutions.

ACKNOWLEDGMENTS

The authors would like to thank the University of Alberta's Division Anatomy for providing access to human cadavers and the necessary aid during dissection.

FUNDING AND/OR CONFLICTS OF INTERESTS/COMPETING INTERESTS

The authors declare that they have no known competing financial interests or personal relationships that could have appeared to influence the work reported in this paper.

This research was sponsored by the Army Research Laboratory and was accomplished under Cooperative Agreement Number W911NF-19-2-0336. The views and conclusions contained in this document are those of the authors and should not be interpreted as representing the official policies, either expressed or implied, of the Army Research Laboratory or the U.S. Government. The U.S. Government is authorized to reproduce and distribute reprints for Government purposes notwithstanding any copyright notation herein.

REFERENCES

- Adanty, K., Bhagavathula, K. B., Tronchin, O., Li, D. X., Rabey, K. N., Doschak, M. R., Adeeb, S., Hogan, J., Ouellet, S., Plaisted, T. A., Satapathy, S., Romanyk, D. L., & Dennison, C. (2022). The Mechanical Characterization and Comparison of Male and Female Calvaria Under Four-Point Bending Impacts. *Journal of Biomechanical Engineering*, 1–47. <https://doi.org/10.1115/1.4056459>
- Adanty, K., Rabey, K. N., Doschak, M. R., Bhagavathula, K. B., Hogan, J. D., Romanyk, D. L., Adeeb, S., Ouellet, S., Plaisted, T. A., Satapathy, S. S., & Dennison, C. R. (2021). Cortical and trabecular morphometric properties of the human calvarium. *Bone*, 148, 115931. <https://doi.org/10.1016/j.bone.2021.115931>
- Anctil, B., Bourget, D., Pagaue, G., Dionne, J. P., Wonnacott, M., Rice, K., & Toman, A. (2008). *The Development of a Ballistic Helmet Test Standard, Personal Armour Systems*. In: Pass conference proceedings, Brussel.
- Brown, A. D., Walters, J. B., Zhang, Y. X., Saadatfar, M., Escobedo-Diaz, J. P., & Hazell, P. J. (2019). The mechanical response of commercially available bone simulants for quasi-static and dynamic loading. *Journal of the Mechanical Behavior of Biomedical Materials*, 90, 404–416. <https://doi.org/10.1016/j.jmbbm.2018.10.032>
- Chattopadhyay, S., & Tripathi, C. (2010). Skull fracture and haemorrhage pattern among fatal and nonfatal head injury assault victims – a critical analysis. *Journal of Injury and Violence Research*, 2(2), 99–103. <https://doi.org/10.5249/jivr.v2i2.46>
- Delille, R., Lesueur, D., Potier, P., Drazetic, P., & Markiewicz, E. (2007). Experimental study of the bone behaviour of the human skull bone for the development of a physical head model. *International Journal of Crashworthiness*, 12(2), 101–108. <https://doi.org/10.1080/13588260701433081>
- Falland-Cheung, L., Waddell, J. N., Chun Li, K., Tong, D., & Brunton, P. (2017). Investigation of the elastic modulus, tensile and flexural strength of five skull simulant materials for impact testing of a forensic skin/skull/brain model. *Journal of the Mechanical Behavior of Biomedical Materials*, 68, 303–307. <https://doi.org/10.1016/j.jmbbm.2017.02.023>
- Gurdjian, E. S., & Lissner, H. R. (1947). Deformations of the skull in head injury as studied by the “stresscoat” technic. *The American Journal of Surgery*, 73(2), 269–281. [https://doi.org/10.1016/0002-9610\(47\)90321-8](https://doi.org/10.1016/0002-9610(47)90321-8)
- Henkel. (2016). *Technical Data Sheet: Speed Set Instant Mix Epoxy*. Henkel. <https://dm.henkel-dam.com/is/content/henkel/tds-10228091-ca-en-lepage-speed-set-instant-mix-epoxy-carded-syringe-14ml>
- Hillier, M. L., & Bell, L. S. (2007). Differentiating Human Bone from Animal Bone: A Review of Histological Methods. *Journal of Forensic Sciences*, 52(2), 249–263. <https://doi.org/10.1111/j.1556-4029.2006.00368.x>

- Hodgson, V. R., & Thomas, L. M. (1972). *BREAKING STRENGTH OF THE HUMAN SKULL VS. IMPACT SURFACE CURVATURE* (Final Rept). Article Final Rept. <https://trid.trb.org/view/112380>
- Hosseini Farid, M., Eslaminejad, A., Ramzanpour, M., Ziejewski, M., & Karami, G. (2018). The Strain Rates of the Brain and Skull Under Dynamic Loading. *Volume 3: Biomedical and Biotechnology Engineering*, V003T04A067. <https://doi.org/10.1115/IMECE2018-88300>
- Hubbard, R. P. (1971). Flexure of layered cranial bone. *Journal of Biomechanics*, 4(4), 251–263. [https://doi.org/10.1016/0021-9290\(71\)90031-5](https://doi.org/10.1016/0021-9290(71)90031-5)
- Hubbard, R. P., & McLeod, D. G. (1974). Definition and Development of A Crash Dummy Head. *SAE Transactions*, 83, 3836–3851.
- JAMES L. UNDERWOOD. (n.d.). *NIJ Standard for Ballistic Helmets*. U.S. DEPARTMENT OF JUSTICE - National Institute of Justice.
- Liu, H., Kang, J., Chen, J., Li, G., Li, X., & Wang, J. (2012). Intracranial Pressure Response to Non-Penetrating Ballistic Impact: An Experimental Study Using a Pig Physical Head Model and Live Pigs. *International Journal of Medical Sciences*, 9(8), 655–664. <https://doi.org/10.7150/ijms.5004>
- Macpherson, B. C. M., Macpherson, P., & Jennett, B. (1990). CT evidence of intracranial contusion and haematoma in relation to the presence, site and type of skull fracture. *Clinical Radiology*, 42(5), 321–326. [https://doi.org/10.1016/S0009-9260\(05\)82145-2](https://doi.org/10.1016/S0009-9260(05)82145-2)
- Marks, P. (2005). HEAD TRAUMA | Pediatric and Adult, Clinical Aspects. In J. Payne-James (Ed.), *Encyclopedia of Forensic and Legal Medicine* (pp. 461–472). Elsevier. <https://doi.org/10.1016/B0-12-369399-3/00186-5>
- Nahum, A. M., Smith, R., & Ward, C. C. (1977). *Intracranial Pressure Dynamics During Head Impact* (SAE Technical Paper No. 770922). SAE International. <https://doi.org/10.4271/770922>
- Nazarian, A., Hermannsson, B. J., Muller, J., Zurakowski, D., & Snyder, B. D. (2009). Effects of tissue preservation on murine bone mechanical properties. *Journal of Biomechanics*, 42(1), 82–86. <https://doi.org/10.1016/j.jbiomech.2008.09.037>
- Ondruschka, B., Lee, J. H. C., Scholze, M., Zwirner, J., Tong, D., Waddell, J. N., & Hammer, N. (2019). A biomechanical comparison between human calvarial bone and a skull simulant considering the role of attached periosteum and dura mater. *International Journal of Legal Medicine*, 133(5), 1603–1610. Scopus. <https://doi.org/10.1007/s00414-019-02102-4>
- Plaisted, T. A., Gardner, J. M., & Gair, J. L. (2015). *Characterization of a Composite Material to Mimic Human Cranial Bone*. 12.
- Roark, R. J., Young, W. C., & Budynas, R. G. (2002). *Roark's formulas for stress and strain* (7th ed). McGraw-Hill.

Roberts, J. C., Merkle, A. C., Carneal, C. M., Voo, L. M., Johannes, M. S., Paulson, J. M., Tankard, S., & Uy, O. M. (2013). Development of a Human Cranial Bone Surrogate for Impact Studies. *Frontiers in Bioengineering and Biotechnology, 1*. <https://doi.org/10.3389/fbioe.2013.00013>

Sharma, V. K., Rango, J., Connaughton, A. J., Lombardo, D. J., & Sabesan, V. J. (2015). The Current State of Head and Neck Injuries in Extreme Sports. *Orthopaedic Journal of Sports Medicine, 3*(1), 2325967114564358. <https://doi.org/10.1177/2325967114564358>

Thali, M. J., Kneubuehl, B. P., Zollinger, U., & Dirnhofer, R. (2002). The “Skin–skull–brain model”: A new instrument for the study of gunshot effects. *Forensic Science International, 125*(2), 178–189. [https://doi.org/10.1016/S0379-0738\(01\)00637-5](https://doi.org/10.1016/S0379-0738(01)00637-5)

Weisenbach, C. A., Logsdon, K., Salzar, R. S., Chancey, V. C., & Brozoski, F. (2018). Preliminary Investigation of Skull Fracture Patterns Using an Impactor Representative of Helmet Back-Face Deformation. *Military Medicine, 183*(suppl_1), 287–293. <https://doi.org/10.1093/milmed/usx210>

PART IV

CONCLUSIONS

The morphometry of male and female human calvarium specimens at the frontal and parietal regions were quantified using micro-CT imaging analyses and was reported in Chapter 1. It was determined that the layer, sex, and location of the calvarium influenced morphometry. Important geometrical properties of the calvarium such as thickness and radius of curvature were reported across Chapters 1 to 3. The mechanical response of 24 and 23 calvarium specimens was then determined by loading the specimens in 4-point quasi-static (Chapter 2) and 4-point dynamic impact bending (Chapter 3) until fracture respectively. For specimens subject to quasi-static loading, it was established that the trabecular bone pattern factor of the diploë was a significant predictor of force and bending moment at fracture. The inner cortical layer contained the greatest number of morphometric and geometric properties as significant predictors of mechanical response including thickness, tissue mineral density, and porosity. In dynamic impact loading, the mechanical response between male and female calvarium was not significantly different.

In Chapter 4, three surrogate prototypes were developed using epoxy and chalk which were readily available at local retail corporations and cost-effective materials. The geometry of the prototypes was constructed based on the average geometrical properties reported on the calvarium specimens including thickness and radius of curvature. The prototypes were loaded in 4-point quasi-static and dynamic impact bending. Under quasi-static loading, the surrogate prototypes on average experienced a greater number of significant differences in mechanical response variables to the calvarium in comparison to dynamic impact loading. It was determined that the epoxy-chalk layered surrogate was the best prototype for further development because, under dynamic impact loading - the testing condition most applicable to real-world head impacts, their force and bending moment at fracture, tensile strain at fracture, tensile and compressive stress at fracture, tensile

effective bending modulus, and tensile strain rate had no statistically significant differences to calvarium specimens.

The epoxy-chalk layered surrogate was comprised of a three-layered sandwich structure similar to the calvarium. Its inner and outer layers comprised a mixture of epoxy and chalk while its middle layer was composed of pure epoxy. The discoveries of this work can be an initial step toward the development of a full-size surrogate model of the calvarium. In the future, the model may be integrated with existing headforms to enable scientists, injury biomechanists or forensic experts to simulate skull fracture events during head impact testing and the evaluation of protective devices.

CONTRIBUTIONS

The contributions of this dissertation are evident in the four articles described in Chapters 1 to 4 but are summarized in this section. The broad contribution of this dissertation in the biomechanical field was the characterization of the morphometry, geometry, and mechanical response of the calvarium followed by the introduction of a simple approach to develop potential surrogate models of the human calvarium to simulate fracture. Readily available and cost-effective materials including epoxy and chalk were employed to fabricate the surrogate models. The specific contributions of this dissertation are the following:

- This dissertation micro-CT scanned 50 human calvarium specimens and employed imaging techniques to provide novel data on the morphometric and geometric properties of the calvarium. Furthermore, the factors of sex and region were considered to determine how morphometry was influenced by each factor. In addition, the radius of curvature of the calvarium was determined for the frontal and parietal regions, and the inner and outer cortical thicknesses and diploë thickness of the calvarium were determined.
- This dissertation identified which morphometric and geometric properties of the diploë and cortical regions of the human calvarium were significant predictors of mechanical response under 4-point quasi-static bending.
- Fiber Bragg gratings (FBG) - optical strain-sensing instrumentation were employed to quantify compressive and tensile strain on both the outer surface and inner surface of the calvarium respectively during 4-point quasi-static and dynamic impact bending. The strains measured were consistent with a similar study that used strain gauges to quantify tensile strain on the inner surface of the calvarium (Hubbard, 1971).

- This dissertation quantified the calvarium under both 4-point dynamic impact bending and 4-point quasi-static bending conditions. The dynamic impact of calvarium specimens was only performed in 3-point bending in previous studies (Motherway et al., 2009; Zwirner et al., 2021). 4-point quasi-static bending of the calvarium was reported in one study but limited to 5 calvarium specimens (Hubbard, 1971).
- The mechanical response between male and female calvarium was statistically compared under 4-point dynamic impact bending.
- Readily available and cost-effective materials, particularly epoxy and chalk accessible at local retail corporations, were used to fabricate preliminary surrogate models of the calvarium.
- The testing conditions between the surrogate models and human calvarium specimens were consistent and occurred within the same study and laboratory settings. This allowed for a reasonable statistical comparison of mechanical responses without inferring if different experimental conditions influenced the results. Previous studies were required to compare the mechanical properties of their surrogate models to calvarium specimens tested in different studies by different researchers that may have not applied parallel testing methodologies to their surrogates (Delille et al., 2007; Falland-Cheung et al., 2017; Ondruschka et al., 2019; Plaisted et al., 2015; Roberts et al., 2013).

LIMITATIONS AND FUTURE RECOMMENDATIONS

Each of the four articles in Chapters 1 to 4 discussed their own set of limitations with some limitations overlapping with previous chapters. This section summarizes these limitations and is followed up with potential future recommendations. Limitations or future recommendations that were not mentioned in Chapters 1 to 4 are also outlined in this section.

- The calvarium specimens were sampled by convenience from human donors restricted to an older age group and to one geographic location. However, a greater sample size centred at an average or median age group and sampled across a diverse geographic location would allow the findings of this work to extend its representation across a wider population. Nonetheless, each article in this dissertation demonstrated a minimum statistical power of 80% ($\beta=0.20$) for hypothesis testing.
- The calvarium specimens were preserved or embalmed using unbuffered aqueous formaldehyde conditions which may have influenced the morphometry and mechanical response. Since formalin was unbuffered, the pH of the formalin solution may have dropped towards acidic levels to chemically react with hemoglobin (the red blood cell protein responsible for transporting oxygen) (Brenner, 2014; Thavarajah et al., 2012). The result would be the formation of dark formalin and phenol precipitates that could have possibly demineralized the tissue and influenced the morphometry of the calvaria (Brenner, 2014). Therefore, future preservation techniques of tissue should consider buffering formaldehyde to prevent any possibility of tissue demineralization. Embalming retards the decomposition of tissue by forming bonds between contiguous proteins that are not generally linked in living tissue (Crandall, 1994). Indeed, the effect of embalming or freezing on mechanical response has been investigated in major load-bearing bones of the

human and animal models (Burkhart et al., 2010; Carothers et al., 1949; Crandall, 1994; Evans, 1973; Lee & Pelker, 1985; Mick et al., 2015; Nazarian et al., 2009; Ohman et al., 2008; Pelker et al., 1984; Topp et al., 2012). However, the effect embalming has on fresh bone tissue remains inconclusive as many of these reported studies have yielded inconsistent results. Therefore, examining the effect of embalming on the mechanical response of fresh human calvarium warrants future investigation.

- In Chapter 2, the study was limited to a series of linear regression analyses whereby each morphometric and geometric property (12 predictors in total) was regressed with each dependent variable (10 in total). In future investigations with a greater sample size of calvarium tissue, it is recommended to perform a multivariable regression analysis that may account for more than one predictor variable in the model in addition to morphometry or geometry including sex, location, or age. The dependent variables derived from Chapter 2 were limited to quasi-static loading. Since the applications of real-world head impacts occur under dynamic impact loading rates with strain rates between $1-10^3\text{s}^{-1}$ (Hosseini Farid et al., 2018), it is recommended that future studies investigate the predictive capabilities of calvarium morphometry and geometry on mechanical response derived from dynamic impact loading.
- To model the calvarium specimens and surrogate prototypes during loading, the Euler-Bernoulli beam theorem was used to estimate bending stress. Combining the estimated bending stress and strain measured from FBGs, an effective bending modulus was derived from the slope of stress-strain curves. Indeed, the calvarium was assumed to be a Euler-Bernoulli beam, however, the calvarium is a non-uniform three-layered structure comprised of bone and pores. Each cross-section is distinctive, particularly the mixture of

pores and trabeculae in the diploë. In addition, the cortical and diploë geometry and morphometry endure slight structural changes, particularly the thickness of the cortical tables and orientation of trabeculae. Therefore, applying Euler-Bernoulli beam theorem on bone tissue like the calvarium is a limitation since it does not agree with some of the assumptions of the theorem (Roark et al., 2002). Although the calvarium specimens and surrogate prototypes were curved, it was ensured that on average, the thickness of the specimens was at least 10 times the ROC to assume a straight beam (Roark et al., 2002). It was assumed that the cross-sections of the specimens and surrogates remained perpendicular to the neutral axis and that the strain or deformation of the beams was small (Adeeb, 2011). Both these assumptions were met since surface strains measured less than 0.5% for the calvarium and less than 3% for the surrogate prototypes. Efforts were also made to apply the curved beam theorem to estimate bending stress, it was determined that tensile and compressive stress differed by less than 5 % compared to the stress derived from the Euler-Bernoulli Beam in 4-point bending impacts (Roark et al., 2002). Future studies may derive or research comprehensive stress models of bone tissue to estimate bending stress, one that accounts for curvature and the three-layered structure of the bone. It can be hypothesized that differences between complex and simple beam models may be negligible if strains until failure remain under 0.5%.

- During the 4-point quasi-static and dynamic bending impacts, a few calvarium specimens and surrogate prototypes experienced fracture initiation under one of the two top impact fixtures as opposed to fracture initiation between the top impact fixtures. In Chapter 3, it was suggested that the impact fixtures may have landed at a vulnerable location of the calvarium where a fracture could initiate such as an area with a single pore of considerable

size or of many pores. This may not necessarily be classified as a limitation since this is the natural structure of the calvarium. However, for the surrogates, fracture may have been initiated under the impact fixtures at a location where unobservable pores or imperfections were present within the internal structure. Therefore, not performing micro-CT scanning on the surrogates to verify if pores or imperfections existed before mechanical testing is a limitation and should be considered in future studies.

- It was ensured that the top impact fixtures would equally impact the calvarium specimens or surrogate prototypes at the same time during 4-point impact loading. However, there may have been small unnoticeable differences in the time when each impact fixture contacted the calvarium or surrogate as the top fixture travelled downward. A future design modification that may prevent this issue and reduce the possibility of fracture initiating under one of the the impact fixtures is pre-resting the impact fixtures on the calvarium or surrogates and then allowing an impactor to impact the top fixture (Figure 1). In addition, to improve the operator's physical ergonomics of reducing back strain and pressure on the knees when setting up the calvaria or surrogates for 4-point impact tests, an additional future design consideration is to elevate the 4-point impact bending fixtures from the floor to a tabletop setup (Figure 1).

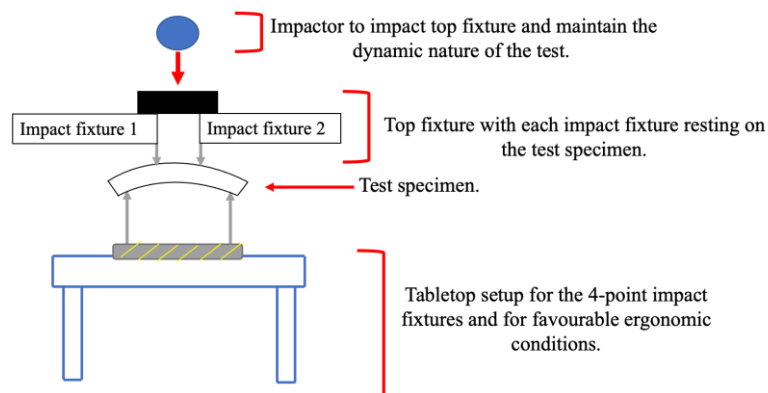


Figure. 1: A schematic of the future design modification for the 4-point dynamic impact bending tests.

- Fracture patterns of the calvarium and surrogate prototypes were not documented during mechanical testing. Future studies may include a qualitative analysis of the fracture patterns of the calvarium to ensure potential surrogates follow similar patterns.
- The mixture of epoxy and chalk for prototypes 2 and 3 was limited to one ratio. Future studies are encouraged to test various ratios of epoxy to chalk to mix to determine optimal ratios that would draw the mechanical response of the surrogates closer to the calvarium.
- Chalk and a single brand of epoxy were employed since they were readily available and cost-effective materials to fabricate the surrogates. In future studies, it is recommended to investigate potential substitutes for chalk with brittle-like characteristics such as glass, ceramic, or graphite. Various cost-effective and readily available epoxies exist in the market that may be considered such as Gorilla Glue Epoxy or Systemthree's T-88. These alternative materials may or may not positively affect the mechanical response of a surrogate when compared to calvarium specimens but are worth exploring.
- The next step in the development of the surrogate prototypes would be the expansion of the surrogates towards a frontal or parietal region. Force versus deflection, force time history curves and strain response may be initial mechanical parameters to be considered when comparing frontal or parietal regions between calvaria and surrogates.

BIBLIOGRAPHY

- Aare, M., & Halldin, P. (2003). A New Laboratory Rig for Evaluating Helmets Subject to Oblique Impacts. *Traffic Injury Prevention*, 4(3), 240–248. <https://doi.org/10.1080/15389580309879>
- Adanty, K., Bhagavathula, K. B., Tronchin, O., Li, D. X., Rabey, K. N., Doschak, M. R., Adeeb, S., Hogan, J., Ouellet, S., Plaisted, T. A., Satapathy, S., Romanyk, D. L., & Dennison, C. (2022). The Mechanical Characterization and Comparison of Male and Female Calvaria Under Four-Point Bending Impacts. *Journal of Biomechanical Engineering*, 1–47. <https://doi.org/10.1115/1.4056459>
- Adanty, K., Clark, J. M., Post, A., Hoshizaki, T. B., & Gilchrist, M. D. (2020). Comparing two proposed protocols to test the oblique response of cycling helmets to fall impacts. *International Journal of Crashworthiness*, 25(6), 648–663. <https://doi.org/10.1080/13588265.2019.1628479>
- Adanty, K., Rabey, K. N., Doschak, M. R., Bhagavathula, K. B., Hogan, J. D., Romanyk, D. L., Adeeb, S., Ouellet, S., Plaisted, T. A., Satapathy, S. S., & Dennison, C. R. (2021). Cortical and trabecular morphometric properties of the human calvarium. *Bone*, 148, 115931. <https://doi.org/10.1016/j.bone.2021.115931>
- Adanty, K., Tronchin, O., Bhagavathula, K. B., Rabey, K. N., Doschak, M. R., Romanyk, D., Hogan, J. D., Ouellet, S., Plaisted, T. A., Satapathy, S. S., & Dennison, C. R. (2020). On the Ability of Morphometric Indices of Skull Diploë to Explain Variation in Bone Fracture Force and Fracture Strain in Four-Point Bending: A Preliminary Step Toward A Simulant Fracture Model. *IRCOBI Conference 2020*, 821–822.
- Adeeb, S. (2011). *Introduction to Solid Mechanics and Finite Element Analysis Using Mathematica* (1st ed.). Kendall Hunt. <https://he.kendallhunt.com/product/introduction-solid-mechanics-and-finite-element-analysis-using-mathematica>
- Alexander, S. L., Rafaels, K., Gunnarsson, C. A., & Weerasooriya, T. (2019a). Structural analysis of the frontal and parietal bones of the human skull. *Journal of the Mechanical Behavior of Biomedical Materials*, 90, 689–701. <https://doi.org/10.1016/j.jmbbm.2018.10.035>
- Alexander, S. L., Rafaels, K., Gunnarsson, C. A., & Weerasooriya, T. (2019b). Structural analysis of the frontal and parietal bones of the human skull. *Journal of the Mechanical Behavior of Biomedical Materials*, 90, 689–701. <https://doi.org/10.1016/j.jmbbm.2018.10.035>
- Al-Fakih, E., Osman, N. A. A., & Adikan, F. R. M. (2012). The Use of Fiber Bragg Grating Sensors in Biomechanics and Rehabilitation Applications: The State-of-the-Art and Ongoing Research Topics. *Sensors (Basel, Switzerland)*, 12(10), 12890–12926. <https://doi.org/10.3390/s121012890>
- Allsop, D., “L,” Perl, T. R., & Warner, C. Y. (1991). Force/Deflection and Fracture Characteristics of the Temporo-parietal Region of the Human Head. *SAE Transactions*, 100, 2009–2018.

- Allsop, D. “L,” Warner, C. Y., Wille, M. G., Schneider, D. C., & Nahum, A. M. (1988). Facial Impact Response—A Comparison of the Hybrid III Dummy and Human Cadaver. *SAE Transactions*, 97, 1224–1240.
- Anctil, B., Bourget, D., Pagaue, G., Dionne, J. P., Wonnacott, M., Rice, K., & Toman, A. (2008). *The Development of a Ballistic Helmet Test Standard, Personal Armour Systems*. In: Pass conference proceedings, Brussel.
- Anderson, B. W., Kortz, M. W., & Al Kharazi, K. A. (2021). Anatomy, Head and Neck, Skull. In *StatPearls*. StatPearls Publishing. <http://www.ncbi.nlm.nih.gov/books/NBK499834/>
- Auperrin, A., Delille, R., Lesueur, D., Bruyère, K., Masson, C., & Drazétic, P. (2014). Geometrical and material parameters to assess the macroscopic mechanical behaviour of fresh cranial bone samples. *Journal of Biomechanics*, 47(5), 1180–1185. <https://doi.org/10.1016/j.jbiomech.2013.10.060>
- Azar, A., Bhagavathula, K. B., Hogan, J., Ouellet, S., Satapathy, S., & Dennison, C. R. (2019). Protective Headgear Attenuates Forces on the Inner Table and Pressure in the Brain Parenchyma During Blast and Impact: An Experimental Study Using a Simulant-Based Surrogate Model of the Human Head. *Journal of Biomechanical Engineering*, 142(4). <https://doi.org/10.1115/1.4044926>
- Boruah, S., Henderson, K., Subit, D., Salzar, R. S., Shender, B. S., & Paskoff, G. (2013). *Response of Human Skull Bone to Dynamic Compressive Loading*. 12.
- Boruah, S., Paskoff, G. R., Shender, B. S., Subit, D. L., Salzar, R. S., & Crandall, J. R. (2015a). Variation of bone layer thicknesses and trabecular volume fraction in the adult male human calvarium. *Bone*, 77, 120–134. <https://doi.org/10.1016/j.bone.2015.04.031>
- Boruah, S., Paskoff, G. R., Shender, B. S., Subit, D. L., Salzar, R. S., & Crandall, J. R. (2015b). Variation of bone layer thicknesses and trabecular volume fraction in the adult male human calvarium. *Bone*, 77, 120–134. <https://doi.org/10.1016/j.bone.2015.04.031>
- Bouxsein, M. L., Boyd, S. K., Christiansen, B. A., Guldborg, R. E., Jepsen, K. J., & Müller, R. (2010). Guidelines for assessment of bone microstructure in rodents using micro-computed tomography. *Journal of Bone and Mineral Research*, 25(7), 1468–1486. <https://doi.org/10.1002/jbmr.141>
- Brenner, E. (2014). Human body preservation – old and new techniques. *Journal of Anatomy*, 224(3), 316–344. <https://doi.org/10.1111/joa.12160>
- Brown, A. D., Walters, J. B., Zhang, Y. X., Saadatfar, M., Escobedo-Diaz, J. P., & Hazell, P. J. (2019). The mechanical response of commercially available bone simulants for quasi-static and dynamic loading. *Journal of the Mechanical Behavior of Biomedical Materials*, 90, 404–416. <https://doi.org/10.1016/j.jmbbm.2018.10.032>
- Bruns, V. (n.d.). *Handbuch der praktischen Chirurgie für Aerzte und Wund~irzte* (Vol. 1). Tiibingen: H. Laupp,.

- Burghardt, A. J., Kazakia, G. J., Laib, A., & Majumdar, S. (2008). Quantitative Assessment of Bone Tissue Mineralization with Polychromatic Micro-Computed Tomography. *Calcified Tissue International*, 83(2), 129–138. <https://doi.org/10.1007/s00223-008-9158-x>
- Burkhart, K. J., Nowak, T. E., Blum, J., Kuhn, S., Welker, M., Sternstein, W., Mueller, L. P., & Rommens, P. M. (2010). Influence of formalin fixation on the biomechanical properties of human diaphyseal bone. *Biomedizinische Technik. Biomedical Engineering*, 55(6), 361–365. <https://doi.org/10.1515/BMT.2010.043>
- Campbell, M. J., Machin, D., & Walters, S. J. (2010). *Medical Statistics: A Textbook for the Health Sciences*. John Wiley & Sons, Incorporated. <http://ebookcentral.proquest.com/lib/ualberta/detail.action?docID=624690>
- Carothers, C., Smith, F., & Calabresi, P. (1949). *Naval Medical Research Report NM 001 056.02.13*.
- Carson, H. J. (2009). Brain trauma in head injuries presenting with and without concurrent skull fractures. *Journal of Forensic and Legal Medicine*, 16(3), 115–120. <https://doi.org/10.1016/j.jflm.2008.08.013>
- Chappard, D., Legrand, E., Haettich, B., Chalès, G., Auvinet, B., Eschard, J.-P., Hamelin, J.-P., Baslé, M.-F., & Audran, M. (2001). Fractal dimension of trabecular bone: Comparison of three histomorphometric computed techniques for measuring the architectural two-dimensional complexity. *The Journal of Pathology*, 195(4), 515–521. <https://doi.org/10.1002/path.970>
- Chattopadhyay, S., & Tripathi, C. (2010). Skull fracture and haemorrhage pattern among fatal and nonfatal head injury assault victims – a critical analysis. *Journal of Injury and Violence Research*, 2(2), 99–103. <https://doi.org/10.5249/jivr.v2i2.46>
- Chen, H., Zhou, X., Fujita, H., Onozuka, M., & Kubo, K.-Y. (2013). Age-Related Changes in Trabecular and Cortical Bone Microstructure. *International Journal of Endocrinology*, 2013. <https://doi.org/10.1155/2013/213234>
- Chen, Q., Bao, N., Yao, Q., & Li, Z.-Y. (2018). Fractal dimension: A complementary diagnostic indicator of osteoporosis to bone mineral density. *Medical Hypotheses*, 116, 136–138. <https://doi.org/10.1016/j.mehy.2018.05.006>
- Chitchumnong, P., Brooks, S. C., & Stafford, G. D. (1989). Comparison of three- and four-point flexural strength testing of denture-base polymers. *Dental Materials*, 5(1), 2–5. [https://doi.org/10.1016/0109-5641\(89\)90082-1](https://doi.org/10.1016/0109-5641(89)90082-1)
- Clark, J. M., Adanty, K., Post, A., Hoshizaki, T. B., Clissold, J., McGoldrick, A., Hill, J., Annaidh, A. N., & Gilchrist, M. D. (2020). Proposed injury thresholds for concussion in equestrian sports. *Journal of Science and Medicine in Sport*, 23(3), 222–236. <https://doi.org/10.1016/j.jsams.2019.10.006>
- Coats, B., & Margulies, S. S. (2006). Material properties of human infant skull and suture at high rates. *Journal of Neurotrauma*, 23(8), 1222–1232. <https://doi.org/10.1089/neu.2006.23.1222>

- Crandall, J. R. (1994). *The preservation of human surrogates for biomechanical studies*. University of Virginia.
- Crandall, J. R., Bose, D., Forman, J., Untaroiu, C. D., Arregui-Dalmases, C., Shaw, C. G., & Kerrigan, J. R. (2011). Human surrogates for injury biomechanics research. *Clinical Anatomy*, 24(3), 362–371. <https://doi.org/10.1002/ca.21152>
- Cripton, P. A., Dressler, D. M., Stuart, C. A., Dennison, C. R., & Richards, D. (2014). Bicycle helmets are highly effective at preventing head injury during head impact: Head-form accelerations and injury criteria for helmeted and unhelmeted impacts. *Accident; Analysis and Prevention*, 70, 1–7. <https://doi.org/10.1016/j.aap.2014.02.016>
- Daughton, S. (1990). Head Injury in the Workplace. *AAOHN Journal*, 38(10), 497–501. <https://doi.org/10.1177/216507999003801008>
- Davis, M. T., Loyd, A. M., Shen, H. H., Mulroy, M. H., Nightingale, R. W., Myers, B. S., & Bass, C. D. (2012). The mechanical and morphological properties of 6 year-old cranial bone. *Journal of Biomechanics*, 45(15), 2493–2498. <https://doi.org/10.1016/j.jbiomech.2012.07.001>
- De Kegel, D., Meynen, A., Famaey, N., Harry van Lenthe, G., Depreitere, B., & Sloten, J. V. (2019). Skull fracture prediction through subject-specific finite element modelling is highly sensitive to model parameters. *Journal of the Mechanical Behavior of Biomedical Materials*, 100, 103384. <https://doi.org/10.1016/j.jmbbm.2019.103384>
- Delaney, J. S. (2004). Head Injuries Presenting to Emergency Departments in the United States From 1990 to 1999 for Ice Hockey, Soccer, and Football. *Clinical Journal of Sport Medicine*, 14(2), 80–87.
- Delille, R., Lesueur, D., Potier, P., Drazetic, P., & Markiewicz, E. (2007). Experimental study of the bone behaviour of the human skull bone for the development of a physical head model. *International Journal of Crashworthiness*, 12(2), 101–108. <https://doi.org/10.1080/13588260701433081>
- Delye, H., Verschueren, P., Depreitere, B., Verpoest, I., Berckmans, D., Vander Sloten, J., Van Der Perre, G., & Goffin, J. (2007). Biomechanics of frontal skull fracture. *Journal of Neurotrauma*, 24(10), 1576–1586. <https://doi.org/10.1089/neu.2007.0283>
- Dennison, C. R., & Wild, P. M. (2008). Enhanced sensitivity of an in-fibre Bragg grating pressure sensor achieved through fibre diameter reduction. *Measurement Science and Technology*, 19, 11pp.
- Dennison, C. R., Wild, P. M., Wilson, D. R., & Gilbert, M. K. (2010). An in-fiber Bragg grating sensor for contact force and stress measurements in articular joints. *Measurement Science and Technology*, 21(11), 115803. <https://doi.org/10.1088/0957-0233/21/11/115803>
- Deuerling, J. M., Rudy, D. J., Niebur, G. L., & Roeder, R. K. (2010). Improved accuracy of cortical bone mineralization measured by polychromatic microcomputed tomography using a novel high

mineral density composite calibration phantom. *Medical Physics*, 37(9), 5138–5145. <https://doi.org/10.1118/1.3480507>

Doube, M., Kłosowski, M. M., Arganda-Carreras, I., Cordelières, F. P., Dougherty, R. P., Jackson, J. S., Schmid, B., Hutchinson, J. R., & Shefelbine, S. J. (2010). BoneJ: Free and extensible bone image analysis in ImageJ. *Bone*, 47(6), 1076–1079. <https://doi.org/10.1016/j.bone.2010.08.023>

Eng, J. (2003). Sample Size Estimation: How Many Individuals Should Be Studied?1. *Radiology*. <https://pubs.rsna.org/doi/abs/10.1148/radiol.2272012051>

Evans, F. G. (1973). *Mechanical Properties of Bone*. Charles C. Thomas.

Evans, F. G., & Lissner, H. R. (1957). Tensile and compressive strength of human parietal bone. *Journal of Applied Physiology*, 10(3), 493–497. Scopus. <https://doi.org/10.1152/jappl.1957.10.3.493>

Fahlstedt, M., Abayazid, F., Panzer, M. B., Trotta, A., Zhao, W., Ghajari, M., Gilchrist, M. D., Ji, S., Kleiven, S., Li, X., Annaidh, A. N., & Halldin, P. (2021). Ranking and Rating Bicycle Helmet Safety Performance in Oblique Impacts Using Eight Different Brain Injury Models. *Annals of Biomedical Engineering*, 49(3), 1097–1109. <https://doi.org/10.1007/s10439-020-02703-w>

Falland-Cheung, L., Waddell, J. N., Chun Li, K., Tong, D., & Brunton, P. (2017). Investigation of the elastic modulus, tensile and flexural strength of five skull simulant materials for impact testing of a forensic skin/skull/brain model. *Journal of the Mechanical Behavior of Biomedical Materials*, 68, 303–307. <https://doi.org/10.1016/j.jmbbm.2017.02.023>

Félizet, G. (1844-1909) A. du texte. (1873). *Recherches anatomiques et expérimentales sur les fractures du crâne / par le Dr G. Félizet,...* <https://gallica.bnf.fr/ark:/12148/bpt6k5740393g>

Félizet, G. (1873). *Recherches anatomiques et expérimentales sur les fractures du crâne* (Vol. 1). A. Delahaye (Paris).

Feltrin, G. P., Macchi, V., Saccavini, C., Tosi, E., Dus, C., Fassina, A., Parenti, A., & Caro, R. D. (2001). Fractal analysis of lumbar vertebral cancellous bone architecture. *Clinical Anatomy*, 14(6), 414–417. <https://doi.org/10.1002/ca.1076>

Feng, X. (2009). Chemical and Biochemical Basis of Cell-Bone Matrix Interaction in Health and Disease. *Current Chemical Biology*, 3(2), 189–196. <https://doi.org/10.2174/187231309788166398>

Ghajari, M., Hellyer, P. J., & Sharp, D. J. (2017). Computational modelling of traumatic brain injury predicts the location of chronic traumatic encephalopathy pathology. *Brain*, 140(2), 333–343. <https://doi.org/10.1093/brain/aww317>

Gong, H., Zhang, M., Yeung, H. Y., & Qin, L. (2005). Regional variations in microstructural properties of vertebral trabeculae with aging. *Journal of Bone and Mineral Metabolism*, 23(2), 174–180. <https://doi.org/10.1007/s00774-004-0557-4>

Gonzales-Barron, U., & Butler, F. (2005). A COMPARISON OF VISUAL ASSESSMENT AND DIGITAL FRACTAL TEXTURE ANALYSIS OF BREAD-CRUMB FEATURES. In S. P.

- Cauvain, S. S. Salmon, & L. S. Young (Eds.), *Using Cereal Science and Technology for the Benefit of Consumers* (pp. 395–400). Woodhead Publishing. <https://doi.org/10.1533/9781845690632.10.395>
- Gosling, J., Harris, P., Humpherson, J., Whitmore, I., & Willian, P. (2017). *Human Anatomy, Color Atlas and Textbook* (6th ed.). Elsevier. <https://www.elsevier.ca/ca/product.jsp?isbn=9780723438274>
- Greenwood, C., Clement, J. G., Dicken, A. J., Evans, J. P. O., Lyburn, I. D., Martin, R. M., Rogers, K. D., Stone, N., Adams, G., & Zioupos, P. (2015). The micro-architecture of human cancellous bone from fracture neck of femur patients in relation to the structural integrity and fracture toughness of the tissue. *Bone Reports*, 3, 67–75. <https://doi.org/10.1016/j.bonr.2015.10.001>
- Gurdjian, E. S. (1975). Re-evaluation of the biomechanics of blunt impact injury of the head. *Surgery, Gynecology & Obstetrics*, 140(6), 845–850.
- Gurdjian, E. S., Hodgson, V. R., Hardy, W. G., Patrick, L. M., & Lissner, H. R. (1964). EVALUATION OF THE PROTECTIVE CHARACTERISTICS OF HELMETS IN SPORTS. *Journal of Trauma and Acute Care Surgery*, 4(3), 309–324.
- Gurdjian, E. S., & Lissner, H. R. (1947a). Deformations of the skull in head injury as studied by the “stresscoat” technic. *The American Journal of Surgery*, 73(2), 269–281. [https://doi.org/10.1016/0002-9610\(47\)90321-8](https://doi.org/10.1016/0002-9610(47)90321-8)
- Gurdjian, E. S., & Lissner, H. R. (1947b). Deformations of the skull in head injury as studied by the “stresscoat” technic. *The American Journal of Surgery*, 73(2), 269–281. [https://doi.org/10.1016/0002-9610\(47\)90321-8](https://doi.org/10.1016/0002-9610(47)90321-8)
- Gurdjian, E. S., Lissner, H. R., Latimer, F. R., Haddad, B. F., & Webster, J. E. (1953). Quantitative determination of acceleration and intracranial pressure in experimental head injury; preliminary report. *Neurology*, 3(6), 417–423. <https://doi.org/10.1212/wnl.3.6.417>
- Gurdjian, E. S., Lissner, H. R., & Webster, J. E. (1947). The mechanism of production of linear skull fracture; further studies on deformation of the skull by the stresscoat technique. *Surgery, Gynecology & Obstetrics*, 85(2), 195–210.
- Gurdjian, E. S., Roberts, V. L., & Thomas, L. M. (1966). Tolerance curves of acceleration and intracranial pressure and protective index in experimental head injury. *The Journal of Trauma*, 6(5), 600–604. <https://doi.org/10.1097/00005373-196609000-00005>
- Gurdjian, E. S., Webster, J. E., & Lissner, H. R. (1950). The Mechanism of Skull Fracture. *Journal of Neurosurgery*, 7(2), 106–114. <https://doi.org/10.3171/jns.1950.7.2.0106>
- Gurdjian, E. S., Webster, J. E., & Lissner, H. R. (1955). Observations on the mechanism of brain concussion, contusion, and laceration. *Surgery, Gynecology & Obstetrics*, 101(6), 680–690.
- Habicht, J. L., Kiessling, C., & Winkelmann, A. (2018). Bodies for Anatomy Education in Medical Schools: An Overview of the Sources of Cadavers Worldwide. *Academic Medicine*, 93(9), 1293–1300. <https://doi.org/10.1097/ACM.0000000000002227>

- Hahn, M., Vogel, M., Pompesius-Kempa, M., & Delling, G. (1992). Trabecular bone pattern factor—A new parameter for simple quantification of bone microarchitecture. *Bone*, *13*(4), 327–330. [https://doi.org/10.1016/8756-3282\(92\)90078-B](https://doi.org/10.1016/8756-3282(92)90078-B)
- Halldin, P., & Aare, M. (2003). A New Laboratory Rig for Evaluating Helmets Subject to Oblique Impacts. *Traffic Injury Prevention*, *4*, 240–248.
- Harrar, K., & Hamami, L. (2008). The fractal dimension correlated to the bone mineral density. *WSEAS Transactions on Signal Processing*, *4*(3), 110–126.
- Hayes, M. D., Edwards, D. B., & Shah, A. R. (2015). 4—Fractography Basics. In M. D. Hayes, D. B. Edwards, & A. R. Shah (Eds.), *Fractography in Failure Analysis of Polymers* (pp. 48–92). William Andrew Publishing. <https://doi.org/10.1016/B978-0-323-24272-1.00004-0>
- Hein, P. R. G., Brancheriau, L., Hein, P. R. G., & Brancheriau, L. (2018). Comparison between three-point and four-point flexural tests to determine wood strength of Eucalyptus specimens. *Maderas. Ciencia y Tecnología*, *20*(3), 333–342. <https://doi.org/10.4067/S0718-221X2018005003401>
- Henkel. (2016). *Technical Data Sheet: Speed Set Instant Mix Epoxy*. Henkel. <https://dm.henkel-dam.com/is/content/henkel/tds-10228091-ca-en-lepage-speed-set-instant-mix-epoxy-carded-syringe-14ml>
- Hildebrand, T., & Rügsegger, P. (1997). A new method for the model-independent assessment of thickness in three-dimensional images. *Journal of Microscopy*, *185*(1), 67–75. <https://doi.org/10.1046/j.1365-2818.1997.1340694.x>
- Hillier, M. L., & Bell, L. S. (2007). Differentiating Human Bone from Animal Bone: A Review of Histological Methods. *Journal of Forensic Sciences*, *52*(2), 249–263. <https://doi.org/10.1111/j.1556-4029.2006.00368.x>
- Hodgson, V. R., & Thomas, L. M. (1972). *BREAKING STRENGTH OF THE HUMAN SKULL VS. IMPACT SURFACE CURVATURE* (Final Rept). Article Final Rept. <https://trid.trb.org/view/112380>
- Hombach-Klonisch, S., Klonisch, T., & Peeler, J. (2019). *Sobotta clinical atlas of human anatomy* (1st edition.). <https://www.clinicalkey.com/dura/browse/bookChapter/3-s2.0-C20150000260>
- Horgan, T. J., & Gilchrist, M. D. (2003). The creation of three-dimensional finite element models for simulating head impact biomechanics. *International Journal of Crashworthiness*, *8*(4), 353–366. <https://doi.org/10.1533/ijcr.2003.0243>
- Hoshizaki, T. B., & Brien, S. E. (2004). The science and design of head protection in sport. *Neurosurgery*, *55*(4), 956.
- Hoshizaki, T. B., Post, A., Kendall, M., Cournoyer, J., Rousseau, P., Gilchrist, M. D., Brien, S., Cusimano, M., & Marshall, S. (2017). The development of a threshold curve for the understanding of concussion in sport. *Trauma*, *19*(3), 196–206. <https://doi.org/10.1177/1460408616676503>

- Hosseini Farid, M., Eslaminejad, A., Ramzanpour, M., Ziejewski, M., & Karami, G. (2018). The Strain Rates of the Brain and Skull Under Dynamic Loading. *Volume 3: Biomedical and Biotechnology Engineering*, V003T04A067. <https://doi.org/10.1115/IMECE2018-88300>
- Hosseini Farid, M., Eslaminejad, A., Ramzanpour, M., Ziejewski, M., & Karami, G. (2019, January 15). *The Strain Rates of the Brain and Skull Under Dynamic Loading*. ASME 2018 International Mechanical Engineering Congress and Exposition. <https://doi.org/10.1115/IMECE2018-88300>
- Houg, K. P., Armijo, L., Doschak, M. R., Major, P. W., Popowics, T., Dennison, C. R., & Romanyk, D. L. (2021). Experimental repeatability, sensitivity, and reproducibility of force and strain measurements from within the periodontal ligament space during ex vivo swine tooth loading. *Journal of the Mechanical Behavior of Biomedical Materials*, *120*, 104562. <https://doi.org/10.1016/j.jmbbm.2021.104562>
- Hubbard, R. P. (1971). Flexure of layered cranial bone. *Journal of Biomechanics*, *4*(4), 251–263. [https://doi.org/10.1016/0021-9290\(71\)90031-5](https://doi.org/10.1016/0021-9290(71)90031-5)
- Hubbard, R. P., & McLeod, D. G. (1974b). Definition and Development of A Crash Dummy Head. *SAE Transactions*, *83*, 3836–3851.
- Igo, B. J., Cottler, P. S., Black, J. S., & Panzer, M. B. (2021). The mechanical and microstructural properties of the pediatric skull. *Journal of the Mechanical Behavior of Biomedical Materials*, *120*, 104578. <https://doi.org/10.1016/j.jmbbm.2021.104578>
- JAMES L. UNDERWOOD. (n.d.). *NIJ Standard for Ballistic Helmets*. U.S. DEPARTMENT OF JUSTICE - National Institute of Justice.
- Jankovic, J., Mazziotta, J. C., & Pomeroy, S. L. (2021). *Bradley and Daroff's Neurology in Clinical Practice, 2-Volume Set*. Elsevier Health Sciences.
- Ji, S., Ghajari, M., Mao, H., Kraft, R. H., Hajiaghamemar, M., Panzer, M. B., Willinger, R., Gilchrist, M. D., Kleiven, S., & Stitzel, J. D. (2022). Use of Brain Biomechanical Models for Monitoring Impact Exposure in Contact Sports. *Annals of Biomedical Engineering*. <https://doi.org/10.1007/s10439-022-02999-w>
- Karton, C., Blaine Hoshizaki, T., & Gilchrist, M. D. (2020). A novel repetitive head impact exposure measurement tool differentiates player position in National Football League. *Scientific Reports*, *10*(1), Article 1. <https://doi.org/10.1038/s41598-019-54874-9>
- Keen, J. A. (1950). A study of the differences between male and female skulls. *American Journal of Physical Anthropology*, *8*(1), 65–80. <https://doi.org/10.1002/ajpa.1330080113>
- Kelsey, S., Gellatly, R. A., & Clark, B. W. (1958). The Shear Modulus of Foil Honeycomb Cores. *Aircraft Engineering and Aerospace Technology*, *30*(10), 294–302. <https://doi.org/10.1108/eb033026>
- Kersh, M. E., Zysset, P. K., Pahr, D. H., Wolfram, U., Larsson, D., & Pandy, M. G. (2013). Measurement of structural anisotropy in femoral trabecular bone using clinical-resolution CT

images. *Journal of Biomechanics*, 46(15), 2659–2666. <https://doi.org/10.1016/j.jbiomech.2013.07.047>

Kim, Y. J., & Henkin, J. (2015). Micro-computed tomography assessment of human alveolar bone: Bone density and three-dimensional micro-architecture. *Clinical Implant Dentistry and Related Research*, 17(2), 307–313. <https://doi.org/10.1111/cid.12109>

Kivell, T. L. (2016). A review of trabecular bone functional adaptation: What have we learned from trabecular analyses in extant hominoids and what can we apply to fossils? *Journal of Anatomy*, 228(4), 569–594. <https://doi.org/10.1111/joa.12446>

Kleiven, S. (2013). Why Most Traumatic Brain Injuries are Not Caused by Linear Acceleration but Skull Fractures are. *Frontiers in Bioengineering and Biotechnology*, 1. <https://doi.org/10.3389/fbioe.2013.00015>

Kleiven, S., & Hardy, W. N. (2002). Correlation of an FE Model of the Human Head with Local Brain Motion—Consequences for Injury Prediction. *Stapp Car Crash Journal*, 46, 123–144.

Knowles, B. M., & Dennison, C. R. (2017). Predicting Cumulative and Maximum Brain Strain Measures From HybridIII Head Kinematics: A Combined Laboratory Study and Post-Hoc Regression Analysis. *Annals of Biomedical Engineering*, 45(9), 2146–2158. <https://doi.org/10.1007/s10439-017-1848-y>

Komisar, V., Dojnov, A., Yang, Y., Shishov, N., Chong, H., Yu, Y., Bercovitz, I., Cusimano, M. D., Becker, C., Mackey, D. C., & Robinovitch, S. N. (2022). Injuries from falls by older adults in long-term care captured on video: Prevalence of impacts and injuries to body parts. *BMC Geriatrics*, 22(1), 343. <https://doi.org/10.1186/s12877-022-03041-3>

Kremer, C., Racette, S., Dionne, C.-A., & Sauvageau, A. (2008). Discrimination of Falls and Blows in Blunt Head Trauma: Systematic Study of the Hat Brim Line Rule in Relation to Skull Fractures. *Journal of Forensic Sciences*, 53(3), 716–719. <https://doi.org/10.1111/j.1556-4029.2008.00725.x>

Kriewall, T. J. (1982). Structural, mechanical, and material properties of fetal cranial bone. *American Journal of Obstetrics & Gynecology*, 143(6), 707–714. [https://doi.org/10.1016/0002-9378\(82\)90119-3](https://doi.org/10.1016/0002-9378(82)90119-3)

Kriewall, T. J., McPherson, G. K., & Tsai, A. Ch. (1981). Bending properties and ash content of fetal cranial bone. *Journal of Biomechanics*, 14(2), 73–79. [https://doi.org/10.1016/0021-9290\(81\)90166-4](https://doi.org/10.1016/0021-9290(81)90166-4)

Laerd Statistics. (2015). Simple linear regression using SPSS Statistics. *Statistical Tutorials and Software Guides*. <https://statistics.laerd.com/>

Lee, J. H. C., Ondruschka, B., Falland-Cheung, L., Scholze, M., Hammer, N., Tong, D. C., & Waddell, J. N. (2019). An Investigation on the Correlation between the Mechanical Properties of Human Skull Bone, Its Geometry, Microarchitectural Properties, and Water Content. *Journal of Healthcare Engineering*, 2019, 1–8. <https://doi.org/10.1155/2019/6515797>

- Lee, K. E., & Pelker, R. R. (1985). Effect of freezing on histologic and biomechanical failure patterns in the rabbit capital femoral growth plate. *Journal of Orthopaedic Research: Official Publication of the Orthopaedic Research Society*, 3(4), 514–515. <https://doi.org/10.1002/jor.1100030415>
- Li, Y., Ouellet, S., Vette, A. H., Raboud, D., Martin, A., & Dennison, C. R. (2021). Evaluation of the Kinematic Biofidelity and Inter-Test Repeatability of Global Accelerations and Brain Parenchyma Pressure for a Head–Brain Physical Model. *Journal of Biomechanical Engineering*, 143(9). <https://doi.org/10.1115/1.4050752>
- Lillie, E. M., Urban, J. E., Weaver, A. A., Powers, A. K., & Stitzel, J. D. (2015a). Estimation of skull table thickness with clinical CT and validation with microCT. *Journal of Anatomy*, 226(1), 73–80. <https://doi.org/10.1111/joa.12259>
- Lillie, E. M., Urban, J. E., Weaver, A. A., Powers, A. K., & Stitzel, J. D. (2015b). Estimation of skull table thickness with clinical CT and validation with microCT. *Journal of Anatomy*, 226(1), 73–80. <https://doi.org/10.1111/joa.12259>
- Liu, H., Kang, J., Chen, J., Li, G., Li, X., & Wang, J. (2012). Intracranial Pressure Response to Non-Penetrating Ballistic Impact: An Experimental Study Using a Pig Physical Head Model and Live Pigs. *International Journal of Medical Sciences*, 9(8), 655–664. <https://doi.org/10.7150/ijms.5004>
- Lorensen, W. E., & Cline, H. E. (1987). Marching cubes: A high resolution 3D surface construction algorithm. *ACM SIGGRAPH Computer Graphics*, 21(4), 163–169. <https://doi.org/10.1145/37402.37422>
- Macpherson, B. C. M., Macpherson, P., & Jennett, B. (1990). CT evidence of intracranial contusion and haematoma in relation to the presence, site and type of skull fracture. *Clinical Radiology*, 42(5), 321–326. [https://doi.org/10.1016/S0009-9260\(05\)82145-2](https://doi.org/10.1016/S0009-9260(05)82145-2)
- Mao, H., Zhang, L., Jiang, B., Genthikatti, V. V., Jin, X., Zhu, F., Makwana, R., Gill, A., Jandir, G., Singh, A., & Yang, K. H. (2013). Development of a Finite Element Human Head Model Partially Validated With Thirty Five Experimental Cases. *Journal of Biomechanical Engineering*, 135(11). <https://doi.org/10.1115/1.4025101>
- Margulies, S. S., & Thibault, K. L. (2000). Infant Skull and Suture Properties: Measurements and Implications for Mechanisms of Pediatric Brain Injury. *Journal of Biomechanical Engineering*, 122(4), 364–371. <https://doi.org/10.1115/1.1287160>
- Marks, P. (2005). HEAD TRAUMA | Pediatric and Adult, Clinical Aspects. In J. Payne-James (Ed.), *Encyclopedia of Forensic and Legal Medicine* (pp. 461–472). Elsevier. <https://doi.org/10.1016/B0-12-369399-3/00186-5>
- McElhaney, J. H., Fogle, J. L., Melvin, J. W., Haynes, R. R., Roberts, V. L., & Alem, N. M. (1970a). Mechanical properties of cranial bone. *Journal of Biomechanics*, 3(5), 495–511. [https://doi.org/10.1016/0021-9290\(70\)90059-X](https://doi.org/10.1016/0021-9290(70)90059-X)

- McGrath, A., & Taylor, R. S. (2022). Pediatric Skull Fractures. In *StatPearls*. StatPearls Publishing. <http://www.ncbi.nlm.nih.gov/books/NBK482218/>
- McIntosh, A. S., Kallieris, D., Mattern, R., & Miltner, E. (1993). *Head and Neck Injury Resulting from Low Velocity Direct Impact* (SAE Technical Paper No. 933112). SAE International. <https://doi.org/10.4271/933112>
- McPherson, G. K., & Kriewall, T. J. (1980). The elastic modulus of fetal cranial bone: A first step towards an understanding of the biomechanics of fetal head molding. *Journal of Biomechanics*, *13*(1), 9–16. [https://doi.org/10.1016/0021-9290\(80\)90003-2](https://doi.org/10.1016/0021-9290(80)90003-2)
- Melvin, J. W., Fuller, P. M., Daniel, R. P., & Pavliscak, G. M. (1969). Human Head and Knee Tolerance to Localized Impacts. *SAE Transactions*, *78*, 1772–1782.
- Melvin, J. W., & Yoganandan, N. (2015). Biomechanics of Brain Injury: A Historical Perspective. In N. Yoganandan, A. M. Nahum, & J. W. Melvin (Eds.), *Accidental Injury: Biomechanics and Prevention* (pp. 221–245). Springer. https://doi.org/10.1007/978-1-4939-1732-7_9
- Messerer, O. (1880). *Über Elasticität und Festigkeit der Menschlichen Knochen*. Stuttgart, Germany.
- Mick, E., Steinke, H., Wolfskämpf, T., Wieding, J., Hammer, N., Schulze, M., Souffrant, R., & Bader, R. (2015). Influence of short-term fixation with mixed formalin or ethanol solution on the mechanical properties of human cortical bone. *Current Directions in Biomedical Engineering*, *1*(1), 335–339. <https://doi.org/10.1515/cdbme-2015-0083>
- Milton, S. (1986). A Sample Size Formula for Multiple Regression Studies on JSTOR. *The Public Opinion Quarterly*, *50*(1), 112–118.
- Motherway, J. A., Verschueren, P., Van der Perre, G., Vander Sloten, J., & Gilchrist, M. D. (2009). The mechanical properties of cranial bone: The effect of loading rate and cranial sampling position. *Journal of Biomechanics*, *42*(13), 2129–2135. <https://doi.org/10.1016/j.jbiomech.2009.05.030>
- Mott, R. L., & Untener, J. A. (2018). *Applied Strength of Materials, Sixth Edition SI Units Version* (6th ed.). Taylor and Francis Group.
- Mukaka, M. (2012). A guide to appropriate use of Correlation coefficient in medical research. *Malawi Medical Journal : The Journal of Medical Association of Malawi*, *24*(3), 69–71.
- Nahum, A. M., Gatts, J. D., Gadd, C. W., & Danforth, J. (1968). *Impact Tolerance of the Skull and Face* (SAE Technical Paper No. 680785). SAE International. <https://doi.org/10.4271/680785>
- Nahum, A. M., Smith, R., & Ward, C. C. (1977). *Intracranial Pressure Dynamics During Head Impact* (SAE Technical Paper No. 770922). SAE International. <https://doi.org/10.4271/770922>
- Nazarian, A., Hermannsson, B. J., Muller, J., Zurakowski, D., & Snyder, B. D. (2009). Effects of tissue preservation on murine bone mechanical properties. *Journal of Biomechanics*, *42*(1), 82–86. <https://doi.org/10.1016/j.jbiomech.2008.09.037>

- Nelson, D. V., Makino, A., Lawrence, C. M., Seim, J. M., Schulz, W. L., & Udd, E. (1998). *Determination of the K-matrix for the multiparameter fiber grating sensor in AD072 fibercore fiber*. 3489, 79–85. <https://doi.org/10.1117/12.323418>
- Nieves, J. W., Formica, C., Ruffing, J., Zion, M., Garrett, P., Lindsay, R., & Cosman, F. (2005). Males Have Larger Skeletal Size and Bone Mass Than Females, Despite Comparable Body Size. *Journal of Bone and Mineral Research*, 20(3), 529–535. <https://doi.org/10.1359/JBMR.041005>
- Ohman, C., Dall’Ara, E., Baleani, M., Jan, S. V. S., & Viceconti, M. (2008). The effects of embalming using a 4% formalin solution on the compressive mechanical properties of human cortical bone. *Clinical Biomechanics*. <https://doi.org/10.1016/j.clinbiomech.2008.07.007>
- Ohman, C., Dall’Ara, E., Baleani, M., Van Sint Jan, S., & Viceconti, M. (2008). The effects of embalming using a 4% formalin solution on the compressive mechanical properties of human cortical bone. *Clinical Biomechanics (Bristol, Avon)*, 23(10), 1294–1298. <https://doi.org/10.1016/j.clinbiomech.2008.07.007>
- Ondruschka, B., Lee, J. H. C., Scholze, M., Zwirner, J., Tong, D., Waddell, J. N., & Hammer, N. (2019). A biomechanical comparison between human calvarial bone and a skull simulant considering the role of attached periosteum and dura mater. *International Journal of Legal Medicine*, 133(5), 1603–1610. Scopus. <https://doi.org/10.1007/s00414-019-02102-4>
- Ono, K., Kikuchi, A., Kobayashi, H., & Nakamura, N. (1985). Human head tolerances to sagittal and lateral impacts—Estimation deduced from experimental dead injury using subhuman primates and human cadaver skulls. In *Head injury prevention past and present research*.
- Osmond, M. H., Klassen, T. P., Wells, G. A., Correll, R., Jarvis, A., Joubert, G., Bailey, B., Chauvin-Kimoff, L., Pusic, M., McConnell, D., Nijssen-Jordan, C., Silver, N., Taylor, B., & Stiell, I. G. (2010). CATCH: A clinical decision rule for the use of computed tomography in children with minor head injury. *CMAJ: Canadian Medical Association Journal*, 182(4), 341–348. <https://doi.org/10.1503/cmaj.091421>
- Parfitt, A. M., Drezner, M. K., Glorieux, F. H., Kanis, J. A., Malluche, H., Meunier, P. J., Ott, S. M., & Recker, R. R. (1987). Bone histomorphometry: Standardization of nomenclature, symbols, and units. Report of the ASBMR Histomorphometry Nomenclature Committee. *Journal of Bone and Mineral Research: The Official Journal of the American Society for Bone and Mineral Research*, 2(6), 595–610. <https://doi.org/10.1002/jbmr.5650020617>
- Pelker, R. R., Friedlaender, G. E., Markham, T. C., Panjabi, M. M., & Moen, C. J. (1984). Effects of freezing and freeze-drying on the biomechanical properties of rat bone. *Journal of Orthopaedic Research: Official Publication of the Orthopaedic Research Society*, 1(4), 405–411. <https://doi.org/10.1002/jor.1100010409>
- Pellman, E. J., Viano, D. C., Tucker, A. M., Casson, I. R., & Waeckerle, J. F. (2003). Concussion in Professional Football: Reconstruction of Game Impacts and Injuries. *Neurosurgery*, 53(4), 799–814. <https://doi.org/10.1227/01.NEU.0000083559.68424.3F>

- Peterson, J., & Dechow, P. C. (2002). Material properties of the inner and outer cortical tables of the human parietal bone. *The Anatomical Record*, 268(1), 7–15. <https://doi.org/10.1002/ar.10131>
- Plaisted, T. A., Gardner, J. M., & Gair, J. L. (2015). *Characterization of a Composite Material to Mimic Human Cranial Bone*. 12.
- Pothuau, L., Benhamou, C. L., Porion, P., Lespessailles, E., Harba, R., & Levitz, P. (2000). Fractal Dimension of Trabecular Bone Projection Texture Is Related to Three-Dimensional Microarchitecture. *Journal of Bone and Mineral Research*, 15(4), 691–699. <https://doi.org/10.1359/jbmr.2000.15.4.691>
- Pritchard, J. J., Scott, J. H., & Girgis, F. G. (1956). The structure and development of cranial and facial sutures. *Journal of Anatomy*, 90(Pt 1), 73-86.3.
- Puvanachandra, P., & Hyder, A. A. (2009). *THE BURDEN OF TRAUMATIC BRAIN INJURY IN ASIA: A CALL FOR RESEARCH*. 4, 6.
- Rafaels, K. A., Cutcliffe, H. C., Salzar, R. S., Davis, M., Boggess, B., Bush, B., Harris, R., Rountree, M. S., Sanderson, E., Campman, S., Koch, S., & ‘Dale’ Bass, C. R. (2015). Injuries of the Head from Backface Deformation of Ballistic Protective Helmets Under Ballistic Impact. *Journal of Forensic Sciences*, 60(1), 219–225. <https://doi.org/10.1111/1556-4029.12570>
- Rahmoun, J., Auperrin, A., Delille, R., Naceur, H., & Drazetic, P. (2014). Characterization and micromechanical modeling of the human cranial bone elastic properties. *Mechanics Research Communications*, 60, 7–14. <https://doi.org/10.1016/j.mechrescom.2014.04.001>
- Reisinger, A. G., Pahr, D. H., & Zysset, P. K. (2011). Principal stiffness orientation and degree of anisotropy of human osteons based on nanoindentation in three distinct planes. *Journal of the Mechanical Behavior of Biomedical Materials*, 4(8), 2113–2127. <https://doi.org/10.1016/j.jmbbm.2011.07.010>
- Roark, R. J., Young, W. C., & Budynas, R. G. (2002). *Roark’s formulas for stress and strain* (7th ed). McGraw-Hill.
- Robbins, D. H., & Wood, J. L. (1969). Determination of mechanical properties of the bones of the skull. *Experimental Mechanics*, 9(5). <https://wblldb.lievers.net/10207541.html>
- Roberts, J. C., Merkle, A. C., Carneal, C. M., Voo, L. M., Johannes, M. S., Paulson, J. M., Tankard, S., & Uy, O. M. (2013). Development of a Human Cranial Bone Surrogate for Impact Studies. *Frontiers in Bioengineering and Biotechnology*, 1. <https://doi.org/10.3389/fbioe.2013.00013>
- Rowson, B., Rowson, S., & Duma, S. M. (2015). Hockey STAR: A Methodology for Assessing the Biomechanical Performance of Hockey Helmets. *Annals of Biomedical Engineering*, 43(10), 2429–2443. <https://doi.org/10.1007/s10439-015-1278-7>
- Sahoo, D., Deck, C., & Willinger, R. (2014). Development and validation of an advanced anisotropic visco-hyperelastic human brain FE model. *Journal of the Mechanical Behavior of Biomedical Materials*, 33, 24–42. <https://doi.org/10.1016/j.jmbbm.2013.08.022>

- Salmon, P. (2009). *MORPHOMETRIC PARAMETERS IN CT_ANALYSER*. 36.
- Salmon, P. (2020). Application of Bone Morphometry and Densitometry by X-Ray Micro-CT to Bone Disease Models and Phenotypes. In K. Orhan (Ed.), *Micro-computed Tomography (micro-CT) in Medicine and Engineering* (pp. 49–75). Springer International Publishing. https://doi.org/10.1007/978-3-030-16641-0_5
- Salmon, P. L., Ohlsson, C., Shefelbine, S. J., & Doube, M. (2015). Structure Model Index Does Not Measure Rods and Plates in Trabecular Bone. *Frontiers in Endocrinology*, 6. <https://doi.org/10.3389/fendo.2015.00162>
- Schneider, D. C., & Nahum, A. M. (1972). *Impact Studies of Facial Bones and Skull* (SAE Technical Paper No. 720965). SAE International. <https://doi.org/10.4271/720965>
- Schweizer, S., Hattendorf, B., Schneider, P., Aeschlimann, B., Gauckler, L., Müller, R., & Günther, D. (2007). Preparation and characterization of calibration standards for bone density determination by micro-computed tomography. *Analyst*, 132(10), 1040–1045. <https://doi.org/10.1039/B703220J>
- Sharma, V. K., Rango, J., Connaughton, A. J., Lombardo, D. J., & Sabesan, V. J. (2015). The Current State of Head and Neck Injuries in Extreme Sports. *Orthopaedic Journal of Sports Medicine*, 3(1), 2325967114564358. <https://doi.org/10.1177/2325967114564358>
- Shields, B. J., Burkett, E., & Smith, G. A. (2011). Epidemiology of balcony fall–related injuries, United States, 1990–2006. *The American Journal of Emergency Medicine*, 29(2), 174–180. <https://doi.org/10.1016/j.ajem.2009.08.023>
- Stables, G., Quigley, G., Basu, S., & Pillay, R. (2005). An unusual case of a compound depressed skull fracture after an assault with a stiletto heel. *Emergency Medicine Journal*, 22(4), 303–304.
- Starmans, M. P. A., van der Voort, S. R., Castillo Tovar, J. M., Veenland, J. F., Klein, S., & Niessen, W. J. (2020). Chapter 18 - Radiomics: Data mining using quantitative medical image features. In S. K. Zhou, D. Rueckert, & G. Fichtinger (Eds.), *Handbook of Medical Image Computing and Computer Assisted Intervention* (pp. 429–456). Academic Press. <https://doi.org/10.1016/B978-0-12-816176-0.00023-5>
- Takhounts, E. G., Ridella, S. A., Hasija, V., Tannous, R. E., Campbell, J. Q., Malone, D., Danelson, K., Stitzel, J., Rowson, S., & Duma, S. (2008). Investigation of traumatic brain injuries using the next generation of simulated injury monitor (SIMon) finite element head model. *Stapp Car Crash Journal*, 52, 1–31.
- Thali, M. J., Kneubuehl, B. P., Zollinger, U., & Dirnhofer, R. (2002). The “Skin–skull–brain model”: A new instrument for the study of gunshot effects. *Forensic Science International*, 125(2), 178–189. [https://doi.org/10.1016/S0379-0738\(01\)00637-5](https://doi.org/10.1016/S0379-0738(01)00637-5)
- Thavarajah, R., Mudimbaimannar, V. K., Elizabeth, J., Rao, U. K., & Ranganathan, K. (2012). Chemical and physical basics of routine formaldehyde fixation. *Journal of Oral and Maxillofacial Pathology : JOMFP*, 16(3), 400–405. <https://doi.org/10.4103/0973-029X.102496>

- Thulung, S., Ranabhat, K., Bishokarma, S., & Gongal, D. N. (2019). Morphometric Measurement of Cranial Vault Thickness: A Tertiary Hospital Based Study. *JNMA: Journal of the Nepal Medical Association*, 57(215), 29–32. <https://doi.org/10.31729/jnma.3949>
- Tian, H., Liu, D., Wang, Y., & Wang, Q. (2019). Effect of adhesive type on the sensitivity coefficient of FBG sensor bonded on the surface of CFRP. *Optoelectronics Letters*, 15(4), 264–268. <https://doi.org/10.1007/s11801-019-8183-5>
- Tivesten, A., Movérare-Skrtic, S., Chagin, A., Venken, K., Salmon, P., Vanderschueren, D., Sävendahl, L., Holmäng, A., & Ohlsson, C. (2004). Additive protective effects of estrogen and androgen treatment on trabecular bone in ovariectomized rats. *Journal of Bone and Mineral Research: The Official Journal of the American Society for Bone and Mineral Research*, 19(11), 1833–1839. <https://doi.org/10.1359/JBMR.040819>
- Topp, T., Müller, T., Huss, S., Kann, P. H., Weihe, E., Ruchholtz, S., & Zettl, R. P. (2012). Embalmed and fresh frozen human bones in orthopedic cadaveric studies: Which bone is authentic and feasible? *Acta Orthopaedica*, 83(5), 543–547. <https://doi.org/10.3109/17453674.2012.727079>
- Ueng, C. E. S. (2003). Sandwich Composites. In R. A. Meyers (Ed.), *Encyclopedia of Physical Science and Technology (Third Edition)* (pp. 407–412). Academic Press. <https://doi.org/10.1016/B0-12-227410-5/00672-4>
- Ural, A., Zioupos, P., Buchanan, D., & Vashishth, D. (2011). THE EFFECT OF STRAIN RATE ON FRACTURE TOUGHNESS OF HUMAN CORTICAL BONE: A FINITE ELEMENT STUDY. *Journal of the Mechanical Behavior of Biomedical Materials*, 4(7), 1021–1032. <https://doi.org/10.1016/j.jmbbm.2011.03.011>
- U.S National Library of Medicine. (2000). *Department of Health and Human Services: Visible Human Database*.
- Van Dessel, J., Nicolielo, L. F. P., Huang, Y., Slagmolen, P., Politis, C., Lambrichts, I., & Jacobs, R. (2016). Quantification of bone quality using different cone beam computed tomography devices: Accuracy assessment for edentulous human mandibles. *European Journal of Oral Implantology*, 9(4), 411–424.
- Van Lierde, C., Depreitere, B., Vander Sloten, J., Van Audekercke, R., Van Der Perre, G., & Goffin, J. (2003). Skull Biomechanics: The Energy Absorbability of the Human Skull Frontal Bone during Fracture under Quasi-Static Loading. *Journal of Applied Biomaterials and Biomechanics*, 1(3), 194–199. <https://doi.org/10.1177/228080000300100306>
- Versace, J. (1971). *A Review of the Severity Index* (SAE Technical Paper No. 710881). SAE International. <https://doi.org/10.4271/710881>
- Viano, D. C., Withnall, C., & Halstead, D. (2012). Impact Performance of Modern Football Helmets. *Annals of Biomedical Engineering*, 40(1), 160–174. <https://doi.org/10.1007/s10439-011-0384-4>

- Vorst, M. V., Stuhmiller, J., Ho, K., Yoganandan, N., & Pintar, F. (2003). Statistically and Biomechanically Based Criterion for Impact-Induced Skull Fracture. *Annual Proceedings / Association for the Advancement of Automotive Medicine*, 47, 363–381.
- Weisenbach, C. A., Logsdon, K., Salzar, R. S., Chancey, V. C., & Brozoski, F. (2018). Preliminary Investigation of Skull Fracture Patterns Using an Impactor Representative of Helmet Back-Face Deformation. *Military Medicine*, 183(suppl_1), 287–293. <https://doi.org/10.1093/milmed/usx210>
- Wilke, H.-J., Krischak, S., & Claes, L. E. (1996). Formalin fixation strongly influences biomechanical properties of the spine. *Journal of Biomechanics*, 29(12), 1629–1631. [https://doi.org/10.1016/S0021-9290\(96\)80016-9](https://doi.org/10.1016/S0021-9290(96)80016-9)
- Wood, J. L. (1971). Dynamic response of human cranial bone. *Journal of Biomechanics*, 4(1), 1–12. [https://doi.org/10.1016/0021-9290\(71\)90010-8](https://doi.org/10.1016/0021-9290(71)90010-8)
- Wu, Y., Adeeb, S., & Doschak, M. R. (2015). Using Micro-CT Derived Bone Microarchitecture to Analyze Bone Stiffness – A Case Study on Osteoporosis Rat Bone. *Frontiers in Endocrinology*, 6. <https://doi.org/10.3389/fendo.2015.00080>
- Yoganandan, N., Pintar, F. A., Sances, A., Walsh, P. R., Ewing, C. L., Thomas, D. J., & Snyder, R. G. (1995). Biomechanics of skull fracture. *Journal of Neurotrauma*, 12(4), 659–668. <https://doi.org/10.1089/neu.1995.12.659>
- Yoganandan, N., Sances, A., Pintar, F. A., Walsh, P. R., Ewing, C. L., Thomas, D. J., Snyder, R. G., Reinartz, J., & Droese, K. (1994). Biomechanical Tolerance of the Cranium. *SAE Transactions*, 103, 184–189.
- Zebaze, R. M., Ghasem-Zadeh, A., Bohte, A., Iuliano-Burns, S., Mirams, M., Price, R. I., Mackie, E. J., & Seeman, E. (2010). Intracortical remodelling and porosity in the distal radius and post-mortem femurs of women: A cross-sectional study. *The Lancet*, 375(9727), 1729–1736. [https://doi.org/10.1016/S0140-6736\(10\)60320-0](https://doi.org/10.1016/S0140-6736(10)60320-0)
- Zech, S., Goesling, T., Hankemeier, S., Knobloch, K., Geerling, J., Schultz-Brunn, K., Krettek, C., & Richter, M. (2006). Differences in the Mechanical Properties of Calcaneal Artificial Specimens, Fresh Frozen Specimens, and Embalmed Specimens in Experimental Testing. *Foot & Ankle International*, 27(12), 1126–1136. <https://doi.org/10.1177/107110070602701220>
- Zhai, X., Nauman, E. A., Moryl, D., Lycke, R., & Chen, W. W. (2020). The effects of loading-direction and strain-rate on the mechanical behaviors of human frontal skull bone. *Journal of the Mechanical Behavior of Biomedical Materials*, 103, 103597. <https://doi.org/10.1016/j.jmbbm.2019.103597>
- Zhang, L., Yang, K. H., & King, A. I. (2004). A Proposed Injury Threshold for Mild Traumatic Brain Injury. *Journal of Biomechanical Engineering*, 126(2), 226–236. <https://doi.org/10.1115/1.1691446>

Zwirner, J., Ondruschka, B., Scholze, M., Workman, J., Thambyah, A., & Hammer, N. (2021). The dynamic impact behavior of the human neurocranium. *Scientific Reports*, *11*(1), 11331. <https://doi.org/10.1038/s41598-021-90322-3>